Phase equilibrium of limonene, *p*-cymene, indane, butylbenzene and 1,2,3-trimethylbenzene at sub-atmospheric conditions

by

Rajesh Gowda

Thesis presented in partial fulfilment of the requirements for the degree of

MASTERS IN ENGINEERING

CHEMICAL ENGINEERING

In the Faculty of Engineering at Stellenbosch University

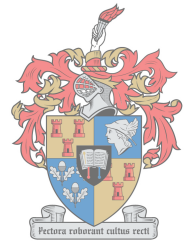

UNIVERSITEIT
iYUNIVESITHI
STELLENBOSCH
UNIVERSITY

Supervisor: Prof C.E. Schwarz

March 2018

Declaration

By submitting this thesis electronically, I declare that the entirety of the work contained therein is my own, original work, that I am the sole author thereof (save to the extent explicitly otherwise stated), that reproduction and publication thereof by Stellenbosch University will not infringe any third party rights and that I have not previously in its entirety or in part submitted it for obtaining any qualification.

Rajesh Gowda	March 2018
Signature	Date

Abstract

Waste tyre pyrolysis has long been seen as a suitable solution to the growing issue of accumulation of waste tyres in our environment. The pyrolysis of waste tyres produces three useful products, namely gas (~15 %), char (~35 %) and oil (~50 %), which can be used as fuel in various processes or as a feedstock for chemicals, one such chemical being limonene.

Limonene is an extremely useful chemical and contributes to a number of industries ranging from household chemical production to aromatherapy. The extraction of this chemical from tyre-derived oil (TDO) could have positive financial benefits to the waste tyre pyrolysis industry and thereby motivate the recycling of tyres through pyrolysis rather than incineration for fuel.

A significant issue faced with the recovery of limonene from waste tyres however, is that a pure fraction is difficult to obtain due to fact that there are other compounds in the TDO that boil at similar temperatures to limonene itself, including *p*-cymene, indane, 1,2,3-trimethylbenzene and butylbenzene. Although a significant amount of literature is available on the pyrolysis process of waste tyres, not much is available on the purification of limonene from the TDO and there is a lack of data in the literature for the concerned compounds vapour-liquid equilibrium (VLE) data. This study therefore focuses on the **experimental determination of the VLE data between limonene, *p*-cymene, indane, butylbenzene and 1,2,3-trimethylbenzene, at sub-atmospheric conditions.**

A setup in which phase equilibrium could be obtained was therefore required to be built as no setup was available for this study. Part of the capabilities required by the setup included accurate pressure measurement and control, accurate temperature measurement and disturbance-free sampling capabilities. The type of setup chosen was a vapour and liquid recirculation still that uses a Cottrell pump to achieve vapour-liquid equilibrium from a boiling feed. The VLE still was constructed using publicly available literature, after which its functional capabilities were commissioned. The experimental methodology was verified through measurement of isobaric VLE for relevant binary systems available in literature, namely ethanol/1-butanol at 101.3 kPa and *n*-decane/2-heptanone, *n*-decane/3-heptanone and *n*-nonane/pentanol at 40 kPa.

Experiments were conducted under Argon environments at 40 kPa in an effort to reduce compound degradation. Additional compound degradation trials conducted at 40 kPa for the experimental systems, **limonene/*p*-cymene, limonene/indane, limonene/butylbenzene, *p*-cymene/butylbenzene and limonene/1,2,3-trimethylbenzene/*p*-cymene/indane** indicated a maximum operation time of 4 hours. This can be used as an indication of the maximum total residence time suitable for an industrial operation involving these compounds if operating at

pressures below 40 kPa. Experimental accuracies, encompassing temperature, pressure and analysis effects, were found to be +/- 0.32 K in terms of temperature and +/- 0.0102 mole fraction in terms of composition. Pure fractions of indane and 1,2,3-trimethylbenzene could not be procured, thereby limiting the compositional range for which data could be obtained for systems including these compounds.

The experimental results showed that **barely any separation was present in the two binary systems, limonene/*p*-cymene and limonene/indane**, with low relative volatilities for *p*-cymene and indane (relative to limonene) respectively, in the regions that separation was present. Both systems contained azeotropes – limonene/*p*-cymene at about 0.25 – 0.30 mole fraction limonene and ~416.2 K and limonene/indane at ~0.55 mole fraction limonene and ~415.9 K. However, only the limonene/indane azeotrope is definite due to the limonene/*p*-cymene system having a slightly narrower temperature range.

The binary systems of **limonene/butylbenzene and *p*-cymene/butylbenzene showed slightly better separation** without the presence of azeotropes and with slightly higher relative volatilities for limonene and *p*-cymene (relative to butylbenzene) respectively. However, measuring this data proved difficult on the newly built still and had to be performed on the existing, additional Pilodist VLE still. This is due to there being insufficient mixing between the mixing and heating chambers of the constructed still for systems involving butylbenzene. Boiling regimes for these systems were noted to be irregular and included sudden vaporisations of the feed coinciding with drops in the measured vapour temperature of ~2 K.

Furthermore, the quarternary system of **limonene/1,2,3-trimethylbenzene/*p*-cymene/indane** showed that purification of limonene from 1,2,3-trimethylebenzene would be difficult to realise on an industrial scale.

All experimentally obtained data, verification and new, were found to be thermodynamically consistent according to the McDermott-Ellis consistency test. Additionally, vapour pressure data for limonene, *p*-cymene and butylbenzene were also obtained.

Finally, the experimentally obtained phase equilibrium data were regressed with the NRTL, Wilson and UNIQUAC activity coefficient models using the Data Regression System by Aspen Plus®. The ability of the models to regress the experimental data were determined through visual comparison and descriptive statistics (*AAD* and *AARD* values). Comparisons showed that the **Wilson activity coefficient model best describes the overall behaviour of the binary systems** with the NRTL model proving better for that of the quarternary system. Nevertheless, all three relevant models do manage to describe the VLE behaviour fairly well. Furthermore, all

the correlative models were compared with the predictive UNIFAC model, which showed that the UNIFAC model could not accurately predict the binary systems' behaviours.

Opsomming

Pirolise van afvalbande word lank reeds as 'n geskikte oplossing vir die toenemende probleem van die ophoping van afvalbande in ons omgewing beskou. Die pirolise van afvalbande lewer drie bruikbare produkte, naamlik gas (~15%), sintel (~35%) en olie (~50%), wat in verskeie prosesse gebruik kan word – as brandstof of as 'n voermateriaal vir chemiese stowwe, waarvan limoneen een is.

Limoneen is 'n uiters nuttige chemikalie wat 'n bydrae tot verskeie nywerhede lewer, van die vervaardiging van huishoudelike chemikalieë tot aromaterapie. Die ekstraksie van hierdie chemikalie van band-afgeleide olie (BAO) kan positiewe finansiële voordele vir die afvalbandpirolisebedryf inhou en daardeur die herwinning van bande deur pirolise, eerder as die verbranding daarvan vir brandstof, motiveer.

Daar is egter 'n probleem met die herwinning van limoneen van afvalbande: dit is moeilik om 'n suiwer fraksie te verkry omdat daar ander verbindings in die BAO is wat teen temperature soortgelyk aan limoneen kook, met inbegrip van *p*-simeen, indaan, 1,2,3-trimetielbenseen en butielbenseen. Alhoewel daar 'n aansienlike hoeveelheid literatuur oor die piroliseproses van afvalbande bestaan, is daar nie veel beskikbaar oor die suiwering van limoneen vanuit BAO nie. Daar is ook 'n gebrek aan damp-vloeistof-ewewig- (VLE-)data van die betrokke verbindings in die literatuur. Hierdie studie fokus dus op die **ekperimentele bepaling van die VLE-data tussen limoneen, *p*-simeen, indaan, butielbenseen en 1,2,3-trimetielbenseen, teen sub-atmosferiese toestande.**

'n Instrumentopstelling waarin fase-ewewig verkry kon word, moes dus gebou word, aangesien daar nie 'n opstelling vir hierdie studie beskikbaar was nie. Die nodige vermoëns van die opstelling het akkurate drukmeting en -beheer, akkurate temperatuurmeting en steuringsvrye monsterneming ingesluit. Die gekose soort opstelling was 'n damp-en-vloeistof-hersirkuleringsdistilleerder wat 'n Cottrell-pomp gebruik om damp-vloeistof-ewewig van die kookvoer te behaal. Die VLE-distilleerder is met behulp van openlik beskikbare literatuur gebou, waarná die funksionele vermoëns daarvan in bedryf gestel is. Die eksperimentele metodologie is deur die meting van isobariese VLE vir relevante binêre stelsels in die literatuur, naamlik etanol/1-butanol teen 101.3 kPa en *n*-dekaan/2-heptanoon, *n*-dekaan/3-heptanoon en *n*-nonaan/pentanol teen 40 kPa, geverifieer.

Eksperimente is onder argontoestande teen 40 kPa gedoen in 'n poging om verbindingsafbreking te beperk. Bykomende verbindingsafbraakproewe vir die eksperimentele stelsels **limoneen/*p*-simeen, limoneen/indaan, limoneen/butielbenseen, *p*-simeen/butielbenseen en limoneen/1,2,3-trimetielbenseen/*p*-simeen/indaan**, wat teen 40 kPa gedoen is, het 'n maksimum bedryfstyd van vier uur aangedui. Dit kan gebruik word as aanduiding van die maksimum totale residensietyd wat vir industriële bedryf met hierdie verbindings geskik is indien daar teen druk van minder as 40 kPa gewerk word. Eksperimentele akkuraatheid, wat temperatuur, druk en ontledingseffek ingesluit het, was +/- 0.32 K ten opsigte van temperatuur en +/- 0.0102 molfraksie ten opsigte van samestelling. Suiwer fraksies kon nie vir indaan en 1,2,3-trimetielbenseen verkry word nie, wat die samestellingsbereik waarvoor data vir stelsels met hierdie verbindings verkry kon word, beperk.

Die eksperimentele resultate het getoon dat daar **nouliks enige skeiding in die twee binêre stelsels limoneen/*p*-simeen en limoneen/indaan** was, met lae relatiewe vlugtigheid vir onderskeidelik *p*-simeen en indaan (relatief tot limoneen), in die gebiede waar daar skeiding was. Albei stelsels het aseotrope bevat – limoneen/*p*-simeen teen ~0.25 – 0.30 molfraksie limoneen en ~416.2 K en limoneen/indaan teen ~0.55 molfraksie limoneen en ~415.9 K. Slegs die limoneen/indaan-aseotroop is egter bepaal as gevolg van die feit dat die limoneen/*p*-simeen-stelsel 'n ietwat kleiner temperatuurbereik het.

Die binêre stelsels **limoneen/butielbenseen en *p*-simeen/butielbenseen het ietwat beter skeiding getoon** sonder die teenwoordigheid van aseotrope en met ietwat hoër relatiewe vlugtigheid vir onderskeidelik limoneen en *p*-simeen (relatief tot butielbenseen). Dit was egter moeilik om hierdie data op die nuutgeboude distilleerder te meet, so dit moes op die bestaande, bykomende Pilodist VLE-distilleerder gedoen word. Die rede hiervoor is ontoereikende vermenging tussen die meng- en verhittingskamers van die geboude distilleerder vir stelsels met butielbenseen. Daar is opgemerk dat kookregimes vir hierdie stelsels onreëlmatig was en skielike verdamping van die voer met gelyktydige afname in die gemete damptemperatuur van ~2 K ingesluit het.

Voorts het die kwartenêre stelsel **limoneen/1,2,3-trimetielbenseen/*p*-simeen/indaan** getoon dat dit moeilik sou wees om limoneen op industriële skaal van 1,2,3-trimetielbenseen te suiwer.

Daar is bepaal dat al die data wat eksperimenteel versamel is, sowel kontrole- as nuwe data, volgens die McDermott-Ellis-konsekwentheidstoets termodinamies konsekwent is. Daarbenewens is dampdrukdata vir limoneen, *p*-simeen en butielbenseen ook versamel.

Laastens is regressieanalise deur middel van die dataregressiestelsel van Aspen Plus® met die NRTL-, Wilson- en UNIQUAC-aktiwiteitskoëffisiëntmodelle gedoen op die fase-ewewigsdata

wat eksperimenteel verkry is. Die vermoë van die modelle om die eksperimentele data te regresseer is deur visuele vergelyking en beskrywende statistiek (absolute gemiddelde afwyking en absolute gemiddelde relatiewe afwyking) bepaal. Vergelyking het getoon dat die **Wilson-aktiwiteitskoëffisiëntmodelle die algehele gedrag van die binêre stelsels die beste beskryf** en dat die NRTL-model beter is in die geval van die kwartenêre stelsel. Nietemin beskryf al drie hierdie modelle die VLE-gedrag redelik goed.

Verder was al die soortgelyke modelle vergelyk met die UNIFAC model, wat daarop gedui het dat die UNIFAC model nie akkuraat is in die voorspelling van ń binêre sisteem se termodinamiese optrede nie.

Acknowledgements

This research has been funded by the Department of Process Engineering at Stellenbosch University and the Department of Environmental Affairs of South Africa. Opinions raised and conclusions drawn are those of the author and not the sponsors. Aspen Plus® is a registered trademark of Aspen Technology Inc.

I would like to personally acknowledge the following people as well:

- My supervisor, Prof Cara E. Schwarz for allowing me the opportunity to complete my masters under her guidance as well as the priceless expertise and consultation that she has provided.
- Dr Cedric Kouakou for his unlimited guidance, expertise and consultation as well.
- Dr Jamie Cripwell for all the free consultations and advice.
- Glasschem South Africa for the industrial knowledge they have brought into this project.
- Mrs. H. Botha and L. Simmers for all their analytical guidance and help.
- My Parents for their support and motivation throughout my years of study.
- Sithandile Ngxangxa and Malusi Mkhize for all their analytical expertise and consultation that they have freely shared with me.

And finally to Master Sri Ramakrishna for blessing me throughout my studies.

Table of contents

Nomenclature

A_i	Antoinne constant for component i	(kPa)
a_{ij}	Binary interaction energy parameter between components i and j	-
B_i	Antoinne constant for component i	(kPa.K)
b_{ij}	Binary interaction energy parameter between components i and j	(K)
C_i	Antoinne constant for component i	(K)
C_p	Heat capacity of a compound	($J.mol^{-1}.K^{-1}$)
D	Deviation in L/W and Mc-Dermott Ellis consistency test	-
D_{max}	Maximum Deviation in Mc-Dermott Ellis consistency test	-
E	Multiple of 10 to the power as indicated	-
e	Intermediate factor in UNIFAC method	-
F	Degrees of freedom	-
$\hat{f}_i^{v,l}$	Fugacity of component i in a particular phase	kPa
G^E	Excess gibbs energy	($J.mol^{-1}$)
G^C	Combinatorial excess gibbs energy	($J.mol^{-1}$)
G^R	Residual excess gibbs energy	($J.mol^{-1}$)
G_{ij}	Intermediate factor	-
ΔH_{vap}	Enthalpy of vaporisation per compound	($J.mol^{-1}$)
i	Denotes a particular species/compound	-
j	Denotes a particular species/compound	-
K_i	Partition coefficient of a compound	-
L	Parameter in L/W consistency test	-
m	Mass of a component	(g)
n	GC calibration curve gradient	-

N	Number of components	-
P	Pressure	(kPa)
P^{sat}_i	Saturated vapour pressure of component i	(kPa)
P_i	Partial pressure of component i	(kPa)
P_c	Critical Pressure	(kPa)
Q	Energy	(J)
Q_k	Subgroup relative surface area	cm^2
q	Relative molecular surface area	cm^2
R	Universal gas constant	$(J.mol^{-1}.K^{-1})$
R_k	Subgroup relative volume	cm^3
R_T	Resistance at a specific temperature	(Ω)
ΔS^*	Entropy of vaporisation	$(J.g^{-1})$
s	Intermediate factor in UNIQUAC equations	-
T	Temperature	(K)
T_b	Boiling temperature	(K)
T_{br}	Boiling/critical temperature ratio	-
T_{bub}	Bubble temperature of mixture	(K)
T_c	Critical temperatutre	(K)
U	Second order group contributions	-
u_k^j	Quantity of subgroups (k) in a molecule (i)	-
V	Volume	(cm^3)
V^L	Liquid molar volume	$(cm^3.mol^{-1})$
V_c	Critical volume	$(cm^3.mol^{-1})$
W	Parameter in L/W consistency test	-

X	Substitute property	-
x_i	Liquid mole fraction of compound i	-
y_i	Vapour mole fraction of compound i	-
Z_T	Total number of data points	-

Greek symbols

Λ_{ij}	Binary interaction energy parameter between components i and j	(J.mol^{-1})
α	Non-randomness parameter in NRTL equation	-
α_{ij}	Relative volatility between species in a mixture	-
β	Intermediate factor in UNIFAC method	-
γ_i	Activity coefficient for component i	-
δ	Difference between derived and experimental	-
ε	B Antoine constant	(kPa.K)
π	Number of phases	-
ρ	Density	(g/cm^3)
ϑ	Intermediate factor in UNIQUAC equation	-
λ	C Antoine constant	(K)
$\mathcal{H}_i$	Henry's constant for compound i in solution	-
$\mu_i^{v,l}$	Chemical potential of phases	(J.mol^{-1})
μ_i	Dipole moment	(Debye)
τ_{ij}	Intermediate factor in activity coefficient models	-
$\varphi_i^{V,l}$	Fugacity coefficient of component i	-
ω	Acentric factor	-

Abbreviations

AC	Alternating current
AAD	Average Absolute Deviation
AARD	Average Absolute Relative Deviation
BP	Boiling Point
DRS	Data Regression System of Aspen Plus®
EoS	Equation of State
exp	Exponential
FID	Flame Ionisation Detector
GC	Gas Chromatography
IS	Internal Standard
MM	Molar Mass
MS	Mass Spectrometry
NRTL	Non-Random Two Liquid
OF	Objective Funtion
PRV	Pressure Relief Valve
RMS	Root Mean Square
RTD	Resistance Temperature Detectors
SSR	Solid State Relay
TDO	Tyre Derived Oil
UNIQUAC	Universal Quasi Chemical Theory
UNIFAC	Universal Functional-group Activity Coefficient
VLE	Vapour-Liquid Equilibrium
ZAR	South African Rands

1. Introduction

The recovery and refining of chemicals from feedstock has long been seen as a profitable process and is most commonly carried out using distillation columns [1]. In the recent decades, environmental concerns has led to an increase in research regarding sustainable energy production. The feedstock from sustainable sources however, also require refining and thus distillation techniques and therefore vapour-liquid equilibrium (VLE) data, will most likely continue to be applicable.

This study looked at the VLE data required in designing a separation process for chemicals within the oil produced during the pyrolysis of waste tyres, as the data is not available in the literature. One particular compound that is present in the tyre-derived oil or TDO, that has caught the eye of many researchers, is limonene (scientific: DL-limonene or dipentene) [1].

TDO is commonly used in the production of fuel, however this study focuses on the recovery of chemicals (specifically limonene) from the TDO due to the unexplored potential of this raw material [1].

1.1 Waste tyre pyrolysis overview

1.1.1 Process

Pyrolysis is a process that consists of thermally degrading volatile matter in the absence of oxygen to produce a product which usually consists of non-condensable gas, liquid oil and solid char components [1]. The pyrolysis of coal and wood has been widely used for the production of solid and gaseous fuel for the past three centuries [2, 8].

Waste tyres are considered to be a growing threat to our environment as an estimated 1.5 billion waste tyres are produced annually worldwide [1]. The use of waste tyres as a combustion fuel source is a familiar sight in South Africa and is a direct contributor to air and water pollution. The landfilling of tyres has also been seen to be very problematic as tyres are very voluminous and do not degrade easily [1]. Waste tyre landfill sites also serve as breeding grounds for pests such as rats and mosquitoes [1].

Thus, pyrolysis may be selected as a suitable solution to the issue of waste tyre accumulation in South Africa and worldwide, as opposed to the incineration and landfilling of waste tyres, due to its low environmental impact and the recovery of liquid and solid material that are useful [8].

Furthermore, products from tyre pyrolysis are easily manageable and can be valorised further depending on various market needs and objectives [2, 8].

In general, there are two types of pyrolysis processes – fast pyrolysis and slow pyrolysis. As the names suggest, these processes depend on the heating rate and residence times of the feedstock to the process, with fast pyrolysis having high heating rates and low residence times and slow pyrolysis having low heating rates and long residence times [8]. Fast pyrolysis generally favours the production of liquid and gas products as opposed to solid char and slow pyrolysis favours the production of solid char as opposed to liquid and gas products [8]. Catalytic pyrolysis is also possible and involves either fast or slow pyrolysis but with the use of a catalyst [8]. The most common reactors used in pyrolysis are fixed bed (batch), screw kiln, rotary kiln, vacuum and fluidised bed type reactors [1].

Tyres mostly consist of various rubbers like natural rubber, synthetic poly-isoprene, butadiene rubber and styrene-butadiene rubber [1]. They do however contain additives such as oils and fillers that are added into the tyre during the manufacturing process [1]. The remainder of a tyre includes steel, which comes from the structural support component in the tyres, as well as zinc, silica and clays [1].

1.1.2 Products

The product from the pyrolysis of a steel-free tyre typically has a composition of 5 – 20 wt. % gas, 40 – 60 wt. % liquid oil and 30 – 40 wt. % solid depending on the process conditions [1, 8]. The steel content in a tyre is roughly around 9 wt. % [7].

The pyrolysis products of a tyre can be significantly influenced by the operating conditions of the pyrolysis process with variables such as temperature, pressure, residence time, particle size, heating rate, whether or not a catalyst is used and the type of tyre brand (chemical composition) that is used as the feedstock playing a key role in the product quality [1]. Figure 1.1 shows a summary of the tyre pyrolysis process and variables that affect the overall performance [1, 8].

The solid char product from tyre pyrolysis typically consists of carbon black and other additives and fillers such as zinc, sulphur, clays and silica that were used in the original tyre or rubber manufacturing process [1, 9, 10]. The gas consists of light hydrocarbons (C_1 – C_4) and is usually fed back to the process as fuel for heat, although it cannot compensate for the total heat required since small quantities are typically retrieved [1, 2]. The steel product can be recovered and resold to scrap metal dealers or ferrous-metal processors to recover a small portion of the production costs [1].

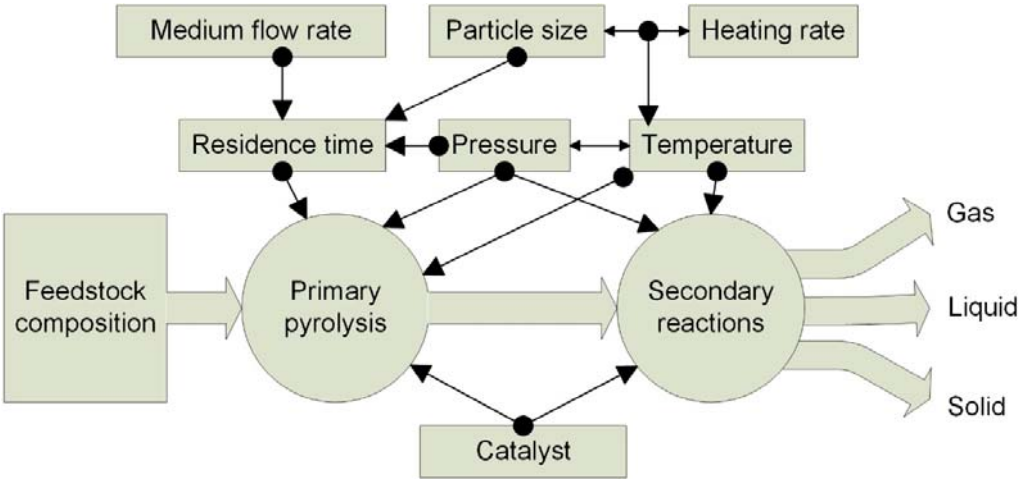

Figure 1.1: Graphical summary of the pyrolysis process and variables that affect the product yields [1]

The liquid oil product however, more commonly known as the tyre-derived oil (TDO), has attracted the most attention due to its applications as either a fuel source or a feedstock for the recovery of valuable chemicals [1]. The TDO is typically a mixture of paraffins, olefins and aromatic compounds and has a high calorific value of 40 – 45 MJ/kg, which is one reason why it could be used as a fuel source [1, 2, 3]. In fact, some of the oil can be used in conjunction with the gas produced in an effort to make the pyrolysis process more self-sustainable [1].

As with any recycling process, there are drawbacks to using the TDO as a fuel source. The pyrolysis process is endothermic, therefore making the incineration of tyres themselves more energy efficient [1, 8]. There is also a lack of industrial acceptance of the waste tyre pyrolysis products with recyclers currently having issues marketing their TDO and char at competitive prices [1].

A portion of the TDO can also be mixed with conventional combustion engine fuels (<473 K), however this portion is also relatively high in sulphur content and requires extra processing such as hydrofining and de-vulcanisation (upstream) before more than 2 wt. % of this portion can be readily mixed with fuels such as petroleum [4, 7].

Fortunately, the TDO can also be used as a feedstock for the recovery of valuable chemicals since it contains many industrially valuable compounds such as limonene, benzene, toluene, xylenes and ethyl benzene to name a few [1]. Limonene however, has been found to be the largest component of the TDO in instances where the pyrolysis process conditions are favourable [1, 8]. It is for this reason that the recovery of limonene from waste tyres has gained

much attention [1]. The commercial viability of the limonene produced from waste tyres however, depends on its quality.

1.2 Purpose and aims

The purpose of this study is to contribute towards research devoted to recovery of limonene from TDO in an effort to improve the economic feasibility of waste tyre pyrolysis. Although research has shown that limonene-rich fractions can be produced from the TDO through simple distillation, an entirely pure fraction has not yet been achieved on an industrial scale [4]. This is one of the difficulties that is currently associated with the waste tyre pyrolysis process [4].

Of the many compounds present in the limonene-rich fractions of TDO, a few have very similar boiling points as that of limonene and thus make separation and purification difficult [68]. These compounds include *p*-cymene, indane, butylbenzene and 1,2,3-trimethylbenzene [1, 4, 68]. The separation of limonene from these compounds could lead to a development in the waste tyre pyrolysis process.

In an effort to determine the feasibility of purifying the limonene-rich fractions via distillation, research has been conducted via Aspen Plus® simulations at vacuum pressures [68]. The simulations required the use of predictive thermodynamic models that describe the thermodynamic behaviour of limonene and the other compounds that boil at similar temperatures [68]. There was however no experimental phase equilibrium data available in the literature to validate these models.

The aim of this study was therefore to provide relevant phase equilibrium data for compounds, with close boiling points to limonene, in the light fraction of the TDO. In addition to being useful in the separation and purification of limonene present in TDO, this data would also be useful in the validation of the thermodynamic model parameters used in Aspen Plus® simulations. Furthermore, it would also give an indication of the quality of limonene that could be extracted from waste tyres.

1.3 Objectives

In order to achieve the above mentioned aim, the following three objectives needed to be met:

1. **Construct a vapour and liquid recirculation equilibrium still in which the phase equilibrium data for this study could be attained.** Although the Department of Process Engineering did already have an existing vapour and liquid recirculation

equilibrium still, it was not available for this project due to prior commitments of other projects. Thus in order to conduct the current project as well as to extend the capacity of the department, an additional setup was required. Furthermore, although the present still was unavailable for the project, it did become available intermittently during projects.

The constructed VLE still should be capable of temperature measurement, pressure measurement as well as vapour and liquid phase sampling. The still was commissioned and verified using binary reference systems from literature to ensure its accuracy and reliability. The reference systems used were ethanol/1-butanol at 101.3 kPa and *n*-decane/2-heptanone, *n*-decane/3-heptanone and *n*-nonane/1-pentanol at 40 kPa [61, 70, 108, 109].

2. **Measure phase equilibrium (vapour pressure and VLE) data at sub-atmospheric pressures for binary mixtures of the compounds limonene, *p*-cymene, indane, butylbenzene and 1,2,3-trimethylbenzene.** The data collected was in the form of temperature-composition data, using the still constructed for the first objective, at a pressure of 40 kPa. The systems obtained were limonene/*p*-cymene, limonene/butylbenzene, *p*-cymene/butylbenzene, limonene/indane and limonene/1,2,3-trimethylbenzene/*p*-cymene/indane.

3. **Determine binary interaction parameters for three relevant activity coefficient models, NRTL, Wilson, and UNIQUAC using Aspen Plus® for the systems investigated.** This was done using the Data Regression System (DRS) available in Aspen Plus® [67].

1.4 Thesis overview

Chapter 2 of this thesis provides a review of the compounds of concern, thermodynamics relevant for experimentally obtained VLE and the basis for the type of setup used in this study.

Chapter 3 addresses Objective 1 as it details the requirements and specifications of the experimental setup's construction, together with the design philosophy employed. The chapter also discusses the experimental methodology as well as the commissioning and verification stages conducted to ensure a proper functioning and reliable experimental setup.

Chapter 4 addresses Objective 2 and briefly describes the experimental plan as well as the effect that compound degradation has on this study, after which the chapter presents and discusses the experimental results obtained for the VLE of five systems comprising limonene, *p*-cymene, indane, butylbenzene and 1,2,3-trimethylbenzene.

Chapter 5 addresses Objective 3 and focuses on the regression of the phase equilibria data obtained using Aspen Plus®. Finally, conclusions are drawn and recommendations made for future projects in Chapter 6.

2. Literature

2.1 Chemical recovery

2.1.1 Limonene (DL-Limonene or dipentene)

Limonene is an alkene and its molecular formula is $C_{10}H_{16}$ [1]. It's scientific name is 1-methyl-4-(1-methylethenyl)-cyclohexene and has a normal boiling point (NBP) of 449.65 K [11, 59]. It is also scientifically known as dipentene [1]. The compound is insoluble in water due its nonpolar nature and has a density (0.839 g/mL) that is less than that of water and a molar mass of 136.237 g/mol [59, 103].

Limonene originates from a family of plant hydrocarbons produced in plants known as terpenes and is classified as a cyclic monoterpene [1, 11]. Terpenes are present in some essential oils such as citrus oil and can be used as a flavour, fragrance and in aromatherapy [1, 3, 11]. Limonene is a colourless oil and is usually extracted from the peel of citrus fruit such as oranges, lemons and grapefruit, it is known to constitute 98 wt. % of the essential oil obtained from orange peels and can also be biosynthetically manufactured [1, 5, 14, 103]. As mentioned previously, a possible alternative source for limonene is TDO [1].

Limonene is typically used in the formulation of industrial solvents, resins and adhesives and as a dispersing agent for pigments [5, 16, 21]. It is also used as a solvent and feedstock for the production of fragrances and flavouring and in a wide range of applications including water-based de-greasers, natural lemon scented all-purpose cleaners, hand cleaners and replacements for chlorofluorocarbon solvents to clean electronic circuit boards [5, 21, 77, 103]. It may be an alternative for some popular but not favourable solvents as it is non-toxic, biodegradable and produced from renewable resources – it has recently been used in the recycling of polystyrene [103]. Furthermore, it can be used for biological purposes to promote weight loss, prevent cancer and treat bronchitis [1, 16]. Therefore, there clearly is a market for the extraction of limonene from TDO as it could help with the valorisation of waste tyre pyrolysis.

Limonene can be found in two forms namely, D-limonene and L-limonene. The two are enantiomers of 1-methyl-4-(1-methylethenyl)-cyclohexene and have the same physical properties [4]. D-Limonene typically smells like oranges and is the R enantiomer, whereas the L-limonene derivative is the S enantiomer and smells like a sour scent mixed with pine (lemons) [1, 11, 103]. The racemic mixture of the enantiomers is known as DL-limonene or dipentene [1]. It is in fact the racemic mixture, DL-limonene which is found in TDO [1]. Figure 2.1 shows the

difference between D- and L-limonene [1]. For the rest of this study, reference to limonene will indicate DL-limonene or dipentene. All molecular structures in this chapter were drawn using ACD Chemsketch Freeware.

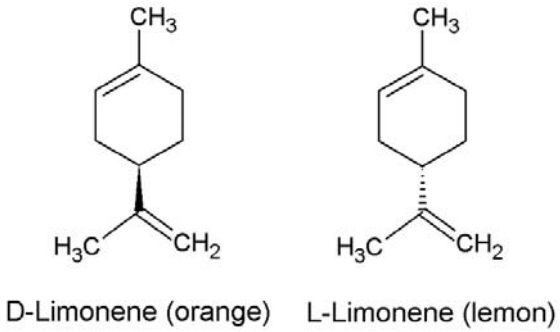

Figure 2.1: Enantiomers D-limonene and L-limonene [1]

2.1.2 Limonene recovery

2.1.2.1 Limonene and pyrolysis

Literature states that at least 2.5 wt. % of a steel free tyre can and has been converted to limonene during pyrolysis [1]. This is a significant amount considering the amount of waste tyres annually generated [1]. As seen in Figure 1.1, the pyrolysis process conditions can significantly influence the limonene yield achievable [1].

The pyrolysis temperature has been seen to be the most important variable to control when trying to achieve a maximum limonene yield, with the optimal temperature ranging between 673 K and 773 K [1]. Literature also states that a tyre with a higher Natural Rubber (NR) content gives way to a higher limonene concentration [8].

Secondary reactions as shown in Figure 1.1 are linked with many variables in the pyrolysis process and are mostly unwanted due to them leading to products such as poly-aromatic hydrocarbons (PAH's) that are carcinogenic and toxic to the environment [1, 4, 8, 13]. It has been seen that the carrier gas or medium is a key variable to control the occurrence of secondary reactions, this is however only been tested at atmospheric conditions [8]. The thermal degradation of limonene also takes place in the form of secondary reactions [8].

At temperatures above 723 K – 753 K, limonene undergoes thermal degradation, as part of secondary reactions, to products such as *p*-cymene, *m*-cymene, indane, *m*-xylene and alkyl-benzenes such as 1,2,3-trimethylbenzene [4, 8, 13, 79]. These products lead to

counterproductive pyrolysis for limonene production firstly because it creates a loss in limonene yield and secondly because the compounds *p*-cymene, *m*-cymene, indane and 1,2,3-trimethylbenzene have normal boiling points that are very similar to limonene, making it very difficult to try and extract pure fractions of limonene [4, 59].

Several researchers have tried to quantify the TDO produced during pyrolysis [20, 22, 24, 25, 87]. Table 2.1 shows such estimations of composition of the TDO (before purification), although only a portion of the TDO could be quantified in each study [22, 24, 25, 87]. Table 2.1 also emphasises the amount of limonene available in the TDO from pyrolysis as compared to other compounds. The peak areas reported in Table 2.1 can be used as an estimation of the respective compounds concentration in the TDO.

Table 2.1: Estimation of composition of TDO from tyres for compounds of significant concentrations [22, 24, 25, 87].

Type of tyre	*Car* [22]	*Truck* [24]	*Motorcycle* [25]	*Car* [87]
Analysis method	*GC-MS*	*GC-MS*	*GC-MS*	*GCxGC-MS & GC-FID*
Operation temperature	*~773 K*	*~923 K*	*~748 K*	*733 - 753 K*
	GC peak area (%)	GC peak area (%)	GC peak area (%)	Concentration wt. (%)
Limonene	13.79	28.78	29.54	6.60
Toluene	3.53	7.53	6.03	0.65
Benzene	-	2.29	0.13	0.12
Ethylbenzene	4.13	2.70	-	0.59
Styrene	2.16	-	-	0.30
Propylbenzene	1.06	4.73	-	0.15
1-Ethyl-3-methylbenzene	1.94	-	-	-
1-Ethyl-4-methylbenzene	-	-	-	0.23
α-Methylstyrene	1.10	1.84	-	-
1,2,3-Trimethylbenzene	-	-	-	0.16
p-Xylene	-	4.30	3.14	0.56
Indene	-	-	-	0.11
Balance	72.29	47.83	61.16	90.53

2.1.2.2 Purification and upgrading of TDO

TDO is a dark brown/black coloured, mildly viscous oil with a sulphurous/aromatic odour [13]. It contains more than a 100 identified compounds and is a mixture of aliphatic, aromatic, heteroatom, polar and non-polar compounds with boiling points ranging between 343 K and 673 K [13, 82]. Limonene, as mentioned previously, is the major component of the TDO [1, 8]. In order to extract a pure fraction of limonene from the TDO, a purification step is clearly necessary [1, 4, 8, 13].

The most common purification technique is distillation of the TDO. TDO is generally classified into four different fractions, namely, light naphtha (NBP < 433 K), heavy naphtha (433 K – 477 K), middle distillate (477 K – 623 K) and heavy fraction/bottom residue (NBP > 623 K), each of which can be used in different applications [1, 4, 6, 7, 23]. Of the total TDO produced, approximately 10 wt. % lies within the heavy naphtha region with a boiling point between 433 K and 473 K, the fraction in which limonene would be recovered [6, 23]. The TDO however typically contains 20 – 25 wt. % of the fraction which has a boiling point below 473 K and this is known as the general naphtha fraction [4, 22, 25].

One group of researchers distilled the TDO twice, to recover a limonene-rich fraction consisting of a varied concentration of between 53 wt. % - 91 wt. % limonene, with an original limonene content of 2.6 wt. % - 3.6 wt. %, respectively in the TDO. [4]. This highly varied concentration could be the effect of the various factors illustrated in Figure 1.1. Table 2.2 shows typical compositions of limonene-rich fractions after two distillation steps of the TDO for different types of tyres [4].

From the table it can be seen that together with limonene, other compounds such as *m*-cymene, butylbenzene, indane and 1,2,3-trimethylbenzene are also present in significant quantities in the limonene-enriched TDO [4].

Other researchers have also tried to obtain a limonene-rich fraction using two distillation steps [84, 85]. The first step was to obtain a naphtha fraction of compounds with boiling points below 463 K and the second step was to obtain a limonene-enriched naphtha fraction [84, 85, 86]. Ultimately, a 16.3 wt. % limonene-enriched naphtha fraction was achieved, however they could not successfully purify the limonene further from the naphtha fraction [86].

Although most of these compounds are formed due to issues such as excess pyrolysis residence times and thermal degradation of limonene at pyrolysis temperatures above 723 K, their presence after two distillation steps is due to their relatively similar boiling points [1, 59].

The similarities in their boiling points' make it difficult to separate them from limonene through distillation without substantial additional operating costs [4].

Table 2.2: Typical chemical composition of limonene-rich fractions of TDO together with the original type of tyre used to perform the pyrolysis [4]

Chemical (wt. %)	Car tyre	Truck tyre 1	Truck tyre 2
Limonene	92	50	62
m-Cymene	2	13	22
Butylbenzene	0.5	3	-
Indane	-	8	1
1,2,3-Trimethylbenzene	-	19	5
2,5-diethylthiophene	Trace	0.2	0.31
1-methyl-4-isopropenyl-Cyclohexene	-	-	3
2-tert-butylthiophene & 3-tert-butylthiophene	Trace	0.4	0.38
4-methyl-1-isopropyl-Cyclohexene	3	-	-
Others	2.5	6.4	6.31

Although *p*-cymene is not included in the analysis presented in Table 2.2, it will be included in this study due to it being found as the second most significant compound after limonene in an analysis of TDO produced by a previous study at Stellenbosch University [11]. *p*-Cymene has also been mentioned in the literature as a product of limonene's thermal degradation [8, 13, 79].

2.1.3 Simulation of limonene purification

Simulation of the limonene enrichment process was conducted in a previous study at Stellenbosch University [68]. Process models using Aspen Plus® V8.2 were developed to separate limonene from TDO at sufficient purity (> 95 wt. %) [68]. Enhanced distillation techniques were employed in the simulation to produce high purity (>95 wt. %) limonene [68].

Thermodynamic models used in the simulation were the non-random-two-liquid (NRTL), the universal quasichemical activity coefficient (UNIQUAC) and universal functional activity coefficient (UNIFAC) models [68].

The process models developed, which describe the thermodynamics and are based on assumptions made, suggested that it was possible to obtain limonene recoveries in excess of 95 wt. % and at purities as high as 99 wt. % [68]. However, after verification with an experimental batch distillation setup, it was found that the models developed could not predict the experimental process precisely, which may be due to model inaccuracy [68]. This therefore emphasised the need for experimental vapour-liquid equilibrium (VLE) data for binary mixtures of interest [68].

2.1.4 Compounds of concern

Table 2.3 summarises the properties of the compounds of concern in this study in addition to limonene, namely, *m*-cymene, *p*-cymene, indane, butylbenzene and 1,2,3-trimethylbenzene [59]. All these compounds are present in limonene-rich fractions of TDO and have similar normal boiling points to that of limonene, as can be seen in Table 2.3 [1, 11, 4, 59, 68]. Figures 2.2 to 2.6 further illustrate 2-D structures of each of the compounds of concern.

Table 2.3: Comparison of properties for compounds of concern [59]

Compound	MM (g/mol)	Normal Boiling Point (K)	Density (g/cm^3)
Limonene ($C_{10}H_{16}$)	136.237	449.65	0.839
m-Cymene ($C_{10}H_{14}$)	134.221	448.23	0.857
p-Cymene ($C_{10}H_{14}$)	134.221	450.28	0.852
Indane (C_9H_{10})	118.178	451.12	0.960
Butylbenzene ($C_{10}H_{14}$)	134.221	456.46	0.858
1,2,3-Trimethylbenzene (C_9H_{12})	120.194	449.27	0.891

In the case of the cymene isomers, *m*-Cymene is an aromatic compound and it is miscible in alcohol and insoluble in water [12]. *p*-Cymene is a geometric isomer of *m*-cymene, as can be seen in Figures 2.2 and 2.3 and is miscible in alcohol and insoluble in water as well [12]. The difference between the two isomers is the positioning of the methyl group on the benzene ring [1, 4, 12, 59].

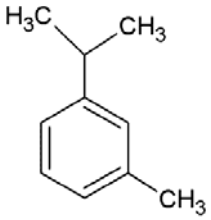

Figure 2.2: *m*-Cymene molecular structure [12]

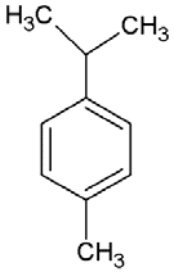

Figure 2.3: *p*-Cymene molecular structure [12]

m-Cymene however, was excluded from this study as it is an extremely expensive chemical in pure fractions, making it difficult to conduct research under budget constraints, since relatively pure fractions are required for the determination of VLE data [12]. Although *m*-cymene should have been included on the premise that it's normal boiling point is very close to that of limonene, it's deviation from ideality should be similar to that of *p*-cymene and it's phase behaviour could thus be modelled based on *p*-cymene. Furthermore, *m*-cymene has an acceptable odour like limonene and therefore does not negatively affect the marketability of limonene produced from waste tyres [4].

Figure 2.4 shows a 2-D structure of Indane [17, 59]. Indane is a clear liquid at room temperature and is usually present in concentrations of between 1 wt. % to 8 wt. % in limonene-enriched fractions of the TDO [4].

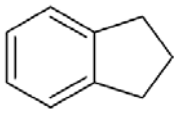

Figure 2.4: Indane molecular structure [17]

Butylbenzene is also present in the limonene-rich fraction of the TDO due to its relatively close boiling point [4]. It is a colourless liquid at room temperature and is shown in Figure 2.5 [18, 59]. The compound is known to be highly flammable, very reactive and insoluble in water but miscible with alcohols and ethers [18].

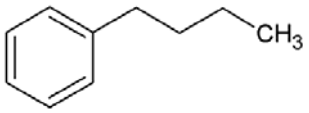

Figure 2.5: Butylbenzene molecular structure [18]

Like the above mentioned chemicals, 1,2,3-trimethylbenzene is also a colourless liquid at room temperature [18]. Figure 2.6 shows its 2-D molecular structure [18, 59].

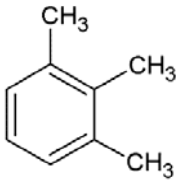

Figure 2.6: 1,2,3-Trimethylbenzene molecular structure [18]

As previously mentioned, the compounds of concern mentioned above are the ones for which phase equilibrium data is required. An advancement in this area of research has high technical and commercial interest [1, 4, 11]. Although a significant amount of literature is available on the pyrolysis process of waste tires, not much is available on the purification of the limonene-rich fractions. Tong *et al.* report VLE data for the system limonene/*p*-cymene at 100.7 kPa, measured in an Ellis equilibrium still [19]. This was the only reference regarding the vapour-liquid equilibrium of either pair of the compounds of concern that was noted [60]. It is for this reason that this project focuses on obtaining the experimental phase equilibrium data for these compounds.

The remainder of this chapter focuses on the thermodynamics behind VLE data generation and the experimental setups suitable for VLE data generation.

2.2 Thermodynamics

Thermodynamics is the basis for all equilibrium problems and this study is no exception. With the determination of experimental VLE data comes the use of thermodynamics to understand and describe the data. A multitude of thermodynamic models are available to describe the equilibrium between phases [46]. This section explains the applicable thermodynamic models used in the Aspen Plus® software to generate parameters for the phase equilibrium data obtained as well as the fundamentals of equilibrium, vapour-liquid equilibrium, partition coefficients and relative volatility. Additional thermodynamic models such as equations of state (EoS) are available in literature [48, 49, 50, 54].

2.2.1 Equilibrium fundamentals

2.2.1.1 Degrees of freedom

The phase rule can be used to explain the fundamental property of equilibrium [54]. It states that at equilibrium, the number of intensive variables that may be independently fixed (degrees of freedom) is restricted by the number of different components and the number of different phases that are present in the system as follows [54]:

$$F = 2 - \pi + N \tag{2.1}$$

Where π is the number of phases, N is the number of components present and F is the number of degrees of freedom [54]. Although trivial, this basic equation can cause confusion if not simply considered at the start of every problem [54].

A binary system at equilibrium has 4 intensive variables namely, temperature, pressure, vapour phase composition and liquid phase composition. In this study, each system has 2 components and 2 phases. Therefore, there are 2 degrees of freedom, which were chosen to be temperature and pressure.

Pressure was chosen since isobaric data is required and temperature was chosen since it is much easier to vary temperature using external heat to obtain equilibrium in a binary mixture than it is to vary composition of either vapour or liquid equilibrium fractions.

2.2.1.2 Phase diagrams

As mentioned above, the type of data required is isobaric vapour-liquid equilibrium data. Therefore, the information retrieved from the experimental setup should be in the form of temperature-composition data for the respective components at a fixed pressure.

Phase diagrams are useful in illustrating temperature-composition (isobaric) and pressure-composition (isothermal) data for mixtures and pure compounds alike as they illustrate the behaviour of components as conditions vary and are also easy to interpret [54]. They are commonly used in industry in combination with other diagrams such as composition diagrams (vapour vs liquid) in the design of separation equipment like distillation columns [54].

Figure 2.7 illustrates a typical temperature-composition phase diagram for a binary mixture at constant pressure [54].

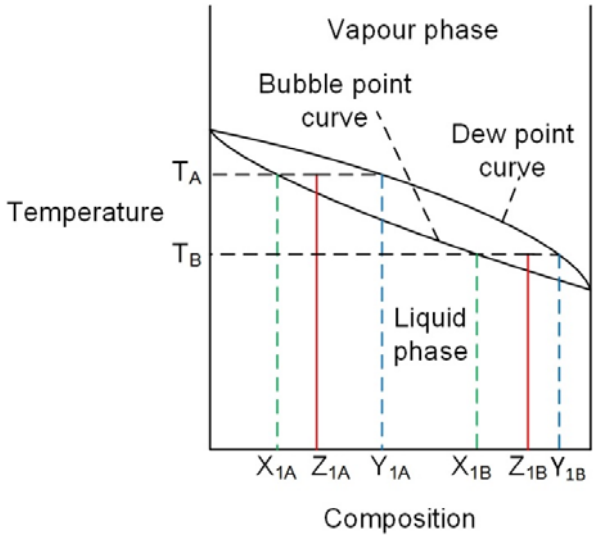

Figure 2.7: Isobaric temperature-composition phase diagram of a typical binary mixture including data generation, X_1 – liquid composition of component 1, Y_1 – vapour composition of component 1, Z_1 – Feed composition of component 1.

The liquid phase lies below the bubble point curve (lower temperatures) and the vapour phase lies above the dewpoint curve (higher temperatures) [54]. Between the two curves lies the two phase region in which both liquid and vapour co-exist in equilibrium. Composition varies from 0 – 1 (mole fraction) of either component from one end of the horizontal axis to the other [54].

Clearly, in order to generate such a diagram, sufficient data points corresponding to the bubble and dew point curves are necessary. As such, records of temperature and composition information are required at isobaric conditions.

Figure 2.7 also illustrates a method in which temperature-composition data can be obtained. For a particular feed composition (Z_1) once the system reaches equilibrium, the temperature (T) is read and the liquid (X_1) and vapour (Y_1) samples are taken, thereafter being analysed, to determine the respective mass and mole fractions for each component. This type of data set will be required for as many feed samples as possible. In Figure 2.7, progressive letters (A and B) indicate each subsequent data point. With this method, the bubble and dew point curves for a system can be generated.

Phase diagrams can also be used to plan and control sample collection for VLE data. As mentioned previously, this system has two degrees of freedom and they have been chosen to be pressure and temperature. Using the lever arm rule as a basis, for a particular feed at a fixed pressure, different equilibrium points in terms of temperature can be obtained. Figure 2.8 illustrates three points, i, ii and iii, that are at equilibrium, however they differ in amount of either liquid or vapour phase present and therefore the temperature (higher temperature would lead to a slightly higher vapour fraction).

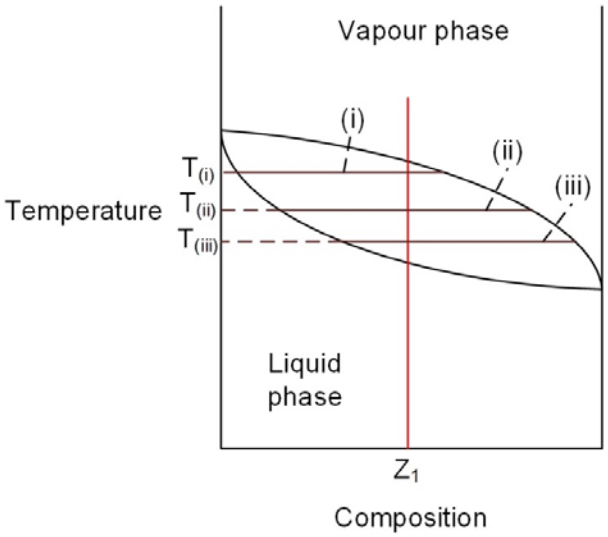

Figure 2.8: Equilibrium phase fraction differentiation using lever arm rule. (i) – larger vapour fraction, (ii) – equal liquid and vapour fractions, (iii) – larger liquid fraction.

2.2.1.3 Azeotropy

Sometimes during equilibrium, a mixture can retain the same composition for both the vapour and liquid phases at a certain pressure, such a point is known as an azeotrope [71, 78]. An azeotrope can be classified as a minimum boiling azeotrope or a maximum boiling azeotrope, with more than 90 % of cases falling within the former [80]. Azeotropic behaviour is common in mixtures where compounds have dissimilar structures and elemental features [81].

In a minimum boiling azeotrope, the presence of dissimilar functional groups cause repulsion forces between molecules, which effectively increase the combined vapour pressure and in turn decrease the boiling point compared to the pure components [71, 83]. In cases where the repulsion forces are extreme, two liquid phases and one vapour phase form in what is known as a heterogeneous minimum boiling azeotrope [71]. In maximum boiling azeotropes, the functional groups cause attractive forces between the molecules, which in turn decrease the combined vapour pressure and increase the mixture's boiling point to higher than that of the pure component [71, 83]. Minimum boiling azeotropes display positive deviations from Raoult's law and vice versa [71, 78].

In general, compounds with small differences in vapour pressures are likely to form azeotropes and as the difference in vapour pressures become larger, the less likely it is that an azeotrope will form [71]. Therefore, the compounds in this study are likely to have azeotropes forming in their binary mixtures as their normal boiling points and hence vapour pressures are very close.

2.2.2 Vapour-liquid equilibrium

Vapour-liquid equilibrium is the state of coexistence between vapour and liquid phases in a closed system and is achieved when the rate of evaporation of the liquid phase is equal to the rate of condensation in the vapour phase [54]. It may seem like no change is taking place on a macroscopic level since temperature, pressure and phase compositions all remain constant, but at a microscopic level, molecules at the phase boundaries are continuously evaporating and condensing from the liquid and vapour phases respectively [54].

Multiple phases at the same temperature and pressure are in equilibrium when the chemical potential (μ) of each species is the same in all phases [54]. The following relations describing chemical, thermal and mechanical equilibrium hold for a system that has achieved vapour-liquid equilibrium [54]:

$$\mu_i^v = \mu_i^l \tag{2.2}$$

$$T^v = T^l \tag{2.3}$$

$$P^v = P^l \tag{2.4}$$

Where μ_i^v and μ_i^l are the chemical potentials of the vapour and liquid phases respectively, for each component i in a mixture. The subscripts *v* and *l* denote the vapour and liquid phases respectively.

Chemical potential is defined in relation to the internal energy and entropy of a species, making it difficult to obtain absolute values for this property [54]. For this reason, fugacity (f) is used in quantifying equilibrium, over the use of chemical potential [54]. Fugacity can be thought of as the tendency of a certain component to escape the phase in which it is [54].

Fugacity by itself is not a fundamental property and is derived using the chemical potential (partial molar Gibbs energy) of a species in a mixture, which is in turn dependent on the temperature and pressure of the system [54, 61]. The fugacity of a species in solution ($\hat{f}_i$) is related to the chemical potential via [54]:

$$\mu_i \equiv \Gamma_i(T) + RTln\left(\hat{f}_i\right) \tag{2.5}$$

Where $\Gamma_i(T)$ is an integration constant at constant temperature and is a species dependent function of temperature only [54]. Therefore, since thermal equilibrium holds between phases for a mixture in vapour-liquid equilibrium, the following relation for corresponding fugacities in each phase also holds [54]:

$$\hat{f}_i^v = \hat{f}_i^l \tag{2.6}$$

Where $\hat{f}_i^v$ is the fugacity of component i in the vapour phase and $\hat{f}_i^l$ is the fugacity of component i in the liquid phase. Hence, two or more phases at the same temperature and pressure are in equilibrium when the chemical potential and fugacity of each species is the same in all phases [54].

Fugacity can be considered as the pressure of an ideal fluid or as the partial pressure of a species in an ideal gas mixture as follows [54, 73]:

$$\hat{f}_i^{ideal\ gas} = y_i P \tag{2.7}$$

However, to account for the effects of a real gas in a mixture, a dimensionless ratio, the fugacity coefficient ($\hat{\varphi}_i$) is used [54, 71]:

$$\hat{f}_i^v = \hat{\varphi}_i^v y_i P \tag{2.8}$$

The fugacity coefficient can also be used for liquids:

$$\hat{f}_i^l = \hat{\varphi}_i^l x_i P \tag{2.9}$$

Where $\hat{\varphi}_i^v$ and $\hat{\varphi}_i^l$ are the fugacity coefficients of component i in the vapour and liquid phases respectively [54]. *P* represents the total system pressure and y_i and x_i are component i's vapour and liquid fractions respectively [54].

In the case of an ideal solution, fugacity can be defined as [54]:

$$\hat{f}_i^{ideal\ solution} = x_i P_i^{sat} \tag{2.10}$$

For an ideal gas and ideal solution at equilibrium, a combination of Equations 2.7 and 2.10 gives Raoult's law [54]. However, just as in the case of a real gas, the non-ideal effects of a real solution are accounted for using a dimensionless ratio, the activity coefficient (γ_i) [54]:

$$\hat{f}_i^l = \gamma_i x_i f_i \tag{2.11}$$

With the fugacity of a pure species (f_i) being [54]:

$$f_i = \varphi_i^{sat} P_i^{sat} \exp\left(\frac{V_i^l (P - P_i^{sat})}{RT}\right) \tag{2.12}$$

Where V_i^l is the liquid molar volume. The exponential term is known as the Poynting correction factor and the derivation for this relation can be found in literature [54]. A combination of Equations 2.8, 2.11 and 2.12 gives:

$$\hat{\varphi}_i^v y_i P = \gamma_i x_i \varphi_i^{sat} P_i^{sat} \exp\left(\frac{V_i^l (P - P_i^{sat})}{RT}\right) \tag{2.13}$$

Finally, at low operation pressures such as that in this study, gases are known to approach ideal gas behaviour and the vapour phase fugacity coefficient, fugacity coefficient of the pure species at saturation as well as the Poynting correction factor all tend to be equal to unity, resulting in the modified Raoult's law [54]:

$$y_i P = \gamma_i x_i P_i^{sat} \tag{2.14}$$

2.2.3 Activity coefficient models

The excess Gibbs energy (G^E) is a commonly used property and it can be proven that the activity coefficient for a particular species is related to the excess Gibbs energy using the following equations [46, 54]:

$$\frac{G^E}{RT} = \sum_i x_i ln\gamma_i \tag{2.15}$$

$$ln\gamma_i = \left[\frac{\partial (nG^E/RT)}{\partial n_i}\right]_{P,T,n_j} \tag{2.16}$$

Various thermodynamic models predict activity coefficients and model phase equilibrium data, with each model being unique in relation to the excess Gibbs energy [46, 54]. The models

mentioned here are Wilson, NRTL (Non-Random Two Liquid), UNIQUAC (Universal Quasi Chemical Theory) and UNIFAC (Universal Functional-group Activity Coefficient) [47, 53, 57]. All of which, except the latter, can be correlated in Aspen Plus® using experimental data [67].

Other models such as Margules and Van Laar are also available [51, 54]. One should note that since the excess Gibbs energy is used to describe deviations from ideal solutions, the excess Gibbs energy for a pure component is zero and the activity coefficient is equal to one [46, 54].

2.2.3.1 Wilson Model

The Wilson model, introduced by G. M. Wilson in 1964, is based on the notion that the interactions between molecules depend primarily on local concentrations, which are portions within a liquid mixture that are different in concentration to the overall mixture [15, 57]. This equation is especially suited for alcohol-hydrocarbon systems and has parameters that can be determined experimentally [51, 53, 54, 57]:

$$\frac{G^E}{RT} = -x_1 \ln(x_1 + x_2\Lambda_{12}) - x_2 \ln(x_2 + x_1\Lambda_{21}) \tag{2.17}$$

Therefore

$$ln\gamma_1 = -\ln(x_1 + x_2\Lambda_{12}) + x_2\left[\frac{\Lambda_{12}}{x_1 + x_2\Lambda_{12}} - \frac{\Lambda_{21}}{x_2 + x_1\Lambda_{21}}\right] \tag{2.18}$$

$$ln\gamma_2 = -\ln(x_2 + x_1\Lambda_{21}) - x_1\left[\frac{\Lambda_{12}}{x_1 + x_2\Lambda_{12}} - \frac{\Lambda_{21}}{x_2 + x_1\Lambda_{21}}\right] \tag{2.19}$$

Λ_{12} and Λ_{21} are given by [54, 57]:

$$\Lambda_{ij} = \frac{V_j}{V_i}\exp\left(\frac{-a_{ij}}{RT}\right) \tag{2.20}$$

Where V_i and V_j are the molar volumes of the pure liquids at a certain temperature and a_{ij} is an adjustable binary interaction parameter [54, 57]. Subscripts i and j identify species. The success of the Wilson equation lead to the development of other models local composition models [54].

2.2.3.2 Non-Random Two liquid (NRTL) Model

Renon and Prausnitz developed a temperature dependent activity coefficient model based on Wilson's local composition concept [53]. The NRTL model has parameters that compensate for the non-randomness of mixing in a two liquid mixture [46, 53, 54]. With proper selection of the non-randomness parameter (α), it could give the best fit for all types of mixtures [53].

$$\frac{G^E}{x_1 x_2 RT} = \frac{G_{21}\tau_{21}}{(x_1 + x_2 G_{21})} + \frac{G_{12}\tau_{12}}{(x_2 + x_1 G_{12})} \quad (2.21)$$

Therefore

$$ln\gamma_1 = x_2^2[\tau_{21}\left(\frac{G_{21}}{(x_1 + x_2 G_{21})}\right)^2 + \frac{G_{12}\tau_{12}}{(x_2 + x_1 G_{12})^2}] \quad (2.22)$$

$$ln\gamma_2 = x_1^2[\tau_{12}\left(\frac{G_{12}}{(x_2 + x_1 G_{12})}\right)^2 + \frac{G_{21}\tau_{21}}{(x_1 + x_2 G_{21})^2}] \quad (2.23)$$

Where

$$G_{12} = \exp(-\alpha\tau_{12}) \quad (2.24)$$

$$G_{21} = \exp(-\alpha\tau_{21}) \quad (2.25)$$

$$\tau_{12} = \frac{b_{12}}{RT} \quad (2.26)$$

$$\tau_{21} = \frac{b_{21}}{RT} \quad (2.27)$$

The parameters α, b_{12} and b_{21} are specific to the compounds per mixture and b_{12} and b_{21} are the binary interaction energy parameters. All three parameters can be determined using experimental data [54]. For the non-polar mixtures in this study however, an α value of 0.3 is recommended [53].

2.2.3.3 UNIQUAC and UNIFAC Models

The UNIQUAC (Universal Quasi Chemical Theory) equation and UNIFAC (Universal Functional-group Activity Coefficient) method are a bit more complex than the methods mentioned before [47, 54, 113].

The UNIQUAC equation assumes the excess Gibbs energy to consist of two parts, a combinatorial part (G^C) and a residual part (G^R) [47, 54]. The combinatorial part accounts molecular size and shape differences and the residual part accounts for intermolecular forces [47, 54]. The UNIQUAC equations are as follows [47, 54]:

$$G^C = \sum x_i \ln\left(\frac{\phi_i}{x_i}\right) + 5\sum q_i x_i \ln\left(\frac{\theta_i}{\phi_i}\right) \quad (2.28)$$

$$G^R = -\sum q_i x_i \ln\left(\sum_j \theta_j \tau_{ij}\right) \quad (2.29)$$

$$\frac{G^E}{RT} = G^C + G^R \quad (2.30)$$

Where

$$\phi_i = \frac{x_i r_i}{\sum_j x_j r_j} \tag{2.31}$$

$$\theta_i = \frac{x_i q_i}{\sum_j x_j q_j} \tag{2.32}$$

$$\tau_{ij} = \exp\left(\frac{-(u_{ji} - u_{ii})}{RT}\right) \tag{2.33}$$

The factors r_i and q_i represent a relative molecular volume and a relative molecular surface area respectively and are pure species parameters [47, 54]. The effect of temperature is taken into account using the intermediate factor, τ_{ij}. The parameters of the UNIQUAC equation are therefore values of $(u_{ji} - u_{ii})$ [47, 54]. The activity coefficient equations are split into two different parts and are as follows [47, 54]:

$$ln\gamma_i = ln\gamma_i^C + ln\gamma_i^R \tag{2.34}$$

$$ln\gamma_i^C = 1 - J_i + lnJ_i - 5q_i\left(1 - \frac{J_i}{Z_i} + ln\frac{J_i}{Z_i}\right) \tag{2.35}$$

$$ln\gamma_i^R = q_i\left(1 - lns_i - \sum_j \frac{\theta_j \tau_{ij}}{s_j}\right) \tag{2.36}$$

Where

$$J_i = \frac{r_i}{\sum_j r_j x_j} \tag{2.37}$$

$$Z_i = \frac{q_i}{\sum_j q_j x_j} \tag{2.38}$$

$$s_i = \sum_l \theta_l \tau_{li} \tag{2.39}$$

With *J* and *Z* being intermediate parameters. All summations are over all species [47, 54].

The UNIFAC method for estimation of activity coefficients depends on the concept that a liquid mixture may be considered a solution of the structural units from which the molecules are formed rather than a solution of the molecules themselves [54, 113]. Theses structural units are called subgroups and each subgroup has a relative volume (R_k) and surface area (Q_k) [54, 69]. The advantage of the UNIFAC method is that it is predictive as opposed to the correlative models previously mentioned [54].

The UNIFAC method is based on the UNIQUAC equation and the activity coefficients are given in Equation 2.34 [54]. Equation 2.35 remains the same with the quantities for J_i and Z_i given by the previous definitions. Equation 2.36, however, becomes [54, 113]:

$$ln\gamma_i^R = q_i\left(1 - \sum_k\left(\frac{\theta_k\beta_{ik}}{s_k} - e_{ki}ln\frac{\beta_{ik}}{s_k}\right)\right) \tag{2.40}$$

Where

$$r_i = \sum_k v_k^{(i)}R_k \tag{2.41}$$

$$q_i = \sum_k v_k^{(i)}Q_k \tag{2.42}$$

$$e_{ki} = \frac{v_k^{(i)}Q_k}{q_i} \tag{2.43}$$

$$\beta_{ik} = \sum_m e_{mi}\tau_{mk} \tag{2.44}$$

$$\theta_k = \frac{\sum_i x_i q_i e_{ki}}{\sum_j x_j q_j} \tag{2.45}$$

$$s_k = \sum_m \theta_m \tau_{mk} \tag{2.46}$$

$$\tau_{mk} = \exp\left(\frac{-a_{mk}}{T}\right) \tag{2.47}$$

Subscripts *k* and *m* identify subgroups [54, 113]. The quantity $v_k^{(i)}$ is the number of subgroups of a certain type in a molecule of species i [54, 113]. The subgroup parameters R_k and Q_k and the group interaction parameters a_{mk} can be found in literature for the different types of subgroups [54, 69].

2.2.4 Partition coefficients and relative volatility

For systems and mixtures comprising of more than two components, conventional correlation of data in terms of phase compositions can be quite challenging. For such systems, data is presented in the form of partition coefficients (K_i) and relative volatility, defined by [96]:

$$K_i = \frac{y_i}{x_i} = \frac{\gamma_i P_i^{sat}}{P} \tag{2.48}$$

$$\alpha_{ij} = \frac{K_i}{K_j} \tag{2.49}$$

Where α_{ij} is the relative volatility between components in the mixture, which is a measure of the relative ease or difficulty of separating the two components [96]. Additionally, *K*-values can be used to determine the accuracy of regressed parameters for the thermodynamic models mentioned previously.

2.2.5 Thermodynamic consistency

Thermodynamic consistency tests bring credibility to a study by building confidence in and ensuring reliability of experimental data obtained and are thus necessary. They also help with the understanding of physical phenomena behind the generation of the data [61].

Thermodynamic consistency tests are based on the Gibbs/Duhem equation. Conformance to this equation denotes thermodynamic consistency at isothermal and isobaric conditions [54, 61]:

$$x_1 \frac{dln\gamma_1}{dx_1} + x_2 \frac{dln\gamma_2}{dx_1} = 0 \tag{2.50}$$

In general, there are two broad classes of thermodynamic consistency tests, namely the area test and the point-to-point consistency test [61]. While the point-to-point test aims to identify inconsistent data as they appear, the area test aims to minimise the total deviation of all points from the Gibbs-Duhem equation [61].

In this sub-section, the L/W and McDermott-Ellis methods for determining thermodynamic consistency are discussed. The L/W method incorporates the area test and the McDermott-Ellis method incorporates the point-to-point test. These methods are also commonly used in testing thermodynamic consistency for low-pressure, isobaric VLE data [61, 65, 66, 72].

Thermodynamic consistency tests alone however, are not sufficient in proving that data obtained is accurate. In order to help build sufficient confidence in data, one should verify their experimental setup as well by repeating experiments that are already available in literature, i.e. experiments that can serve as references.

2.2.5.1 The L/W method

The L/W method was developed by Wisniak and is used to evaluate isobaric systems [65]. It is based on the relationship between the excess Gibbs energy and its equilibrium boiling temperature for a mixture [65]. This method is therefore not a direct derivative of the Gibbs/Duhem equation and the consistency tests done using this method need to be considered together with tests using other methods such as the McDermott-Ellis method [61, 65, 72].

Wisniak used the following assumptions to determine the L/W method [65]:

- All non-idealities of the fluid are concentrated in the liquid phase
- Heats of vaporisation of each component are either constant or an average value for the range of boiling temperatures used
- Liquid molar volume is negligible compared with that of the vapour

Through integration and manipulation of thermodynamic equations, the above assumptions lead to the definition of the following terms [65]:

$$L = \int_0^1 \left(\sum_k \frac{T_{bi} x_i \Delta S_i^*}{\Delta S} - T_{bub}\right) dx_1 = \int_0^1 \left(\frac{G^E}{\Delta S} - \frac{RTf}{\Delta S}\right) dx_1 = W \tag{2.51}$$

$$f = \sum_i x_i \ln\left(\frac{y_i}{x_i}\right) \tag{2.52}$$

$$\Delta S = \sum_i x_i \, \Delta S_i^* \tag{2.53}$$

Where ΔS_i^* is the entropy of vaporisation of component i and T_{bub} is the bubble temperature of the mixture [65]. The equality of L and W is derived through equilibrium expressions and is thus a test for thermodynamic consistency [65].

However, real experimental data has some degree of error, making the constraint of equality between L and W limiting as the error could be on either side (L or W). Thus, Wisniak defined a deviation [65]:

$$D = 100 \frac{|L-W|}{L+W} \tag{2.54}$$

Wisniak proposed a maximum value for D of 3 to 5, with the lower limit based on the Herington area test and the higher limit based on the uncertainty involved when estimating heats of vaporisation for components [61, 65, 66].

PRO-VLE 2.0 software was used to test the data according to the L/W method, although the software does offer consistency test capabilities for other methods [61, 65, 112]. The method requires inputs such as the actual data to be tested, Antoine constants, the critical properties, acentric factors (ω), liquid molar volumes (V^L), dipole moments (μ) and enthalpies of vaporisation (ΔH_v) and boiling points (at operation pressures) of the compounds involved [65]. It then calculates the ratio L/W and one can immediately determine if the data is thermodynamically consistent or not depending on how close the values are to unity [61, 65].

Table 2.4 presents the parameters required to conduct the L/W consistency test [95]. The parameters are from the Design Institute for Physical Properties (DIPPR) database, which is a

highly reliable source of thermophysical and environmental property data [95]. Parameters from other databases as well as from group contribution methods can be found in literature as well [29, 30, 31, 58, 59].

Table 2.4: Critical properties, acentric factors, liquid molar volumes, enthalpies of vaporisation and dipole moments for the compounds of concern in this study, obtained from DIPPR [95]

Parameter	α-Pinene	Limonene	*p*-Cymene	Butylbenzene	Indane	1,2,3-Trimethylbenzene
T_b @ 40 kPa (K)	395.65	415.7	415.63	422.06	416.48	415.48
T_c (K)	644	653	652	660.5	684.9	664.5
P_c (MPa)	2.76	2.82	2.8	2.89	3.95	3.45
V_c (cm^3/mol)	454	470	497	497	396	414
ω	0.221	0.381	0.374	0.394	0.309	0.367
V^L (cm^3/mol)	159	162.2	157.5	156.6	123.1	134.9
ΔH_v (kJ/mol)	39307.6	40777.6	41799.4	42654.6	41853.4	42222
μ (D)	0.36	0.639	0	0.369	0.54	0.561

2.2.5.2 The McDermott-Ellis method

Using the Gibbs/Duhem equation as a starting point, the McDermott-Ellis consistency test is derived by integrating Equation 2.50 over all considered data points using the trapezoidal rule [72]:

$$0 = \sum_{i=1}^{N}(x_{ia} + x_{ib})(ln\gamma_{ib} - ln\gamma_{ia}) \tag{2.55}$$

With the summation being over all components for every two consecutive experimental points, taken in pairs of *a* and *b* [72]. The test was chosen to be applied on a point to point basis, considering each pair of consecutive data independently [72, 73].

In an ideal case, perfect data would strictly adhere to Equation 2.55, however, experimental data is known to have some inherent error [72]. The authors therefore suggested that the criteria used to distinguish between consistent and inconsistent data was dependent upon the accuracy with which the vapour and liquid fractions were reported, giving an example of a maximum deviation in Equation 2.55 of 0.01 for accuracies in composition of +/- 0.001 mole fraction [61, 72].

It was initially stated that a maximum deviation be allowed relating to the cube of the difference of mole fraction in the liquid phase at the two points [72]. The maximum deviation (D_{max}) was later refined to be a function of the accuracies of the considered parameters [74]:

$$D_{max} = \sum_{i=1}^{N}(x_{ia} + x_{ib})\left(\frac{1}{x_{ia}} + \frac{1}{y_{ia}} + \frac{1}{x_{ib}} + \frac{1}{y_{ib}}\right)\Delta x + 2\sum_{i=1}^{N}|ln\gamma_{ib} - ln\gamma_{ia}|\,\Delta x + \sum_{i=1}^{N}(x_{ia} + x_{ib})\frac{\Delta P}{P} + \sum_{i=1}^{N}(x_{ia} + x_{ib})\,\varepsilon_i\left(\frac{1}{|T_a + \lambda_i|^2} + \frac{1}{|T_b + \lambda_i|^2}\right)\Delta T \qquad (2.56)$$

Where the Δ terms are the accuracies of the experimental mole fractions, pressure and temperatures. The ε_i and λ_i are the B_i and C_i Antoine constants respectively [72]. The value for D can be calculated using Equation 2.55, which should be less than that of D_{max}.

2.2.6 Antoine constants and vapour pressure

The Antoine constants for the compounds of concern in this study were obtained from Yaws' Handbook of Antoine Coefficients for Vapor Pressure [75]. These values were comparable to those calculated using the DIPPR source [95] Table 2.5 shows the values that were obtained, with the pressure and temperature being in mm Hg and K respectively [75].

Using the Antoine constants, a theoretical vapour pressure graph was generated as shown in Figure 2.9 for the all the compounds of concern in this study [75]. As can be seen in Figure 2.9, the plots are all very close to each other for the whole pressure range, indicating possible azeotropic behaviour [71, 96].

An interesting point to note in this section is the Bancroft point, which indicates the possibility of azeotropic behaviour for a system at a point (or points) where vapour pressures of two compounds cross each other [96]. From Figure 2.9, it can be seen that the vapour pressure curves of limonene, indane, *p*-cymene and 1,2,3-trimethylbenzene almost overlap each other between 10 kPa and 100 kPa. Taking this into account, it can be expected that the systems planned in this study would contain azeotropes, except those including butylbenzene as it's vapour pressure curve is away from the rest. The approximate Bancroft points for the systems limonene/*p*-cymene, limonene/indane and limonene/1,2,3-trimethylbenzene are shown in Table 2.6, calculated using linear interpolation [75].

In an effort to reduce thermal degradation during experiments in this study, using Figure 2.9 and previous research, an operational pressure of 40 kPa was chosen [68, 106]. The boiling points of the concerned compounds also imply better separation at this pressure than at atmospheric pressure, as can be seen in Figure 2.9. From Figure 2.9, it is clear that lower pressures would

be better in avoiding azeotropic behaviour and thermal degradation, however, the constructed still was seen as stable at pressures above 30 – 35 kPa.

Table 2.5: Antoine constants for the compounds of concern in this study with applicable temperature ranges (P: mmHg; T: K) [75]

Compound	A	B	C	T_{min} (K)	T_{max} (K)
Limonene	7.30194	1831.70	236.306	198.65	660.00
p-Cymene	7.13238	1671.47	216.013	205.25	653.15
Indane	7.19185	1723.24	221.757	221.74	684.90
Butylbenzene	7.18472	1720.37	216.413	185.30	660.55
1,2,3-Trimethylbenzene	7.29803	1789.65	229.034	247.79	664.53

Table 2.6: Approximate Bancroft points for the systems limonene/*p*-cymene, limonene/indane and limonene/1,2,3-trimethylbenzene [75]

System	*P* (kPa)	*T* (K)
Limonene/*p*-cymene	26.0	402.2
Limonene/indane	94.4	448.0
Limonene/1,2,3-trimethylbenzene	6.5	363.3

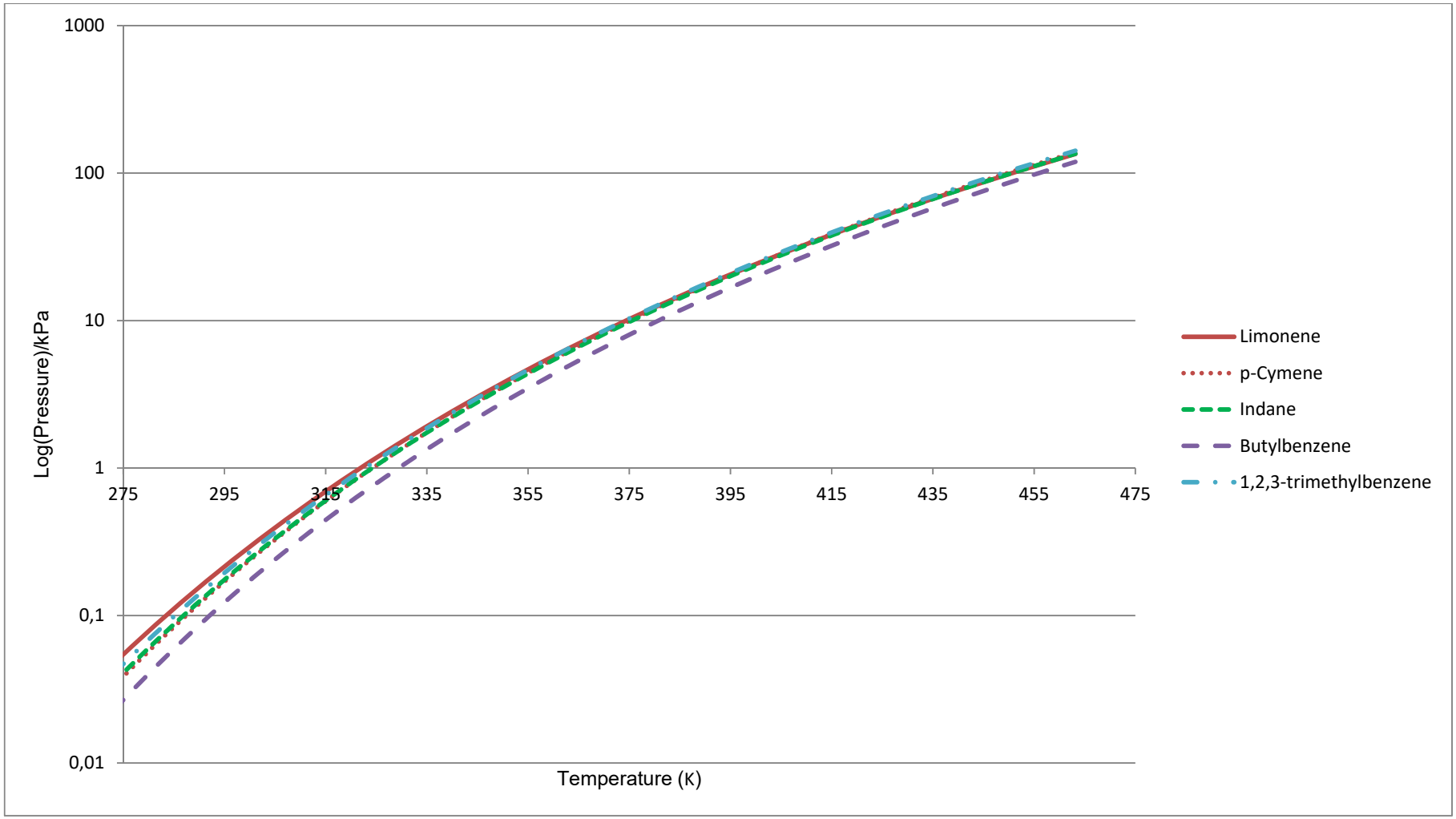

Figure 2.9: Theoretical vapour pressure data for compounds in this study [75]

2.3 Measurement of phase equilibria

This section focuses on the different types of equipment used to determine vapour-liquid equilibrium (VLE) data in the past and present.

As will be seen in this section, the materials of construction for all apparatus used are metals, polymers (such as Teflon) and most importantly, borosilicate glass, as it has very favourable chemical and physical properties for use in laboratory environments [89].

Through history, a number of developments have been made regarding the experimental determination of VLE data on a lab scale [41]. The most common form of apparatus used to determine low pressure isobaric VLE data are recirculation stills due to their convenience [41].

Additionally, static methods are also able to determine VLE. This type of still was not however considered since the recirculation still is a more versatile for the intended operation and can be adapted, if needed, to obtain VLLE data in addition to VLE data, which the static synthetic setup cannot. The static synthetic method also requires a degassing step involving temperature and pressure changes which could easily increase the effects of compound degradation.

2.3.1 Recirculation stills

Recirculation stills allow for quick and fairly accurate measurement of VLE data [27]. They are based on the continuous separation of vapour evolved from boiling of the liquid phase and recirculation of the vapour phase back into the system [27]. As this process progresses, equilibrium is reached between the vapour and liquid phases inside the still at a specific pressure and temperature. In order to function accurately and in a user-friendly manner, a recirculation still's design must encompass the following aspects [27, 40]:

- Simple design
- Small samples of vapour and liquid attainable
- Accurate temperature and pressure measurements
- Quick attainment of equilibrium if disturbances are made to the system (sample taking)
- Prevention of vapour condensation onto a temperature sensor, as this leads to incorrect readings
- Steady flow of the recirculated vapour
- Accumulation of chemicals in the system should be prevented
- Sampling and feeding should not cause a big disturbance in boiling of the liquid phase.
- Entrainment of liquid particles into the vapour phase should be prevented

- Recirculated vapour and the liquid phase should be well mixed to maintain uniform composition

Pioneers of the recirculation still noted that measuring the temperature of the boiling liquid is not a true indication of the equilibrium temperature [36]. Placement of the temperature sensor in the vapour phase is not ideal either as this can be inhibited by the condensation of the vapour phase onto the probe [27]. The temperature sensor should therefore be placed in a position where condensation of the vapour onto it will not take place [27].

In industry there are two types of recirculation stills, those that recirculate only the vapour phase and those that recirculate both the liquid and the vapour phase [41]. The latter is the preferred method since this helps with maintaining consistency during the mixing of the two phases during recirculation [36, 40, 41]. It also allows for convenient sampling of the liquid phase.

Therefore, a discussion of only vapour and liquid recirculation stills follows. Prior to that however, the development of recirculation stills through their use of the ebulliometer is discussed.

2.3.2 The Ebulliometer and its use in the development of the recirculation still

An ebulliometer is an apparatus used to accurately measure the boiling temperature of a substance and is used as the basis for development of the modern day recirculation still [27].

The Cottrell ebulliometer introduced by Cottrell in 1919 (Figure 2.10) was basically an ebulliometer with a tube placed in the boiling liquid to lift up the boiling liquid, which would flow back down onto a thermometer after being condensed [33]. The tube entrained liquid together with a vapour phase and became known as a pump because of the way the liquid travelled up the tube, together with its vapour phase, with such ease [33].

This design was later modified for the liquid coming out of the tube to be splashed onto a thermometer [43]. That way the thermometer would be in immediate contact with the liquid and vapour phase [43]. The modified design also includes features that prevent the condensed vapours from coming into contact with the thermometer as well as a sampling point for the boiling liquid phase [43].

Another designer, Swietoslawski also incorporated the Cottrell pump in his ebulliometer in 1929 [36]. One of his designs included a Cottrell pump used to pump the boiling liquid and vapour phase onto the temperature sensor in a similar way to the Cottrell ebulliometer [36].

Although Swietoslawski's design did not however have any sampling points, it does highlight the modern day equilibrium still in terms of the way the vapour condensate returns to the boiling chamber as shown in Figure 2.11 [36].

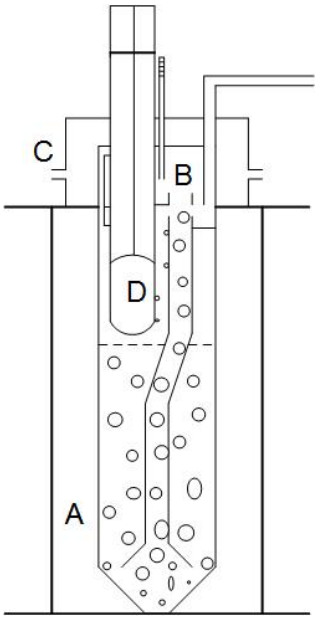

Figure 2.10: Cottrell ebulliometer [33]. A – Boiling chamber; B – Cottrell pump; C – Condenser; D – Thermometer. Figure obtained with permission and redrawn using Microsoft Visio® [27].

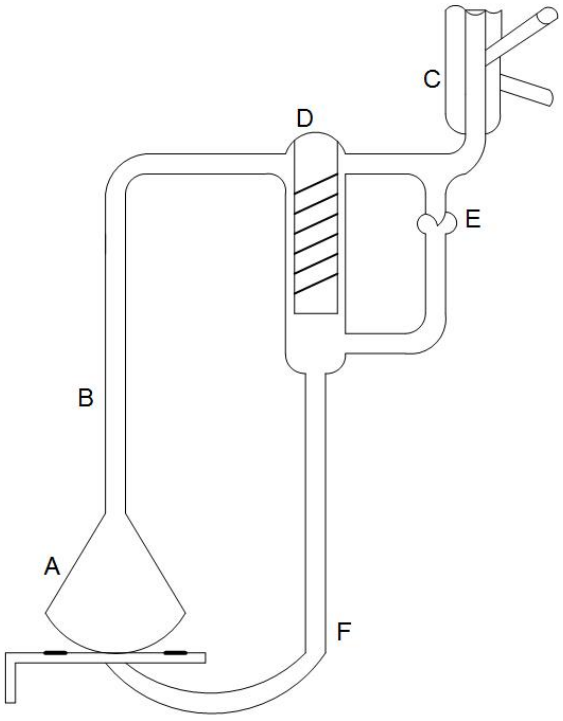

Figure 2.11: Swietoslawski ebulliometer [36]. A – Boiling chamber; B – Cottrell pump; C – Condenser; D – Temperature sensor; E – Drop counter; F – Vapour condensate return. Figure obtained with permission and redrawn using Microsoft Visio® [27].

Swietoslawski's ebulliometer also included a useful "drop counter" feature that allowed one to relate boiling intensity to the rate at which drops (vapour condensate) are formed [36].

2.3.3 Different types of vapour and liquid recirculation stills

In the early stages of the recirculation equilibrium still's development, samples would be taken by interrupting the boiling process (for vapour samples) or by taking samples out of the boiling chamber (for liquid samples) and this could lead to inaccurate samples [26, 27, 37, 38, 40].

In 1946, Gillespie proposed an equilibrium still that was able to retrieve vapour phase equilibrium samples without interrupting the boiling process using the still shown in Figure 2.12 [35]. The liquid phase, however, was still taken in the boiling chamber [35].

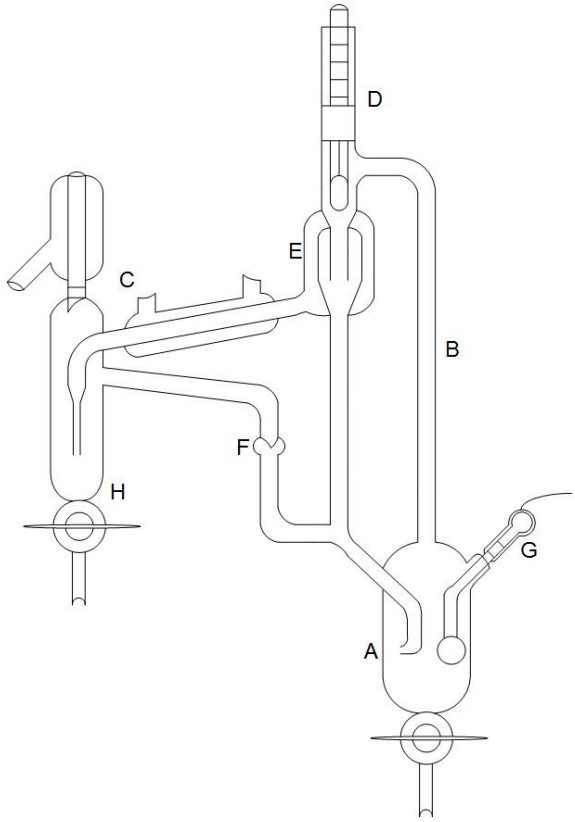

Figure 2.12: Gillespie equilibrium still [35]. A – Boiling chamber; B – Cottrell tube; C – Condenser; D – Thermometer; E – Vapour disengagement chamber; F – Drop counter; G – Internal heater; H – Vapour sample well. Figure obtained with permission and redrawn using Microsoft Visio® [27].

The Gillespie still had some unique features such as an internal heater which was a heated platinum wire immersed in the boiling chamber [35]. With reference to Figure 2.12, the feed would be boiled in the boiling chamber and rise as a boiling liquid entraining vapour bubbles, splashing onto the thermometer [35]. The liquid would then flow back into the boiling chamber while the vapour would pass through the disengagement chamber and condense on its way to the vapour sample well [35]. The overflow of the well would flow back into the boiling as a recirculate [35].

Liquid samples as taken in the Gillespie still are not indicative of the equilibrium liquid's composition since equilibrium is actually reached inside the Cottrell tubing, the liquid sample should therefore be taken after coming out of the Cottrell pump/tube [41]. This raised concern and modifications were made to the liquid sampling method by adding a liquid sampling well before the equilibrium liquid phase made its way back to the boiling chamber [32, 38].

Although the Cottrell pump is where equilibrium is achieved, caution must be taken in ones design to ensure that the tube is not too short [41]. For better performance of the Cottrell pump/tube, one could implement a spiral design to increase the tube length, ensuring the achievement of equilibrium [41]. Research has showed that through the use of a spiralled Cottrell tube, an increase in interfacial areas and contact times and therefore improved mass transfer may be achieved [41]. Nevertheless, the achievement of equilibrium can be verified by the temperature stabilisation, the design modification of a spiral Cottrell pump simply ensures the achievement of equilibrium [35]. The Cottrell tube can also be inclined for increased length [39, 44].

Other modifications to improve the achievement of equilibrium include:

- Jacketing the equilibrium chamber surrounding the Cottrell pump, minimising heat loss [40, 41, 45]
- Stirring of the recirculating liquid and vapour phases as this ensures uniform composition and better mixing of the two phases, it also prevents flashing [34]
- Usage of a packed equilibrium chamber or Cottrell tube [42].

One design that incorporates some of these modifications is the Malanowski Low Pressure VLE still [40]. It is based on the Swietoslawski ebulliometer and is shown in Figure 2.13 [40]. The boiling chamber is manufactured with sintered glass as this promotes bubble formation and the Cottrell tube then pumps a vapour liquid mixture into the equilibrium chamber to splash onto the temperature sensor [40].

The equilibrium liquid phase then passes through a sample point and into the mixing chamber [40]. The equilibrium vapour phase passes through a condenser, drop counter and sample point and finally mixes with the recirculated liquid phase in the mixing chamber [40].

The vapour phase is jacketed before it reaches the condenser in order to prevent condensation of the vapour phase as this would flow back into the equilibrium chamber [40].

Condensation of the vapour phase can be prevented by building the equilibrium chamber at a higher height than the condensers, which will also result in a longer Cottrell tube [40]. The Malanowski still shown however does not incorporate a spiral Cottrell tube [40].

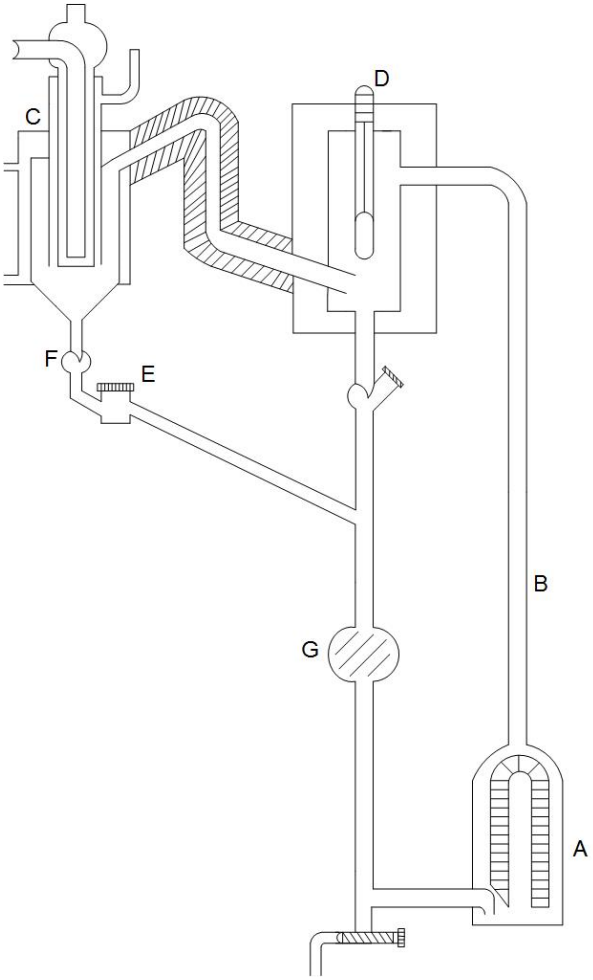

Figure 2.13: Malanowski Low Pressure VLE Still [40]. A – Boiling chamber, B – Cottrell tube; C – Condenser; D – Temperature sensor and jacketed equilibrium chamber; E – Vapour sample chamber; F – Drop counter; G – Mixing chamber. Figure obtained with permission and redrawn using Microsoft Visio® [27].

So far, the equilibrium stills that have been discussed are the ones that have led to the development of the modern day VLE still. The last type of VLE still discussed, developed by Stage and Fischer, is one of the most commonly used apparatus for experimental equilibrium data measurements and is an example of the modern day VLE still [28].

A design of the VLE still by Stage and Fischer, based on the original Gillespie equilibrium still, is shown in Figure 2.14 [28, 35]. A similar type of VLE still was also designed by Schuberth and was named the G15 [91]. This VLE still design eliminated all the sources of error that were pointed out by researchers over the years, which is why it became so widely used thereafter [91].

The process starts with the feed being boiled in the boiling chamber and then liquid being pumped up the spiral Cottrell tube by vapour bubbles while reaching equilibrium and finally splashing onto the thermometer [27, 89]. The Cottrell tube is housed in what will be referred to as a Gillespie chamber for the purposes of this study and is vacuum-insulated. The liquid phase is drained from the equilibrium chamber and passes through a well from which the overflow goes back to the mixing chamber. The vapour phase passes through the higher end of the equilibrium chamber into a primary condenser and then through a secondary condenser as well, to ensure that all vapour is condensed [27, 89]. The vapour condensate also passes through a well, where the over-flow is sent back to the mixing chamber. The contents of the mixing chamber then pass through to the boiling chamber forming a recycle process [27, 89]. The liquid and vapour condensate wells are used to capture samples for the respective phases [27, 89].

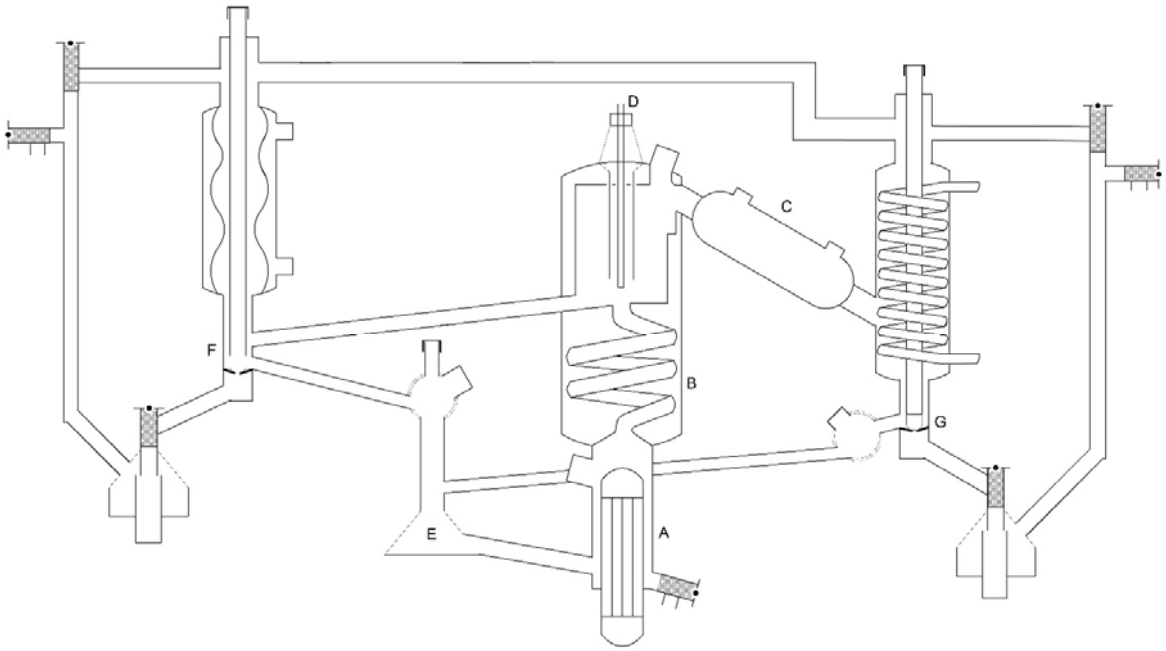

Figure 2.14: Stage and Fischer VLE still [28]. A – Boiling chamber; B – Spiral Cottrell tube; C – Condenser; D – Thermometer; E – Magnetically stirred mixing chamber; F – Liquid phase sample point; G – Condensed vapour phase sample point. Figure obtained with permission and redrawn using Microsoft Visio® [27].

Furthermore, the design by Stage and Fischer eliminates the following sources of error that were present in previous designs of the equilibrium still [28, 89]:

1. Concentration gradients in the heating chamber or boiling flask
2. Partial condensation above the heating chamber
3. Entrainment of droplets by the vapour

4. Total evaporation of feed liquid
5. Withdrawal of large samples so as to upset equilibrium
6. Sample contamination

Another type of VLE still, the Low Pressure VLE still of Raal and Muhlbauer is a modern day alternative available in industry and makes use of a packed equilibrium chamber [41].

The last two equilibrium stills mentioned are both excellent designs and have culminated the work of many researchers over time. Therefore, the experimental work required in this study employs a modified version of the still pioneered by researchers Stage and Fischer as well as Schuberth *et al.* [28, 89, 91]. This type of still with its use of a Cottrell tube has also been proven to be suitable for systems with relatively high volatilities (normal BP > 373 K) and requires only around 100 mL of feed at a time, making the research cost effective [89].

From this section it is clear that, although not a simple task, the determination of experimental VLE data has been commonly practised by many professionals around the world and the equipment for such experiments is readily available either commercially or through public literature for manufacturing and modification purposes. The following chapter therefore discusses the details of the construction aspect regarding the experimental VLE still used in this study.

3. Design and verification of equipment

This chapter looks at the core requirements and specification the VLE still, major components vital to the setup's functioning and the design philosophy behind it's construction. The chapter also discusses the experimental method followed, setup commissioning and verification procedure.

3.1 Setup requirements and specifications

The main requirements of the constructed setup in this study were to:

- Obtain vapour-liquid equilibrium within a reasonable time. This can be done by ensuring sufficient power is delivered to the system quickly and efficiently. This would also require sufficient circulation and re-boiling of both vapour and liquid fractions.
- Maintain vapour-liquid equilibrium by ensuring stable temperatures and pressures. This can be done by ensuring low pressure drops across process equipment as well as eliminating fluctuations in energy input to the system.
- Have the ability to take samples during recirculation of vapour and liquid fractions without disturbing equilibrium. The VLE still of Stage and Fischer allows for samples to be taken without disturbing equilibrium [28].
- Accurate temperature and pressure measurement. This would require temperature and pressure instruments with high accuracies to ensure that small changes in temperature and pressure can be picked up, especially since the compounds of concern in this study have very close vapour pressures.

The rest of this sub-section introduces the design and discusses the specifications of the core of the constructed setup, the Cottrell tube, as well as the housing around it, labelled as the Gillespie chamber for the purpose of this study.

3.1.1 Cottrell tube

The Cottrell tube was first developed by Frederick Cottrell in 1919 and is a simple tube, which allows vapour bubbles to entrain liquid during boiling [33]. The tube therefore acts as a pump and ensures that both liquid and vapour phases are firstly in intimate contact during boiling and secondly in contact with a temperature sensing element [61, 71, 100]. The basis of this study, vapour-liquid equilibrium, is achieved at the vapour-liquid phase boundary as bubbles produced

pump liquid through the Cottrell tube. The tube is thus crucial to the proper functioning of the setup and therefore this study by extension.

From a design perspective, a smooth spiralled Cottrell tube was chosen for ideal mass transfer as well to ensure a negligible pressure drop across the tube [41, 89, 92, 94]. The Stage and Fischer VLE still as well as commercial VLE stills employ spiralled Cottrell tubes as well [28]. A vacuum jacket for insulation of the tube was also employed, which forms part of the Gillespie chamber [93]. In terms of the dimensions, the specification of the Cottrell tube used was based on what was available in literature, upon which the rest of the still was based [27, 89].

It was found that the G15 equilibrium apparatus by Schubert employed a Cotrrell tube with an inner diameter of 4 mm and a heating chamber with an inner diameter of 15 mm [89, 91]. The heating chamber is connected directly to the Cottrell tube and is where the bubbling of the feed takes place.

Practise has shown that if the Cottrell tube diameter is too small relative to the heating chamber diameter, only liquid will be pumped through the Cottrell tube and if it is too big, vapour would only pass through the tube. The initial design estimate for the inner diameter of the Cottrell tube was chosen to be 8 mm – keeping the tube/heating chamber ratio similar to that in literature as an initial estimate [89]. A larger diameter for the Cottrell tube found in literature for laboratory studies was 11 mm (OD) for the packed equilibrium chamber by Yerazunis in 1964, the heating chamber diameter for his setup is unknown [41].

3.1.2 Gillespie chamber

The Gillespie chamber is one of the most important and delicate sections of the setup in this study as it houses the Cottrell tube. Figure 3.1 shows a specific design for it. The specifications for this chamber can be found in Appendix D as well, together with the detailed specification of the rest of the still.

As can be seen in Figure 3.1 the Cottrell tube extends from the heating chamber (A) into the Gillespie chamber. It then winds up until half the height of the vessel and opens onto the temperature probe, this allows for the determination of the vapour temperature as the vapour-liquid mixture is pumped out of the Cottrell tube [89]. The length of the tube is approximately 45 cm – 50 cm in length (3 coils of tube in a 10 cm diameter coil) with an inner diameter of approximately 8 mm and an outer diameter of approximately 12 mm.

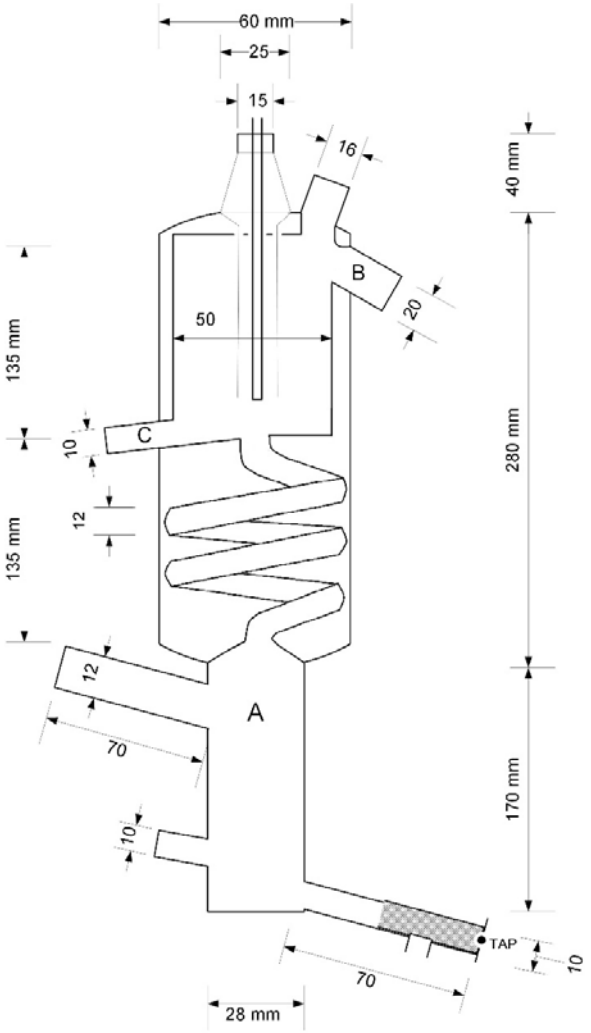

Figure 3.1: Gillespie chamber specifications

The Gillespie chamber is vacuum sealed and insulated, mainly to prevent heat loss. The top part of the Gillespie chamber has an outlet through which the vapour can pass (B) into the primary condenser [89]. The liquid exit (C) allows for the recirculation of the liquid fraction back to the mixing chamber [89].

3.2 Design philosophy

This section looks at an overview of the construction aspects and the major decisions taken in constructing the VLE still. A detailed specification of the constructed equilibrium still is available in Appendix D.

As a summary, the major pieces of equipment used are listed in Table 3.1, together with a brief description and the manufacturer/supplier.

Table 3.1: Major components of constructed VLE still [52, 55, 56, 90, 107, 114]

Component	Description	Manufacturer/supplier
Glass structure	Borosilicate	Glasschem South Africa
Cartridge heater	600W	Glasschem South Africa
Pressure transmitter	4 – 20 mA; absolute pressure	Yokogawa Pty Ltd
Temperature sensors	1/10th DIN 4-wire Pt-100	Wika South Africa
Proportional valve	PD controlled; gear motor	Glasschem South Africa
Electrical wiring & interface	-	Glasschem South Africa
Insulation and heating jacket	70cmØ x 17.5cm – 24Vac; 36W	Eltherm South Africa
Magnetic stirrer	230 Vac Cimarec Telemodul	Separation Scientific
Vacuum pump	0.25 kW; 220V; 5m^3/hr Speedivac	Vacuum SA
Fume hood housing	1m x 1.1m Stainless steel	Stellenbosch University

3.2.1 Materials of construction

As seen in literature and practise, borosilicate glass is a very common material of construction in laboratory equipment [89]. Advantages such as being able to visualise a process (transparency), adiabatically promote a process through the use of vacuum jackets up to temperatures of 393 K, resistance to corrosion and being easy to clean all form part of the advantages when using glass as a material of construction in the laboratory [89]. Most importantly though, glass also has the valuable property of being unreactive and inert [89].

The material of construction, therefore, in this study was borosilicate glass. The taps selected are made of Teflon due to its high temperature resistance and harsh chemical resistance properties [96, 97].

During operation, the still has sections through which the material passing is at temperatures that are above 373 K, these are known as hot sections. All hot sections of the still are able to operate up to temperatures of 520 K. Butylbenzene has the highest normal boiling point among all the compounds that were going to be tested for this study, 456 K, so 520 K as a limit was deemed sufficient. Figure 3.2 highlights the hot sections of the equilibrium still.

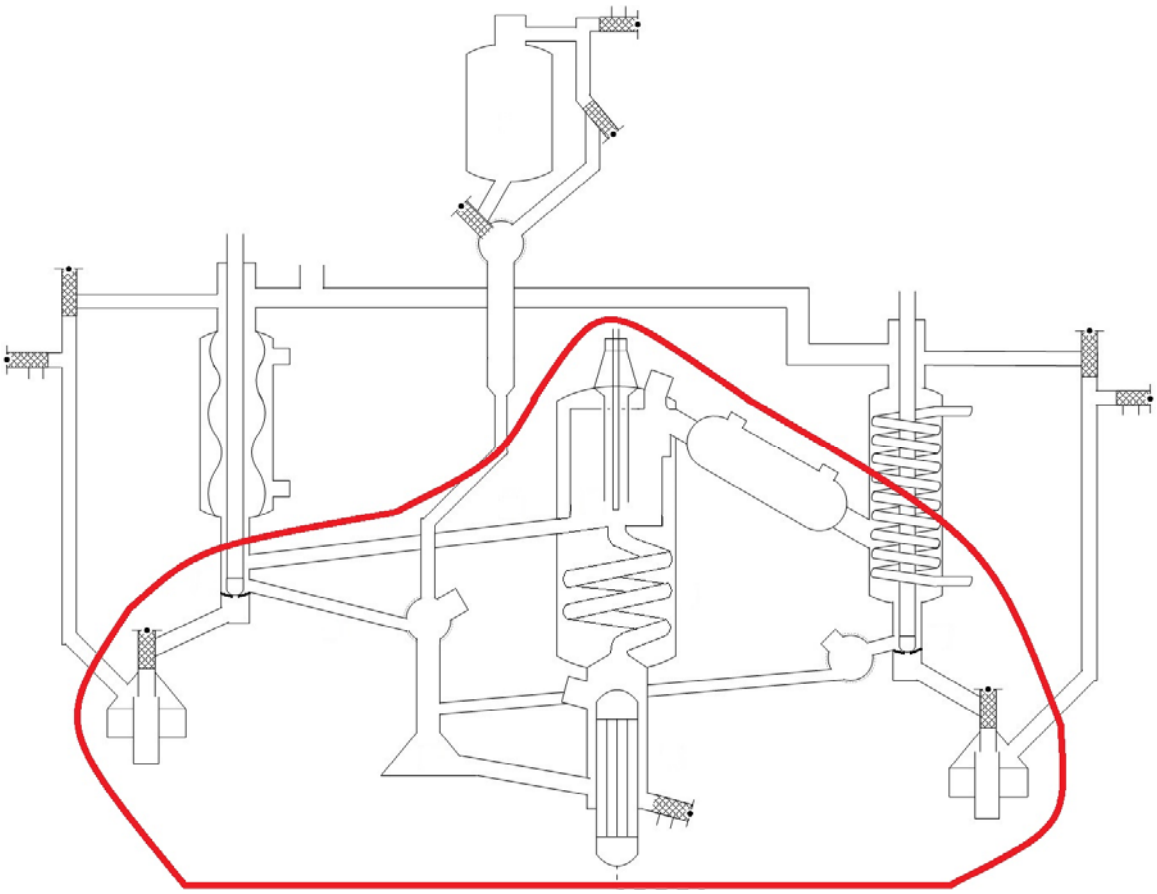

Figure 3.2: Highlighted area of the still indicating hot sections

3.2.2 Boiling and insulation

A continuous, steady supply of energy, in the form of heat, is required to start and maintain the boiling process during experiments [89]. As in every process however, heat losses occur and need to be accounted for [89].

3.2.2.1 Heating

Heating of feed can be done either directly, by gas or electricity, or indirectly using a heat carrier, the former being more applicable to this study as it is based in a laboratory [89]. Accurate temperature control can be achieved with direct electrical heating and can be applied in the various forms [89, 96]:

1. Open heating
2. Shaped heaters
3. Infrared heaters

4. Immersion heaters

Open heating elements such as hot plates are common and can provide sensitive control [89]. Shaped heaters have resistance wires conforming to the shapes of the surfaces to be heated such as that of a round-bottom flask [89]. Infrared heaters have more uniform heating than the others and are suitable for the power range of 250 Watt and 1000 Watt respectively [89].

Immersion heaters provide sensitive control, efficient heat transfer and require the presence of heating wells such as a typical cartridge heater available in the heating chamber of the VLE still of Stage and Fischer [89].

In the experimental setup for this study, a cartridge immersion heater was seen to be the most suitable for the energy supply as it was the most likely to conform to the dimensions of the planned setup [61].

In order to determine the required heater's capacity, the compounds' heat capacities and enthalpies of vaporisation were used to determine the amount of heat required to boil each compound, in atmospheric conditions and based on the temperature range of 293 K to the respective normal boiling points (NBP) [59]. After calculations, it was noted that ~30 W of power would be required to boil ~100 mL of either compound within 30 minutes.

A cartridge heater with a maximum power output of 600 W was obtained from Glasschem as this was the lowest power rating available from the supplier [90]. It uses an AC input, of which the output is controlled via pulse skip modulation (PSM) [88, 90].

Although it is clear that the heater has been over-specified, an advantage is that the heater can be used in future projects which might have higher heat requirements. An additional advantage is that equilibrium can be quickly obtained with such heater as the heat can be raised much higher than required to bring the feed to a quick boil. In practise it was noted that the time taken to reach equilibrium could be reduced by at least 10 minutes if the initial power was specified to be ~100 W and reducing it back to ~15 W (experimentally observed plateau region) once the liquid started to boil. This practise however, was not adopted in this study due to the effects of compound degradation most likely increasing with such a practise.

3.2.2.2 Bubble nucleation

The purpose of the cartridge heater is to provide the energy input to the system in the form of heat. With this in mind, energy should be transferred as efficiently as possible in order to prevent superheating from taking place.

The bubbles formed during heating of the liquid are responsible for the heat and mass transfer that takes place between the liquid and vapour phases [51]. These exchanges take place at the interface of the two phases, therefore, the greater the surface area available, the better the heat and mass transfer [51, 101]. The total phase boundary surface area can therefore be increased by increasing the number of bubbles that nucleate on the surface of the cartridge heater [51].

Proper bubble nucleation is thus vital in reaching equilibrium [96]. It also ensures the proper functioning of the Cottrell tube in pumping the liquid phase up the tube in a regulated fashion [102, 111]. Furthermore, it helps prevent superheating of the liquid phase, which could lead to incorrect temperature measurements or even a safety hazard.

Bubble nucleation during boiling usually takes place in gas pockets or surface cracks – this process is shown in Figure 3.3 [51]. Bubble nucleation also obviously depends on the surface tension and viscosity of the medium being heated – which in turn depend on the temperature and pressure [59, 96]. Surface-level gas pockets can also fill up with liquid as the process is repeated. Bubble nucleation sites further prevent superheating by allowing initial amounts of heat being directed to the formation of vapour instead of even heat distribution without any form of agitation.

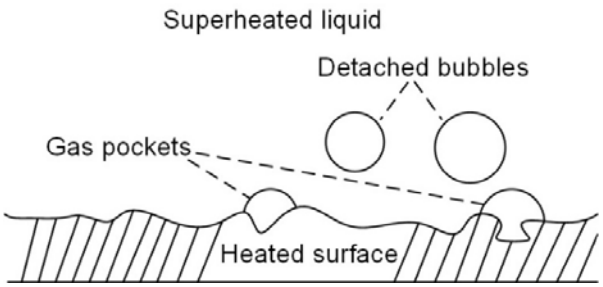

Figure 3.3: Bubble nucleation on a heated surface [51]

In an effort to optimise the boiling originating from the selected cartridge heater, various methods to increase and improve bubble nucleation taking place on the cartridge heaters' stainless steel (SS) sheath's surface were tested.

After various attempts (including sandblasting, etching and general machining), the crude approaches of physically drilling 1 mm cavities and grinding rough edges onto the SS cartridge heater sheath resulted in a surface which frequently produces well-rounded bubbles, ideal for pumping liquid through the Cottrell tube. As expected, the methods employed had an additional benefit in that they prevented the feed from superheating during boiling.

3.2.2.3 Insulation and heat loss prevention

The Gillespie chamber of the constructed VLE setup, which experiences operation temperatures above 373 K, requires not only good insulation, but some form of heating additional to the insulation as well [89].

In this study, a vacuum jacket as well as an electrical heater in an insulation jacket is employed to insulate the process and prevent vapour condensation inside the Gillespie chamber, which causes the vapour fraction to run back down with the liquid fraction [61]. The Gillespie chamber therefore has a vacuum jacket as well as a thermal insulation jacket.

The temperature of the thermal insulation jacket need not go above the boiling and equilibrium temperatures, literature states that it could be at least 15 K lower than the equilibrium temperature [61]. The thermal insulation jacket was procured from Eltherm South Africa and has a power rating of 36 W, with a 24V AC input [56].

3.2.3 Ancillary equipment

In constructing the setup for this study, various pieces of standard laboratory equipment were required to complete the still and ensure the proper functioning of the core equipment. Equipment such as condensers, receivers and adapters were therefore used to complete the construction.

3.2.3.1 Condensers

Condensers are required in this study to condense the vapour fractions for sample collection and to try and maintain complete vapour and liquid reflux. Various types of condensers are available and the more commonly used ones have been standardised [89]:

1. Condensers with a smooth tube
2. Condensers with augmented parallel cooling surfaces
3. Condensers with coils

Condensers with smooth tubes include Liebig condensers with cooling jackets and is suitable for applications that require a low pressure drop such as this study [89]. Condensers with augmented parallel cooling surfaces include Allihn’s condenser with a cooling surface formed by a series of bulbs, suitable to ensure the condensation of evaporating liquids [89]. Lastly, condensers with coils include Dimroth condensers with a coil for the cooling medium and is highly effective [89].

The Liebig and Dimroth condensers were seen as suitable for condensing vapour fractions in the setup due to their high effectiveness. A Liebig condenser with an area of 1800 mm^2 was calculated to be more than sufficient to ensure condensation of the vapour fractions produced. The Allihn condenser was utilised in condensing vapours from the hot liquid fraction. Furthermore, all condensers used in this setup have low pressure drops across them.

3.2.3.2 Standard equipment

Receivers are typically used in laboratory distillation setups for collection of liquefied samples but can also be used in the measurement of feed being loaded into a system [89]. The Anschutz-Thiele receiver is very common for use in laboratory based vacuum distillation setups and a setup based on this technique is employed in the current setup in isolating the setup from the environment during the loading of feed and collection of samples. An illustration of an Anschutz-Thiele receiver is shown in Figure 3.4.

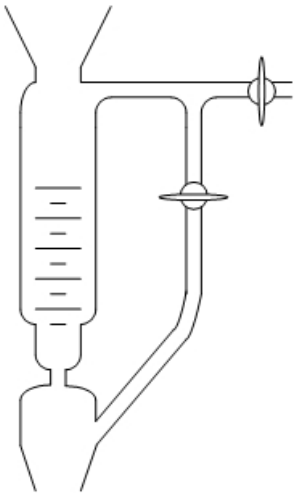

Figure 3.4: Anschutz-Thiele receiver for vacuum systems [89]

Additional standard equipment such as adapters, sample rods, drop counters and precision stopcock valves were also used to complete the construction of the VLE still such that it would function properly and in a user-friendly way.

3.3 Measurement and control: Pressure, Temperature and Composition

This section describes the overall philosophy employed in controlling the temperature and pressure during experiments to ensure that phase equilibrium is attained within a reasonable time and maintained. It also discusses the analysis techniques and errors involved in measuring composition.

As part of a degrees of freedom analysis, there are two degrees of freedom for each experiment due to each system being a binary mixture with two phases (with the exception of the final quarternary phase). This implies that two of the four intensive variables in each experiment (pressure, temperature, vapour phase composition and liquid phase composition), can be controlled.

The two variables chosen to be varied were the pressure and temperature as it would be impractical to control the phase compositions. However, temperature was not explicitly controlled, instead the energy input was controlled which results in a specific temperature output. This is due to the relatively long periods of time required for stabilisation during temperature loops [76].

The basic requirements regarding measurement and control for the experimental setup are therefore as follows:

- Accurate pressure measurement and control – to maintain isobaric conditions and thus mechanical equilibrium
- Accurate temperature measurement – to measure VLE temperature data
- Manual variation of heater output – to maintain a constant energy input and thus thermal equilibrium
- Accurate sample analysis – to quantify VLE composition data accurately

The rest of this section discusses the basic requirements in more detail. Before that, a few issues noted from the operation of similar setups are mentioned. Furthermore, Figure 3.5 illustrates a basic summary of the instrumentation and control employed in terms of temperature and pressure. The touch screen displays all required information such as vapour and boiling temperatures, pressure set points, heater output and heating jacket set points. Appendix C contains the Process Flow Diagram (PFD) and the Piping & Instrumentation Diagram (P&ID) of the equilibrium still respectively.

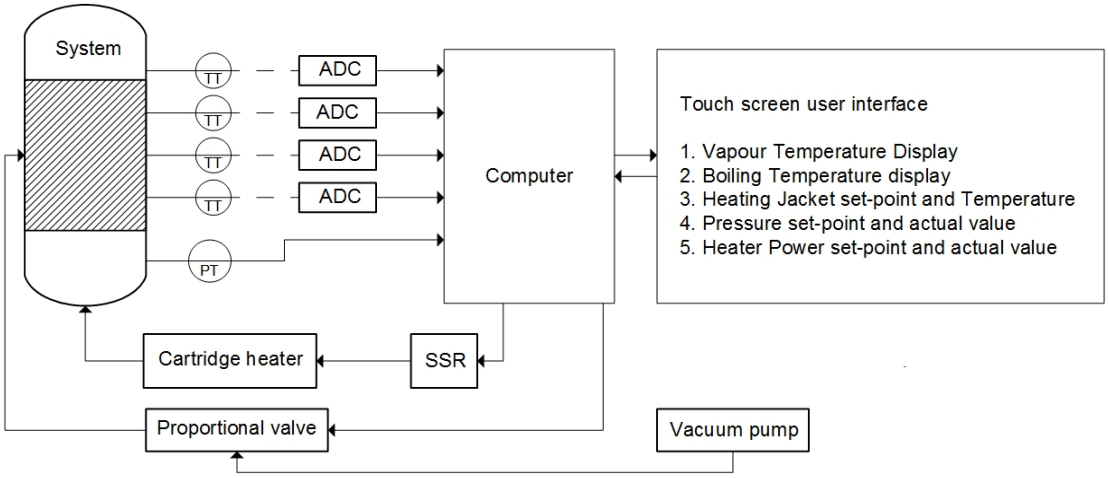

Figure 3.5: Instrumentation and control summary for temperature and pressure. ADC – analog-to-digital converter. SSR – solid state relay.

3.3.1 Existing operations

From experience with operations of similar setups, the following issues were noted and addressed accordingly [61]:

- Manual valves used to control vacuum pressure can be very sensitive, making pressure control rather tough. This is avoided in the new setup by implementing a controlled proportional valve.
- None of the data recorded are necessary to be logged since the samples required are planned to be taken during steady state equilibrium conditions – meaning that the temperature will not vary significantly. However, the setup allows for modifications such that if logging is required in future, it will be possible.

3.3.2 Pressure measurement and control

The experiments in this study were conducted at a sub-atmospheric pressure of 40 kPa in an effort to reduce thermal degradation. The ability to operate at sub-atmospheric pressures also contributes to the constructed setup's versatility. In order to measure and maintain constant pressure, pressure measurement devices are required.

Electrical pressure transmitters were seen to be the most suitable for measuring vacuum pressures in this study and are also very accurate in general [89, 90, 96]. Therefore, different pressure transmitters of the same types were compared and the Yokogawa model EJX 510A

was found to be the most suitable and hence chosen for this setup. The pressure transmitter was calibrated by Wika South Africa, of which the certificate can be found in Appendix A and details of the specification are provided in Table 3.2 [107, 114].

Table 3.2: Yokogawa model EJX 510A pressure transmitter specification [114]

Supplier	Yokogawa
Model	EJX 510 A
Range [0 to _] (bar abs)	2
Accuracy (% of range) (Linearity and repeatability included)	0.04%
(mbar)	0.8
Stability	0.2%/10 yr
(mbar)	4
Total thermal effect	0.30%
(mbar)	6
Turndown ratio	200 to 1
Max Process Temp (K)	393
Weight (kg)	2.7
Output signal	4 - 20 mA HART ®

Figure 3.6 illustrates the setup in terms of pressure control. A more detailed description of the rest of the process can be found in the PFD and P&ID in Appendix C.

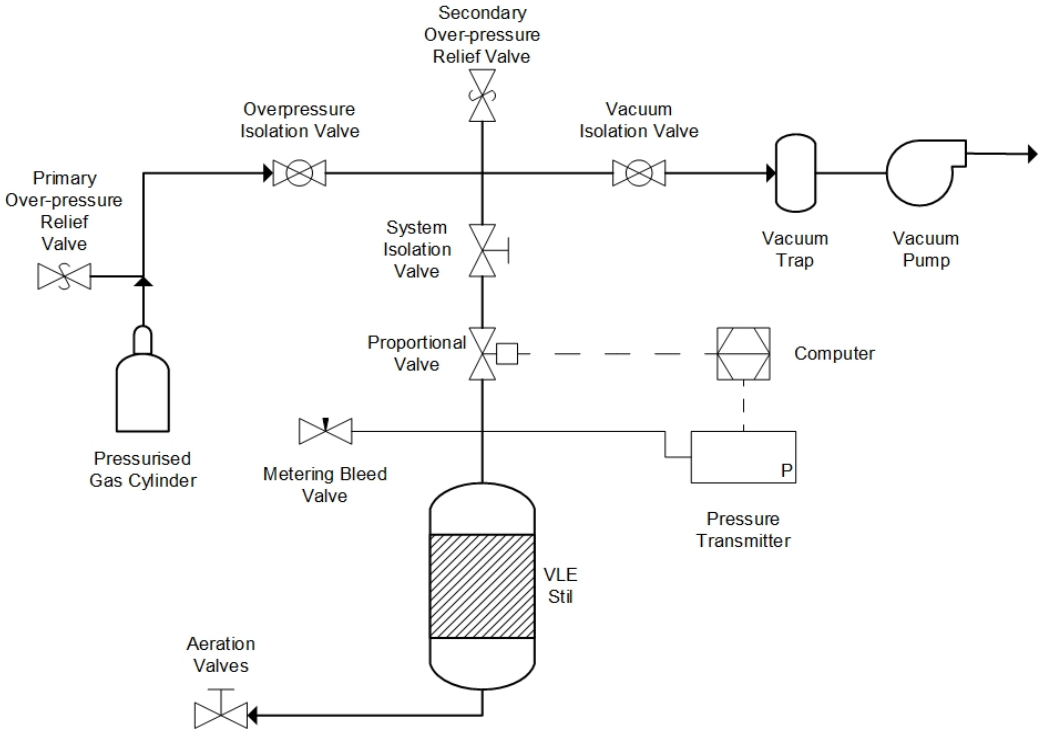

Figure 3.6: Pressure control setup for both vacuum and over-pressure scenarios

There are two pressure settings for the equilibrium still built, namely, vacuum and overpressure, and the Yokogawa pressure transmitter covers the entire range.

3.3.2.1 Vacuum

As Figure 3.6 illustrates, vacuum in the still is achieved using a 0.25 kW rotary vane vacuum pump. This type of pump was chosen as it is commonly known to provide stable suction pressures [52, 96].

Vacuum is controlled using the proportional metering valve and manual metering bleed valve, the former of which is operated through a computing system, as shown in Figure 3.6 [90, 96].

The control of action of the proportional valve was only used for vacuum pressure scenarios as the majority of this study was conducted under vacuum pressures. However, if control action is required during overpressure scenarios, the setup is designed to accommodate it.

The absolute pressure in the system is displayed on the pressure transmitter. The touch screen allows the user to input a desired pressure level. The pressure input by the user serves as a set point for the pressure, which is controlled by adjusting the position of the proportional valve [90]. This is a closed loop system in which the pressure is the control variable and the valve position is the manipulated variable. A hysteresis (upper and lower limit) value for the control variable is also used. This maintains a very narrow vacuum range in which the control takes place.

The proportional valve employs typical proportional and derivative action in controlling vacuum [76, 90]. However, integral action is obtained using the manual metering valve to shift the vacuum pressure level when stabilised [76]. Furthermore, a manual throttle valve is installed between the proportional valve and the pump for situations in which vacuum from the pump is excessive or difficult to control [90]. Throttling this valve helps reduce the vacuum pump's pulling force.

The proportional metering valve is controlled using a threaded actuator and a motor with 6 mm thread length and 3592 counts per revolution respectively [90]. Each revolution can shift the needle up or down by 0.5 mm [90]. This equates to a resolution of 0.14 µm of movement per shift. The motor for the valve has a 74.83:1 gearbox which is able to deliver substantial power in a small package [90]. The gearbox is controlled using the 4 – 20 mA signal from the pressure transmitter [90].

3.3.2.2 Overpressure

The overpressure scenario on the setup is currently controlled manually, without the use of the proportional valve (although possible if required). High purity nitrogen gas (>99.999 %) was used to pressurise the system when required [110].

The metering valve is used to control the overpressure scenario as well. One should ensure that during vacuum settings, the overpressure isolation valve is closed and during the overpressure settings, the vacuum isolation valve is closed.

3.3.3 Temperature measurement and heater control

The accurate temperature measurements necessary consist of the equilibrium vapour temperature inside the Gillespie chamber section and the boiling temperature inside the cartridge heater section of the still.

Two Resistance Temperature Detector (RTD) probes were therefore chosen for temperature measurements in this study due to their relatively high accuracy, robustness and reliability [96]. The probe selected was the 4-wire Pt-100 1/10th DIN Class B, as it has the lowest uncertainty, of 0.03 K at 273.15 K and 0.08 K at 373.15 K, in the conventional Pt-100 range [90, 107].

Although only the vapour temperature is required for the temperature composition data in this study, the feed temperature probe was also specified for high accuracy to ensure that future projects that could possibly involve vapour-liquid-liquid equilibria would have a high accuracy probe available. The probes were procured from Wika Instruments Pty Ltd. and the vapour temperature probe was calibrated by Thermon South Africa [107]. The calibration certificate can be found in Appendix A.

The signal from the probes is converted from an analog format to a digital format, using an Analog-to-digital converter (ADC), which allows it to be read by the computer chip, to a resolution of 22 bit [90]. This resolution has been seen as sufficient due to the operational temperature range being from 273 – 458 K. The resolution is therefore 0.00004 K (458 K /(2^22)), which is lower than the highest accuracy of the Pt-100 probes of 0.03 K [90].

In addition to the two temperature measurements mentioned, one more temperature is measured. This is used to control the thermal insulation jacket of the Gillsepie chamber. High accuracy is not required since this temperature is not crucial to the operation of the still. A Type K thermocouple is employed in the measurement of this temperature [90]. Power to the insulation jacket is controlled using the computer and a solid state relay (SSR) [90].

The two accurate temperatures are displayed and are not used for direct control purposes. However, the boiling rate is used to assess the power required from the cartridge heater. The 600 W alternating current (AC) cartridge heater is manually controlled with the power being input as a percentage of the heater's wattage, on the touch screen user interface. Each mixture is unique and requires a different amount of energy to boil appropriately, i.e. enough to vaporise the feed material but not so much as to only produce a vapour return [61].

The heater has simple on/off control with a desired set-point that the heater can reach [88, 90]. As long as the temperature is below the set-point, the heater will remain switched on and if the temperature rises above the set-point, the heater will be switched off. A hysteresis is used to maintain constant power delivery.

The heater employs a SSR as well, with no moving parts and is therefore not prone to wear and tear. Furthermore, to switch the heater off, an input value of zero power is required on the touch screen user-interface.

3.3.4 Composition: sample analysis and compositional error

3.3.4.1 Sample analysis

Samples were analysed using a Gas Chromatography (GC) Flame Ionisation Detector (FID). GC methods of analysis are the most common that are noted in the literature for TDO analysis [1].

For the analysis, an Agilent 7820A GC FID was used [99]. A non-polar Rxi®-5Sil MS Crossbond® column with dimensions 60 m x 0.18 mmID x 0.1 µm df was employed in generating the peaks obtained. The temperature programme was set to ramp up at a rate of 0.7 K/min from 313 K until 335 K, followed by a rate of 20 K/min up till 553 K. Samples of approximately 500 ppm in concentration were used for analysis due to the relatively small diameter of the column. Although the split ratio is typically increased in order to improve the resultant peaks, increasing the split ratio was insufficient to provide good peaks and also wasted carrier gas (Helium).

Areas produced by the GC-FID for each compound were correlated to mass values using calibration curves, which were generated for each compound by preparing four samples with fixed masses of the internal standard and varying masses of the mixture compounds. Each calibration curve had a specific gradient and all calibration curve gradients for each compound can be found in Appendix I. A detailed method for calculating the calibration curves is also available in Appendix I.

A proper internal standard would be one that has the same functional groups, similar normal boiling point and activity as the target compounds [99]. Toluene was chosen as the internal standard (IS) due to its similarity in functional groups, boiling point and activity to the aromatic compounds as well as *α*-pinene and limonene. This ensured similar elution behaviour through the GC column.

Samples from two of the verification trials however, the ethanol/1-butanol and *n*-nonane/1-pentanol systems, employed 1-pentanol and 1-octanol as internal standards, respectively [108, 109].

3.3.4.2 Compositional error

The compositional error in this study is a combination of temperature, pressure and analysis effects. Heater power does not vary during operation of the still, therefore its effect on the compositional error can be considered to be negligible. In order to confidently report uncertainty values obtained in this study, the expanded uncertainty method defined by the Guide to the Uncertainty in Measurement and NIST is employed [60]. In this method, the standard uncertainty obtained is multiplied by a coverage factor (usually between 2 and 3) in order to have a certain amount of confidence in the reported uncertainty, where a coverage factor of 2 indicates a 95% confidence level and a coverage factor of 3 indicates a 99% confidence level [60].

Pressure fluctuations during operation were noted to be +/- 0.1 kPa, which translated to a maximum fluctuation of +/- 0.1 K in temperature measurements. For pressure and temperature uncertainties, a coverage factor of 2 was employed in order to have 95% confidence in the reported value. This is in keeping with international standards [60]. The expanded uncertainty for pressure was therefore +/- 0.2 kPa.

Temperature errors, in addition to that caused by the pressure fluctuations, such as a calibration reference error of +/- 0.05 K and a calibration reference offset of 0.02 K lead to a combined temperature error of +/- 0.16 K. Using a coverage factor of 2, the expanded uncertainty for temperature becomes +/- 0.32 K with 95 % confidence in this value.

Analysis effects were accounted for using dummy samples with known compound masses to test accuracy of the calibration curves developed after obtaining data for a relevant system [61]. The process for each system included 3 samples of known masses being analysed and the resultant peaks used together with calibration curves to generate the analysed compositions. The error between the analysed compositions and gravimetrically determined compositions were thus considered.

The maximum analysis error from all dummy samples tested was noted to be +/- 0.011 mole fraction. The average analysis error from all dummy samples tested was noted to be +/- 0.0034 mole fraction. This shows that most of dummy samples exhibited less than half of the maximum analysis error. For this reason, the average analysis error was used in calculating the expanded uncertainty together with a coverage factor of 3, even though it is more than required. The expanded uncertainty for composition therefore becomes +/- 0.0102 mole fraction. The compositional error for this study was therefore noted to be relatively low, fulfilling the accurate VLE composition data requirement.

3.4 Experimental methodology

This section explains the experimental methodology employed during operation of the experimental setup.

3.4.1 Process summary

Here, a summary of the process in which vapour-liquid equilibrium is achieved in the still is described. Figure 3.7 illustrates the constructed VLE still for this study. A detailed specification of the still can be found in Appendix D [28]. The experimental methodology described in this as well as following sections, is adapted from Cripwell in 2015 [61].

To start the process, around 100 mL of liquid mixture is loaded in to the mixing chamber (E) via the feed loading chamber (L) above it. The micro-stirrer in the mixing chamber (E) and cartridge heater in the heating chamber (A) are then switched on. An RTD (J) allows for temperature measurement of the boiling liquid.

Once the liquid starts to boil, a liquid-vapour mixture travels from the heating chamber (A) through the Cottrell tube (B) where equilibrium between the two phases is reached. The vapour and liquid phases exit the tube where they split. An RTD (D) then allows for temperature measurement of the vapour.

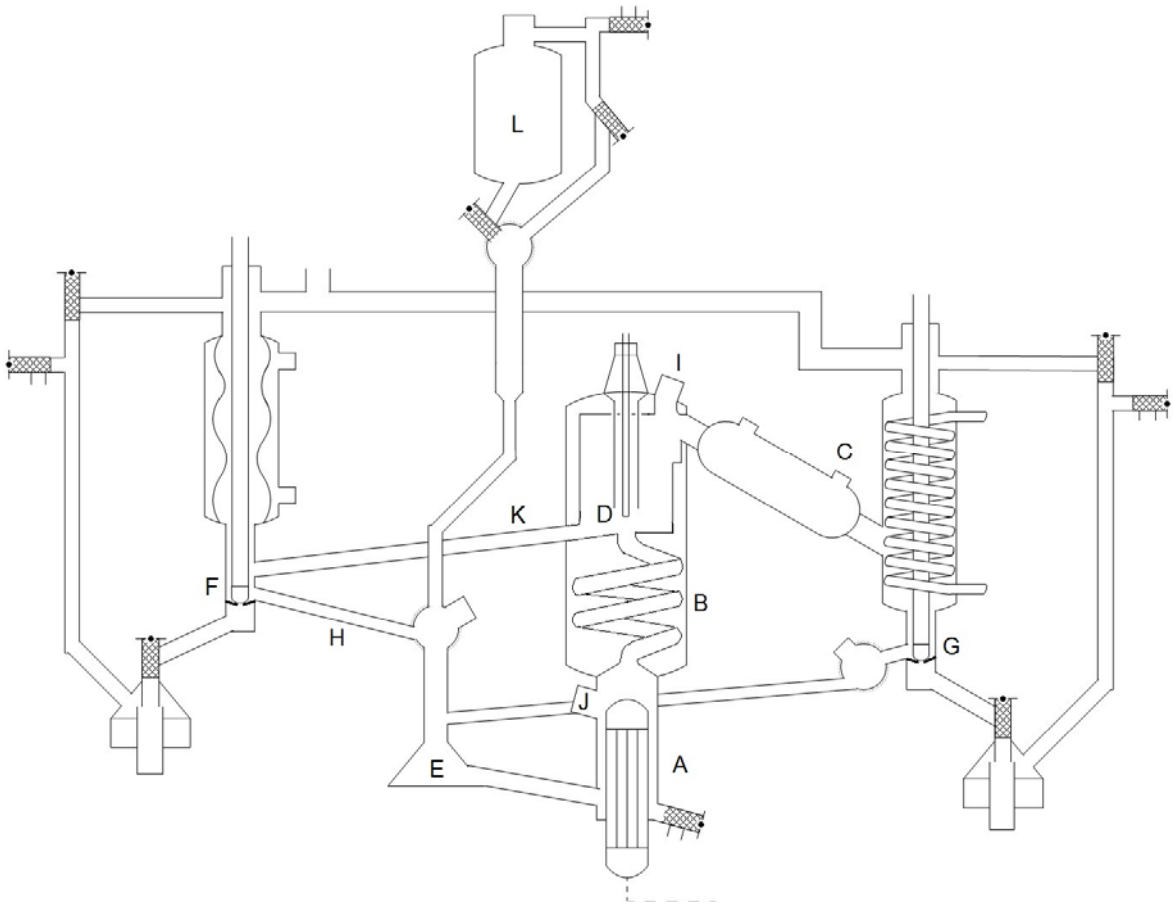

Figure 3.7: General setup of the vapour-liquid equilibrium still [28]. A – Cartridge heater; B – Cottrell tube; C – Condensers; D – Vapour RTD; E – Magnetically stirred mixing chamber; F– Liquid sample well; G – Condensed vapour sample well; H – Future Liquid online GC port; I – Future vapour online GC port; J – Feed RTD; K – Equilibrium liquid tube; L – Feed loading chamber.

Equilibrium is reached when the temperature of the liquid-vapour mixture coming out of the Cottrell tube becomes steady. The Cottrell tube is housed in the Gillespie chamber, which also insulates it, allowing for equilibrium to be reached as easily as possible.

The liquid then flows through a drain (K) and into the bottom of a condenser where any vapours coming off the hot liquid portion can be condensed. The liquid flows through the sampling well F and back into the mixing chamber (E).

The vapour exiting the Cottrell tube travels to the top of the Gillespie chamber and into a primary condenser (C). This primary condenser and secondary condenser try to ensure that all the vapours are condensed. The condensed vapour flows into a well (G) and then back into the mixing chamber (E), which is then fed back into to the heating chamber (A) [28].

The wells in which the liquid and vapour condensate accumulates (F and G respectively) are equipped with stoppers (glass rods embedded with magnetic rods) to allow for sampling.

Modification provisions were made for possible aspects of future projects such as on-line sampling or vapour-liquid-liquid (VLLE) experiments. As such, easy modification will be possible to allow connection of an on-line GC to ports H and I.

3.4.2 Still preparation and operation

This sub-section provides a brief overview of how the still is prepared and operated at sub-atmospheric pressures. A more detailed step-by-step procedure can be found in Appendix E.

Before commencing with the experiments on the still, one should ensure that it has been cleaned. This can be done by running solvent such as dichloromethane (or acetone) at atmospheric conditions through the still the previous day or after running an experiment - instead of dedicating an entire day to cleaning the still. This reduces the risk of contamination and errors as well.

The first step to operation would be to ensure that all the relevant valves are open and the rest closed. The next step would be to achieve the desired pressure for the system. This can be done by adjusting the vacuum pump as well as the system software to the desired pressure after switching it on and calibrating the touch screen. The cooling water can now be pumped through the condensers by switching the cooling water pump on.

To start an experiment, pure component is loaded into the mixing chamber via the funnel at the top, enough to cover the cartridge heater, this is to maximise the electricity usage and to prevent burnout of the cartridge heater. Pure component is loaded because the first reading is the boiling temperature of that component at the experimental pressure, which is vapour pressure data, as well as a test to check that the temperature is being measured correctly. This is also the simplest way to generate a temperature-composition diagram using the least amount of chemicals.

To heat up the mixture, the power output of the cartridge heater needs to be adjusted to a level where sufficient liquid boils without excessive amounts of vapour being produced since the system is under vacuum. In this study, a power setting of 15 W was used, this was found to meet the energy requirements of the compounds of concern, in order to reach vapour-liquid equilibrium within 90 minutes. This power setting of 15 W can thus be seen as being part of the plateau region in terms of power input.

A safe way to check if the cartridge heater has been set correctly is to make sure the feed is not experiencing rapid evaporation upon entering the heating chamber. Additionally, the liquid phase and condensed vapour phase drop rate returning to the mixing chamber should be appropriate. This should not be too high as this indicates either too much power input or too much liquid feed being in the system.

3.4.3 Sampling

The concave nature of the sampling wells requires regular flushing of the collected condensate to prevent contamination of the equilibrium sample. Flushing should also be done prior to sampling. The sample is taken by opening the sample wells in order to drop some of the collected flushed vapour condensate and flushed liquid sample into the sample collection vial, thereafter removing the vial. In order to remove any collected sample, one would have to isolate the system first as it is under vacuum conditions. The system can be isolated by closing off the valves that allow outside air into the system.

Before isolating the system however, one should remove all flushed liquid by draining it into the collection vials. After isolating the system and collecting the flushed liquid, the vials are to be replaced with clean ones for collection of actual sample. Once the clean vials for sample collection are put into place and the system reintegrated, the magnetic valves could be opened up, allowing the desired equilibrium sample to pass through. This sample could be directed into the sample vials using the relative taps. To remove the samples, one would simply have to isolate the system again and remove the sample vials. Each time the system is isolated and reintegrated, at least 20 minutes would be required for it to reach equilibrium again, however sampling is only recommended after 45 minutes due to flushing at the 20 minute mark being necessary.

3.4.4 Shut down

The system can be shut down using the touch screen user interface. The vacuum pump can be switched off and the aeration valves should be opened slightly to allow the system to get back to atmospheric pressure. The cartridge heater should also be switched off.

Once the system is open, the liquid should be allowed to cool off. The cooling water pump can be switched off after a few minutes. Once the liquid is cool, it can be drained using the drain valve at the bottom of the still. The still can then be washed by running solvent such as dichloromethane if required. The solvent should be heated and run in the still as well so that any

build up would be easier to remove. The magnetic valves should also be opened as per flushing procedure during washing.

The solvent can be allowed to run for about 30 minutes before switching the system off completely as described above. The aeration valves can be left open for the still to dry. The still is enclosed in a fume hood so contamination effects from outside sources are negligible.

The experimental methodology described here was followed during the commissioning and verification stages of this project, which are discussed in the following sections.

3.5 Commissioning

With the development of every setup comes the compulsory task of commissioning to ensure that the constructed setup works properly. A significant portion of the commissioning for the setup in this study was conducted simultaneously with the verification process. With regard to the setup this study, some of the features that could lead to significant error in data capturing were the temperature measurement and pressure measurement and control.

The still was commissioned using VLE data for the atmospheric reference system ethanol/1-butanol at 101.3 kPa [61, 70]. To start off the commissioning, vapour pressure data was collected for both ethanol and 1-butanol and compared to that of literature [103, 104].

3.5.1 Calibration

The first step in commissioning is the calibration of all physical phenomena-sensing electronics. This is required to increase and ensure the accuracy of measurements taken during experimental runs.

In this study, pressure sensing equipment and the temperature probe used to measure data were calibrated according to the South African National Accreditation System (SANAS). Both certificates can be found in Appendix A.

The temperature calibration was further used to provide an updated temperature reading on the existing setup display in addition to the original measurement. The updated temperature reading had a combined temperature offset of 0.02 K from the actual temperature values.

3.5.2 Pressure control

Figure 3.8 shows the initial setup of the proportional valve's connection to atmosphere while controlling the vacuum pressure in the still.

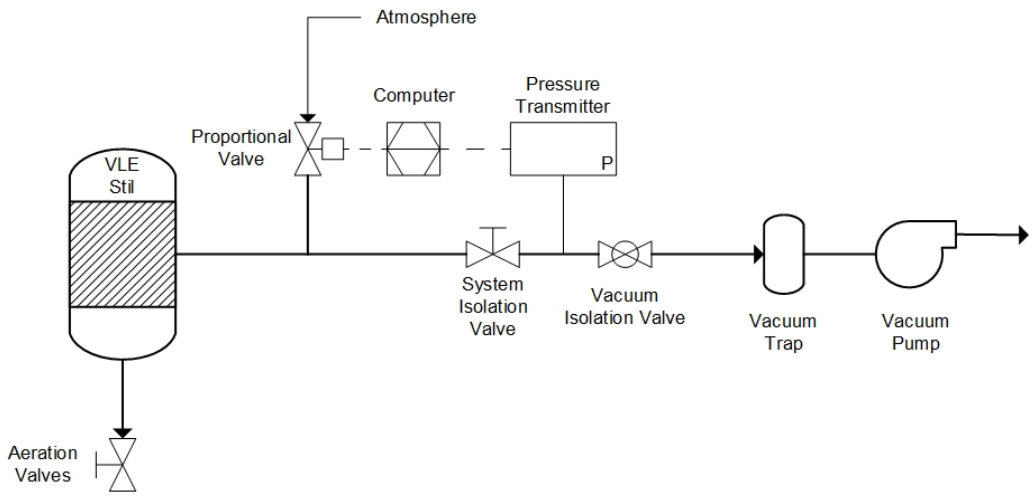

Figure 3.8: Basic description of initial vacuum line setup

As illustrated by Figure 3.8 the proportional valve initially controlled vacuum within the still and was vented to the atmosphere. Basically, the proportional valve would close (to pull in less atmospheric air) if more vacuum was required and would therefore open if less vacuum was required, to pull in more atmospheric air.

During operation, the proportional valve was always open to atmosphere to a significant extent in order to control vacuum. This caused large amounts of atmospheric air to be pulled into the vacuum pump oil chamber and purged into the laboratory air via the vacuum pump exhaust port together with some of the heated vacuum pump oil vapours. For this reason, it is normally recommended that vacuum pumps are fitted with exhaust filters to prevent oil mist from exiting the pump [105].

To rectify the oil mist issue, the vacuum line setup was altered as shown in Figure 3.9. The setup of the proportional valve was changed to an in-line setup and an additional bleed valve (connected to atmosphere) was added to the line to help control vacuum. The additional bleed valve would serve the same control function that the proportional valve previously did, but pull in much smaller amounts of air into the line and in turn preserve the lifespan of the pump. A new pump, which was fitted with exhaust filters, was also obtained.

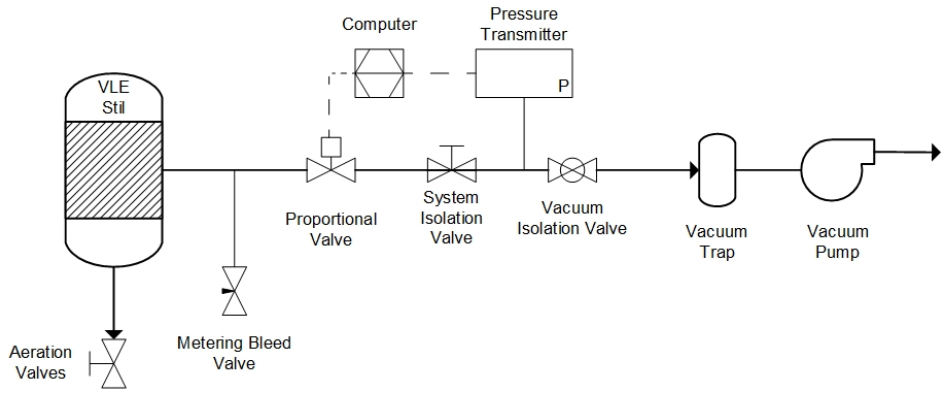

Figure 3.9: Basic description of current vacuum line setup employing metering bleed valve and in-line proportional valve

Another issue encountered with the pressure control was that the proportional valve had difficulty managing disturbances to the pressure. Initially, the proportional valve employed only proportional control action but this was later seen to be insufficient in controlling the pressure. This was identified by isolating the valve and manually trying to control the pressure. It was noticed that the rate at which the pressure changed also needed to be taken into account when controlling the pressure at a specific point [76, 96]. The valve was then re-programmed to incorporate proportional and derivative action.

The type of valve used initially was a 1/8” needle valve. Although suitable to most pressure regulating systems, this type of valve had a much smaller “window” in which the actual flow of fluid could be controlled [90]. For this reason, the 1/8” needle valve was exchanged with a 1/8” metering valve. The metering valve was chosen because of its restricted design and ability to control flow as tested in its application as a bleed valve.

3.5.3 Temperature and pressure measurement

As previously mentioned, vapour pressure data for ethanol and 1-butanol were obtained and compared literature [103, 104]. This was done to be certain that temperature and pressure were being measured accurately.

The process began by loading the system with 99.8 wt. % ethanol into the system and heating it with ~20 W of power providing equal vapour and liquid return. The pressure was decreased incrementally from atmospheric levels down to a minimum of 15 kPa in order to determine the vapour pressure curves as accurately as possible. At the various pressures, values of temperature and pressure were recorded once the equilibrium temperature and pressure had

stabilised. For certainty reasons, a second component, 99.6 wt. % 1-butanol feed, was run through the still as well, using the same procedure.

These records were compared to literature values from a trusted source and some error was noted in the measurements. The following two types of plots were used to troubleshoot the problem:

- Temperature difference (experimental – literature) vs pressure
- Pressure difference (experimental – literature) vs temperature

The initial plots had significant temperature and pressure deviations from literature values. It was seen that the problem arose from a drift in the pressure transmitter's reading and an impure feed. The pressure transmitter's drift was then corrected by adjusting the zero point using a screw on the pressure transmitter itself. This did not affect the calibration of the transmitter. The still was also thoroughly cleaned twice before a new load of 1-butanol feed was run through the still for the collection of vapour pressure data. This was followed by the collection vapour pressure data of the 99.8 wt. % ethanol feed.

Figures 3.10 and 3.11 illustrate the final temperature and pressure difference plots obtained. The deviations from literature for temperature are within that of the temperature error in this project (+/- 0.32 K) and that for pressure is predominantly within +/- 0.2 kPa.

The final temperature and pressure difference plots for both ethanol and 1-butanol showed that the measurements were now acceptable and the setup's temperature and pressure measurement capability was commissioned. This also showed that even the slightest contamination of feed can cause significant errors in measurements and that one should be as concise as possible when operating the setup in order to obtain accurate data.

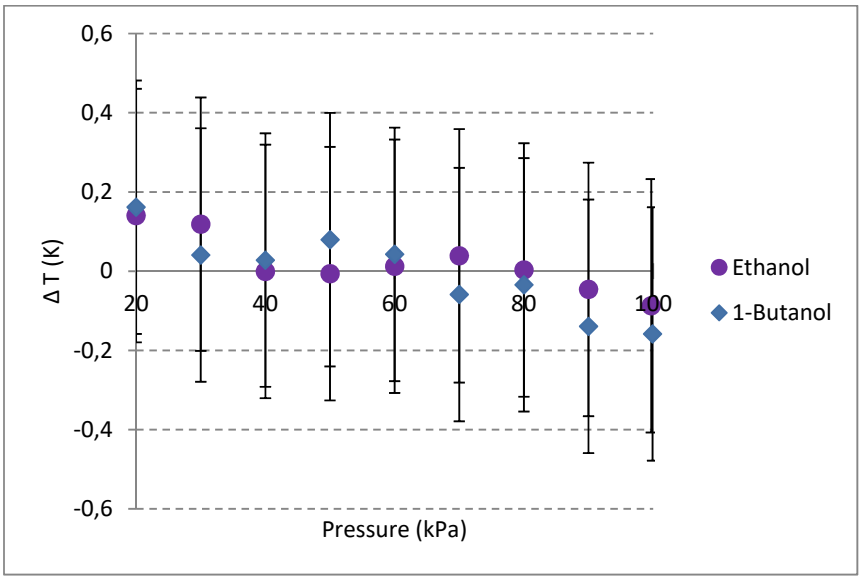

Figure 3.10: Final temperature difference plot for vapour pressures of ethanol and 1-butanol [103, 104]

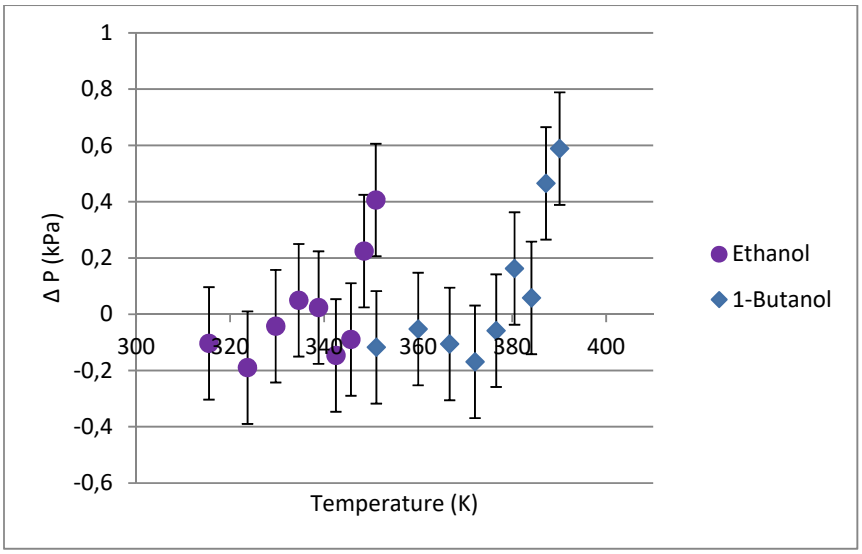

Figure 3.11: Final pressure difference plot for vapour pressures of ethanol and 1-butanol [103, 104]

3.6 Verification

Just as thermodynamic consistency tests bring credibility to a study by indicating whether or not data is unreliable, so too does equipment verification bring credibility to a study, by ensuring the reliability and repeatability of an experimental setup and procedure respectively. To verify an

experimental setup, one would have to repeat experiments that have already been performed or are similar in nature to that of the current study, i.e. an experiment that can serve as a reference.

In this study, the isobaric vapour liquid equilibrium at reduced pressures between the compounds limonene, indane, butylbenzene, 1,2,3-trimethylbenzene and *p*-cymene was determined. Since the measurements were done at sub-atmospheric conditions, ideally, verification should be done at sub-atmospheric pressures as well. However, it was decided that the setup's performance at atmospheric conditions should be tested first. Therefore, instead of testing the newly built still with only one prior set of data, a combination of reference systems at atmospheric and sub-atmospheric conditions were used to verify the constructed setup.

3.6.1 System selection

The first verification system is the binary mixture of ethanol/1-butunol at 101.3 kPa and is a relatively common system in the literature [61, 70]. One of the references is the work of Cripwell, measured on a similar setup in the same department as the current study [61]. The data passed the L/W and the McDermott-Ellis consistency tests and were acceptable.

The remainder of the three reference systems were all sub-atmospheric verifications performed at 40 kPa, the planned operation pressure for experiments and therefore more pertinent to this study. [61, 62, 108, 109]. The sub-atmospheric reference systems were:

- limonene/*α*-pinene at 40 kPa [62]
- *n*-decane/2-heptanone at 40 kPa [61, 108]
- *n*-decane/3-heptanone at 40 kPa [61, 108] and
- *n*-nonane/1-pentanol at 40 kPa [109]

The components of the first sub-atmospheric system are comparable to those in this study [63]. The latter three sub-atmospheric systems were measured in the same department as this study [61, 108, 109].

Consistency tests for the sub-atmospheric reference systems, using the L/W and the McDermott-Ellis consistency test methods, were performed and the data was found to be consistent, therefore the data was seen as suitable as reference systems. PRO-VLE 2.0 Software package was used to perform the L/W consistency test [65]. The reference data for all the verifications systems are presented in Appendix B together with their consistency test results.

3.6.2 Materials

The use of pure chemicals are vital in obtaining reliable experimental VLE data. The purity of compounds used in this study was of high importance and the verification process was no exception. Supplier details, CAS numbers and assays of the chemicals used for verification trials in this project are presented in Table 3.3. Unfortunately for *n*-decane, no recorded analysis could be found, however the exact same bottle of *n*-decane sample was used in a previous study and the analysis results from that study are reported as it is the only available record [61]. The reported analysis is also what is generally supplied by the respective supplier.

Table 3.3: Chemicals used in this project together with assay and supplier name

Chemical	Supplier	CAS #	Assay (wt. %)
Ethanol	Illovo Sugar Africa	64-17-5	99.81*
1-Butanol	Sigma-Aldrich	71-36-3	99.24*
1-Pentanol	Sigma-Aldrich	71-41-0	98.91*
n-Nonane	Merck	111-84-2	98.97*
n-Decane	Sigma-Aldrich	124-18-5	> 99.0***
2-Heptanone	Sigma-Aldrich	110-43-0	99.6**
3-Heptanone	Sigma-Aldrich	106-35-4	98.3**

* - As per in-house GC and KF analysis
** - As per supplier certificate of analysis
*** - As per [61]

3.6.3 Results

The following sub-section illustrates the comparisons between experimentally obtained data to that of the reference systems. All experimentally obtained data during the verification process, together with the results of their consistency tests, can be found in Appendix K.

3.6.3.1 Atmospheric pressure verification

The first set of verification was conducted for the ethanol/1-butanol system at 101.3 kPa. The data collected passed the McDermott-Ellis consistency tests and most of the data were consistent according to the L/W method as well. Figures 3.12 and 3.13 show the experimental vapour pressure data obtained, during the commissioning phase, on the current setup compared to that of literature values from the trusted sources for ethanol and 1-butanol respectively [103, 104].

The temperature-composition (T-x-y) diagram for the ethanol/1-butanol binary system at 101.3 kPa compared to that of literature is shown in Figure 3.14 [61, 70]. As seen, the experimental values are in visual agreement with the literature values. This initial verification step provided the confidence required to go ahead with subsequent verification steps.

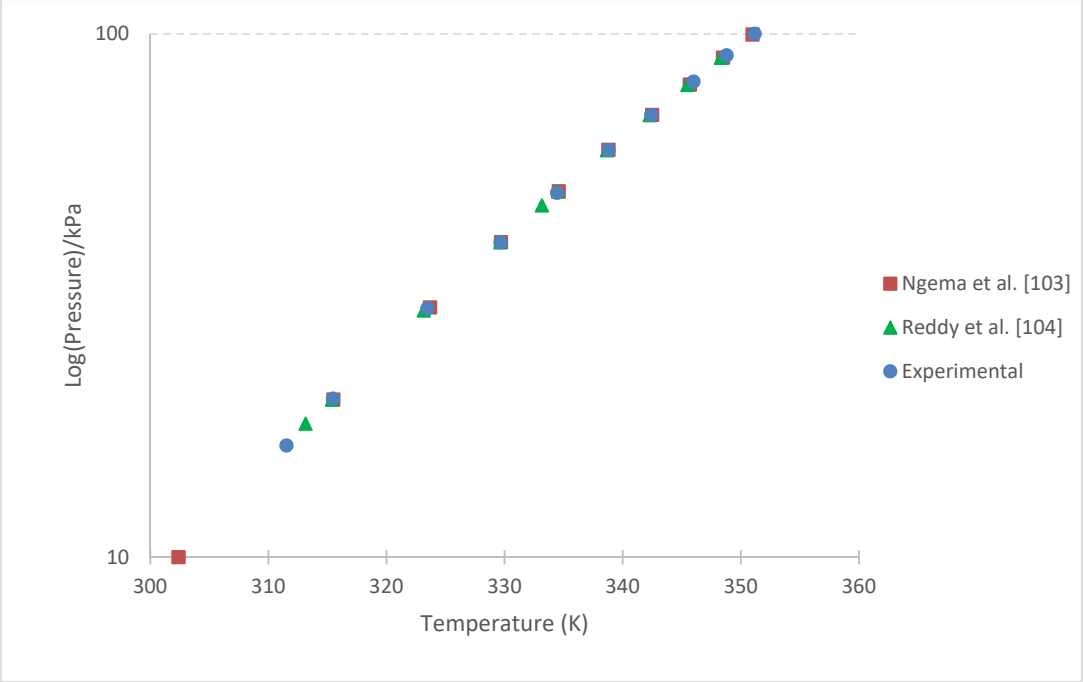

Figure 3.12: Vapour pressure data obtained for ethanol compared with literature [103, 104]

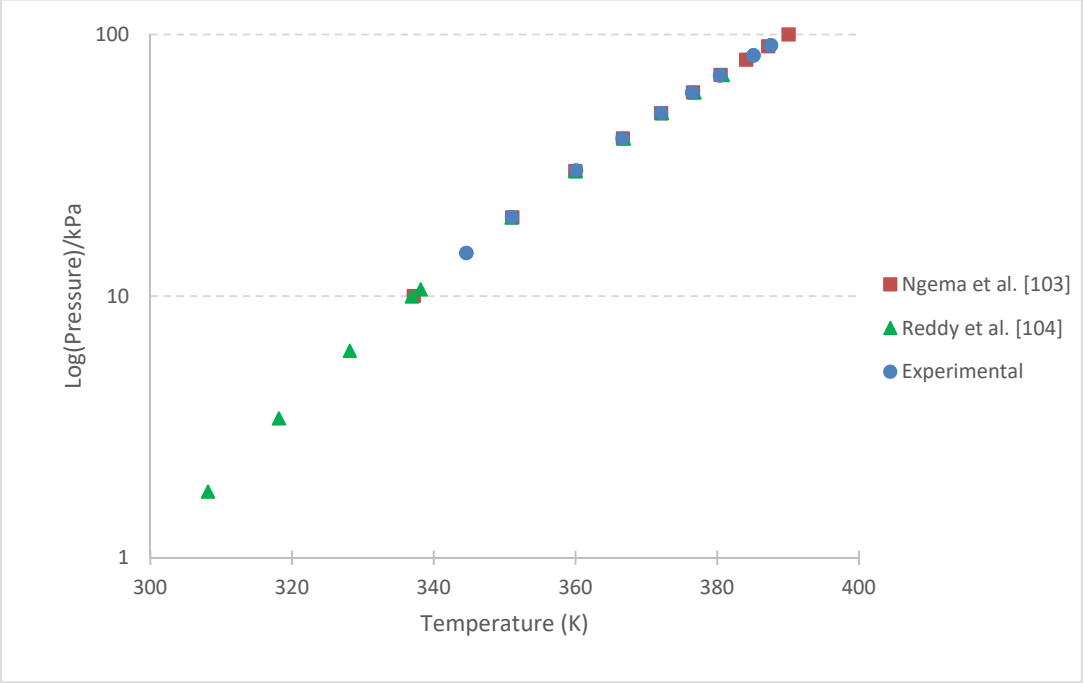

Figure 3.13: Vapour pressure data obtained for 1-butanol compared with literature [103, 104]

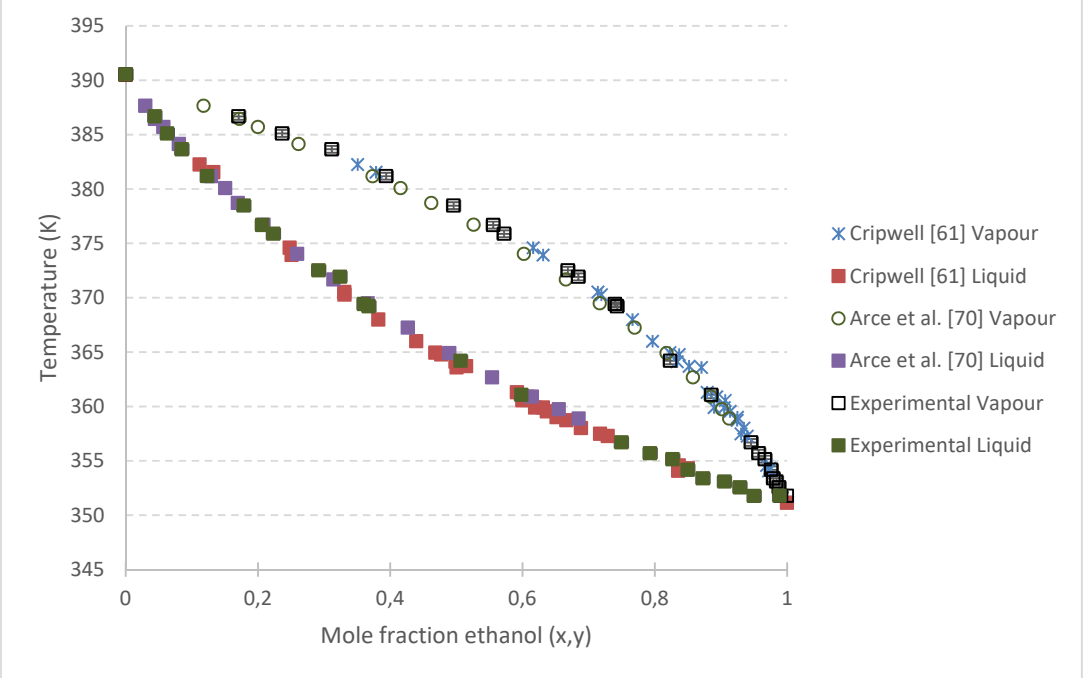

Figure 3.14: Temperature-composition diagram for ethanol/1-butanol binary mixture at 101.3 kPa [61, 70]

3.6.3.2 Sub-atmospheric pressure verification

The following verifications were all performed at 40 kPa for relevant comparison with the data being generated in this study. The first verification system was obtained from literature and used an experimental setup that was different to that in this study [62, 63, 64]. Although a different setup was used, it should not matter if uncertainties were well estimated. The remaining systems were obtained by researchers in the same department as the current study, all of which is published data and obtained from the additional VLE still available in the same department as this study [61, 108, 109].

During verification efforts of the limonene/*α*-pinene system at 40 kPa, it was noticed that the experimental data obtained displayed significant deviation from the reference data of Nadais and Bernardo-Gil [62]. The data obtained illustrated irregular temperature-composition data such as that shown in Figure 3.15. The x-y plot for the data obtained compared to the reference data is shown in Figure 3.16 [62]. The error bars of the experimental data are +/- 0.32 K for temperature and +/- 0.0102 mole fraction for composition. From the figures, it can be seen that the experimentally determined data deviates from that of Nadais and Bernardo-Gil in terms of temperature as well as composition, more so however in terms of the temperature values in which the maximum deviation is ~4 K.

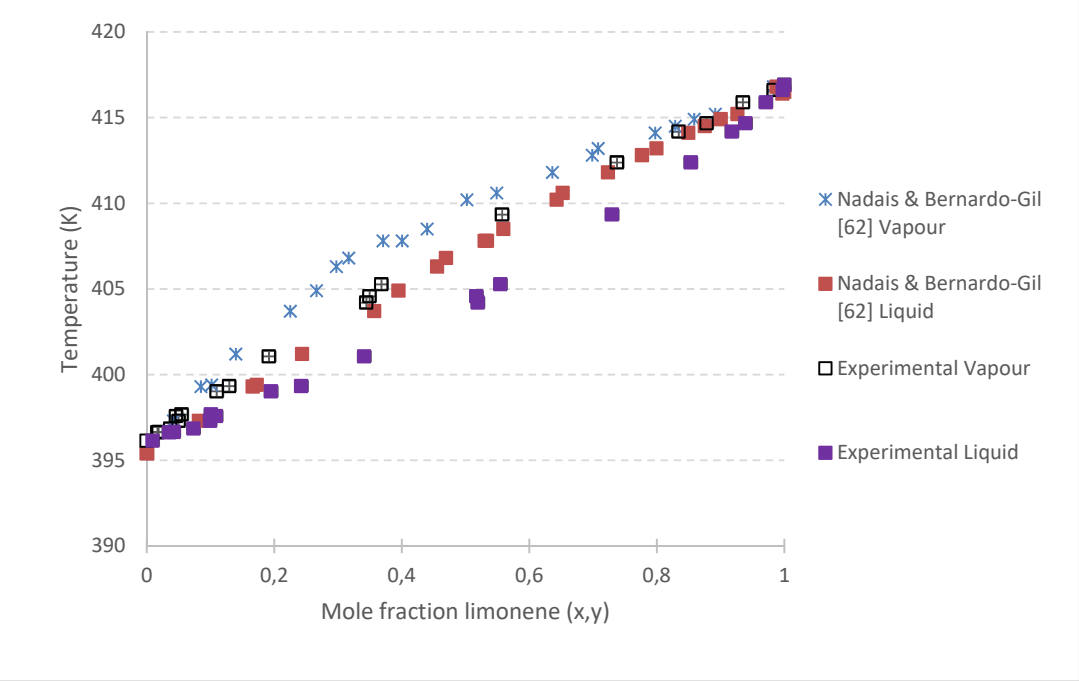

Figure 3.15: Temperature-composition diagram for limonene/*α*-pinene reference system at 40 kPa comparing experimental and reference data [62]

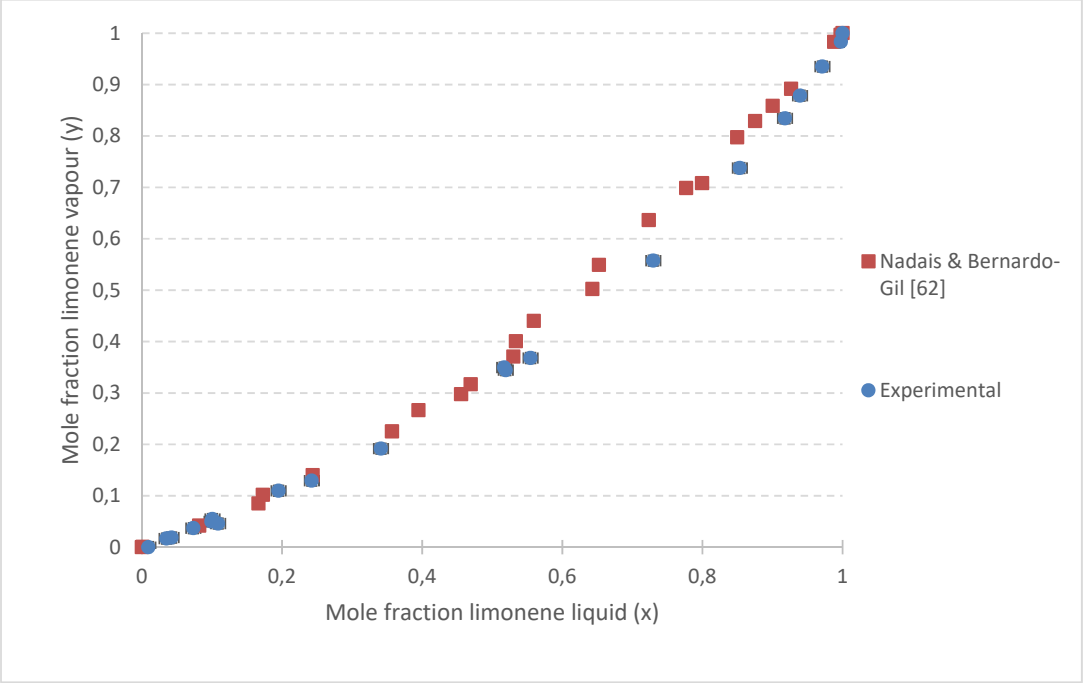

Figure 3.16: x-y plot for limonene/*α*-pinene data obtained experimentally as well as from reference data at 40 kPa.

Despite significant effort (including multiple repeatability runs and various sampling techniques), unsuccessful results with high deviations between experimental data and that of Nadais and Bernardo-Gil were still obtained.

After performing thermodynamic consistency tests, it was seen that although the data from Nadais and Bernardo-Gil passes both the L/W and McDermott-Ellis consistency tests, the experimentally obtained data only passes McDermott-Ellis consistency test, and not the L/W consistency test. This raised concern over the accuracy of this experimental verification. Furthermore, after going through the work of Nadais and Bernardo-Gil thoroughly, it was noticed that although the authors had previously measured data for the same system, no external (second) verification of their data was provided [62, 63, 64]. This is not to say that the reference system is erroneous, but rather that the absence of a second verification raises some concern over the accuracy of their temperature and composition measurements. For these reasons, additional reference systems were included in the verification part of this study.

The binary system *n*-decane/2-heptanone at 40 kPa was the next sub-atmospheric reference system tested [108]. After plotting the experimentally obtained data against the data of Cripwell *et al.*, it was noticed that the two sets of data were generally within the confines of their error

bars as shown in Figures 3.17 and 3.18. The data collected had passed both the L/W and McDermott-Ellis consistency tests.

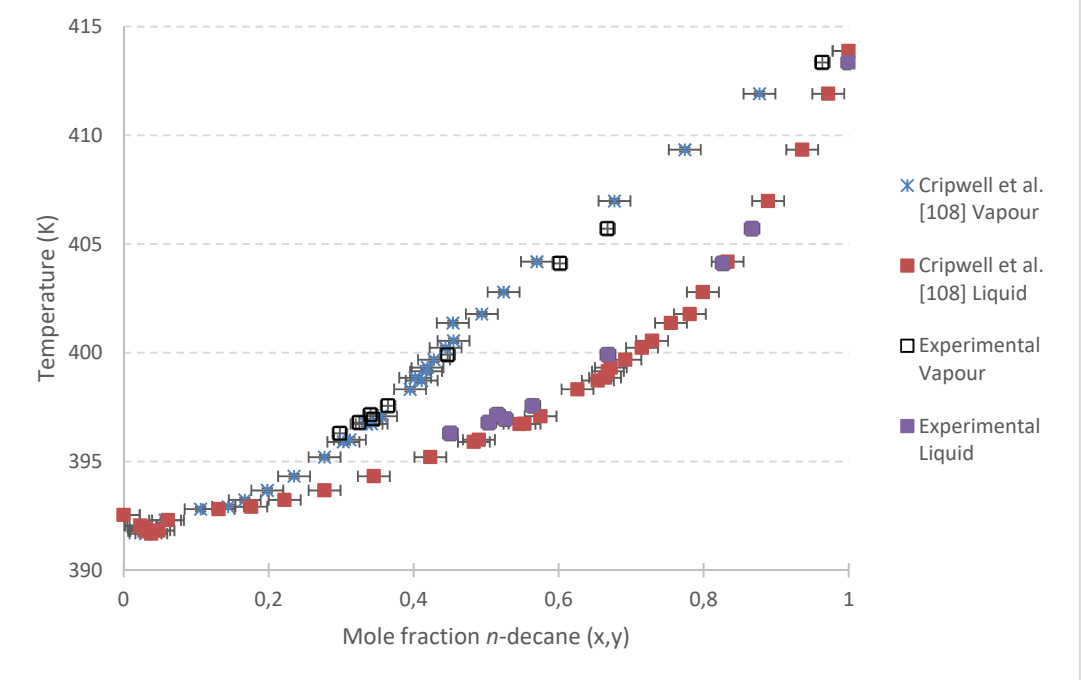

Figure 3.17: Temperature-composition diagram for the *n*-decane/2-heptanone reference system at 40 kPa with error bars [108].

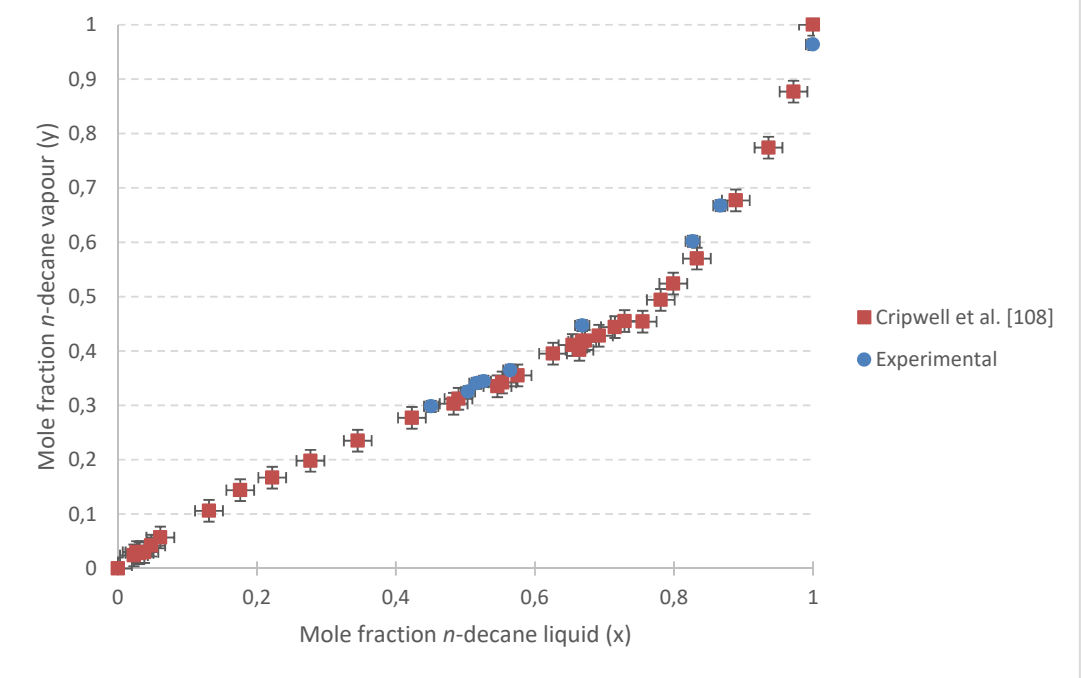

Figure 3.18: x-y plot for the *n*-decane/2-heptanone reference system at 40 kPa [108]

Further verification of the setup was done using the similar *n*-decane/3-heptanone binary system at 40 kPa [108]. The experimentally obtained data and that of Cripwell *et al.* for the *n*-decane/3-heptanone system at 40 kPa are shown in Figures 3.19 and 3.20 [108]. Error bars shown for the experimental data are +/- 0.32 K for temperature and +/- 0.0102 mole fraction for composition. Error bars for the reference data are as per the original source [108]. This data set has also passed both the L/W and McDermott-Ellis consistency tests. As it can be seen in Figure 3.19, the data are in agreement and are within the error bars. Figure 3.20 shows the x-y plot for this system comparing the experimental data and that of Cripwell *et al.*, further illustrating the agreement in data.

The third sub-atmospheric reference system of *n*-nonane/1-pentanol at 40 kPa is shown in Figures 3.21 and 3.22. The figures show good agreement between the experimentally obtained data and that of Ferreira [109]. Error bars displayed are +/- 0.32 K for temperature and +/- 0.0102 mole fraction for composition. Furthermore, the data obtained for this system has passed both the L/W and McDermott-Ellis consistency tests.

Lastly, vapour pressure data for the compounds *n*-decane, 2, heptanone, 3-heptanone, *n*-nonane and 1-pentanol was not measured as their pure component boiling points matched that of literature at 40 kPa.

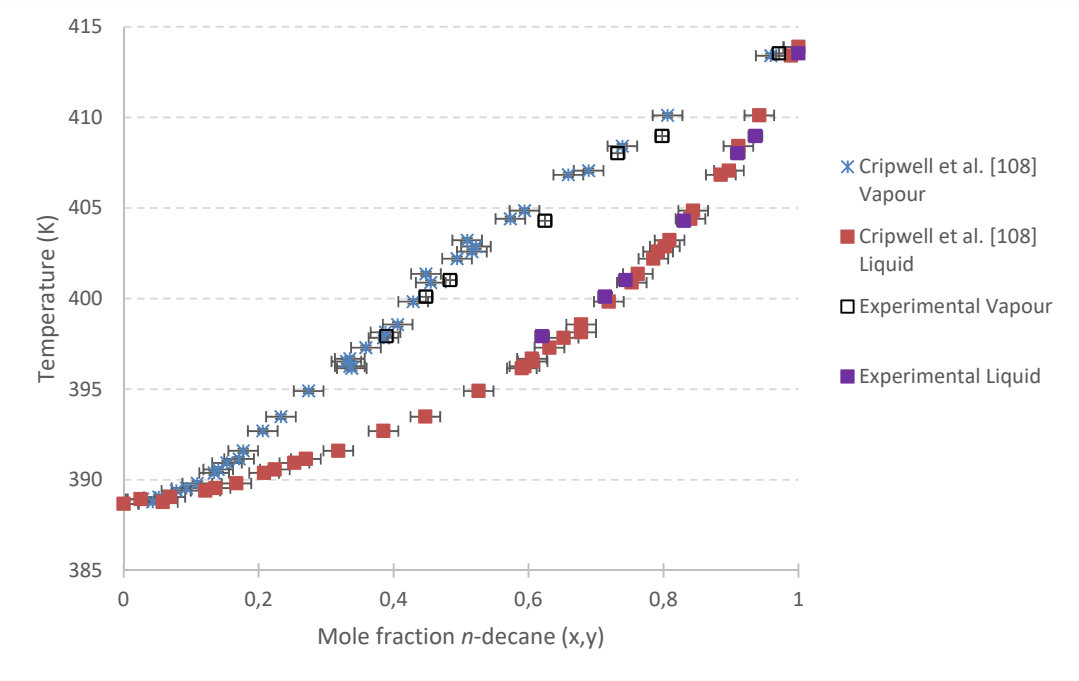

Figure 3.19: Temperature-composition diagram for the *n*-decane/3-heptanone reference system at 40 kPa with error bars [108].

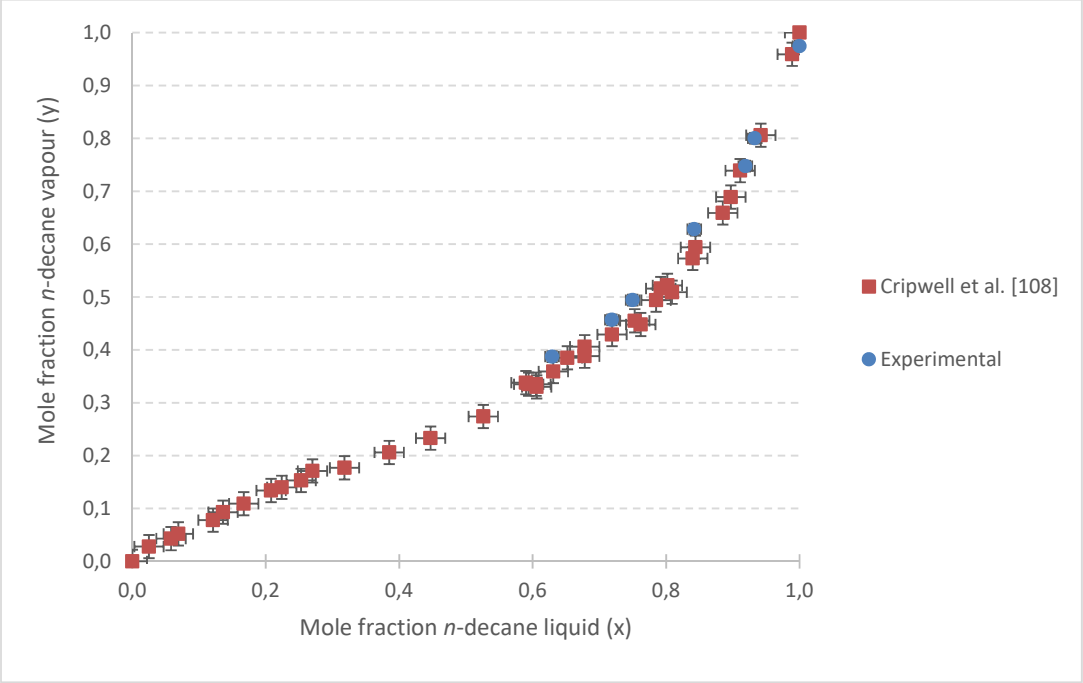

Figure 3.20: x-y plot for the *n*-decane/3-heptanone reference system at 40 kPa with [108]

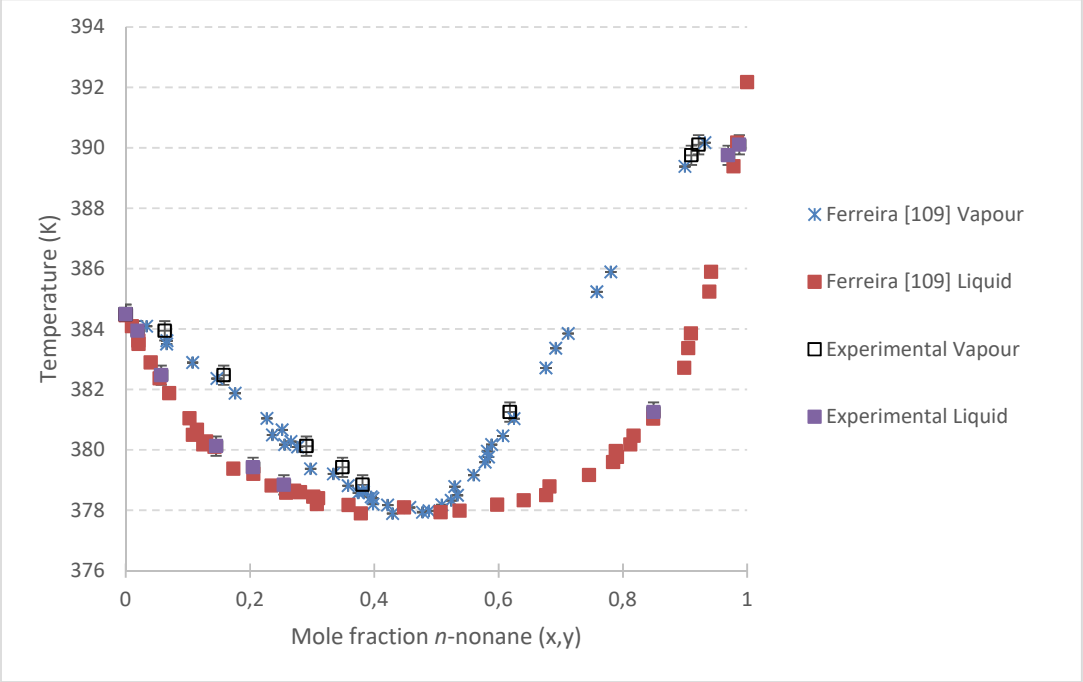

Figure 3.21: Temperature-composition diagram for the *n*-nonane/1-pentanol reference system at 40 kPa showing good agreement between experimental and reference data [109]

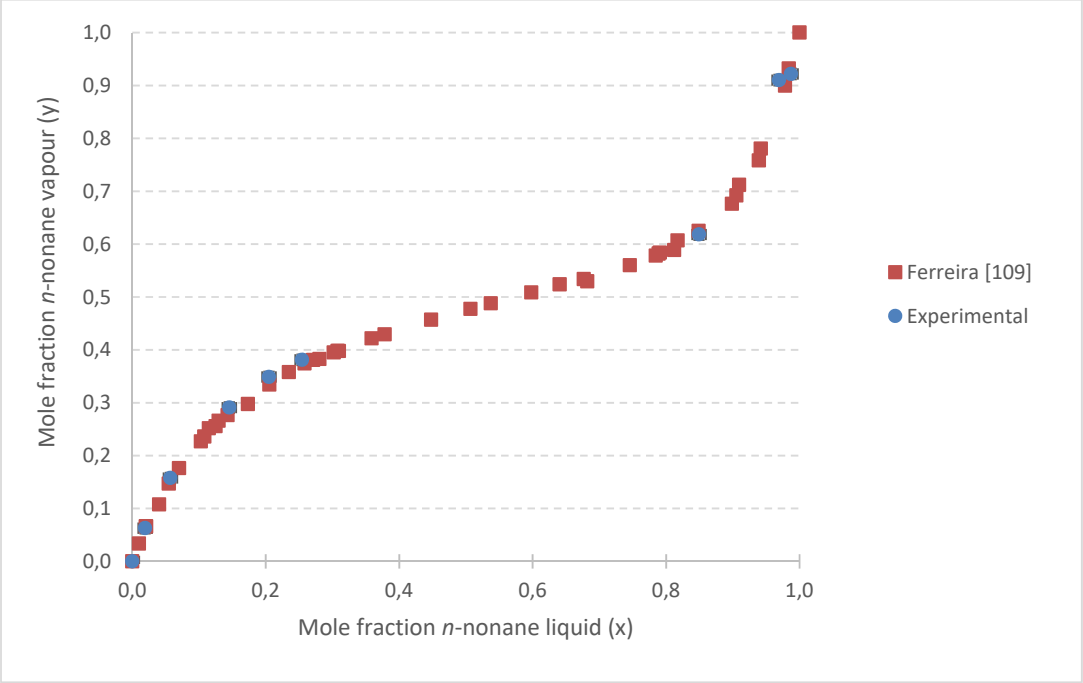

Figure 3.22: x-y plot for the *n*-nonane/1-pentanol reference system at 40 kPa with error bars [109]

The verification trials performed showed that the constructed setup could provide accurate and reliable temperature and pressure measurements within the whole range of it's specification. The trials also showed that additional requirements for the setup such as accurate sample capturing and analysis (in terms of the method) were repeatable as well. This therefore confirmed the successful fulfilment of the first objective in this project.

4. Results and discussion: Experimental measurements

This chapter focuses on the second objective in this study, obtaining VLE data at sub-atmospheric pressures for the compounds limonene, *p*-cymene, indane, butylbenzene and 1,2,3-trimethylbenzene. As such, the chapter discusses the experimental design approached and follows with the results obtained, thereafter discussing them.

4.1 Experimental design

4.1.1 Materials

As mentioned previously, the purity of compounds used in this study was one of high importance. However, pure fractions (>98 wt. %) of indane and 1,2,3-trimethylbenzene could not be obtained. Supplier details and assays of the chemicals used for experiments in this project are presented in Table 4.1.

Table 4.1: Chemicals used in this project together with assay and supplier name

Chemical	Supplier	CAS #	Assay (wt. %)
Toluene	Sigma-Aldrich	108-88-3	99.89*
α-Pinene	Sigma-Aldrich	7785-70-8	98.86*
Limonene	Sigma-Aldrich	5989-27-5	98.38*
p-Cymene	Sigma-Aldrich	99-87-6	98.97*
Butylbenzene	Sigma-Aldrich	104-51-8	98.97*
Indane	Shanghai Terppon Chemical	496-11-7	95.86*
1,2,3-Trimethylbenzene	Shanghai Terppon Chemical	526-73-8	80.51*

* - As per in-house GC and KF analysis

4.1.2 Experimental plan

All experiments were run at a fixed sub-atmospheric pressure of 40 kPa. The data was obtained in the form of equilibrium mole fractions of the liquid and vapour phases at a range of equilibrium temperature values between the boiling points of each of the pure components at 40 kPa. Table 4.2 shows the binary systems measured and their operation pressures. An additional

quarternary system at 40 kPa comprising limonene, 1,2,3-trimethylbenzene, *p*-cymene and indane was measured as well.

Table 4.2: Binary systems measured for this study

System	Compound 1		Compound 2		System Pressure
(order)	Name	BP (K) [59]	Name	BP (K) [59]	(kPa)
1	Limonene	449.65	*p*-Cymene	450.28	40
2	Limonene	449.65	Butylbenzene	456.46	40
3	*p*-Cymene	450.28	Butylbenzene	456.46	40
4	Limonene	449.65	Indane	451.12	40

The experimental methodology followed was of that explained in Section 3.4. In summary, pure component would be loaded into the equilibrium still and run until its equilibrium data and samples could be taken. The medium inside the still would then be loaded with small amounts of the second component to reach the next equilibrium point.

At the end of a run, the process would be stopped and the setup cleaned and dried in preparation for the next run. The next run would commence with the still being loaded with concentrations of the next desired data point. This procedure would be repeated and would ultimately provide a full set of data and samples which were then analysed and tested for thermodynamic consistency.

During the verification process, a discoloration in the compounds during operation lead to the suspicion that the compounds of concern in this study were undergoing structural degradation during operation due to their exposure to light, oxygen and mainly heat [106]. It was therefore decided to minimise the effects of oxygen as it was most tangible since the effects of light and heat were unavoidable.

Therefore, prior to each experiment, the still was purged with high purity Afrox Baseline® Argon gas (99.999 wt. %) for about 30 minutes while opening a valve in the upper part of the still. This would help purge the oxygen in the system as Argon has a higher density than that of air. The vacuum pump was then switched on, taking the still to the desired pressure (40 kPa), after which feed would be added.

Furthermore, degradation tests were conducted on each mixture planned and a summary of the results are provided in the next sub-section. The tests indicated that a maximum run time of 4 hours was suitable before the compounds started to degrade [106]. Therefore, each experiment

was run for a maximum of 4 hours at a time. This meant that two data points were collected per day due to the operation requiring at least 1 hour to achieve equilibrium.

4.1.3 Degradation trials

As mentioned previously, the compounds of concern were suspected of undergoing degradation [106]. Although compound degradation was not the cause for being unable to obtain VLE data within acceptable deviation for the limonene/*α*-pinene binary system at 40 kPa, visual degradation of the compounds after prolonged use was noticed. A discoloration from clear to yellowish was noticed in all compounds after ~8 hours of operation. Figure 4.1 illustrates the typical discoloration of limonene after ~10 hours of operation. Degraded compounds were also analysed for purity using a GC FID and peaks eluting in addition to those for the pure compounds were noticed.

In order to quantify the degradation taking place in a single binary system, degradation trials were run at 40 kPa under an Argon environment. A 100 mL feed mixture of a fixed feed concentration was used to start up the still. Once equilibrium was reached in each experiment, samples were taken regularly and the times recorded. Figures 4.2 and 4.3 illustrate the degradation for the limonene/*p*-cymene binary system at 40 kPa in terms of temperature and composition respectively. Similar results were obtained for all systems tested. The complete results of all degradation tests can be found in Appendix H. Figures 4.2 and 4.3 show that an operation time of 6 hours would be acceptable, however, a maximum operation time of 4 hours was chosen for each system obtained. In addition to the figures, compound analysis showed the elution of significant extra peaks after roughly 8 – 9 hours of operation, confirming the degradation taking place.

Figure 4.1: Discoloration of limonene after ~10 hours of operation indicating degradation

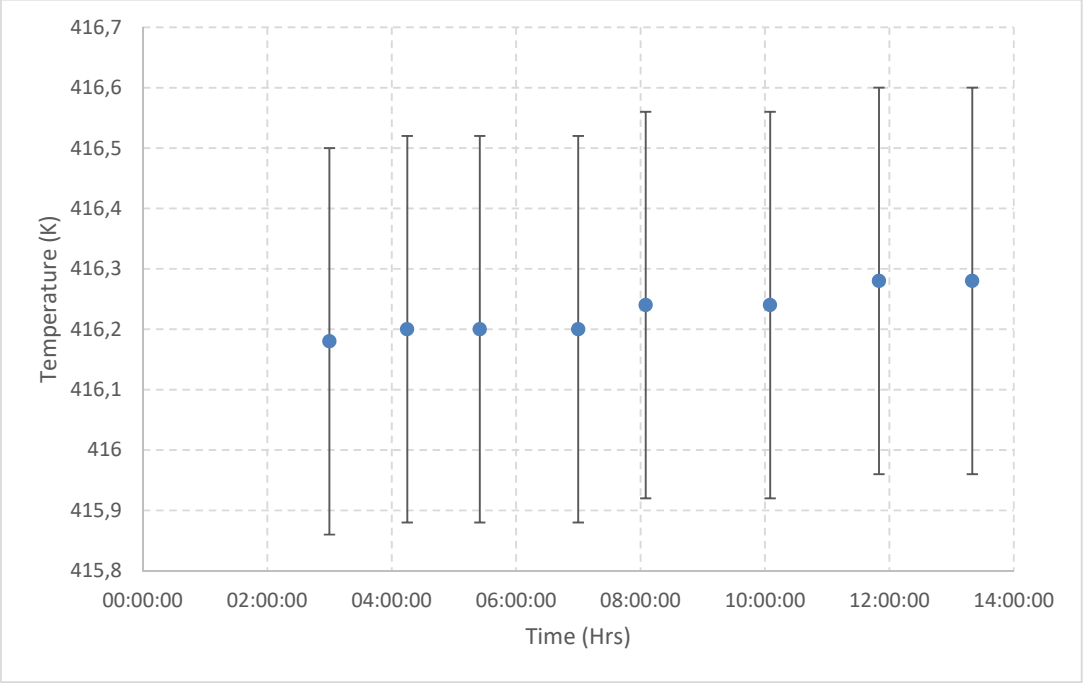

Figure 4.2: Temperature degradation profile for limonene/*p*-cymene system at 40 kPa with +/- 0.32 K error bars illustrating negligible drift within 6 hours of operation

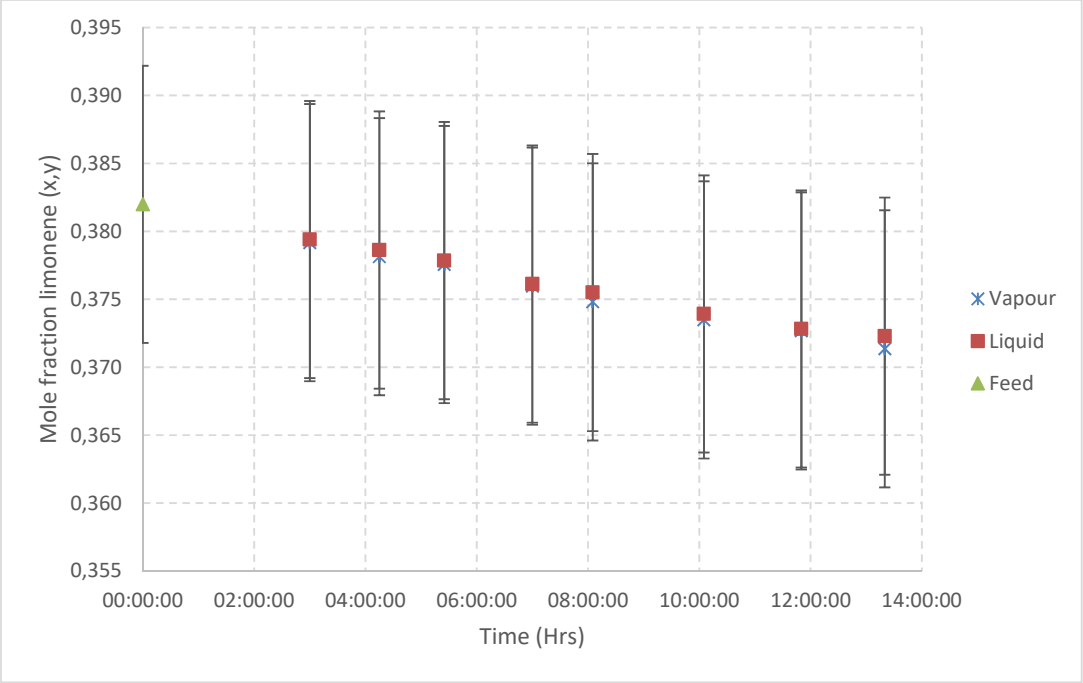

Figure 4.3: Concentration degradation profile for limonene/*p*-cymene system at 40 kPa with +/- 0.0102 mole fraction error bars illustrating reasonable drift within 6 hours of operation

4.2 Experimental results

The experimental results for the systems limonene/*p*-cymene, limonene/butylbenzene, *p*-cymene/butylbenzene, limonene/1,2,3-trimethylbenzene/*p*-cymene/indane and limonene/indane are presented in this section. Additionally, vapour pressure data collected for limonene, *p*-cymene and butylbenzene can be found in Appendix G. The actual VLE data for all the systems can be found in Appendix J together with details of the consistency tests.

All the data sets obtained pass the point-to-point consistency test of McDermott-Ellis, however fail the L-W consistency tests. This could be due to the fact that there is little to no separation between the components in each system. It could also be due to the fact that the boiling points across the composition range for some systems are within the confines of the error bars and that there is barely any difference between the respective pure component boiling points for those systems.

4.2.1 Limonene/*p*-cymene

The measured data for the system limonene/*p*-cymene at 40 kPa can be found in Figures 4.4 to 4.6. Figure 4.4 shows the temperature-composition diagram illustrating negligible separation between the two components at 40 kPa. There is however, slight separation within the 0.50 – 0.90 mole fraction limonene range, with an average relative volatility of less than 1.04 for *p*-cymene in this region.

Figure 4.4 also indicates the possibility of a homogenous azeotrope at about 0.25 – 0.30 mole fraction limonene and at ~416.2 K. This is however difficult to see due to the large temperature error relative to the narrow temperature range. The temperature and composition error bars, are +/- 0.32 K and +/- 0.0102 mole fraction respectively. Figure 4.5 further illustrates that there is barely any separation between these two components at this pressure. Figure 4.6 shows the (y-x) vs x plot, also indicating a strong possibility of an azeotrope, although this is difficult to confirm due to the error bars crossing over the horizontal axis throughout the composition range.

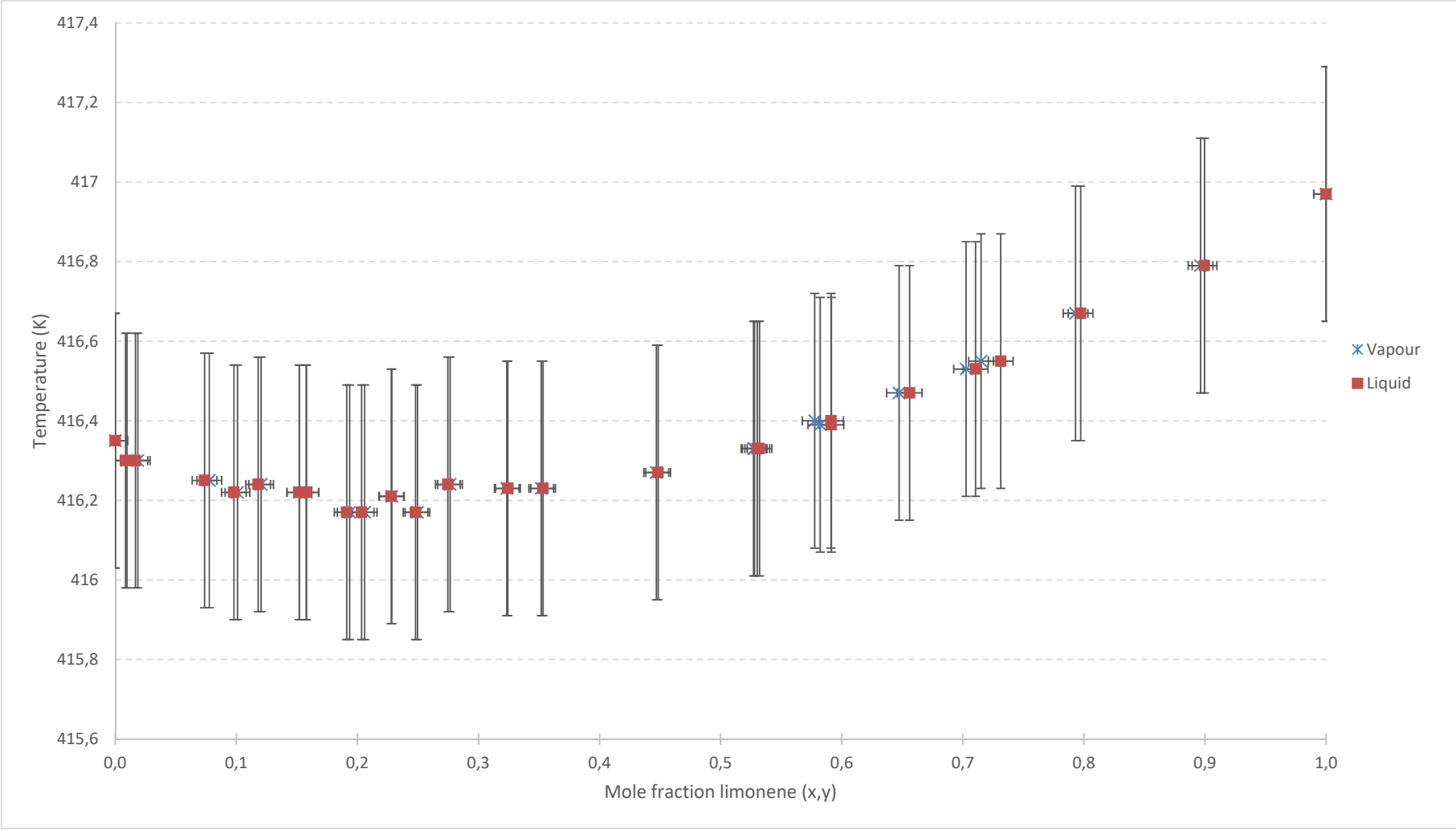

Figure 4.4: Temperature-composition diagram for limonene/*p*-cymene binary system at 40 kPa

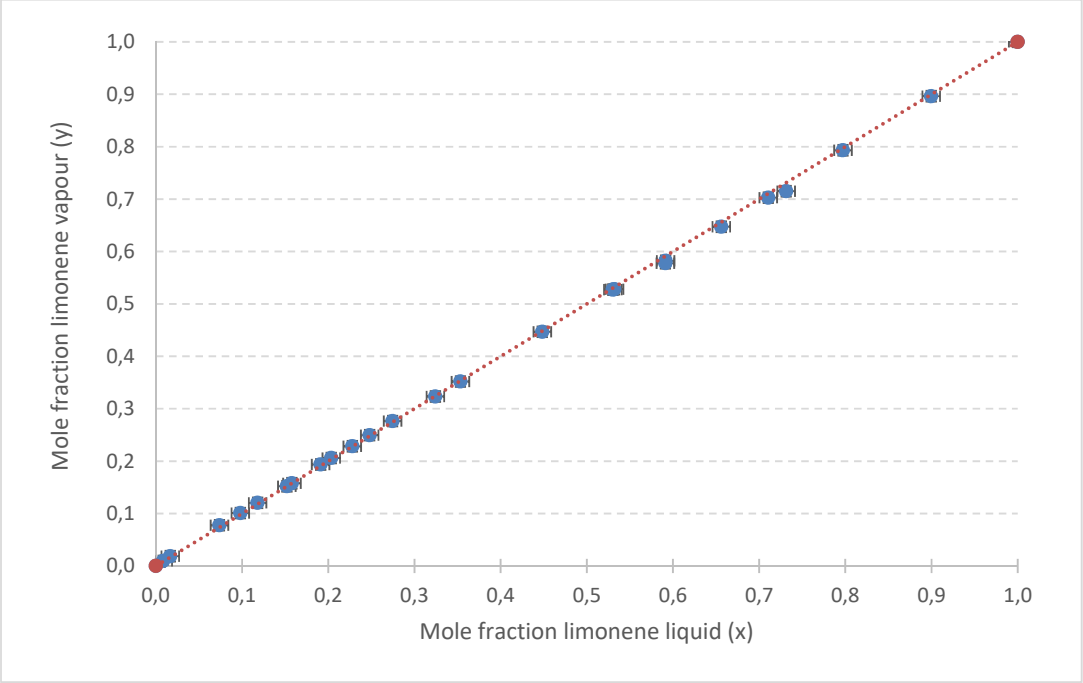

Figure 4.5: x-y plot for the limonene/*p*-cymene binary system at 40

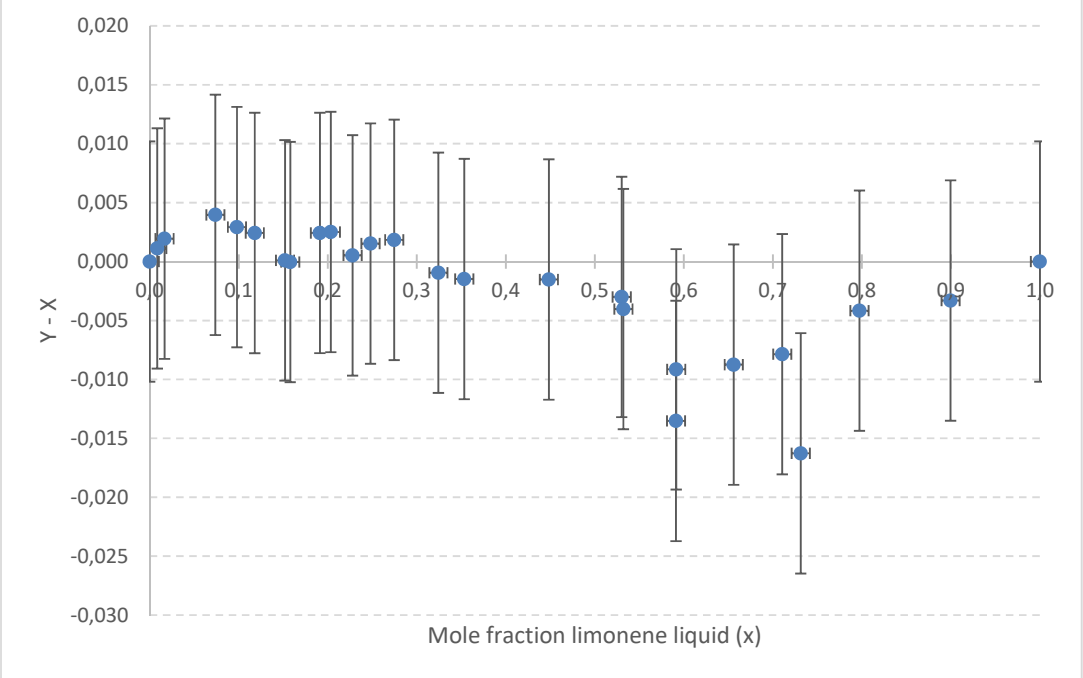

Figure 4.6: (y-x) vs x plot for the limonene/*p*-cymene binary system at 40 kPa

4.2.2 Limonene/butylbenzene

During experiments for the limonene/butylbenzene binary system at 40 kPa, strange data was noticed, as shown in Figure 4.7.

The temperature composition data obtained at the extremes of the concentration ranges had regular trends, however data within the ~0.20 mole fraction and ~0.70 mole fraction limonene regions of the composition range experienced a significant temperature drop much larger than value of the error bar.

Accurate temperature and pressure measurements and composition data were however obtained and verified with various sources to ensure that reliable data was being collected [109]. This lead to trials on the additional Pilodist VLE 100 vapour-liquid equilibrium setup in our department being conducted, which resulted in much more regular data as can be seen in Figure 4.7. The Pilodist VLE 100 setup functions in the same way as the current setup with vapour and liquid recirculation employed.

An initial explanation for the weird phenomena was that a two-phase liquid-liquid equilibrium region could be forming due to differences in physical properties between the limonene and butylbenzene. In order to verify this, measurements of density and surface tension of the two compounds as well as *p*-cymene (as will be seen in the following sub-section) were taken using a KSV Sigma 702 Tensiometer. The results are shown in Table 4.3 and conversely show minimal differences between butylbenzene's density and surface tension and limonene and *p*-cymene's density and surface tension. This was therefore not the cause. It should however be noted that this data was measured at atmospheric conditions.

Table 4.3: Density and surface tension measurements for limonene, *p*-cymene and butylbenzene highlighting minimal differences in physical properties between the compounds

	ρ (g/cm^3)	Surface Tension (mN/m)
Limonene	0.8395	27.96
Limonene/ butylbenzene	0.8435	28.29
Butylbenzene	0.8538	28.97
p-Cymene /butylbenzene	0.8523	28.35
p-Cymene	0.8519	27.93

The actual reason therefore, could be because there is insufficient mixing taking place between the mixing chamber and the heating chamber for this system. This reason is compounded by the fact that boiling for this system as well as the next was irregular such that sudden

evaporation of the feed was noticed at times coinciding with drops in the vapour temperature. A similar phenomenon was noticed in literature by other researchers while quantifying vapour-liquid-liquid equilibrium experiments [71, 115]. High oscillations in temperature of ~2 K were noticed at concentrations of ~0.20 mole fraction and ~0.70 mole fraction limonene in this system. Similar temperature oscillations were noticed in the next system as well.

The result is that hot and cold regions are forming within the heating chamber, leading to “cold layer” and a “hot layer”. Once the hot layer is bubbled through the Cottrell tube, the cold layer requires heating but is not sufficiently heated to be at the same temperature. By this time the bubbles formed are already pumping the previously cold layer through the Cottrell tube. There is a high possibility that this layer would not have reached the equilibrium temperature and is therefore not at equilibrium. In order to overcome these issues therefore, a modification of the setup would be required, such as merging the mixing and heating chambers into one chamber, as this would eliminate the possibility of hot and cold regions forming by providing better mixing. The high oscillations in temperature could also be linked to superheating due to lack of mixing, which would also be rectified by merging the mixing and heating chambers to provide better mixing.

The experiments for the two systems involving butylbenzene were therefore conducted on the Pilodist setup [61]. The new data obtained on the Pilodist setup is shown in Figure 4.7 and illustrates better separation compared to the limonene/*p*-cymene system at 40 kPa. This was expected since there is a larger difference in boiling points of the pure components. Figures 4.8 and 4.9 display the x-y and (y-x) vs x plots for this system, respectively. Figure 4.8 illustrates the marginally better separation compared to the previous system, however relative volatility is generally below 1.3 for limonene throughout the entire composition range. No azeotrope is present for this system at 40 kPa and Figure 4.9 confirms this.

Error bars for this system remain as +/- 0.0102 mole fraction for composition and +/- 0.32 K for temperature for both the original data and the new data. For the temperature uncertainty, fluctuations in temperature and pressure during measurement amounted to +/- 0.06 K and a calibration offset of +/- 0.1 K was noted, adding up to +/- 0.16 K, which becomes +/- 0.32 K after multiplying with a coverage factor of 2. When these relatively large error bars are taken into account, the overlap in data between the original data and new data, at the extremes of the composition range, can be visualised.

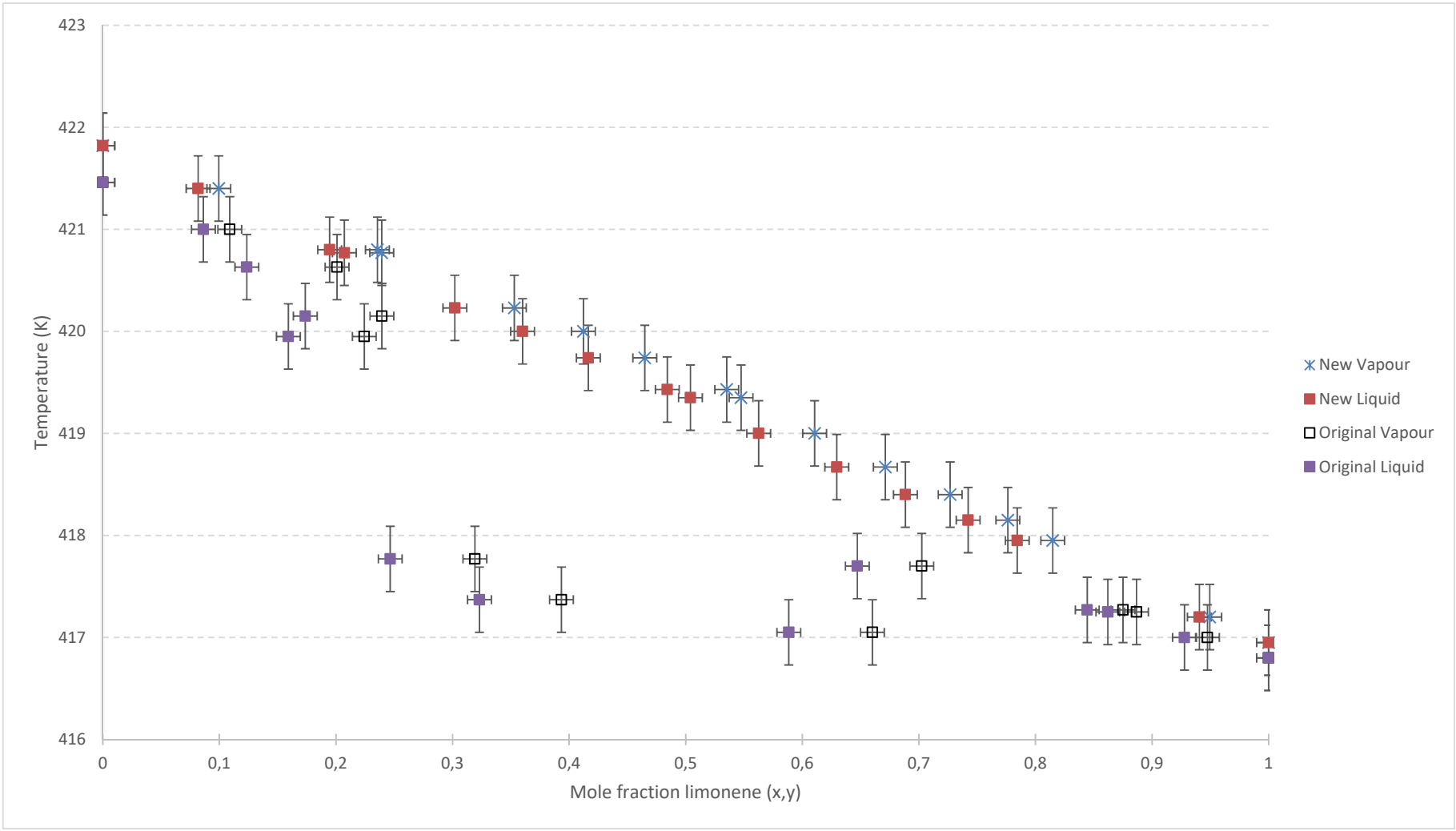

Figure 4.7: Temperature-composition diagram for limonene/butylbenzene binary system at 40 kPa

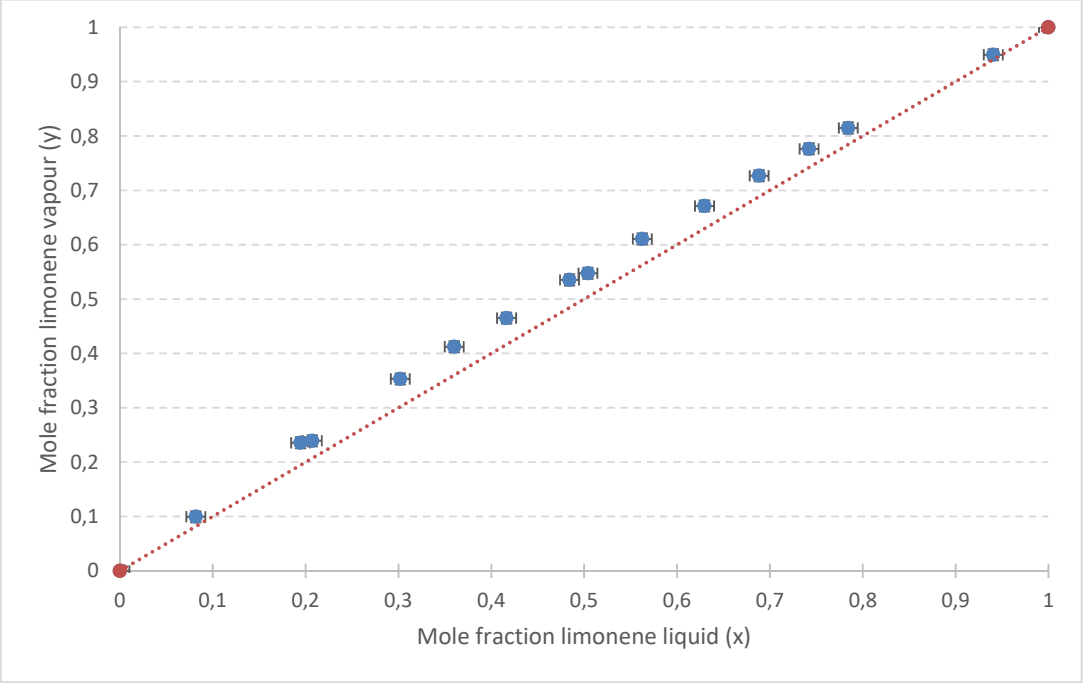

Figure 4.8: x-y plot for the limonene/butylbenzene binary system at 40 kPa

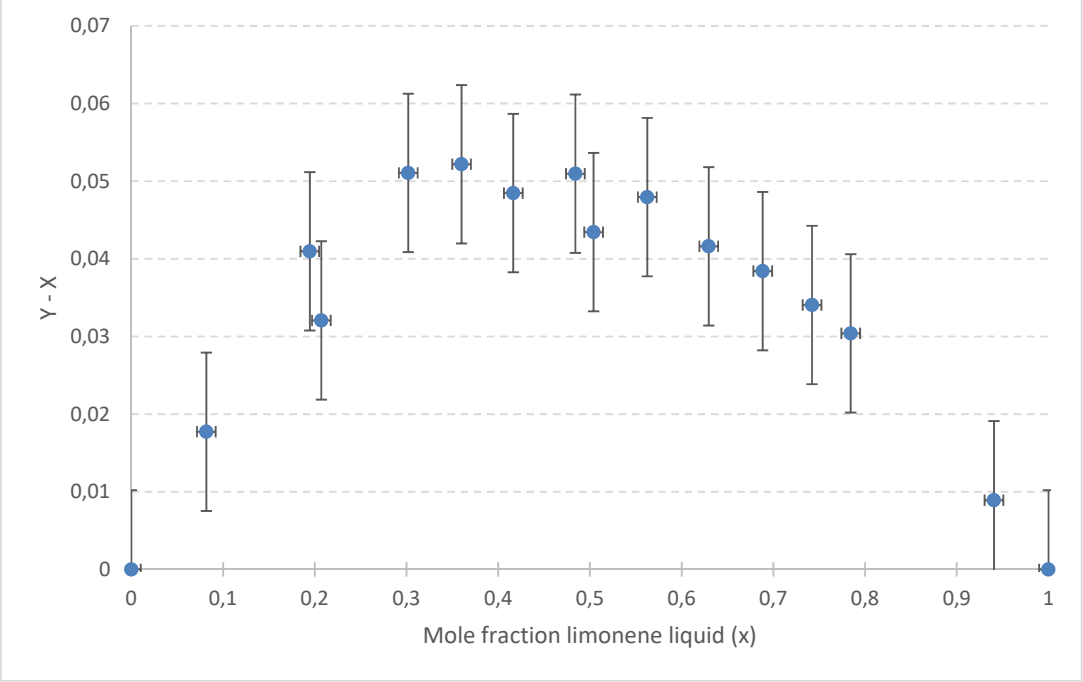

Figure 4.9: (y-x) vs x plot for the limonene/butylbenzene binary system at 40 kPa

4.2.3 *p*-Cymene/butylbenzene

The same irregular behaviour in data collected for the limonene/butylbenzene binary system at 40 kPa was noticed in the *p*-cymene/butylbenzene binary system at 40 kPa. Trials were therefore shifted to be conducted on the Pilodist VLE setup just as in the previous system [61]. The results obtained are shown in Figures 4.10 to 4.12.

When the error bars are taken into account in Figure 4.10 at the extremes of the composition range, the overlap in data between the original data and new data can be visualised. Once again, the error bars for this system remain as +/- 0.0102 mole fraction for composition and +/- 0.32 K for temperature for both the original data and the new data.

The same explanation that hot and cold regions could be forming is maintained to explain the irregular data obtained for this system. Temperature oscillations of ~2 K were noticed at concentrations of ~0.20 mole fraction and ~0.70 mole fraction *p*-cymene in this system, just as in the previous system. As shown in Table 4.3, there are little to no differences in physical properties between *p*-cymene and butylbenzene.

Figures 4.10 and 4.11 nevertheless show that separation data as good as the previous system, with relative volatility generally being below 1.3 for *p*-cymene throughout the entire composition range, is obtained in the current *p*-cymene/butylbenzene system at 40 kPa. This was expected due to the similar temperature range relative to the other systems. Figures 4.10 and 4.12 confirm the absence of any azeotrope in this system at 40 kPa.

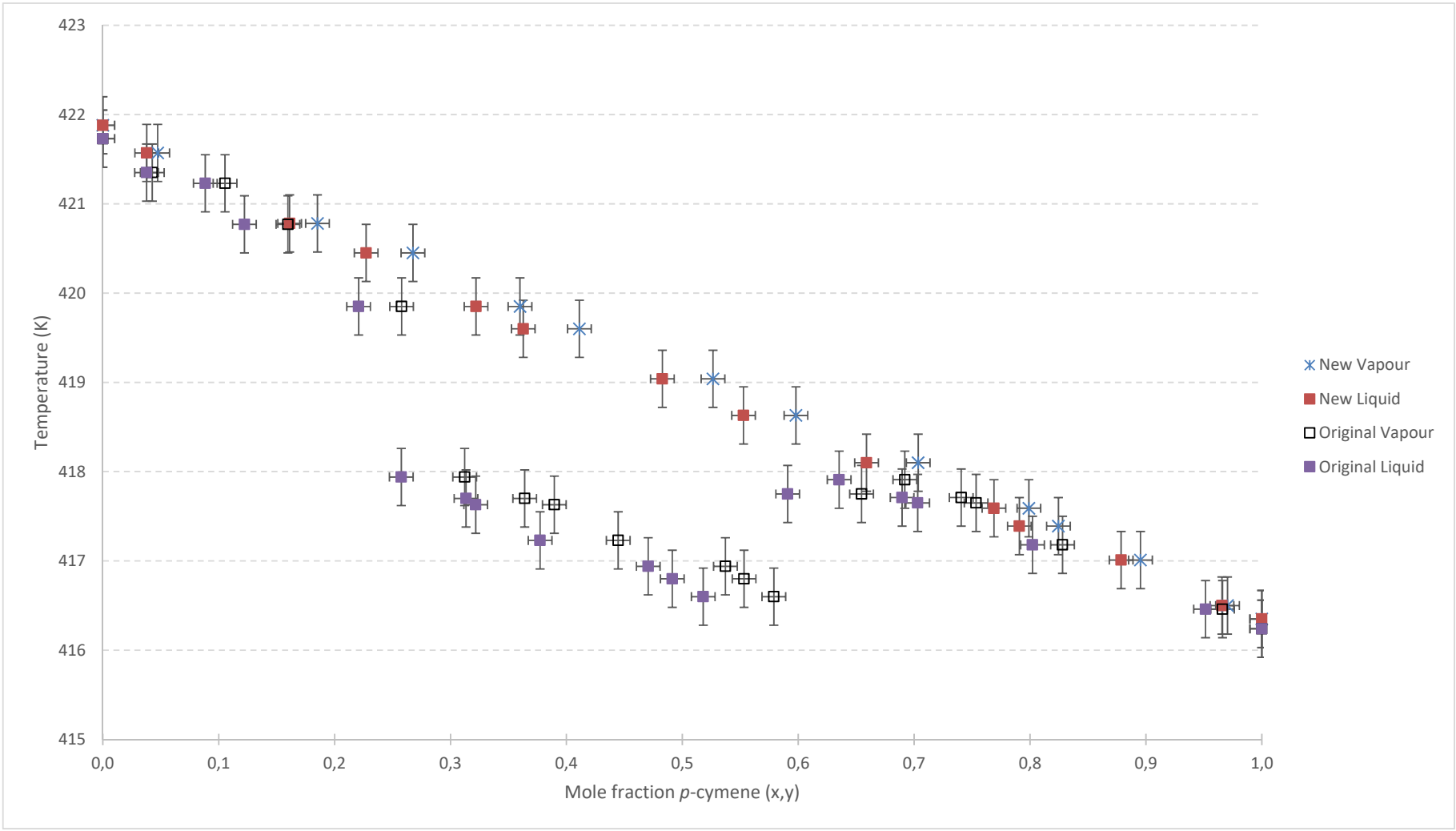

Figure 4.10: Temperature-composition diagram for *p*-cymene/butylbenzene binary system at 40 kPa

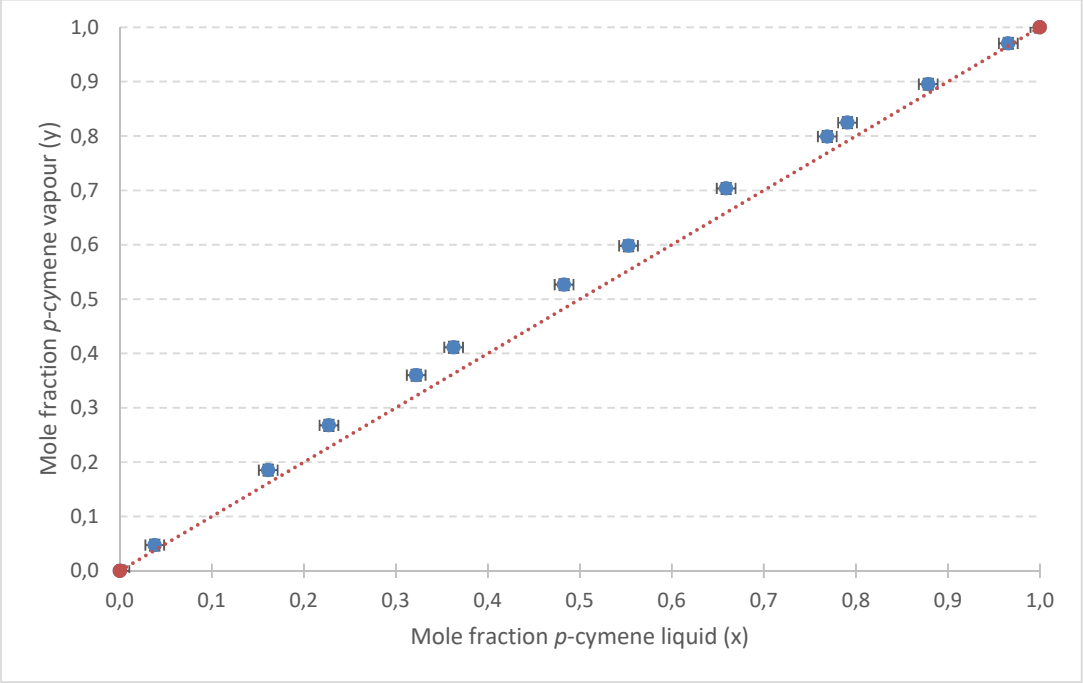

Figure 4.11: x-y plot for the *p*-cymene/butylbenzene binary system at 40 kPa

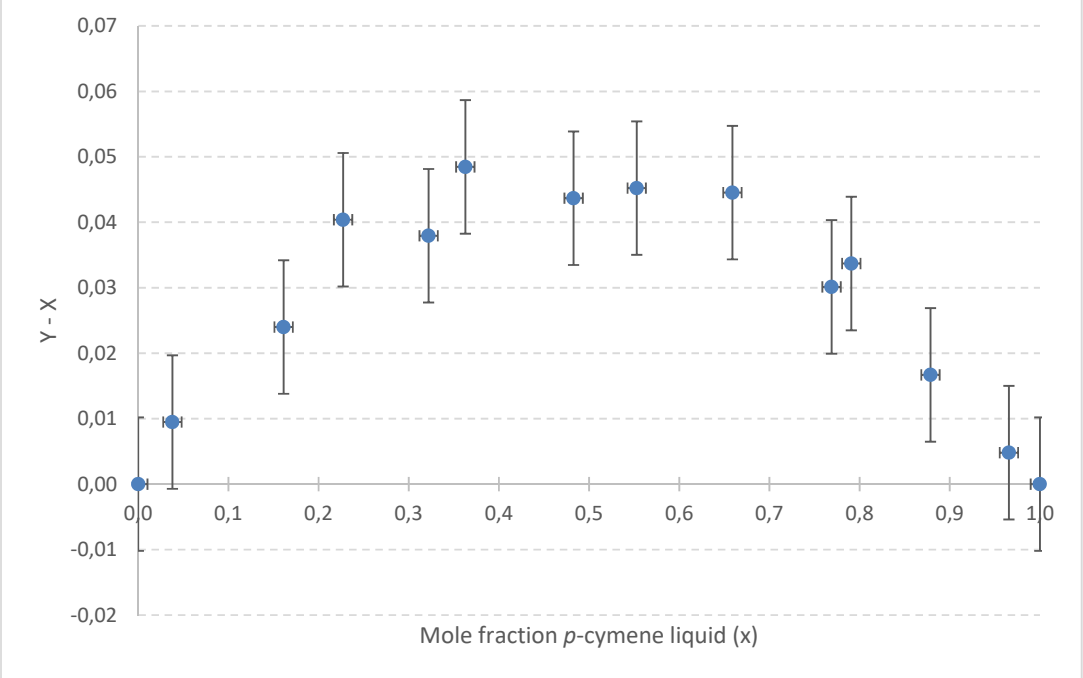

Figure 4.12: (y-x) vs x plot for the *p*-cymene/butylbenzene binary system at 40 kPa

4.2.4 Limonene/indane

A shortcoming for this system was that a pure fraction of indane (>98 %) could not be procured. The indane sample procured was quantified to be 95.89 wt. % pure according to in-house GC-MS analysis, as shown in Table 4.4. The main impurity noticed was benzonitrile, which would have affected the temperature and composition measurements in the indane region of the composition range. Therefore, data could not be obtained for the entire composition range, but rather from pure limonene up until ~0.25 mole fraction limonene.

Table 4.4: Composition of indane sample procured as feed

Compound	Composition (wt. %)
Indane	95.89
Benzonitrile	2.77
1-ethyl-2,3-dimethylbenzene	0.70
1-propynylbenzene	0.64

The measured data for the system limonene/indane at 40 kPa can be found in Figures 4.13 to 4.15. Figure 4.13 shows the temperature-composition diagram illustrating negligible separation between the compounds at 40 kPa. Slight separation between the two compounds can be noticed between 0.6 mole fraction and 1.0 mole fraction limonene of the composition range, with relative volatility generally being below 1.1 for indane in this region. Slight separation below ~0.5 mole fraction limonene of the composition range can also be noticed.

Figure 4.13 also shows that a homogenous azeotrope is present. The temperature point of the azeotrope is ~415.9 K, this is however difficult to visualise due to the large temperature error relative to the narrow temperature range. The error bars being +/- 0.32 K for temperature and +/- 0.0102 mole fraction for composition. The azeotrope is confirmed by Figure 4.15 where the data tends to cut the horizontal axis at ~0.55 mole fraction limonene. Figure 4.14 simply emphasises the fact that there is generally little to no separation between these two compounds at 40 kPa.

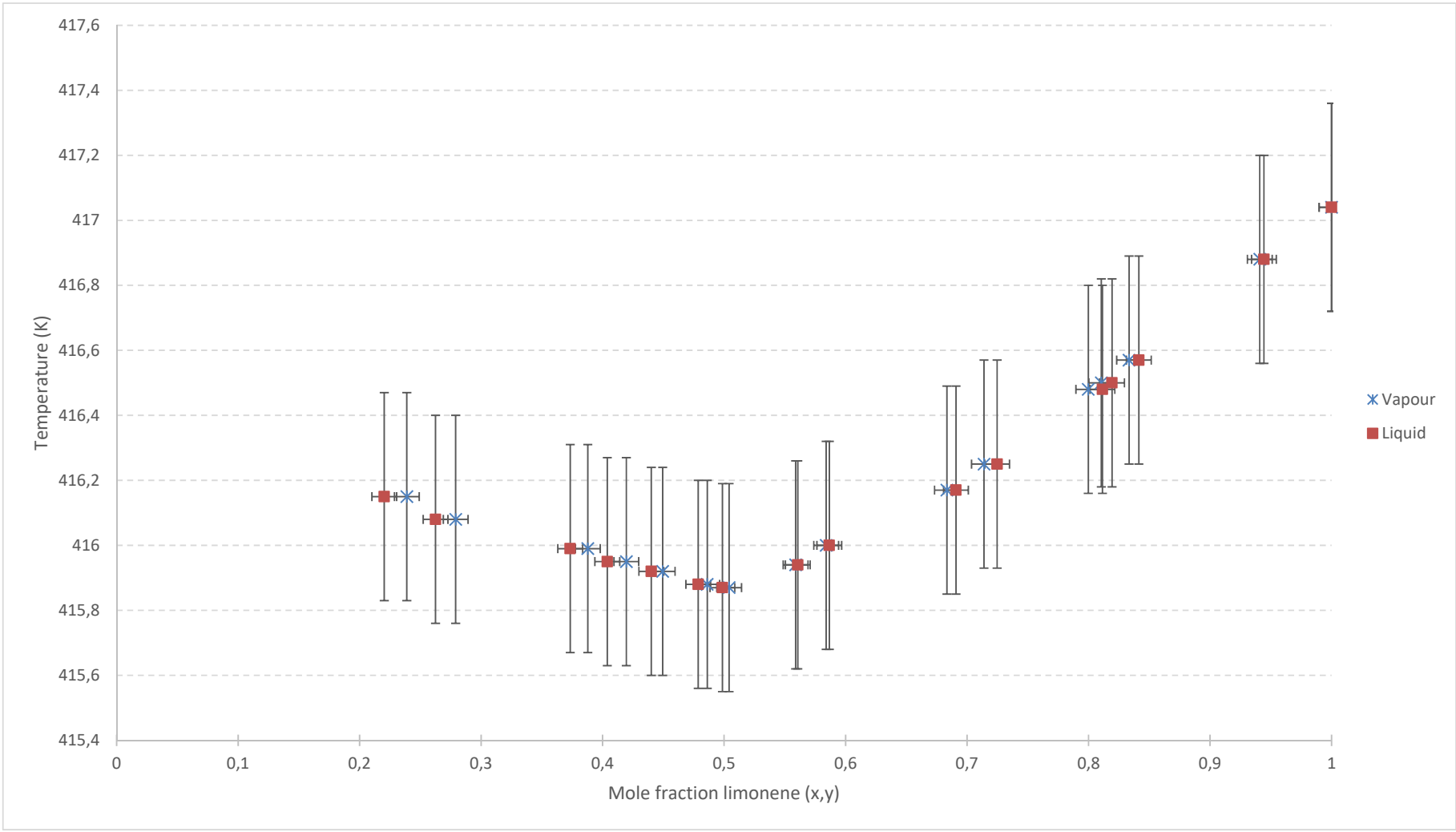

Figure 4.13 Temperature-composition diagram for limonene/indane binary system at 40 kPa

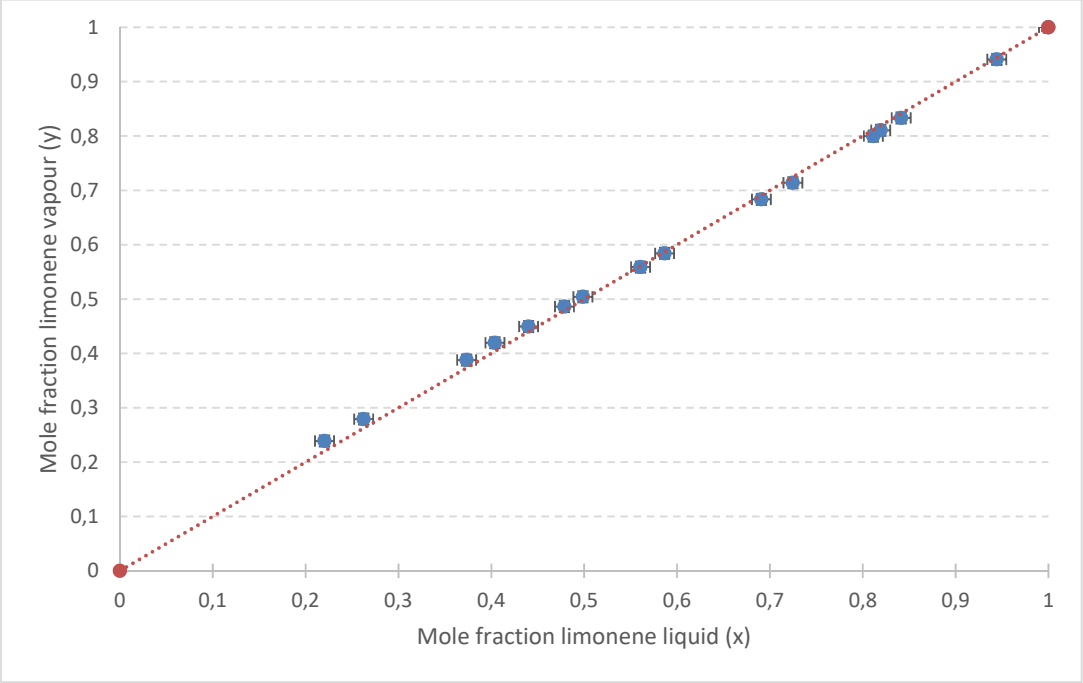

Figure 4.14: x-y plot for the limonene/indane binary system at 40 kPa

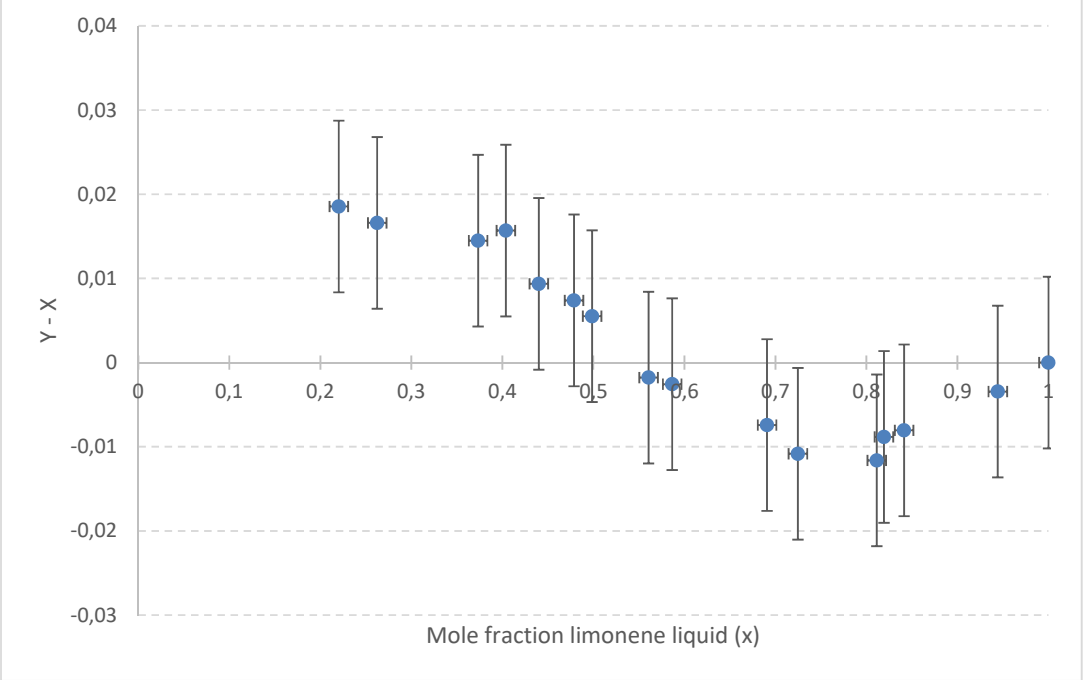

Figure 4.15: (y-x) vs x plot for the limonene/indane binary system at 40 kPa

4.2.5 Limonene/1,2,3-trimethylbenzene/*p*-cymene/indane

A pure fraction of 1,2,3-trimethylbenzene (>98 %) could not be procured either. Fortunately however, the main impurities of the 1,2,3-trimethylbenzene procured were *p*-cymene and indane in the proportions listed in Table 4.5. The sample was quantified using in-house GC-MS analysis.

Table 4.5: Composition of 1,2,3-trimethylbenzene sample procured as feed

Compound	Composition (wt. %)
1,2,3-Trimethylbenzene	80.53
Indane	15.25
p-cymene	3.71
o-cymene	0.50

Therefore, data for a quarternary VLE system could be obtained. The data collected for this system is shown in Table 4.6.

The partition coefficients for the respective components (*K*-values) and relative volatilities (α) indicate that 1,2,3-trimethylbenzene would theoretically be the easiest to separate out of this mixture, however, this is due to the fact that it has the lowest normal boiling point. Furthermore, the minimal differences in *K*-values also indicate that it would be very difficult to realise separation on an industrial scale.

The same uncertainty of +/- 0.32 K for temperature and +/- 0.0102 mole fraction for composition apply to this system. The compositional error encapsulates the fluctuations noted with regard to the partition coefficients and relative volatilities, as presented in Table 4.6.

Table 4.6: Temperature-composition, partition coefficient (K_i) and relative volatility (α_{ij}) data for the quarternary system of limonene(1)/1,2,3-trimethylbenzene(2)/*p*-cymene(3)/indane(4) at 40 kPa

T (K)	x_1	x_2	x_3	x_4	y_1	y_2	y_3	y_4	$K_{limonene}$	$K_{1,2,3\text{-}trimeth}$	K_{cymene}	K_{indane}	$\alpha_{lim/tri}$	$\alpha_{lim/cym}$	$\alpha_{lim/ind}$
415.40	0.251	0.618	0.013	0.118	0.250	0.620	0.013	0.117	0.994	1.004	0.990	0.991	0.990	1.004	1.003
415.47	0.294	0.583	0.012	0.111	0.291	0.587	0.012	0.110	0.990	1.007	0.967	0.991	0.983	1.025	0.999
415.56	0.351	0.536	0.011	0.102	0.347	0.540	0.011	0.102	0.989	1.008	0.991	0.999	0.982	0.998	0.989
415.67	0.400	0.490	0.016	0.095	0.395	0.500	0.010	0.095	0.987	1.020	0.633	1.009	0.967	1.559	0.978
415.72	0.432	0.464	0.014	0.090	0.423	0.470	0.016	0.091	0.979	1.013	1.146	1.009	0.966	0.854	0.970
415.90	0.503	0.402	0.016	0.079	0.493	0.412	0.015	0.080	0.981	1.023	0.978	1.009	0.959	1.003	0.972
416.05	0.585	0.335	0.014	0.065	0.573	0.345	0.015	0.067	0.979	1.028	1.040	1.031	0.952	0.941	0.950
416.19	0.656	0.275	0.014	0.055	0.645	0.286	0.013	0.056	0.984	1.038	0.932	1.018	0.948	1.055	0.967
416.20	0.673	0.262	0.013	0.052	0.658	0.274	0.014	0.054	0.978	1.042	1.097	1.046	0.938	0.891	0.935
416.40	0.757	0.190	0.013	0.041	0.747	0.202	0.011	0.040	0.987	1.063	0.858	0.995	0.929	1.151	0.992
416.63	0.870	0.110	0.000	0.021	0.859	0.119	0.000	0.022	0.987	1.084	-	1.085	0.911	-	0.910
416.77	0.945	0.045	0.000	0.010	0.936	0.053	0.000	0.011	0.991	1.170	-	1.130	0.847	-	0.876
416.89	1.000	0.000	0.000	0.000	1.000	0.000	0.000	0.000	1.000	-	-	-	-	-	-

4.3 Discussion

This section summarises the discussions related to the degradation trials, consistency of data obtained and interpretation of the VLE data obtained.

The degradation trials in this study limited the operation time to 4 hours per run for each experiment. This means that any industrial process, operating at 40 kPa or below, will have a maximum residence time of 4 hours. Although this is more than sufficient for process equipment such as distillation columns, it should be noted that this residence time applies to all high temperature process operations, i.e. pyrolysis reactor, condenser, distillation column, piping, etc.

All measured data passed the thermodynamic consistency test of McDermott-Ellis. However, all the data conversely fail the L/W consistency test. This could be due to the fact that there is little to no separation between the components in each system. It could also be due to the fact that the boiling points across the composition range for some systems are within the confines of the error bars and that there is barely any realistic difference between the respective pure component boiling points for those systems. Furthermore, although the parameters used in calculating the L/W consistency test were obtained from a very reliable source, the accuracies of these parameters (generally below 5 %) could contribute to the data failing the L/W test. Nevertheless, this does raise slight concerns over the accuracy of the data itself, even though all data did pass the McDermott-Ellis consistency test.

The experimental VLE data showed that barely any separation was present in two binary systems, limonene/*p*-cymene and limonene/indane, with close bubble and dew point data indicating that an industrial distillation column for this process would require infinite stages. Both systems contained azeotropes, although only the limonene/indane azeotrope is definite due to the slightly larger temperature range. Both systems also had very low relative volatilities for the volatile components in the regions that separation was present.

The fairly similar relative volatilities of limonene in relation to 1,2,3-trimethylbenzene, *p*-cymene and indane in the limonene/1,2,3-trimethylbenzene/*p*-cymene/indane quarternary system indicate that purification of limonene from 1,2,3-trimethylebenzene would be difficult.

The combined lack of separation in the systems limonene/*p*-cymene, limonene/indane and limonene/1,2,3-trimethylbenzene/*p*-cymene/indane, as well as the azeotropic nature of the systems limonene/*p*-cymene and limonene/indane, indicate and assure that it would be very difficult and almost impossible to purify limonene from *p*-cymene and indane using ordinary distillation techniques.

The binary systems of limonene/butylbenzene and *p*-cymene/butylbenzene showed slightly better separation without the presence of azeotropes, however still minimal in realistic terms. Measuring this data proved difficult on the newly built still and had to be performed on the additional Pilodist VLE still of the department. This was due to there being insufficient mixing between the mixing and heating chambers of the constructed setup. A modification to the constructed setup, whereby the mixing and heating chambers are combined to provide better mixing could rectify this issue.

Although a number of shortcomings were experienced in completing the second objective, it was completed to the most achievable extent. The following chapter addresses the third and final objective in this study.

5. Modelling

This chapter focuses on the third objective in this study, regressing the VLE data presented in the previous chapter. Future projects at the Department of Process Engineering would ultimately involve using the data obtained in this study to develop process models for the pyrolysis of waste tyres using Aspen Plus®. Aspen Plus® was therefore used to regress the data obtained. The chapter therefore explains the approach taken, followed by the results of the regression and a discussion.

5.1 Approach

The Aspen Plus® Data Regression System (DRS) was used to fit binary interaction parameters from the activity coefficient models to the phase equilibrium data measured in this study. The Aspen Plus® DRS database however, uses different formulae for the calculation of the binary interaction parameters compared to those commonly found in literature [54]. The formulae used by the Aspen Plus® DRS database and consequently those that are used in this study to calculate the binary interaction parameters for the NRTL, Wilson and UNIQUAC activity coefficient models are shown in Equations 5.1, 5.2 and 5.3 respectively [67].

NRTL: $$\tau_{ij} = a_{ij} + {}^{b_{ij}}/_{T} \quad (5.1)$$

Wilson: $$ln\Lambda_{ij} = a_{ij} + {}^{b_{ij}}/_{T} \quad (5.2)$$

UNIQUAC: $$\tau_{ij} = \exp\left(a_{ij} + {}^{b_{ij}}/_{T}\right) \quad (5.3)$$

The non-randomness parameter for the NRTL model (α_{ij}) remains at 0.3 since the compounds of concern are basically non-polar [53]. Two parameters (a_{ij} and b_{ij}) for the NRTL, Wilson and UNIQUAC models were considered in this study as this was seen to be common practise in literature [108]. Furthermore, all correlations were compared with the UNIFAC model as well. The DRS calculated the parameters by minimising the activity coefficient objective function, which is suitable for *T*, *P*, *x*, *y* measurements [67]. This was chosen as such since it minimises the error between activity coefficient values, of which the experimental values usually have more noise than measurable variables, making the regression more accurate. Equation 5.4 illustrates the activity coefficient objective function used by the Aspen Plus® DRS [108].

$$OF = \sum_{n}^{1}(\gamma_1^{exp} - \gamma_1^{calc})_i^2 + \sum_{n}^{1}(\gamma_2^{exp} - \gamma_2^{calc})_i^2 \quad (5.4)$$

To assess the ability of these activity coefficient models to predict the phase equilibrium behaviour, their regressed values for temperature and composition need to be compared with the experimental values [116]. This can be done either visually, by plotting the experimental and calculated values on a single graph, or using descriptive statistics such as the Average Absolute Deviation (*AAD*) and Average Absolute Relative Deviation (*AARD*) between the experimental and calculated values [116]. Equations 5.5 and 5.6 illustrate how the *AAD* and *AARD* values are calculated, respectively [116].

$$AAD\ (x_i) = \frac{1}{Z_T} \sum_1^{Z_T} \left| x_i^{calc} - x_i^{measured} \right| \tag{5.5}$$

$$AARD\ (x_i)\ \% = \frac{100}{Z_T} \sum_1^{Z_T} \left| \frac{x_i^{calc} - x_i^{measured}}{x_i^{measured}} \right| \tag{5.6}$$

Where Z_T is the total number of data points measured.

The *AAD* is a suitable assessment because it is less affected by extreme data as it does not square the distance of the data point from the mean, unlike the variance and standard deviation calculations [116]. The *AARD* is similar to the *AAD*, but also takes into account the relative size of the data point [116].

The following sections present the binary interaction parameters determined for each system measured using the Aspen Plus® DRS. Both visual plots and descriptive statistics (*AAD* and *AARD* values) are presented for each of the relevant models' correlations. *AAD* and *AARD* values were calculated by comparing the final temperature (*T*) and vapour mole fractions (y_i) calculated with raw experimental values at their respective liquid mole fractions (x_i).

Vapour pressure data obtained for limonene, *p*-cymene and butylbenzene were regressed together with the VLE data obtained. As such, different boiling points (from each vapour pressure set) for these pure compounds were regressed, all of which however, are within the limits of the temperature error bars. Lastly, the uncertainties reported in this study were used as the STD-DEV in the Aspen Plus® correlations.

5.2 Results

5.2.1 Limonene/*p*-cymene

From Table 5.1 and Figures 5.1 and 5.2, it can be seen that all the models correlate the data in very much the same manner both visually and in terms of the *AAD* and *AARD* values. Although the azeotrope temperature is slightly under-estimated by ~0.12 K, the models are still within the

limits of the error bars for this data. The figures also show that the correlative models estimate an azeotrope at ~0.2 mole fraction limonene compared to 0.25 – 0.30 mole fraction limonene. UNIFAC model predicts the azeotrope to be ~0.4 mole fraction limonene.

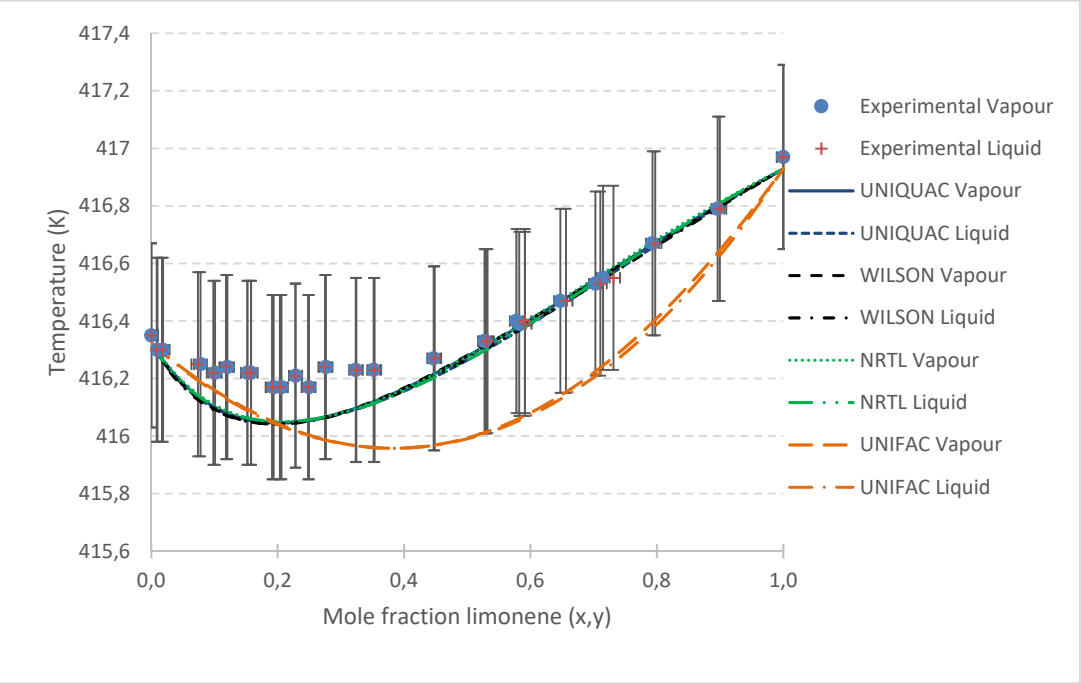

Figure 5.1: Temperature-composition diagram for limonene/*p*-cymene at 40 kPa

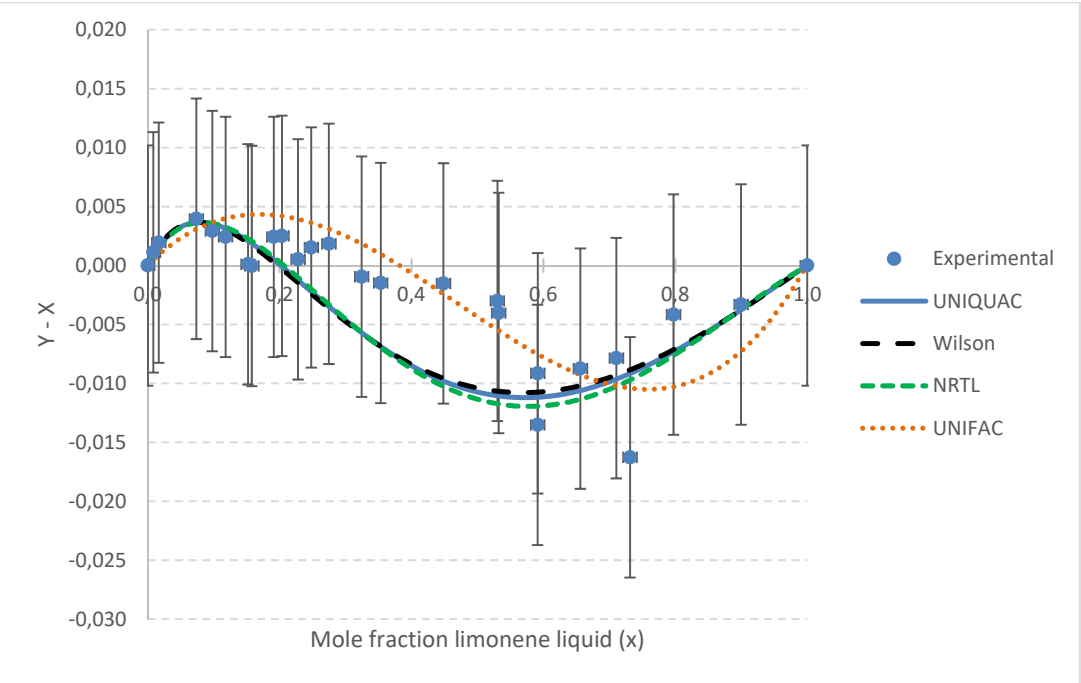

Figure 5.2: (y-x) vs x plot for limonene/*p*-cymene at 40 kPa

Table 5.1: NRTL, Wilson and UNIQUAC binary interaction parameters for the limonene(1)/*p*-cymene(2) binary system

	a_{12}	a_{21}	b_{12}	b_{21}	*AAD* (T)	*AAD* (y_1)	*AARD* (T)	*AARD* (y_1)
			K	K	K	mol frac	%	%
NRTL	-3.463	25.19	1100.47	-10000.0	0.07	0.005	0.018	1.699
WILSON	-24.98	4.402	10000.0	-1580.93	0.08	0.003	0.019	1.353
UNIQUAC	6.782	-14.08	-2644.02	5630.90	0.08	0.003	0.018	1.386
UNIFAC	-	-	-	-	0.19	0.002	0.046	1.530

5.2.2 Limonene/butylbenzene

Table 5.2 and Figures 5.3 and 5.4 illustrate the fit of the models to the experimental data and a comparison of the models' estimates. After taking in to account the visual comparisons as well as the *AAD* and *AARD* values, it can be seen that the Wilson model correlates the data slightly better than the UNIQUAC and NRTL models for this system. The UNIFAC model seems to predict the data with quite bit of error for this system.

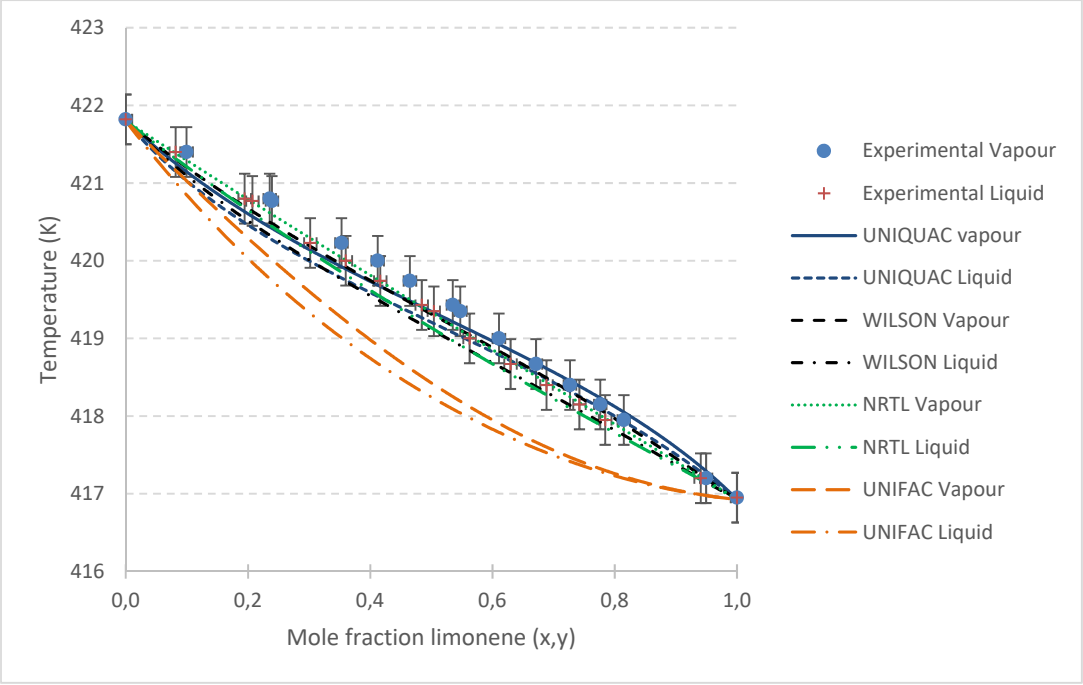

Figure 5.3: Temperature-composition diagram for limonene/butylbenzene at 40 kPa

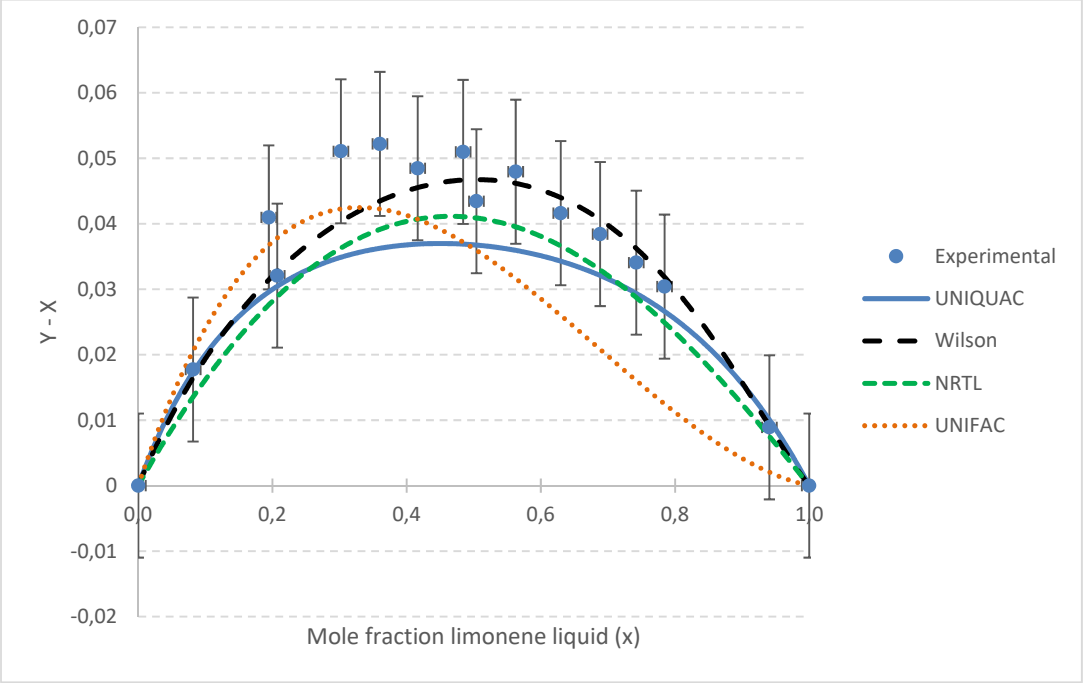

Figure 5.4: (y-x) vs x plot for limonene/butylbenzene at 40 kPa

Table 5.2: NRTL, Wilson and UNIQUAC binary interaction parameters for the limonene(1)/butylbenzene(2) binary system

	a_{12}	a_{21}	b_{12}	b_{21}	*AAD* (T)	*AAD* (y_1)	*AARD* (T)	*AARD* (y_1)
			K	K	K	mol frac	%	%
NRTL	5.035	2.587	-1689.35	-1400.22	0.12	0.027	0.029	6.737
WILSON	-12.59	-12.66	5607.95	4701.95	0.16	0.003	0.038	0.972
UNIQUAC	-1.440	-1.570	627.540	634.312	0.15	0.007	0.036	1.728
UNIFAC	-	-	-	-	0.73	0.010	0.174	1.894

5.2.3 *p*-Cymene/butylbenzene

Table 5.3 and Figures 5.5 and 5.6 illustrate the fit of the models to the experimental data and the similarities in the models' estimates. From a visual perspective, all the models' estimates are identical. However, looking at the *AAD* and *AARD* values, it can be argued that the Wilson and UNIQUAC models provide slightly better estimates than the NRTL model for this system. For this system, the UNIFAC model seems to predict the data fairly well as it falls within the error bars.

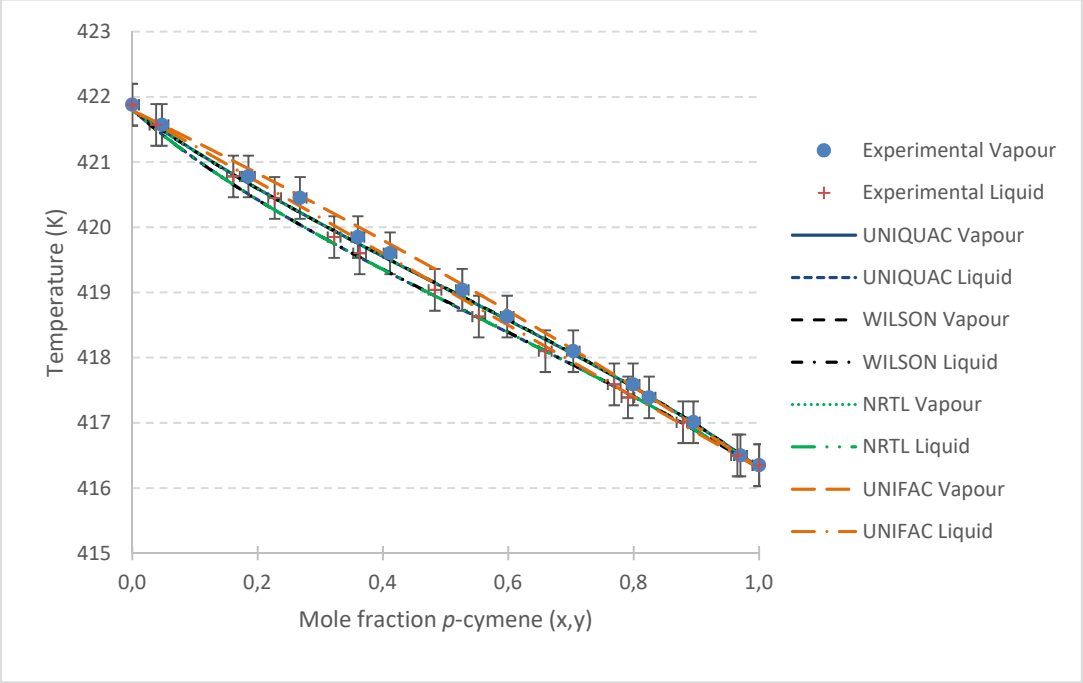

Figure 5.5: Temperature-composition diagram for *p*-cymene/butylbenzene at 40 kPa

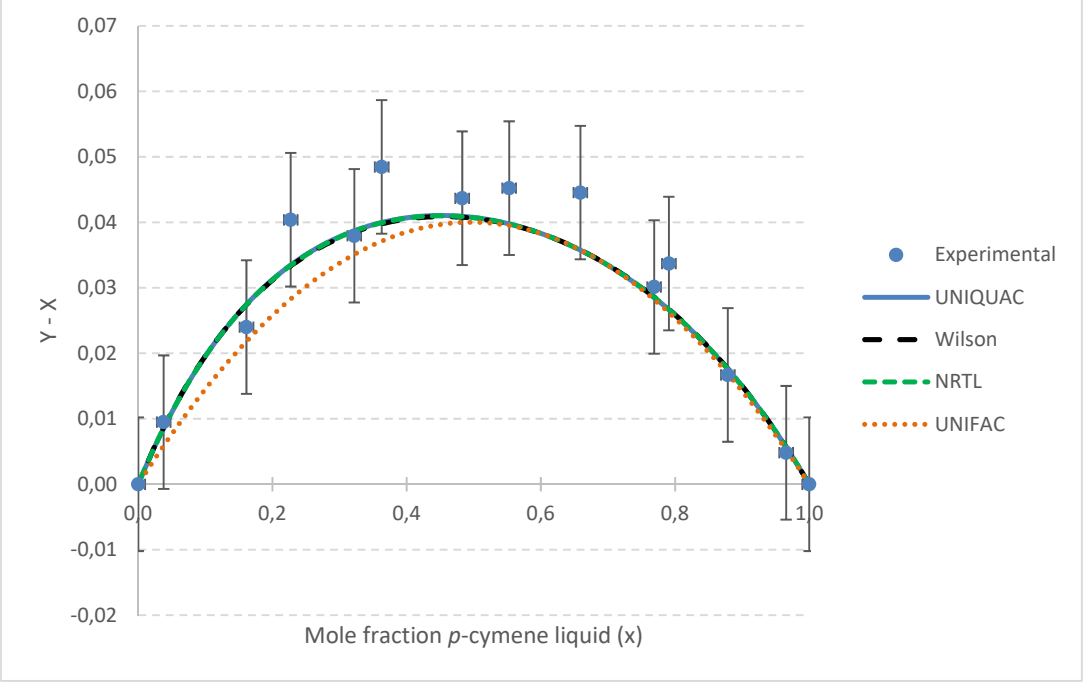

Figure 5.6: (y-x) vs x plot for *p*-cymene/butylbenzene at 40 kPa

Table 5.3: NRTL, Wilson and UNIQUAC binary interaction parameters for the *p*-cymene(1)/butylbenzene(2) binary system

	a_{12}	a_{21}	b_{12}	b_{21}	*AAD* (T)	*AAD* (y_1)	*AARD* (T)	*AARD* (y_1)
			K	K	K	mol frac	%	%
NRTL	3.651	2.789	-1445.71	-1240.95	0.06	0.580	0.015	7.364
WILSON	-2.448	-4.118	1096.04	1640.49	0.06	0.577	0.015	0.866
UNIQUAC	-0.724	-0.665	266.212	312.830	0.07	0.577	0.016	0.873
UNIFAC	-	-	-	-	0.08	0.004	0.020	1.405

5.2.4 Limonene/indane

Visual comparisons of the regressions for this system are presented in Figures 5.7 and 5.8. Visually, it can be seen that the NRTL and UNIQUAC models provide better estimates of the experimental data, than the Wilson model, while remaining within the confines of the error bars. The *AAD* and *AARD* values, as presented in Table 5.4, are very similar for each models' regression but indicate that the NRTL model provides the best estimate. Once again, the UNIFAC model fails to accurately predict the experimental data as it falls outside the error bars for this system. The azeotrope is also inaccurately predicted by UNIFAC in terms of temperature.

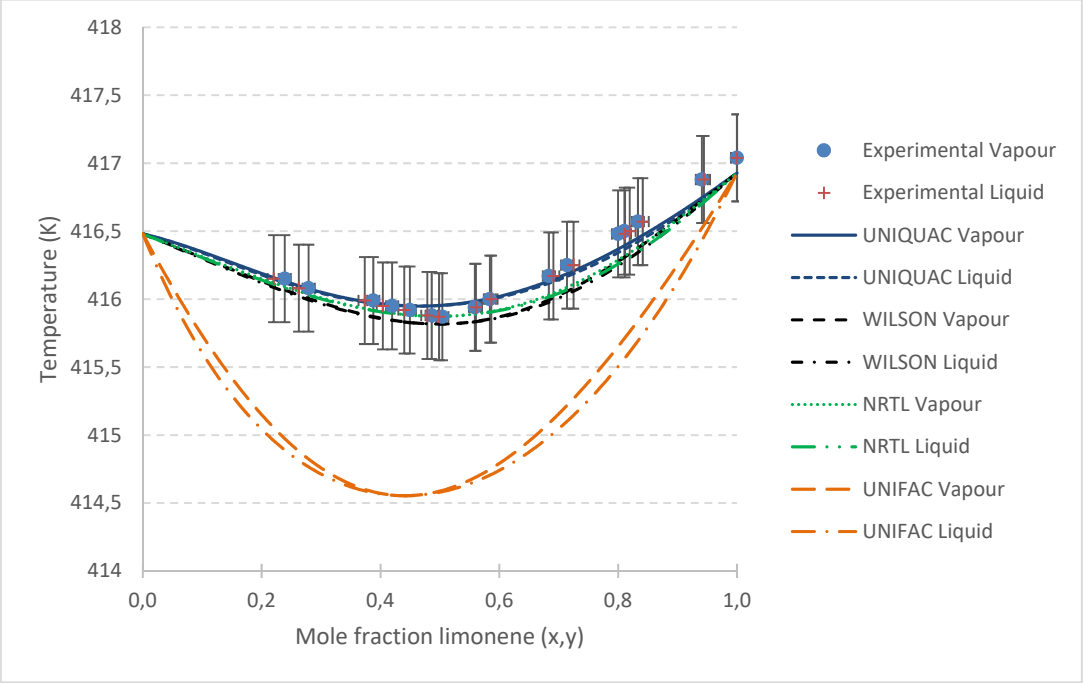

Figure 5.7: Temperature-composition diagram for limonene/indane at 40 kPa

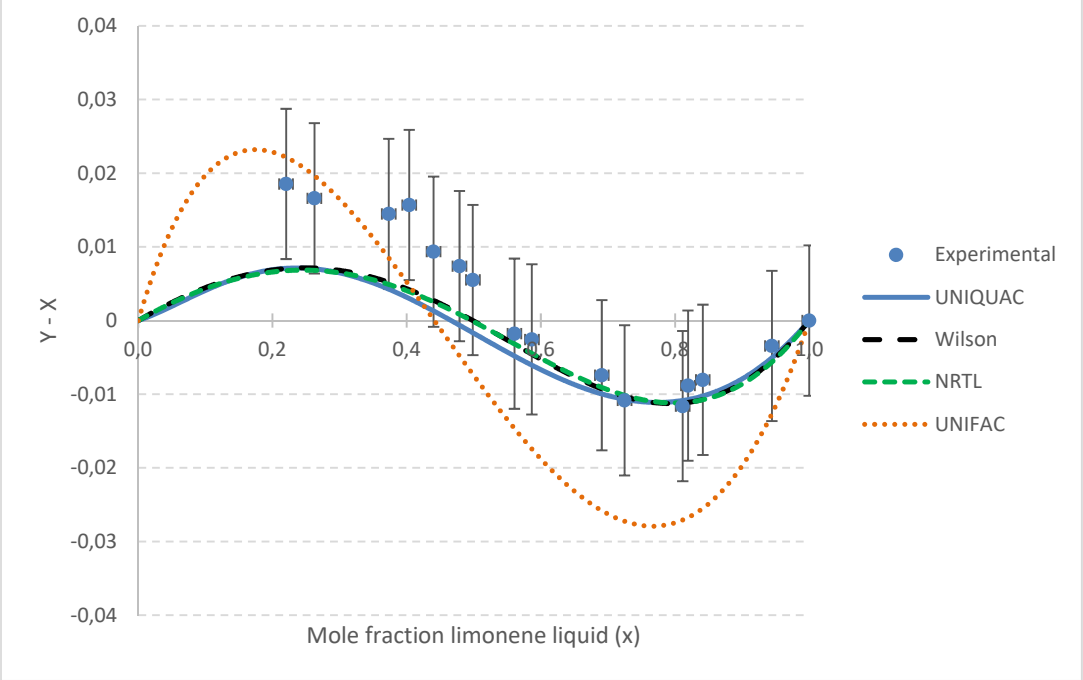

Figure 5.8: (y-x) vs x plot for limonene/indane at 40 kPa

Table 5.4: NRTL, Wilson and UNIQUAC binary interaction parameters for the limonene(1)/indane(2) binary system

	a_{12}	a_{21}	b_{12}	b_{21}	*AAD* (T)	*AAD* (y_1)	*AARD* (T)	*AARD* (y_1)
			K	K	K	mol frac	%	%
NRTL	-3.269	-6.512	1650.82	2504.03	0.10	0.006	0.023	-3.269
WILSON	8.955	4.847	-3588.08	-2235.07	0.13	0.005	0.031	8.955
UNIQUAC	0.419	1.068	-42.326	-573.882	0.06	0.006	0.015	0.419
UNIFAC	-	-	-	-	1.08	0.012	0.259	1.898

5.2.5 Limonene/1,2,3-trimethylbenzene/*p*-cymene/indane

Table 5.5 presents the binary interaction parameters obtained for the limonene/1,2,3-trimethylbenzene/*p*-cymene/indane quarternary system. No visual representations for the regressed data have been provided. *AAD* and *AARD* values indicate a better fit with the NRTL model than the UNIQUAC and Wilson models, as presented in Table 5.6. Tables 5.5 and 5.6 highlight the fact that insufficient data were used to fit too many parameters. It could therefore be deduced that better models could have been used to correlate this system. The UNIFAC model does seem to predict this quarternary system better than the NRTL model however and would therefore be the best choice for this system.

Table 5.5: NRTL, Wilson and UNIQUAC binary interaction parameters for the limonene(1)/1,2,3-trimethylbenzene(2)/*p*-cymene(3)/indane(4) quarternary system

	NRTL		Wilson		UNIQUAC	
Ij	a_{ij}	b_{ij}	a_{ij}	b_{ij}	a_{ij}	b_{ij}
		K		K		K
12	79.537	397.27	25.074	-10000	-46.276	-46.276
13	31.302	12170	1.5360	-0.0680	-7.9510	-7.9510
14	29.421	18159	-89.626	-29217	-27.544	-27.544
21	0.2690	-69.202	-69.051	-5629.6	25.284	25.284
31	64.776	6494.0	-85.199	-115.82	119.91	119.91
41	-4.6450	3324.4	-2.0310	-1582.7	17.064	17.064
23	72.486	5267.6	-22.025	10000	-43.428	-43.428
24	0.2280	-936.13	26.010	-10000	-44.940	-44.940
32	30.034	3879.6	-80.000	-10000	-22.382	-22.382

34	0.5590	354.27	-80.000	-10000	-41.154	-41.154
42	1.0550	450.55	-80.000	-10000	25.323	25.323
43	62.943	115.01	-80.000	-10000	-43.615	-43.615

Table 5.6: *AAD* and *AARD* values for the limonene(1)/1,2,3-trimethylbenzene(2)/*p*-cymene(3)/indane(4) quarternary system

	Unit	NRTL	Wilson	UNIQUAC	UNIFAC
AAD (T)	K	1.085	2.173	377.1	0.575
AAD (y_1)	mol frac	0.014	0.025	0.508	0.006
AARD (T)	%	0.261	0.522	90.57	0.138
AARD (y_1)	%	2.540	4.493	92.10	1.451

5.3 Discussion

Regression of the generated data showed that all three correlative thermodynamic models chosen, NRTL, Wilson and UNIQUAC, manage to describe the binary VLE behaviour. However, the systems involving butylbenzene favoured the Wilson model. When compared with the UNIFAC models, it was seen that the UNIFAC models could not accurately predict the systems' behaviour, except for that of the system *p*-cymene/butylbenzene – meaning that the usage of UNIFAC in previous studies could have caused errors in simulations.

Furthermore, the NRTL model best correlated the quarternary system as this model managed to fit the data the best, statistically. The UNIFAC model did however manage to predict the data better according to the *AAD* and *AARD* values, although the NRTL model's correlation was not perfect in the first place.

Nevertheless, it could be argued that the Wilson model best describes the overall behaviour of the binary systems in general and that the UNIFAC model is unsuitable for predicting the system behaviour.

From a point of ideality, activity coefficients for each compound in all the systems were seen to be close to 1. Although some are below 1, indicating negative deviations from Raoult's law, and some above 1, indicating positive deviations from Raoult's law. In this study as azeotropic behaviour is seen with the experimental data indicating non-ideal behaviour. For this reason,

Raoult's law would not be able to accurately predict the phase behaviour for these systems either.

The regression conducted further emphasises the lack of separation between limonene and the remaining compounds of concern as well as the difficulty that would be experienced if limonene were to be purified from these compounds using ordinary distillation. Furthermore, the presented regression results could be used to further investigate the potential of advanced distillation techniques in purifying naphtha fractions of the TDO.

.

6. Conclusions and recommendations

The aim of this study was to provide relevant phase equilibrium data which would be useful in the separation of limonene from compounds in the naphtha fraction of the TDO that have similar boiling points to it. These compounds are mainly *p*-cymene, indane, 1,2,3-trimethylbenzene and butylbenzene.

In order to carry out this task, an experimental rig which could measure temperatures, pressures and sample vapour and liquid compositions accurately and reliably, had to first be constructed. The constructed rig was then commissioned for the accuracy of its' temperature and pressure measurement capabilities.

After the verification of the experimental methodology was completed, vapour pressure and vapour liquid equilibrium data were collected for the binary systems limonene/*p*-cymene, limonene/butylbenzene, *p*-cymene/butylbenzene, limonene/indane and the quaternary system limonene/1,2,3-trimethylbenzene/*p*-cymene/indane. All of the vapour-liquid equilibrium data were collected at 40 kPa in an effort to reduce the effects of thermal degradation on these compounds.

The collected vapour-liquid equilibrium data were then regressed using Aspen Plus® DRS to obtain binary interaction parameters between the respective compounds in each measured system. The models chosen for the regression were the NRTL, Wilson and UNIQUAC activity coefficient models due to their applicability to the compounds and systems measured in this study.

Thus, the projects first, second and third objectives, as well as how they were ultimately attained, are discussed.

The first objective of this project was to construct a vapour and liquid recirculation equilibrium still in which the phase equilibrium for this study could be attained. This meant that temperature and pressure could be measured accurately and reliably at sub-atmospheric conditions. The still also had to have the ability to sample the vapour and liquid phases separately after equilibrium was reached, without significantly disturbing the equilibrium itself.

The author of this work designed the equilibrium still with the required capabilities. The constructed still, together with ancillary electrical equipment, offers temperature measurement, pressure measurement, vacuum pressure operation and control, vapour phase sampling and liquid phase sampling without significantly interrupting equilibrium operations.

After the calibration of temperature and pressure measuring instruments and commissioning of the still, as per the experiments in this study, a temperature measurement accuracy of +/- 0.32 K and composition measurement accuracy of +/- 0.0102 mole fraction has been realised, this is including pressure fluctuations of +/- 0.1 kPa at vacuum conditions. The composition error comprises of error originating from the analytical technique as well, although this simply further emphasises the accurate sampling capability of the still.

The operation of the constructed still has been verified using four binary VLE systems in total, one at atmospheric conditions (ethanol/1-butanol) and three at 40 kPa (*n*-decane/2-heptanone; *n*-decane/3-heptanone and *n*-nonane/1-pentanol). This confirmed the successful completion of the first objective.

The second objective was to generate phase equilibrium data at sub-atmospheric pressures for the compounds of concern in this study, limonene, *p*-cymene, indane, butylbenzene and 1,2,3-trimethylbenzene. Throughout this project, vapour-liquid equilibrium data has been collected for four binary systems at 40 kPa, limonene/*p*-cymene; limonene/butylbenzene; *p*-cymene/butylbenzene and limonene/indane as well as one quarternary system at 40 kPa. Additionally, vapour pressure data for limonene, *p*-cymene and butylbenzene has been collected and compared to literature, being in visual agreement.

The VLE data collected showed that negligible separation was evident between limonene and two close boiling compounds, *p*-cymene and indane, at 40 kPa. Both *p*-cymene and indane, when paired with limonene, exhibited azeotropes at about 0.25 – 0.30 mole fraction limonene and ~416.2 K and at ~0.55 mole fraction limonene and ~415.9 K respectively, although only the limonene/indane azeotrope is definite due to the temperature error bars being relatively smaller to the slightly larger temperature range. The data indicated that purification of limonene from these compounds would be very difficult using ordinary distillation.

The data of the systems limonene/butylbenzene and *p*-cymene/butylbenzene at 40 kPa exhibited slightly better separation, however still minimal in realistic terms. No azeotropes were present in these systems. The limonene/1,2,3-trimethylbenzene/*p*-cymene/indane quarternary system illustrated minimal separation between the compounds as well, although this data could prove useful in future research when designing separation systems for the naphtha fraction of the TDO.

Furthermore, all data has passed the thermodynamic consistency test of McDermott-Ellis but failed the L/W consistency test. The failing of the L/W test could be attributed to the fact that there is barely any separation between the compounds in each system and that the boiling

points across the composition range for some systems are within the confines of the error bars. This does, albeit slightly, raise concerns over the accuracy of the data.

Another shortcoming in achieving the second objective was that pure feedstock samples of indane and 1,2,3-trimethylbenzene could not be procured, which is why vapour pressure data of these two compounds could not be obtained. Overall, although shortcomings were present in achieving the second objective, the phase equilibrium data obtained was collected to the most achievable extent. Therefore, the second objective of this project has been achieved.

The third objective was to regress the collected phase equilibrium data in order to obtain binary interaction parameters for relevant activity coefficient models. This was done by using the Data Regression System (DRS) available in Aspen Plus®.

Binary interaction parameters for the NRTL, Wilson and UNIQUAC activity coefficient models were determined. The models' correlations were evaluated using *AAD* and *AARD* values as well as visual inspection, which produced a fair fit between the experimental data and model estimates. Evaluations showed that the Wilson activity coefficient model best correlates the overall behaviour of the binary systems in general with the NRTL model proving better for that of the quarternary system. The UNIFAC model was also used for comparison and showed inability to accurately predict the behaviour of the systems. This means that UNIFAC could have caused the error experienced in previous studies from a simulation point of view. This also means that UNIFAC is not suitable for accurate predictions in future studies involving the systems tested in this study. This confirmed the completion of the third objective.

In conclusion, the three objectives of this study have been completed in an effort to fulfil the purpose and aim of this research project. Furthermore, the following recommendations are made for future work:

- If the still is modified to merge the mixing and heating chambers, this could eliminate the effects of a possible heat-induced two-liquid phase and possibly produce better results than that obtained in this study. However, this will also eliminate the capability of the still to measure vapour-liquid-liquid equilibrium in future.
- The data obtained in this study can be used in future projects in order to develop process models and simulations for the purification of limonene from the naphtha fraction of TDO.
- As the results of this study have pointed out, purifying the TDO via ordinary distillation would not be a simple solution. Previous researchers have also studied the applicability of advanced distillation to this issue. It is therefore recommended that future projects investigate the potential of advanced distillation techniques in purifying the TDO.

- Industrial operations involving limonene or any of the other compounds of concern in this study should limit their total operation time to a maximum of 4 hours if operating at pressures below 40 kPa.
- The compound *m*-cymene is a highly valuable compound. Extra research could be focused on trying to increase the yield of this compound from the TDO, possibly via thermal degradation or conversion of limonene and *p*-cymene.

7. References

[1] B. Danon, P. van der Gryp, C.E. Schwarz, J. F. Gorgens, A *review of dipentene (DL – Limonene) production from waste tyre pyrolysis*, Journal of Analytical and Applied Pyrolysis 112 (2015) 1 – 13.

[2] N, Nkosi, and E. Muzenda, *A review and discussion of waste tyre pyrolysis and derived products*, International Association of Engineers 2 (2014).

[3] M. Bajus and N. Olahova, *Thermal conversion of scrap tyres*, Petroleum & Coal 53 (2011) 98 – 105.

[4] H. Pakdel, D. M. Pantea, C. Roy, *Production of dl-limonene by vacuum pyrolysis of used tyres*, Journal of Analytical and Applied Pyrolysis 57 (2001) 91 – 107.

[5] L. Sun, D. Liao, Z. Yang, X. Chen, Z. Tong, *Measurement and correlation of (vapour + liquid) equilibrium data for {α-pinene + p-cymene + (S)-(-)-limonene} ternary system at atmospheric pressure*, Journal of Chemical Thermodynamics 58 (2013) 416 – 421.

[6] I. de Marco Rodriguez, M. F. Laresgoiti, M. A. Cabrero, A. Torres, M. J. Chomon, B. M. Caballero, *Pyrolysis of scrap tyres*, Fuel Processing Technology 72 (2001) 9 – 22.

[7] B. Benallal, C. Roy, H. Pakdel, S. Chabot, M.A. Poirier, *Characterization of pyrolytic light naphtha from vacuum pyrolysis of used tyres – comparison with petroleum naphtha,* Fuel 74 (1995) 1589 – 1594.

[8] J.D. Martínez, N. Puy, R. Murillo, T. García, M.V. Navarro, A.M. Mastral, *Waste tyre pyrolysis – a review*, Renewable and Sustainable Energy Reviews 23 (2013) 179 – 213.

[9] E. L. K. Mui, D. C. K. Ko, G. McKay, *Production of active carbons from waste tyres – a review*, Carbon 42 (2004) 2789 – 2805.

[10] B. Sahouli, S. Blacher, F. Brouers, H. Darmstadt, C. Roy, S. Kaliaguine, *Surface morphology and chemistry of commercial carbon black and carbon black from vacuum pyrolysis of used tyres*, Fuel 75 (1996) 1244 – 1250.

[11] N. M. Mkhize, B. Danon, P. van der Gryp, J. F. Gorgens, *Condensation of the hot volatiles from waste tyre pyrolysis by quenching*, Journal of Analytical and Applied Pyrolysis 124 (2017) 180 – 185.

[12] Sigma-Aldrich (2015) [https://www.sigmaaldrich.com/south-africa.html], [2/25/2015].

[13] P.T. Williams, *Pyrolysis of waste tyres: A Review*, Waste Management 33 (2013) 1714 – 1728.

[14] W. R. Alonso, J. I. M. Rajaonarivony, J. Gershenzon, R. Croteau, *Purification of 4S-Limonene Synthase, a Monoterpene Cyclase from the Glandular Trichromes of Peppermint (Mentha x piperita) and spearmint (Mentha spicata)*, The Journal of Biological Chemistry 267 (1992) 7582 – 7587.

[15] S. M. Walas, *Phase Equilibria in Chemical Engineering*, Butterworth Publishers, Boston, 1985.

[16] A. M. Cunliffe, P.T. Williams, *Composition of oils derived from the batch pyrolysis of tyres*, Journal of Analytical and Applied Pyrolysis 44 (1998) 131 – 152.

[17] Chem-Spider (2015) *Indane* [http://www.chemspider.com/Chemical-Structure.9903.html], [7/3/2015].

[18] Chemical Book (2010) *Butylbenzne* [https://www.chemicalbook.com/], [7/3/2015].

[19] Z. F. Tong, Z. Y. Yang, D. K. Liao, T. Y. Wei, X. P. Chen, *Measurement and correlation of VLE data for α-pinene +limonene and p-cymene + limonene*, Journal of Chemical Industry and Engineering (China) 60 (2009) 1877 – 1881.

[20] S. Mirmiran, H. Pakdel, C. Roy, *Characterisation of used tyre vacuum pyrolysis oil: nitrogeneous compounds from the naphtha fraction*, Journal of Analytical and Applied Pyrolysis 22 (1992) 205 – 215.

[21] M. R. Islam, M. Parveen, H. Hainu, M. R. I. Sarker, *Innovation in Pyrolysis Technology for Management of Scrap Tire: a Solution of Energy and Environment*, International Journal of Environmental Science and Development 1 (2010) 89 – 96.

[22] M. Kyari, A. Cunliffe, P. T. Williams, *Characterisation of oils, gases and char in relation to the pyrolysis of different brands of scrap automotive tyres*, Energy Fuels 19 (2005) 1165 – 1173.

[23] M. F. Laresgoiti, B. M. Caballero, I. de Marco, A. Torres, M. A. Cabrero, M. J. Chomon, *Characterisation of the liquid products obtained in tyre pyrolysis*, Journal of Analytical and Applied Pyrolysis 71 (2004) 917 – 934.

[24] S. Ucar, S. Karagoz, A. R. Ozkan, J. Yanik, *Evaluation of two different scrap tyres as hydrocarbon source by pyrolysis*, Fuel 84 (2005) 1884 – 1892.

[25] M. R. Islam, H. Haniu, M. R. A. Beg, *Liquid fuels and chemicals from pyrolysis of motorcycle tyre waste: product yields, compositions and related properties*, Fuel 87 (2008) 3112 – 3122.

[26] R. M. Rieder and A. R. Thompson, *Vapor-Liquid equilibria measured by a Gillespie Still*, Journal of Industrial and Engineering Chemistry, 41 (1949) 2905 – 2908.

[27] M. Soni, D. Ramjugernath, J. D. Raal, *Vapour-Liquid Equilibria and Infinite Dilution Activity Coefficient Measurements of Systems Involving Diketones*, University of Natal – Durban, 2003.

[28] H. Stage, W. G. Fischer, Glass Instrumenten Technik 12 (1968) 1167 – 1173.

[29] K. Magoulas, D. Tassios, *Thermophysical Properties of n-Alkanes from C1 to C20 and their prediction for higher one*, Fluid Phase Equilibria 56 (1990) 119 – 140.

[30] C. Tsonopoulos, Z. Tan, *The Critical Constants of Normal Alkanes From Methane to Polyethylene*, Fluid Phase Equilibria 83 (1993) 127 – 138.

[31] M. R. Riazi, T. A. Al-Sahhaf, *Physical Properties of Heavy Petroleum Fractions and Crude Oils*, Fluid Phase Equilibria 117 (1996) 217 – 224.

[32] I. Brown, *Liquid-Vapour Equilibria. III. The Systems Benzene-n-Heptane, n-Hexane-Chlorobenzene and Cyclohexane-Nitrobenzene*, Australian Journal of Scientific Research 5 (1952) 530-540.

[33] F. G. Cottrell, *On the Determination of Boiling Points of Solutions*, Journal of the American Chemical Society 41 (1919) 721 – 728.

[34] K. Dvorak, T. Boublik, Liquid-vapour Equilibria. XXIX. *Measurement of Equilibrium Data in Systems with High Equilibrium Ratio of Components*, Collection of Czechoslovak Chemical Communications 28 (1963) 1249 – 1255.

[35] D. T. C. Gillespie, *Vapor-liquid Equilibrium for Miscible Liquids*, Industrial and Engineering Chemistry, Analytical Edition 18 (1946) 575 – 577.

[36] E. Hala, J. Pick, V. Fried, O. Vilim, *Vapour-Liquid Equilibrium*, Pergamon Press, New York, 1957.

[37] M. A. Joseph, D. Ramjugernath, J. D. Raal, *Phase Equilibrium Properties for Binary Systems with Diacetyl from a Computer Controlled Vapour-Liquid Equilibrium Still*, Fluid Phase Equilibria 182 (2001) 157 – 176.

[38] S. C. Lee, *Partial Pressure Isotherms*, Journal of Physical Chemistry 35 (1931) 3558 – 3582.

[39] H. Li, Y. Han Sand Teng, *Bubble Point Measurement for Systems Chloroform-Ethanol-Benzene by Inclined Ebulliometer*, Fluid Phase Equilibria 113 (1995) 185 – 195.

[40] S. Malanowski, *Experiemental Methods for Vapour-Liquid Equilibria. Part 1. Circulation Methods*, Fluid Phase Equilibria 8 (1982) 197 – 219.

[41] J. D. Raal, A. L. Muhlbauer, *Phase Equilibria: Measurement and Computation*, Taylor and Francis, Bristol PA, 1998.

[42] S. Yerazunis, J. D. Plowright, F. M. Smola, *Vapor-Liquid Equilibrium Determination by a New Apparatus*, American Institute of Chemical Engineers Journal 10 (1964) 660 – 665.

[43] R. Washburn, J. W. Read, *The Laws of "Concentrated" Solutions. VI. The General Boiling Point Law*, Journal of the American Chemical Society 41 (1919) 729 – 741.

[44] Y. X. Yu, J. G. Liu, G. H. Gao, *Isobaric Vapor-Liquid Equilibria for Three Aromatic Hydrocarbon-tetraethylene Glycol Binary Mixtures*, Fluid Phase Equilibria 157 (1999) 299 – 307.

[45] W. B. Altsheler, E. D. Unger, P. Kolachov, *Improved Still for Liquid-Vapor Equilibria Data on Systems: Ethanol-Water and Acetic Acid-Water*, Industrial and Engineering Chemistry 43 (1951) 2559.

[46] F. J. Conradie, P. L. Crouse, *Batch Separation of Tetrafluoroethylethylene, Hexafluoropropylene and Octofluorocyclobutane*, University of Pretoria, 2011.

[47] D. Abrams, J. M. Prausnitz, *Statistical thermodynamics of liquid mixtures: A new expression for the excess Gibbs energy of partly or completely miscible systems*, American Institute of Chemical Engineers Journal 21 (1975) 116 – 128.

[48] D. Peng, D. B. Robinson, *A new two-constant equation of state*, Industrial & engineering Chemistry Fundamentals, 15 (1976) 59 – 64.

[49] K. S. Pitzer, R. F. Curl, *The Volumetric and Thermodynamic Properties of Fluids. III. Empirical Equation for the Second Virial Coefficient*, Journal of the American Chemical Society 79 (1957) 2369 – 2379.

[50] J. M. Prausnitz, *Molecular Thermodynamics of Fluid Phase Equilibria*, Prentice Hall Inc, 1969.

[51] J. M. Prausnitz, R. N. Lichtenthaler, E. G. Azevedo, *Molecular Thermodynamics of Fluid-phase Equilibria*, Prentice Hall PTR, USA, 1999.

[52] Vacuum SA cc. (2017) http://vacuumsa.co.za/ [17/03/2017].

[53] H. Renon, J. M. Prausnitz, *Local compositions in thermodynamic Excess Functions for Liquid Mixtures*, American Institute of Chemical Engineers Journal 14 (1968) 135 – 144.

[54] J. M. Smith, H. C. Van Ness, M. M. Abbott, *Introduction to Chemical Engineering Thermodynamics*, The Mc-Graw-Hill Companies, Inc. New York, USA, 2001.

[55] Separation Scientific (2017) https://www.sepsci.co.za/ [03/09/2015].

[56] Eltherm South Africa (2017) https://eltherm.com/en-za/ [11/01/2016].

[57] G. M. Wilson, *Vapour Liquid Equilibrium. XI. A new expression for the excess free energy of mixing*, Journal of the American Chemical Society 86 (1964) 127 – 130.

[58] L. Constantinou, R. Gani, *New Group Contribution Method for Estimating Properties of Pure Compounds*, American Institute of Chemical Engineers Journal 40 (1994) 1697 – 1710.

[59] Knovel (2015) *Yaws' Handbook of Thermodynamic and Physical Properties of Chemical Compounds: Critical Properties and Acentric Factor* https://app.knovel.com/web/toc.v/cid:kpYHTPPCC4/viewerType:toc/root_slug:yaws-handbook-thermodynamic/url_slug:critical-properties-acentric [4/22/2015].

[60] ThermoLit: NIST (2015) *Literature Report Builder for Thermochemical Property Measurements: Binary mixture* http://trc.nist.gov/thermolit/main/home.html#property/syssel:2:form:form:form/props:1:0:0 [4/22/2015].

[61] J. T. Cripwell, *Assessment of the Capabilities of Two Polar SPC-SAFT Terms Through Application to Measured Ketone-Alkane Phase Equilibria Data (Master's Thesis)*, Stellenbosch University, Stellenbosch, 2014.

[62] M. H. Nadais, M. G. Bernardo-Gil, *Vapour-Liquid Equilibria of α-pinene + Limonene at Reduced pressures*, Fluid Phase Equilibria 91 (1993) 321 – 330.

[63] M. F. Rodrigues, M. G. Bernardo-Gil, *Vapor-Liquid Equilibrium of Binary Mixtures of Limonene with α-pinene and of β-pinene at Reduced Pressures*, Journal of Chemical engineering Data 40 (1995) 1193 – 1195.

[64] M. G. Bernardo-Gil, M. A. Ribeiro, *Vapor-Liquid Equilibria of binary Systems Based on Pine Resin*, Fluid Phase Equilibria 53 (1989) 15 – 22.

[65] J. Wisniak, *A new test for the thermodynamic consistency of vapour-liquid equilibrium*, Industrial and Engineering Chemistry Research 32 (1993) 1531 – 1533.

[66] J. Wisniak, *The herington test for thermodynamic consistency*, Industrial and Engineering Chemistry Research 33 (1994) 177 – 180.

[67] Aspentech (2015) *Design and optimize chemical processes with Aspen Plus*: https://www.aspentech.com/products/aspen-plus.aspx [7/3/2015].

[68] M. M. Ngwetjana, *Fractionation of tyre derived oil (TDO) (Master's Thesis)*, Stellenbosch University, Stellenbosch, 2017.

[69] H. K. Hansen, P. Rasmussen, A. Fredenslund, M. Schiller, J. Ghemling, Industrial & Engineering Chemistry Research, 30 (1991) 2352 – 2355

[70] A. Arce, E. Rodil, A. Soto, *Extractive distillation of 2-methoxy-2-methylpropane + ethanol using 1-Butanol as entrainer: Equilibria and simulation*, Canadian Journal of Chemical Engineering 77 (1999) 1135 – 1140.

[71] L. Brits, *Vapour-liquid-liquid equilibria measurements for the dehydration of low molecular weight alcohols via heterogeneous azeotropic distillation (Master's Thesis)*, Stellenbosch University, 2015.

[72] C. McDermott, S. R. M. Ellis, *A multicomponent consistency test*, Chemical Engineering Science 20 (1965) 293 – 296.

[73] S. I. Sandler, *Chemical, biochemical, and engineering thermodynamics*, John Wiley & Sons, Inc. New Jersey, USA, 2006.

[74] J. Wisniak, A. Tamir, *Vapor-liquid equilibria in the ternary systems water-formic acid-acetic acid and water-acetic acid-propionic acid*, Journal of Chemical and Engineering Data 22 (1977) 253 – 260.

[75] Knovel (2015) *Yaws' Handbook of Antoine Coefficients for Vapor Pressure (2nd Electronic Edition)* https://app.knovel.com/web/toc.v/cid:kpYHACVPEH/viewerType:toc/root_slug:yaws-handbook-antoine/url_slug:antoine-equation-coefficients [10/1/2015].

[76] W. L. Luyben, *Process Modelling, Simulation and Control for Chemical Engineers – Second Edition*, McGraw-Hill, New York, USA, 1996.

[77] H. Pakdel, C. Roy, H. Aubin, G. Jean, S. Coulombe, *Formation of dl-limonene in used tyre vacuum pyrolysis oils*, Environmental Science and Technology 25 (1991) 1646.

[78] M. F. Doherty, J. P. Knapp, *Distillation, Azeotropic, and Extractive.* Kirk-Othmer Encyclopedia of Chemical Technology. John Wiley & Sons, Inc. New Jersey, USA, 2000.

[79] H. Pines, J. Ryer, *Pyrolysis of d-Limonene and of related hydrocarbons, mechanisms of pyrolysis*, Journal of American Chemical Society 77 (1955) 4370.

[80] R. W. Rousseau, J. R. Fair, *Handbook of separation process technology.* Wiley-IEEE. pp. 261–262, 1987.

[81] E. J. Hoffman, *Azeotropic and extractive distillation,* Wiley-Interscience, New York, USA, 1964.

[82] R. Murillo, A. Aranda, E. Aylon, M.S. Callen, A.M. Mastral, *Process for the separation of gas products from waste tyre pyrolysis*, Industrial & Engineering Chemistry Research 45 (2006) 1734.

[83] W. L. Luyben, I. L. Chien, *Design and Control of Distillation Systems for Separating Azeotropes,* Wiley, New Jersey, USA, 2010.

[84] M. Stanciulescu, M. Ikura, *Limonene ethers from tyre pyrolysis oil. Part 1: Batch experiments,* Journal of Analytical and Applied Pyrolysis 75 (2006) 217 – 225.

[85] M. Stanciulescu, M. Ikura, *Limonene ethers from tyre pyrolysis oil. Part 2: Continuous flow experiments,* Journal of Analytical and Applied Pyrolysis 78 (2007) 76 – 84.

[86] A. Quek, R. Balasubramanian, *Liquefaction of waste tyres by pyrolysis for oil and chemicals - A review,* Journal of Analytical and Applied Pyrolysis 101 (2013) 1 – 16.

[87] P. Rathsack, F. Riedewald, M. S. Gallagher, *Analysis of pyrolysis liquid obtained from whole tyre pyrolysis with molten zinc as the heat transfer media using comprehensive gas chromatography mass spectrometry*, Journal of Analytical and Applied Pyrolysis (2015).

[88] S. Ramamurthy, R. P. Vanaja, *Pulse skipping modulated buck converter – modelling and simulation*, Circuits and systems 1 (2010) 59 – 64.

[89] E. Krell, *Handbook of laboratory distillation: with an introduction into the pilot plant distillation*, Elsevier Science Publishing Company, New York, USA, 1982.

[90] Glasschem (2016) http://www.glasschem.co.za/ [20/1/2016].

[91] R. Schmidt, G. Werner, H. Schuberth, Zeitschrift für Physikalische Chemie 242 (1969) 381 – 390.

[92] K. Thormann, Dechema-Erfahrungsaustausch, *Arbeitsmethoden und Gerate, Destillieren und Rektifizieren*, Dechema, Frankfurt/Main, 1950.

[93] E. Jantzen, O. Wieckhorst, Chemie Ingenieur Technik 16 (1954). 302 – 396.

[94] P. C. Wankat, *Separation Process Engineering: Second edition*, Prentice Hall, Boston, USA.

[95] AIChE – DIPPR (2017) https://www.aiche.org/dippr [4/02/2017].

[96] D. W. Green, R. H. Perry, *Perry's Chemical Engineers' Handbook: 8th Edition*, McGraw-Hill, New York, USA.

[97] Chemours (2016) https://chemours.com/Viton/en_US/ [12/02/2016].

[98] M. Rausand, A. Hoyland, *System Reliability Theory: Models, Statistical Methods, and Applications (2nd Edition)*, John Wiley & Sons, Hoboken, New Jersey, USA, 2004.

[99] S. Ngxangxa, *Development of GC-MS methods for the analysis of tyre pyrolysis oils (Master's Thesis)*, Stellenbosch University, Stellenbosch, 2016.

[100] J.A. Duran, F.P. Cordoba, I. Gil, G. Rodriguez, A. Orjuela, *Vapor-liquid equilibrium of the ethanol + 3-methyl-1-butanol system at 50.66, 101.33 and 151.99 kPa*, Fluid Phase Equilibria 338 (2013) 128 – 134.

[101] J.R. Welty, C.E. Wicks, R.E. Wilson, G.L. Rorrer, *Fundamentals of Momentum*, Heat and Mass Transfer, John Wiley & Sons, Hoboken, New Jersey, USA.

[102] S. Gong, P Cheng, X. Quan, *Two-dimensional mesoscale simulations of saturated pool boiling from rough surfaces. Part I: Bubble nucleation in a single cavity at low superheats*, International Journal of Heat and Mass Transfer 100 (2016) 927 – 937.

[103] P. T. Ngema, D. Matkowska, P. Naidoo, T. Hofman, D. Ramjugernath, *Vapor−Liquid Equilibrium Data for Binary Systems of 1-Methyl-4-(1-methylethenyl)-cyclohexene + {Ethanol, Propan-1-ol, Propan-2-ol, Butan-1-ol, Pentan-1-ol, or Hexan-1-ol} at 40 kPa*, Journal of chemical & engineering data 57 (2012) 2053 – 2058.

[104] P. Reddy, T. P. Benecke, D. Ramjugernath, *Isothermal (vapour + liquid) equilibria for binary mixtures of diisopropyl ether with (methanol, or ethanol, or 1-butanol): Experimental data, correlations and predictions*, The Journal of Chemical Thermodynamics 58 (2013) 330 – 339.

[105] Scientific instrument services (2000) http://www.sisweb.com/referenc/applnote/app-83.htm [9/6/2016].

[106] C. Turek, F. C. Stintzing, *Stability of Essential oils*, Comprehensive reviews in Food Science and Food Safety 12 (2013) 40 – 53.

[107] Wika South Africa (2017) http://www.wika.co.za/ [6/12/2015].

[108] J. T. Cripwell, C. E. Schwarz, A. J. Burger, *Vapor-Liquid Equilibria Measurements for the Nine n-Alkane/Ketone pairs Comprising 2-,3-, and 4-Heptanone with n-Octane, n-Nonane and n-Decane*, Journal of Chemical and Engineering Data 60 (2015) 602 – 611.

[109] M. Ferreira, *Phase Equilibria and Thermodynamic modelling of the ternary system CO_2 + 1-decanol + n-tetradecane (PhD Thesis)*, Stellenbosch University, Stellenbosch, To be done by: December 2018.

[110] Afrox South Africa (2017) https://www.afroxshop.co.za/shop/en/za/home [25/10/2016].

[111] R. E. Cavicchi, T. Avedisian, *Bubble nucleation, growth and surface temperature oscillations on a rapidly heated microscale surface immersed in a bulk subcooled but locally superheated liquid under partial vacuum*, International Journal of Heat and Mass Transfer 54 (2011) 5612 – 5622.

[112] A. Fredenslund, J. Gmehling, P. Rasmussen, *Vapor-Liquid equilibria Using UNIFAC. A Group Contribution Model*, Elsevier, Amsterdam, 1977.

[113] A. Fredenslund, R. L. Jones, J. M. Prausnitz, *Group contribution method for the estimation of activity coefficients in non-ideal solutions*, American Institute of Chemical Engineers Journal 21 (1975) 1086 – 1099.

[114] Yokogawa South Africa (2017) https://www.yokogawa.com/za/ [25/10/2015].

[115] V. Gomis, F. Ruiz, J. C. Asensi, *The application of ultrasound in the determination of isobaric vapour-liquid-liquid equilibrium data*, Fluid Phase Equilibria 172 (2000) 245 – 259.

[116] C. Pienaar, *Evaluation for entrainers for the dehydration of C_2 and C_3 alcohols via azeotropic distillation (Master's Thesis)*, Stellenbosch University, Stellenbosch, 2012.

[117] T. Guetachew, J. Jose, A. Voilley, *Experimental and estimated saturated vapour pressures of aroma compounds*, Fluid Phase Equilibria 157 (1999) 257 – 270.

[118] W. V. Steele, R. D. Chirico, A. B. Cowell, S. E. Knipmeyer, A. J. Nguyen, *Thermodynamic Properties and Ideal-Gas Enthalpies of Formation for Methyl Benzoate, Ethyl Benzoate, (R)-(+)-Limonene, tert-Amyl Methyl Ether, trans-Crotonaldehyde, and Diethylene Glycol*, Journal of Chemical and Engineering Data 47(4) (2002) 667 – 688.

[119] R. A. McDonald, S. A. Shrader, D. R. J. Stull, *Vapor Pressures and Freezing Points of 30 Organics*, Journal of Chemical and Engineering Data 4 (1959) 311.

[120] A. F. Forziati, W. R. Norris, F. D. J. Rossini, *Vapor Pressures and Boiling Points of Sixty API-NBS Hydrocarbons*, Journal of Research of the National Bureau of Standards (U. S.) 43 (1949) 555.

8. Appendices

Appendix A: Calibration certificates

This Appendix contains calibration certificates for the vapour temperature probe and pressure transmitter used in the experimental setup.

Thermon
South Africa (Pty) Ltd.

unitemp

sanas
Calibration Laboratory
1573, 373

Calibration certificate CAL-UC-S-T-160411L04
certificate number

	INSTRUMENT	PROBE
Type	Temperature Display	Pt100 1/10 4-wire Probe A
Manufacturer	PlayingwithFusion	Wika
Part Nr.	n/a	SS 316
Serial Nr.	SEN 30201: MAX 31865	W321728

Calibration of hi-accuracy digital thermometer with Pt100 1/10 4-wire Probe A

Location
Laboratory - Thermon South Africa (Pty) Ltd.
47 Flamingo Crescent
Lansdowne
Cape Town

CAL-UC-S-T-160411L04

Customer Address
University of Stellenbosch
Process Engineering
Bag X1, Stellenbosch University
Matieland, 7602

Order Nr. TZAFS007708
Date of calibration 11-Apr-2016

Was adjustment of the instrument done?
☐ yes ☑ no

The reported expanded uncertainty is based on a standard uncertainty multiplied by a coverage factor k = 2 providing a level of confidence of approximately 95%, the uncertainty of measurement has been estimated in accordance with the principles defined in the GUM, guide to uncertainty of measurement, ISO, Geneva, 1993

This calibration certificate may not be reproduced other than in full, and with the permission of SANAS & Thermon Laboratory.

Calibration certificates without an authorized signature and seal are not valid.

Person Responsible: F Fernandez-Rivera

Technical Signatory: Roy MacGregor

CALIBRATION LABORATORY Thermon SA (Pty) Ltd. 2016 -04- 12 CAPE TOWN

page 1 of 2

Calibration • Validation • Training
Email: sales.za@thermon.com **Web**: www.thermon.co.za
Thermon South Africa (Pty) Ltd. Reg. No. 2015/020118/07, VAT No. 4750268387, **Directors**: G.P. Alexander, R.L. Bingham, J.C. Peterson

Figure 8.1: Temperature calibration certificate part 1

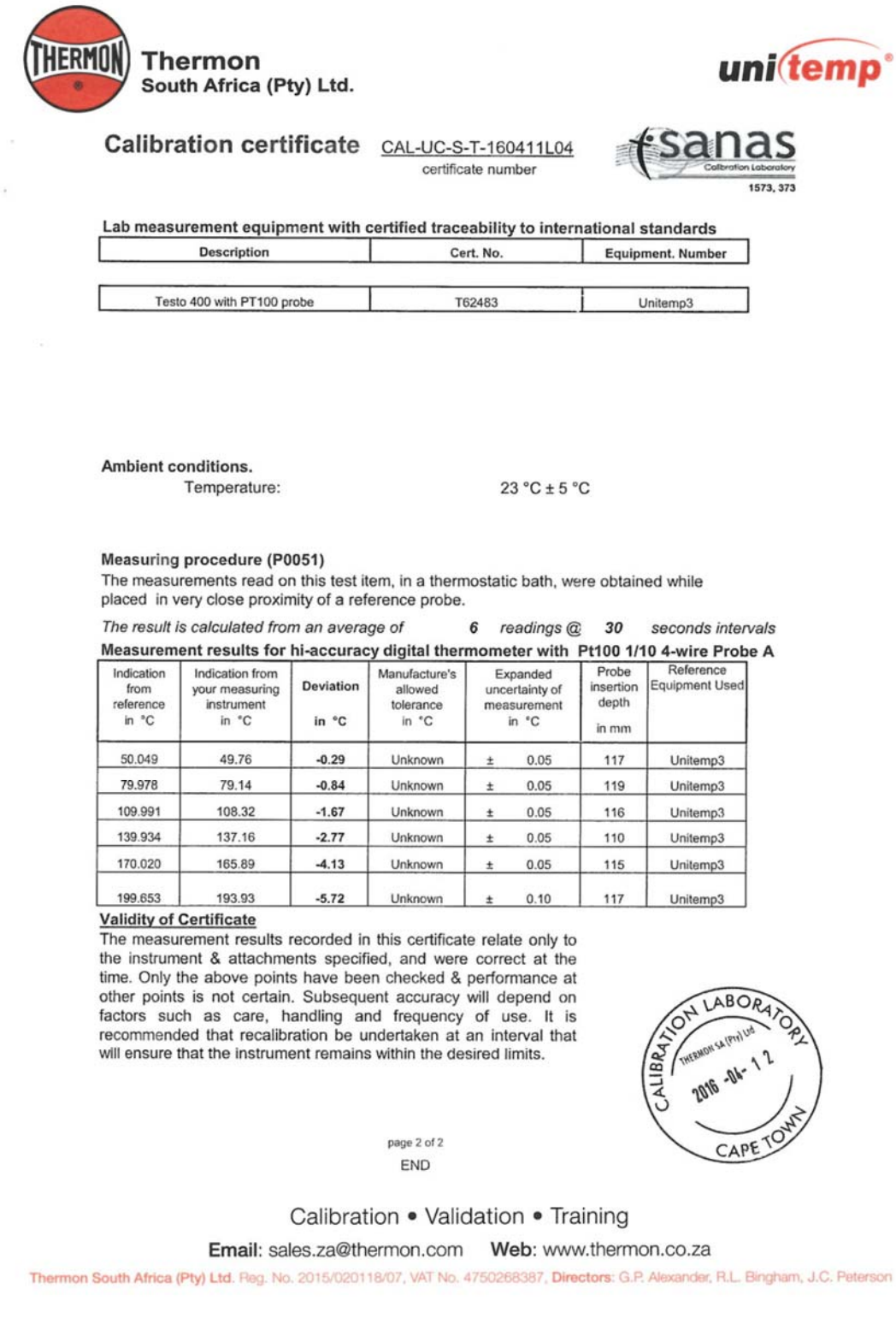

Thermon
South Africa (Pty) Ltd.

unitemp

Calibration certificate CAL-UC-S-T-160411L04
certificate number

sanas Calibration Laboratory
1573, 373

Lab measurement equipment with certified traceability to international standards

Description	Cert. No.	Equipment. Number
Testo 400 with PT100 probe	T62483	Unitemp3

Ambient conditions.

Temperature: 23 °C ± 5 °C

Measuring procedure (P0051)

The measurements read on this test item, in a thermostatic bath, were obtained while placed in very close proximity of a reference probe.

The result is calculated from an average of ***6*** *readings @* ***30*** *seconds intervals*

Measurement results for hi-accuracy digital thermometer with Pt100 1/10 4-wire Probe A

Indication from reference in °C	Indication from your measuring instrument in °C	Deviation in °C	Manufacture's allowed tolerance in °C	Expanded uncertainty of measurement in °C	Probe insertion depth in mm	Reference Equipment Used
50.049	49.76	**-0.29**	Unknown	± 0.05	117	Unitemp3
79.978	79.14	**-0.84**	Unknown	± 0.05	119	Unitemp3
109.991	108.32	**-1.67**	Unknown	± 0.05	116	Unitemp3
139.934	137.16	**-2.77**	Unknown	± 0.05	110	Unitemp3
170.020	165.89	**-4.13**	Unknown	± 0.05	115	Unitemp3
199.653	193.93	**-5.72**	Unknown	± 0.10	117	Unitemp3

Validity of Certificate

The measurement results recorded in this certificate relate only to the instrument & attachments specified, and were correct at the time. Only the above points have been checked & performance at other points is not certain. Subsequent accuracy will depend on factors such as care, handling and frequency of use. It is recommended that recalibration be undertaken at an interval that will ensure that the instrument remains within the desired limits.

CALIBRATION LABORATORY
THERMON SA (Pty) Ltd
2016 -04- 12
CAPE TOWN

page 2 of 2

END

Calibration • Validation • Training

Email: sales.za@thermon.com **Web**: www.thermon.co.za

Thermon South Africa (Pty) Ltd. Reg. No. 2015/020118/07, VAT No. 4750268387, **Directors**: G.P. Alexander, R.L. Bingham, J.C. Peterson

Figure 8.2: Temperature calibration certificate part 2

SOUTH AFRICAN NATIONAL ACCREDITATION SYSTEM

WIKA Instruments (Pty) Ltd - South Africa

CALIBRATION LABORATORY FOR PRESSURE MEASUREMENT

Certificate Number A 20217 SANAS 246

Certificate of Calibration

Calibration of a	Transmitter
Manufacturer	YOKOGAWA
Type	EJX510A
Range	0 ... 110 kPa
Serial number	91NC08447
Tag number	n/a
Customer	University of Stellenbosch Room C101 Process Engineering Banghoeg Weg Engineering Campus Stellenbosch 7602 South Africa
Order No.	249210028
Number of pages of the certificate	4
Date of calibration	10/02/2016
Recalibration Date As Per Customer	**February 2017**

This calibration certificate documents the traceability to national standards and international standards, which realise the units of measurement according to the International System of Units (SI).

The South African National Accreditation System (SANAS) is a member of the International Laboratory Accreditation Committee (ILAC) for the Mutual Recognition Agreement. This arrangement allows for the mutual recognition of technical test and calibration data by the member's accreditation bodies worldwide. For more information on the MRA please consult www.ilac.org

The values in this certificate are correct at the time of calibration/certification. Subsequently the accuracy will depend on such factors as operating temperature, the care exercised in handling, frequency of use and its use under conditions other than specified by the manufacturer and/or conditions of calibration/certification. Recertification should be performed after a period that has been chosen by the user to ensure that the equipment's accuracy remains within the desired limits. The user is obliged to have the object recalibrated at these intervals.

The reported results are only valid for the object calibrated. Legal liability shall be limited to the cost of recalibration and or certification, but the applicant indemnifies WIKA INSTRUMENTS against any consequential or other loss.

This calibration certificate may not be reproduced other than in full except with the permission of the issuing laboratory. Calibration certificates without Technical Signatory's signature and seal are not valid.

Seal	Date of Issue	Checked by Laboratory Assisstant	Calibrated by SANAS Authorised Technical Signatory
SOUTH AFRICAN NATIONAL ACCREDITATION SYSTEM SANAS 246	10/02/2016	Mlotha L.	Wellcome P.

WIKA Instruments (Pty) Ltd. Chilvers St., Denver, 2094
Johannesburg, South Africa
PO Box 75225, Gardenview, 2047

Tel.: (011) 621 0000
Fax: (011) 621 0059
email: sales@wika.co.za

Figure 8.3: Pressure transmitter calibration certificate part 1

WIKA Instruments (Pty) Ltd - South Africa

page 4 of 4: Date of calibration 10/02/2016 Certificate No. A 20217 SANAS 246

Uncertainty

The reported expanded uncertainty of measurement is valid after a correction of the reading value with the systematical deviation (see table "evaluation").

The reported expanded uncertainty of measurement is stated as the standard uncertainty of measurement multiplied by the coverage factor k=2, which for a normal distribution corresponds to a coverage probability of 95,45%, the uncertainty of measurement has been estimated in accordance with the principles defined in the GUM, 'Guide to Uncertainty of Measurement, ISO, Geneva, 1993'.

Graphic representation of the relative uncertainty

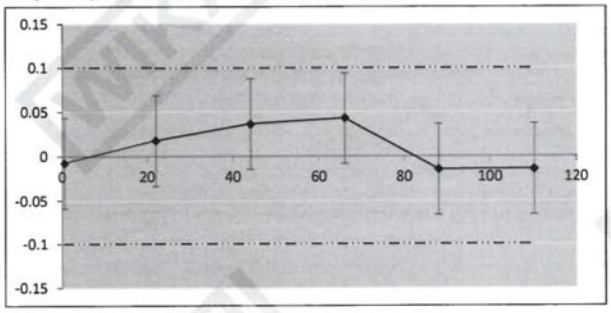

Legend	
X-axis	P_e in kPa
Y-axis	rel. uncertainty in %

Accuracy of instrument

+/- 0.103 kPa = +/- 0.094 % referred to span

Label

The calibration object is labelled, which shows the number of this calibration certificate, serial/tag number and the date of calibration.

END OF CERTIFICATE.

The South African National Accreditation System (SANAS) is a member of the International Laboratory Accreditation Committee (ILAC) for the Mutual Recognition Agreement. This arrangement allows for the mutual recognition of technical test and calibration data by the member's accreditation bodies worldwide. For more information on the MRA please consult www.ilac.org

SOUTH AFRICAN NATIONAL ACCREDITATION SYSTEM SANAS 246

WIKA Instruments (Pty) Ltd. Chilvers St.,
Denver, 2094
Johannesburg, South Africa
PO Box 75225, Gardenview, 2047

Tel.: (011) 621 0000
Fax: (011) 621 0059
email: sales@wika.co.za

Figure 8.4: Pressure transmitter calibration certificate part 2

Appendix B: Reference system data

This Appendix presents the atmospheric and sub-atmospheric reference system data that was used for verification of the experimental setup in this study [61, 62, 70,108, 109]. The data for the systems presented in Tables 8.4 to 8.6 have been shown to pass the L/W consistency and McDermott-Ellis consistency tests by the original authors and are thus not displayed together with the data.

Table 8.1: Atmospheric reference system data of ethanol(1)/1-Butanol(2) at 101.3 kPa together with L/W consistency test results [61]

Temperature (K)	x_1	y_1	L/W	Comment
351.14	1	1	N/A	N/A
354.08	0.8353	0.972	0.93	Acceptable
358.01	0.6883	0.9346	0.93	Acceptable
358.73	0.6662	0.9243	0.93	Acceptable
359.00	0.6514	0.9248	0.93	Acceptable
359.55	0.6367	0.9136	0.93	Acceptable
360.56	0.5999	0.9064	0.93	Acceptable
363.59	0.5003	0.8704	0.93	Acceptable
364.78	0.4771	0.8367	0.93	Acceptable
367.99	0.3821	0.7663	0.94	Acceptable
370.27	0.3308	0.719	0.95	Acceptable
381.54	0.1326	0.3783	0.96	Acceptable
382.25	0.1118	0.3506	0.97	Acceptable
373.93	0.2509	0.6309	0.95	Acceptable
374.59	0.2479	0.6161	0.95	Acceptable
370.52	0.3305	0.7139	0.94	Acceptable
354.31	0.8501	0.9738	0.92	Acceptable
354.58	0.8364	0.9689	0.92	Acceptable
357.28	0.7288	0.9396	0.92	Acceptable
357.48	0.7172	0.9303	0.92	Acceptable
359.89	0.6192	0.9048	0.93	Acceptable
359.9	0.6308	0.8896	0.93	Acceptable
360.89	0.6073	0.8934	0.92	Acceptable
361.31	0.5917	0.8791	0.92	Acceptable

363.7	0.5147	0.8518	0.93	Acceptable
364.11	0.4986	0.8339	0.93	Acceptable
364.95	0.4682	0.8227	0.94	Acceptable
366	0.4393	0.7965	0.94	Acceptable
390.49	0	0	N/A	N/A

Table 8.2: Atmospheric reference system data of ethanol(1)/1-Butanol(2) at 101.3 kPa together with L/W consistency test results [70]

Temperature (K)	x_1	y_1	L/W	Comment
387.65	0.0297	0.1178	0.99	Acceptable
386.44	0.0444	0.1719	0.98	Acceptable
385.7	0.057	0.2	0.98	Acceptable
384.14	0.0804	0.2614	0.97	Acceptable
381.17	0.1292	0.3734	0.96	Acceptable
380.08	0.1505	0.4157	0.96	Acceptable
378.71	0.1696	0.4622	0.96	Acceptable
376.71	0.2087	0.5261	0.95	Acceptable
374.03	0.2594	0.602	0.95	Acceptable
371.68	0.3139	0.6657	0.94	Acceptable
369.48	0.3661	0.7168	0.94	Acceptable
367.25	0.4266	0.7697	0.93	Acceptable
364.9	0.4895	0.8178	0.93	Acceptable
362.68	0.554	0.8577	0.92	Acceptable
360.9	0.6142	0.8847	0.92	Acceptable
359.74	0.6548	0.9016	0.92	Acceptable
358.88	0.685	0.9126	0.91	Acceptable

Table 8.3: Sub-atmospheric reference system data of limonene(1)/*α*-pinene(2) at 40 kPa together with L/W consistency test results [62]

Temperature (K)	x_1	y_1	L/W	Comment
416.5	1	1	N/A	N/A
416.4	0.9973	0.9965	3.76	Not Acceptable
416.8	0.9881	0.9829	0.88	Acceptable
415.2	0.9267	0.8917	0.81	Acceptable
414.9	0.9005	0.8586	0.87	Acceptable
414.5	0.8753	0.8289	0.89	Acceptable
414.1	0.8496	0.7974	0.9	Acceptable
413.2	0.7996	0.708	0.9	Acceptable
412.8	0.7769	0.6987	0.91	Acceptable
411.8	0.7236	0.6363	0.91	Acceptable
410.6	0.6524	0.5489	0.91	Acceptable
410.2	0.6431	0.5021	0.91	Acceptable
408.5	0.5594	0.4399	0.91	Acceptable
407.8	0.5338	0.4006	0.9	Acceptable
407.8	0.5303	0.3707	0.9	Acceptable
406.8	0.4695	0.3167	0.91	Acceptable
406.3	0.4556	0.2975	0.9	Acceptable
404.9	0.3949	0.2663	0.89	Acceptable
403.7	0.357	0.2251	0.86	Acceptable
401.2	0.2438	0.1398	0.83	Acceptable
399.4	0.1728	0.1018	0.72	Acceptable
399.3	0.1664	0.0849	0.74	Acceptable
397.3	0.0818	0.0416	0.54	Acceptable
395.4	0.001	0.0005	-0.28	Not Acceptable
395.4	0	0	N/A	N/A

Table 8.4: Sub-atmospheric reference system data of *n*-decane(1)/2-heptanone(2) at 40 kPa [108]

Temperature (K)	x_1	y_1
413.88	1	1
411.91	0.972	0.877
409.34	0.936	0.774
406.98	0.889	0.677
404.19	0.833	0.570
402.79	0.799	0.524
401.78	0.781	0.494
401.37	0.755	0.454
400.55	0.729	0.455
400.23	0.715	0.444
399.68	0.692	0.428
399.32	0.672	0.419
399.15	0.668	0.417
398.85	0.664	0.402
398.72	0.654	0.411
398.32	0.626	0.395
397.08	0.575	0.355
396.73	0.553	0.342
396.72	0.546	0.335
396.00	0.490	0.312
395.90	0.483	0.303
395.20	0.423	0.277
394.32	0.345	0.235
393.67	0.277	0.198
393.23	0.222	0.167
392.92	0.176	0.144
392.81	0.131	0.106
392.30	0.061	0.057
391.82	0.048	0.042
391.68	0.038	0.030
391.79	0.031	0.028
391.87	0.031	0.030
391.96	0.027	0.030
392.05	0.023	0.024
392.54	0	0

Table 8.5: Sub-atmospheric reference system data of *n*-decane(1)/3-heptanone(2) at 40 kPa [108]

Temperature (K)	x_1	y_1
413.88	1	1
413.4	0.989	0.959
410.11	0.942	0.806
408.41	0.911	0.739
407.06	0.897	0.689
406.83	0.885	0.659
404.85	0.844	0.594
404.40	0.840	0.573
403.22	0.809	0.509
402.87	0.802	0.522
402.59	0.792	0.516
402.20	0.785	0.494
401.36	0.762	0.448
400.88	0.753	0.455
399.83	0.719	0.429
398.57	0.678	0.406
398.14	0.678	0.388
397.83	0.652	0.385
397.29	0.631	0.359
396.53	0.606	0.330
396.68	0.605	0.335
396.26	0.594	0.335
396.15	0.590	0.338
394.90	0.526	0.274
393.48	0.447	0.233
392.69	0.385	0.206
391.60	0.318	0.177
391.15	0.270	0.171
390.93	0.253	0.153
390.57	0.224	0.140
390.38	0.208	0.134
389.8	0.167	0.109
389.54	0.136	0.093
389.40	0.121	0.078
389.05	0.069	0.052
388.77	0.058	0.043
388.93	0.025	0.028
388.67	0	0

Table 8.6: Sub-atmospheric reference system data of *n*-nonane(1)/1-pentanol(2) at 40 kPa [109]

Temperature (K)	x_1	y_1
384.45	0	0
384.09	0.01002	0.0335
383.61	0.02058	0.0662
383.5	0.02063	0.0659
382.89	0.04029	0.1076
382.36	0.05469	0.1468
381.87	0.07020	0.1761
381.04	0.10278	0.2270
380.49	0.10813	0.2361
380.66	0.11476	0.2517
380.17	0.12493	0.2557
380.27	0.12945	0.2659
380.09	0.14306	0.2765
379.37	0.17337	0.2974
379.2	0.20550	0.3342
378.81	0.23478	0.3578
378.57	0.25833	0.3744
378.64	0.27116	0.3808
378.59	0.28058	0.3825
378.44	0.30199	0.3950
378.2	0.30776	0.3980
378.39	0.30970	0.3976
378.17	0.35873	0.4215
377.89	0.37839	0.4293
378.09	0.44797	0.4569
377.93	0.50686	0.4775
377.98	0.53748	0.4879
378.18	0.59806	0.5086
378.32	0.64065	0.5239
378.49	0.67676	0.5338
378.78	0.68197	0.5294
379.16	0.74584	0.5600
379.59	0.78454	0.5783
379.95	0.78886	0.5819
379.76	0.79074	0.5837
380.17	0.81218	0.5888
380.46	0.81737	0.6070
381.03	0.84889	0.6248
382.71	0.89885	0.6761
383.36	0.90547	0.6920
383.85	0.90967	0.7120

385.23	0.93925	0.7582
385.89	0.94210	0.7806
389.38	0.97839	0.8997
390.17	0.98398	0.9319
392.17	1.00000	1.0000

Appendix C: Process Flow Diagram and Piping & Instrumentation Diagram

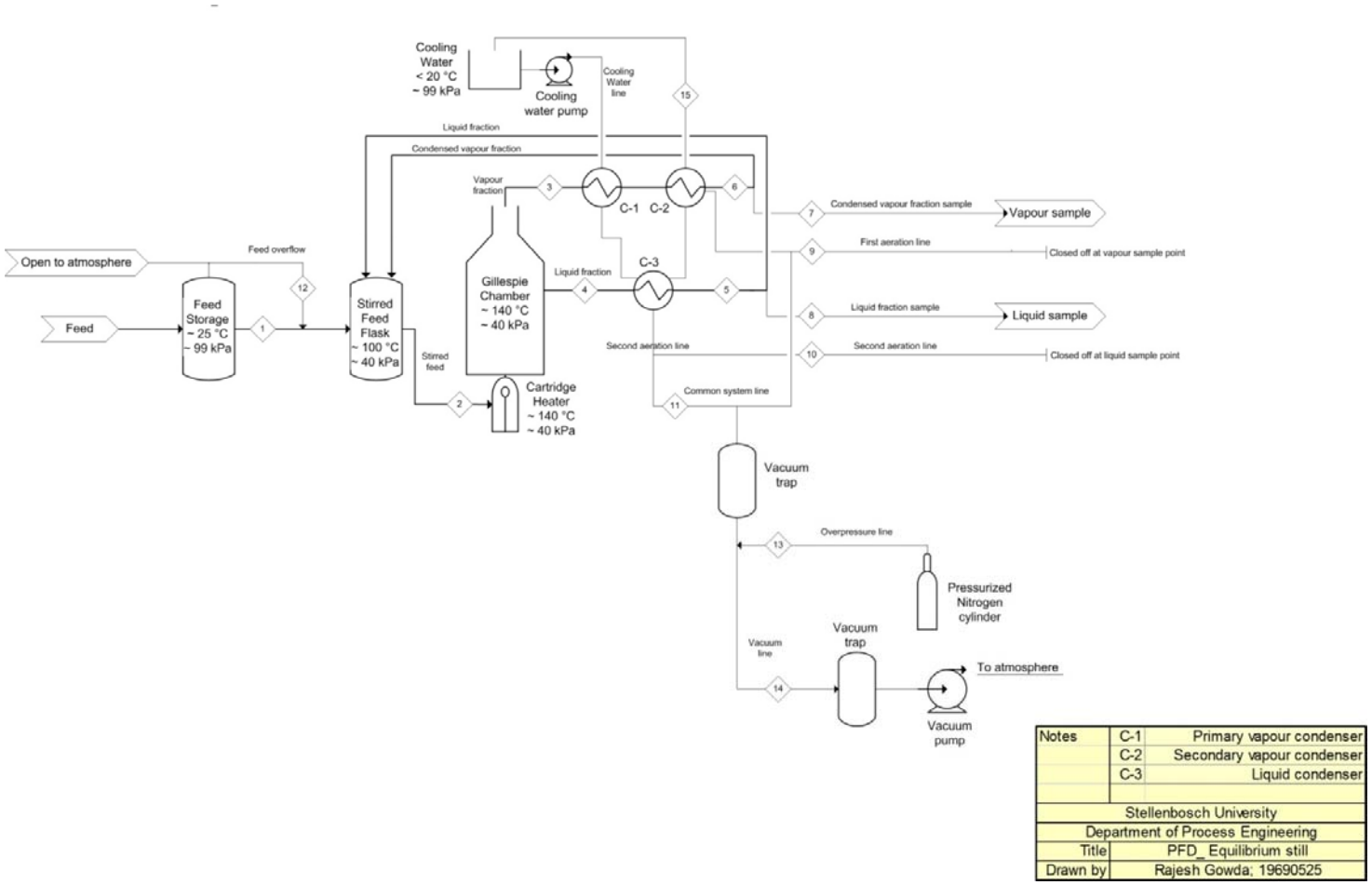

Figure 8.5: Process Flow Diagram (PFD) of equilibrium still setup

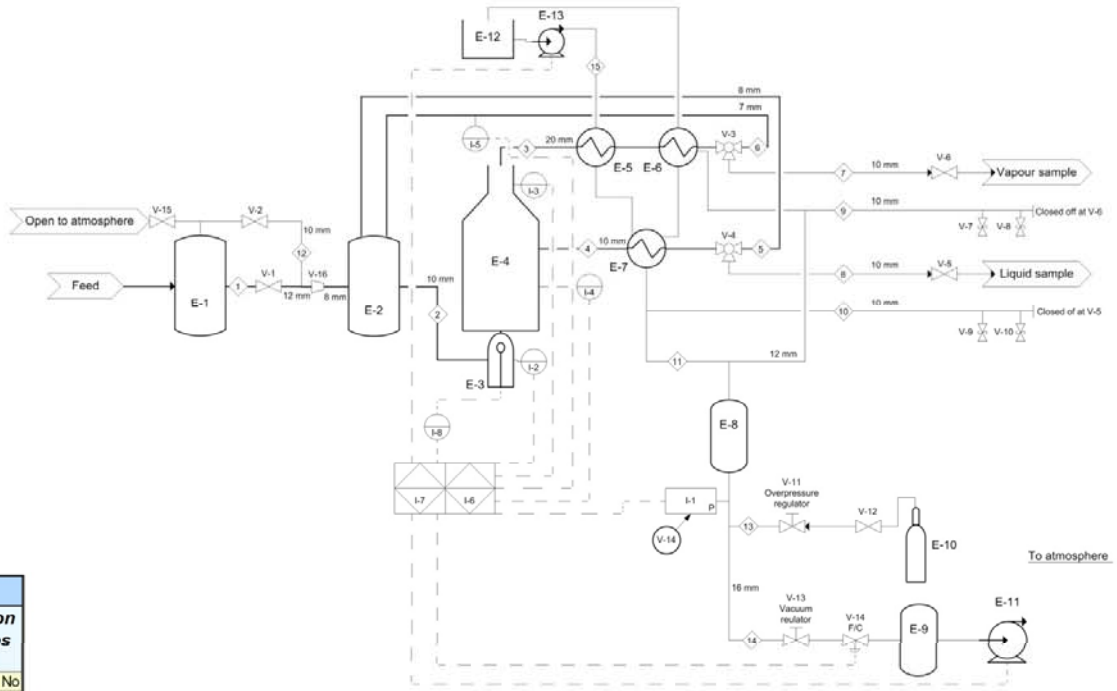

Valve List

Displayed Text	Description	Material	Line Size (OD) [mm]
V-1	Screwcock needle	Teflon	10
V-2	Screwcock needle	Teflon	10
V-3	Solenoid	Glass; steel	16
V-4	Solenoid	Glass; steel	16
V-5	Screwcock needle	Teflon	10
V-6	Screwcock needle	Teflon	10
V-7	Screwcock needle	Teflon	10
V-8	Screwcock needle	Teflon	10
V-9	Screwcock needle	Teflon	10
V-10	Screwcock needle	Teflon	10
V-11	Needle	316 Stainless steel	16
V-12	Pressure regulator	Steel	-
V-13	Needle	316 Stainless steel	16
V-14	Solenoid controlled	Brass; 316 Stainless steel	16
V-15	Screwcock needle	Teflon	10
V-16	Reducer	Glass	-

Equipment List

Displayed Text	Description	Length (mm)	Diameter (mm)	Material of construction	Insulation /thickness
E-1	Feed storage	220	52	Borosilicate Glass	No
E-2	Stirred feed flask	160	12	Borosilicate Glass	No
E-3	Cartridge heater	170	28	Quartz	No
E-4	Gillespie chamber	280	60	Borosilicate Glass	Yes - 30 mm
E-5	Primary vapour condenser	90	40	Borosilicate Glass	No
E-6	Secondary vapour condenser	170	40	Borosilicate Glass	No
E-7	Liquid condenser	170	40	Borosilicate Glass	No
E-8	Vacuum trap	220	70	Borosilicate Glass	No
E-9	Vacuum trap	220	70	Borosilicate Glass	No
E-10	Nitrogen Cylinder	1500	230	Steel	No
E-11	Vacuum pump; 180 W	-	-	-	No
E-12	Cooling water storage	200 x 250 x 310		Perspex	No
E-13	Cooling water pump; 16 W	-	-		No

Instrument List

Displayed Text	Description	Purpose	Manufacturer	Model
I-1	Pressure Transmitter	Pressure control; V-14	Wika	UPT-20
I-2	Temperature transmitter	Display		1/10 DIN 4-wire Pt-100
I-3	Temperature transmitter	Display		1/10 DIN 4-wire Pt-100
I-4	Temperature transmitter	Display		Class A 3-wire Pt-100
I-5	Temperature transmitter	Display		Class A 3-wire Pt-100
I-6	PLC unit Input modules	Display and calculation	Delta	AH 500
I-7	PLC unit output card	Control	Delta	AH 500
I-8	Soild state realy	Heater energy regulation		

Notes:	1. OD Pipe diameters
	2. Soild lines - Process
	3. Dashed lines - Signals
Stellenbosch University	
Department of Process Engineering	
Title	P&ID_ Equilibrium still
Drawn by	Rajesh Gowda; 19690525

Figure 8.6: Piping & Instrumentation Diagram (P&ID) of equilibrium still setup

Appendix D: Equilibrium still construction

This section provides a detailed overview of the sizes of each part of the equilibrium still that was built. It follows with a slightly more detailed description of the Gillespie chamber in which the Cottrell pump sits as well since this was the most delicate section of construction.

Figure 8.7 shows a detailed description of the equilibrium still to be constructed with numbered parts. Each part is given a description in this section. All valves indicated as taps are made from Teflon. All ports need external tapping. Table 8.7 also provides a quick reference to the parts labelled in Figure 8.7, indicating the name, most relevant outer diameter and length of the part if possible.

Table 8.7: Descriptions for the various parts in Figure 8.7

Part	Name	Outer Diameter (mm)	Length (mm)
1	Mixing chamber	12	160
2	Connector	10	100
3	Heating chamber	28.2	170
4	Temperature probe port	12	70
5	Cartridge heater element	<25	~130
6	Drain port	10	70
7	Cottrell tube coil	12	450
8	Vapour phase compartment	50	140
9	Temperature probe port	25	40
10	Temperature probe	15	140
11	Vapour sampling port	16	30
12	Vapour phase tube	20	140
13	Primary condenser	40	90
14	Secondary vapour condenser	40	170
15	Vapour condensate sample well	16	90
16	Connector tube	10	50
17	Vapour condensate droplet counter	30	30
18	Vapour condensate sample vial	12	90
19	Liquid sample return tube	10	200
20	Liquid sample condenser	40	170
21	Liquid sample well	16	90

22	Connector tube	10	50
23	Liquid sample vial	12	90
24	Connector tube	8	40
25	Connector tube	8	50
26	Liquid sample droplet counter	30	30
27	Connector tube	8	90
28	Connector tube	12	50
29	Feed vessel	52	220
30	Feed droplet counter	30	30
31	Feed port	16	60
32	Connector tube	10	440
33	Vacuum pipe port	12	30
34	Pneumatic valve rod port	19	60
35	Pneumatic valve rod port	19	60
36	Connector tube	10	40
37	Connector tube	10	40
38	Connector tube	10	350
39	Connector tube	10	350
40	Main common tube	12	400
41	Coil condenser tubes	7	120

Part 1 is the mixing chamber. It is basically a volumetric flask of approximately 50 mL in volume and has a total height of about 160 mm. Part 2 connects the mixing chamber to the heating chamber and is of 10mm in outer diameter and about 100 mm in length. It attaches to slightly above the bottom of the heating chamber.

Part 3 is the heating chamber and should be externally tapped. A cartridge heater is to be placed inside the heating chamber. The heating chamber has 2 ports, parts 4 and 6. Their dimensions are shown in Table 8.7. Part 4 should be externally tapped as it will have a temperature probe fitting into it. Part 5 is the cartridge heater. Part 6 is a stopcock valve that acts as a drain and is slanted towards the bottom.

The heating chamber is basically a port to the Gillespie chamber which holds part 7, the Cottrell tubing. As mentioned before, the tubing should be around 8 mm in inner diameter and approximately 450 mm in length. As can be seen in Figure 8.7, the Cottrell tube opens up into another chamber, part 8. Part 8 was fairly complex to build as it houses a temperature probe

(part 10). There should be no spaces between the temperature probe housing and the walls of part 8 as this will lead to inaccurate experiments. The chamber has a drain at the bottom (part 19) for the liquid and a vapour exit which opens into part 12.

The vessel housing parts 7 and 8 is the Cottrell pump chamber, it is approximately 70 mm in internal diameter and 280 mm in height. Part 9 is the port into which the temperature probe (part 10) will fit, for this reason, part 9 has to be externally tapped. Part 11 is a port which has to be externally tapped as well, it will be used in future to take direct samples of the vapour phase.

Part 12 is the tube that the vapour phase passes through and is about 20 mm in diameter. It passes through part 13, which is a primary condenser. The condenser needs to surround the vapour phase tube (part 12). It is a Liebig type of condenser and should be of approximately 40 mm thick and 90 mm long. Part 12 connects into part 14, which is the secondary condenser and is a coil type (dimroth) of condenser (part 41). The condenser itself is 40 mm wide and approximately 170 mm in length.

The bottom of the secondary condenser extends into a sample well, part 15. The well is housed in a chamber which is 16 mm in diameter and 90 mm in length. The well has a pneumatic stopper (part 35) which allows liquid to pass through part 16 into the vapour condensate sample well (part 18) when open or pass through a droplet counter (part 17) and back into the mixing chamber (part 1) when closed. Part 16 is approximately 10 mm in diameter. Part 17 is the vapour condensate droplet counter and is 30 mm in diameter. It should have an externally tapped port of 12 mm in diameter. It is connected to the sample well (part 15) with a tube of 10 mm in diameter and to the mixing chamber (part 1) with a tube of 7 mm in diameter.

Part 18 is the vapour condensate sample vial and is 12 mm in diameter. The chamber housing the sample vial is to be 22 mm in external diameter and 60 mm long. It should be externally tapped for the lid of the sample vial to screw on.

Part 19 is the tube through which the liquid phase passes from the Cottrell tube housing vessel and into the liquid sample well (part 21). It is approximately 10 mm in diameter.

Part 20 is an Allihn type of condenser and has a function of cooling any vapour produced from the heated liquid sample. It is approximately 40 mm thick and 170 mm in height. At the bottom of the condenser is the liquid sample well (part 21). The well is also housed in 16 mm diameter and 90 mm long chamber like part 15 and has a pneumatic stopper as well (part 34).

The sample well (part 21) and it's stopper (part 34) allow liquid to pass through a connector tube (part 22) and into the liquid sample vial (part 23) when open or into the liquid droplet counter (part 26) and back into the mixing chamber (part 1) when closed. Part 22 is approximately 10 mm in diameter and the liquid sample vial (part 23) is 12 mm in diameter. The chamber housing the sample vial (part 23) is to be 22 mm in external diameter and 60 mm long. It should be externally tapped for the lid of the sample vial to screw on.

Part 24 is a connector tube between the liquid sample well (part 21) and the liquid droplet counter (part 26) and is approximately 8 mm in diameter. The droplet counter (part 26) is 30 mm in diameter and should have an externally tapped port of 12 mm in diameter. The droplet counter is joined to the mixing chamber. Parts 25 and 27 are connector tubes joined to the liquid sample droplet counter and are both 8 mm in diameter. Part 28 is an expansion to part 27 and is 12 mm in diameter, it connects the feed droplet counter (part 30) to part 27.

Part 29 is the feed vessel into which the amount of feed being loaded can be measured. It is a normal measuring vessel and is approximately 250 mL in volume, 52 mm in diameter and 220 mm in height. Part 30 is the feed droplet counter and is connected to the feed vessel via a 10 mm connector tube. The feed from the feed vessel to the feed droplet counter is controlled using a precision stopcock valve.

Part 31 is a port attached to the feed vessel (part 29) and is open on the top. This port does not have to be externally tapped, it has a diameter of 16 mm and is about 60 mm in length. Part 32 represents a connector tube manifold from the top of the feed vessel (part 29) to the feed droplet counter (part 30), these tubes are 10 mm in diameter.

Part 33 is a vacuum pipe port attached to the main common tube (part 40). Part 33 is 12 mm in diameter and is the port that the vacuum pump needs to be attached to. This port does not need to be externally tapped. Part 40 is also 12 mm diameter and approximately 400 mm in length.

Parts 34 and 35 as mentioned earlier are pneumatic valve rods. These are made of glass as well and are approximately 7 mm in diameter. The rods fit into ports that are connected to the secondary vapour phase condenser and the liquid sample condenser. The ports should both be externally tapped and should be 19 mm in diameter.

Parts 36 and 37 are both connector tubes and are 10 mm in diameter and approximately 40 mm in length. Parts 38 and 39 are also connector tubes both 10 mm in diameter.

Parts 1, 13, 14, 20 and 29 are basically standard laboratory glassware equipment. Table 8.8 highlights the catalogue number on which a visual description of these parts can be found in the attached link for a similar product from Sigma-Aldrich.

Table 8.8: Common parts description found in Sigma-Aldrich website [12]

Part	Name	Sigma-Aldrich link [12]
1	Volumetric flask	http://www.sigmaaldrich.com/catalog/product/sigma/z326747?lang=en&region=ZA
13	Liebig condenser	http://www.sigmaaldrich.com/catalog/product/aldrich/z530964?lang=en&region=ZA
14	Dimroth condenser	http://www.sigmaaldrich.com/catalog/product/aldrich/sync124200?lang=en&region=ZA
20	Allihn condenser	http://www.sigmaaldrich.com/catalog/product/aldrich/sync621200?lang=en&region=ZA
29	Measuring cylinder	http://www.sigmaaldrich.com/catalog/product/aldrich/z647381?lang=en&region=ZA

As part of the construction of the experimental setup, a number of different tubes and fittings were used to either connect parts of the process or to simply direct air flow. Some of the fittings used were:

- ½” female NPT T-piece fitting to connect the regulator to the PRV (1/2” male NPT end) and main nitrogen line
- ¼” nuts and ferrules
- ½” to 3/8” reducing bush to connect the regulator to the T-piece
- ½” to ¼” reducing bush for the main nitrogen line
- ¼” insert fittings
- ¼” silicon flexible pipe
- ¼” ball valves with male NPT ends for isolation puproses
- ¼” needle valves with male NPT ends for air flow regulation purposes
- ¼” 4-way female NPT fitting

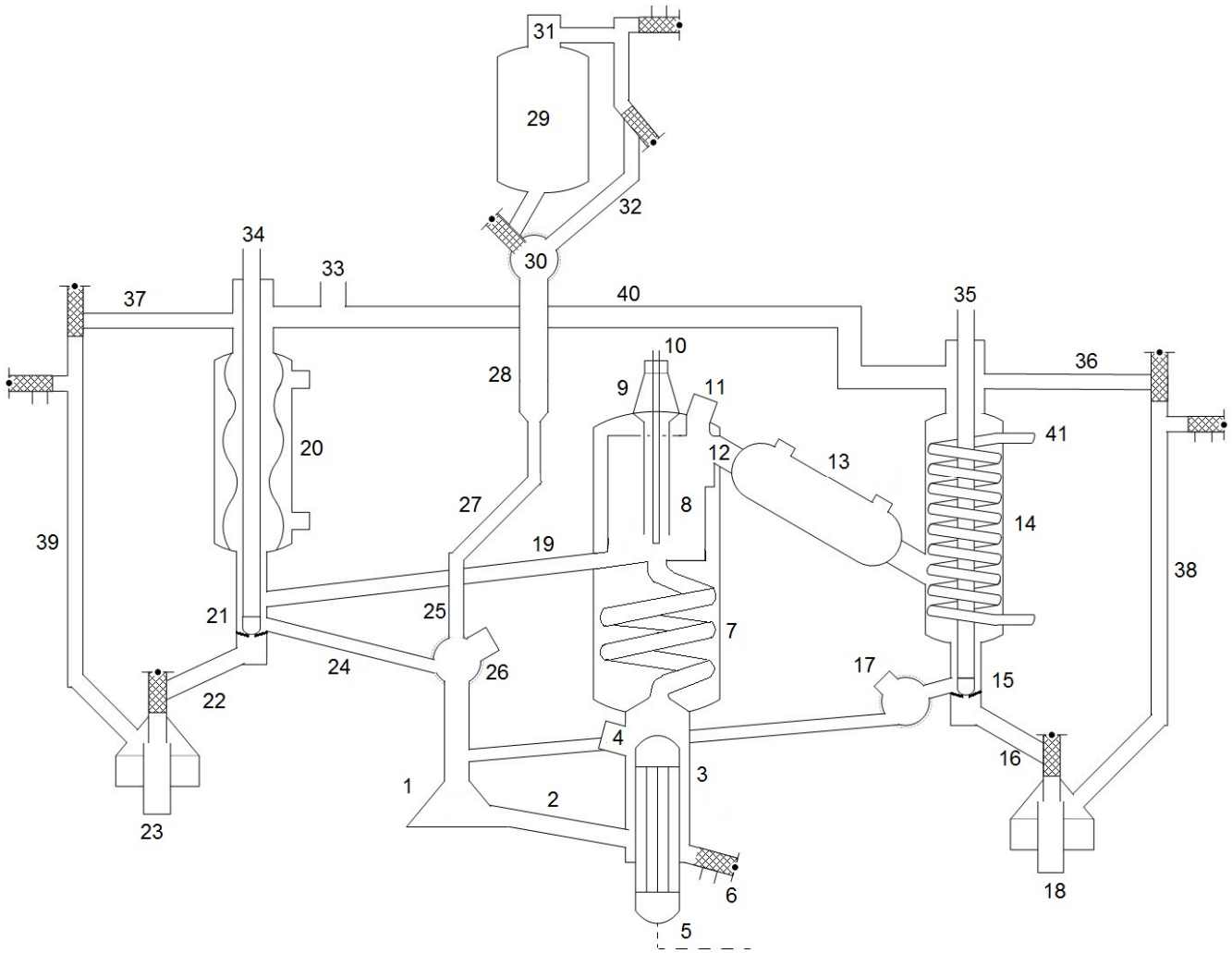

Figure 8.7: Detailed description of still to be built

The Gillespie chamber (vessel that houses the Cottrell tubing) is shown in detail in this section. Figure 8.8 shows a technical drawing of the chamber/vessel together with measurements for the different parts. All sizes are in mm. All ports need to be externally tapped. The Cottrell tube is in the shape of a coil and is about 450 mm – 500 mm in length and 135 mm in height. Each tube outer diameter is around 8 mm and the coil diameter will be less than 60 mm, since that is the diameter of the chamber. The Gillespie chamber has to fit in both the Cottrell tubing (coil) and the section in which the vapour and liquid phases separate.

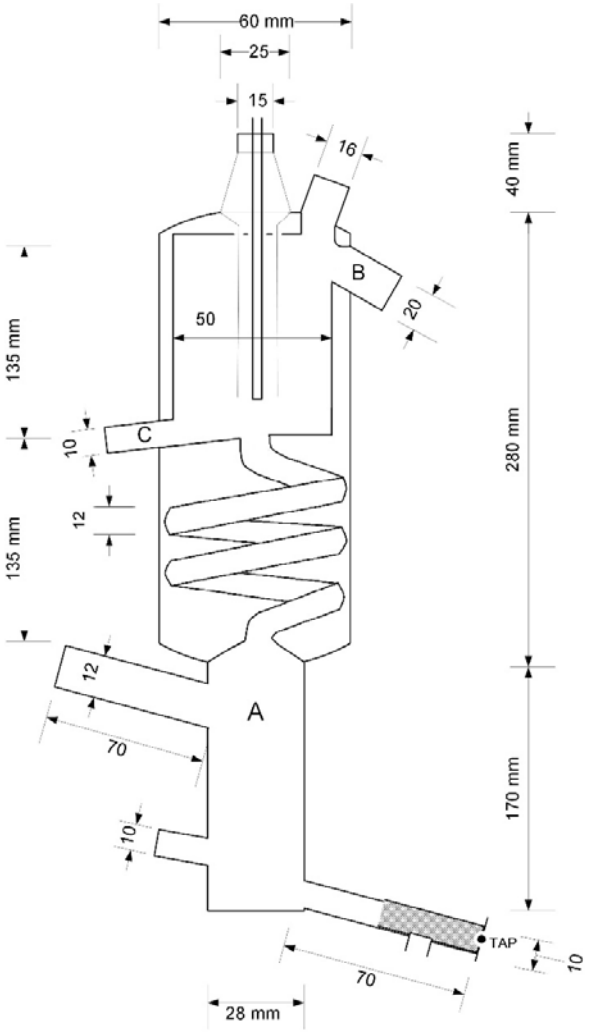

Figure 8.8: Detail measurements of the Gillespie chamber. A – Heating chamber; B – Vapour exit; C – Liquid exit.

Appendix E: Equilibrium still operation

This Appendix describes the operation procedure for the newly built VLE still. Aspects of preparation, start-up, steady state operation, sampling and analysis, shut down, emergency shut down and draining and washing procedures are all explained.

E-1: Preparation

The preparation of the still is required to make sure that no hiccups are experienced during operation of the still. The following should be checked prior to the commencement of each new experimental run:

- Open the fume hood doors and inspect the glass still to make sure that everything is still in place and that there are no cracks anywhere on the glass.
- The still should have been washed with acetone or dichloromethane as per the draining and washing procedure to be explained below.
- The still should be completely dried with compressed air having been passed through each and every nuke and corner in the setup to prevent contamination of any planned runs. The stop valves on the still can be manipulated to direct air flow through whichever part requires drying.
- The cooling water should be available in a bucket behind the still and the water pump should be operational.
- The magnetic stirrer should be operational.
- The oil level in the vacuum pump should be sufficient and the maintenance of the pump should be confirmed.
- The nitrogen or argon air cylinder pressures should be confirmed.

The still can now be started up by switching on the main power switch connected to the wall socket in the lab.

E-2: Start-up

The following steps should be followed for starting up the still:

- Load the system with feed using a beaker and the feed loading chamber, directing it to the mixing chamber using the appropriate stop valve.
- Switch on the power switch located on the left side panel of the stainless steel housing.

- Switch on the water pump and magnetic stirrer at the back of the setup by switching on the power supply to these two elements at the wall socket.
- Calibrate the touch screen interface using the available stylus (or your finger – stylus preferable) by touching the indicating dots as they appear.
- Ensure that the level of feed in the mixing and heating chamber is sufficient such that it covers the top of the cartridge heater – this is to prevent burnout of the heater.
- Pressure setting: For the vacuum setting, ensure all valves connecting the still to atmosphere are closed.
- Switch the vacuum pump on and select the desired absolute pressure by clicking on “Pressure” on the touch screen interface and vary the amount using either the slider bar or increment buttons.
- Select the amount of power required from the cartridge heater by clicking on the “Power” button on the touch screen interface and vary the amount using either the slider bar or increment buttons. Each system would require a certain amount of power depending on the volatility of the mixture itself.
- Select the temperature of the insulation heating jacket required by clicking on the “Jacket” button on the touch screen interface and vary the amount using either the slider bar or increment buttons. The jacket is used for insulation purposes and is usually set to 15 K less than the mixtures boiling point.
- Once the feed starts to boil and the insulation jacket reaches its appropriate temperature, the system can be closed off from atmosphere by ensuring that all atmosphere-connecting stop valves and caps are tightly closed.
- Ensure that the sample vials are also tightly closed.

For overpressure systems, ensure that the bleed valve is open and that the overpressure line is correctly directed to the setup. Then open the nitrogen cylinder’s regulator slightly. Pressure can be maintained by balancing the amount of nitrogen entering the system through the regulator on the cylinder and manual needle valve on the pressure line with the amount passing through the bleed valve. This way, the contents of the experiment stay within the still and do not exit with the passing nitrogen.

For vacuum systems, ensure that the bleed valve is open to a maximum of one revolution from the closed position and that the vacuum line is correctly directed to the setup with the in-line vacuum trap and proportional valve. The proportional valve will try to control the vacuum level in the still, once it stabilizes, adjust the bleed valve very slightly to achieve minimal error between the set pressure and actual pressure displayed on the pressure transmitter.

E-3: Operation

Within almost 20 minutes after the start-up procedure is completed, the system should be approaching stability and a liquid return would indicate that the amount of feed in the system is sufficient. The liquid return however should be more or less equal to the vapour return, this ensures that the vapour bubbles are sufficiently pumping the liquid through the Cottrell tube and that vapour and liquid phase mass and energy transfer taking place in the tube itself.

If the liquid return is far greater than that of the vapour return, it means that there is too much feed in the system or that the energy input from the cartridge heater is excess of that required. This can be rectified by first checking the boiling characteristic in the heating chamber and bubble flow through Cottrell tube if possible.

If the bubbles forming on the heater are larger than roughly 1 cm in diameter and there isn't a liquid film covering the heater's metal surface, it means that the energy input is too high and it should be decreased by reducing the power on the touch screen interface.

If the bubbles being formed are smaller than roughly 1 cm in diameter and allow the heater's metal surface to have a liquid film mostly surrounding it, the energy input is fine and the feed is too much. The amount of feed can be decreased using the drain at the bottom of the heating chamber.

Another issue that requires attention during operation is the pressure of the system, especially during overpressure operation since there is not automatic valve to control overpressure. The automatic valve can be modified to control overpressure however it was not seen as necessary in this study since the majority of work will be done at vacuum conditions. Overpressure can however be steadily maintained by adjusting the bleed valve to balance the amount of nitrogen passing through.

Once the pressure is stable and the liquid and vapour returns are fairly equal (~80 droplets per minute) and stable as well, the temperature reading would start to stabilise. This is the equilibrium temperature being measured as the vapour and liquid bubbles exit the Cottrell tube. This reading can be seen on the touch screen as the left hand side value of Temperature Probe A – it is the calibrated value as compared to the value displayed on the right hand side.

Temperature stabilisation indicates equilibrium is being achieved and at least 30 minutes should be given to ensure that all the samples in the well are flushed out with the equilibrium liquid and vapour fractions before sampling.

E-4: Sampling and analysis

Sampling

Sampling is a fairly concise procedure as well. Taking too much sample of the vapour and liquid phases may shift the equilibrium. Taking too little sample may lead to evaporation of a component. Neglecting to clean the sample vials may lead to contamination. Precautions against these mistakes need to be taken carefully while sampling.

Before sampling of the phases commences, the sampling wells need to be flushed and sample vials replaced with clean vials. Flushing can be performed by using a magnet to levitate the glass rods (with metal rods inside them), causing the liquid to pass through the sample wells and into the sample collection area which can then be directed into a sample vial using the sample collection stop valve.

One flush on the liquid side and three flushes on the vapour side (liquid sample well hole is larger and vapour sample well hole) are sufficient to flush the wells and not disturb the equilibrium temperature drastically. If the temperature does change drastically, one should restart the operation process, however, it is advised to wait a further 20 minutes before actually sampling since the equilibrium has been disturbed albeit slightly.

Before replacing the sample vials, the system needs to be isolated using the isolation and aeration valves. After the system is isolated and the sample vials are at atmospheric pressure, the vials can be gently screwed out and the replaced with clean ones.

Phase sampling can then commence by basically flushing the sample wells and recording the temperature and pressure. Once again, one flush on the liquid sample well and three flushes on the vapour sample well is sufficient (for analysis). This should give roughly 150 µL to 200 µL of each sample. This process can be repeated if insufficient sample is collected. One should be careful however to ensure that the equilibrium temperature does not change more than 0.1 K while doing this. It will however slightly change as sample is taken and the second temperature can be recorded.

Sample vials and the system can then be isolated and removed, followed by the sample being collected using a micropipette.

Analysis

The samples can be stored in 2 mL sample vials for further analysis. Samples should be stored in the fridge and analysed within 24 hours of collection to reduce the risk of any components evaporating due to their volatility.

Before analysis of any samples can be analysed, a method for analysis and calibration curve need to be developed. The method will comprise of the following:

- Amount of sample to be analysed
- Amount and type of internal standard to be injected with sample for sample identification purposes
- Type of solvent to be used
- Temperature profile of GC for analysis
- Pressure characteristic of analysis
- Injection procedure

The calibration curve can then be developed between the individual components and internal standard using the suitable method and known masses of the components and internal standards.

The analysis procedure is as follows:

- Take 20 µL of required sample and add it to a 2mL sample vial
- Add 20 µL of internal standard and take not of the mass using the scale available in the GC lab on the fourth floor (lab C402)
- Top up the sample vial with solvent until the 2 mL mark
- Insert the sample in the GC holder and use the developed method to analyse the peaks produced

The samples in this study were analysed using the Agilent 7820A GC equipped with an auto sampler and Flame Ionisation Detector (FID). The column is a non-polar capillary column with dimensions 60 m x 0.18 mmID x 0.10 µm and can run at a maximum temperature of 623 K.

Each system will require a unique analysis method and calibration curve in order to accurately determine the mass fractions of each component in a sample.

E-5: Shut down

After all required equilibrium samples have been collected and the runs complete, the system can be switched off. The shut down procedure can be conducted in the following steps:

- If working at overpressure conditions, close the nitrogen cylinder and open the bleed valves such that the system comes back to being open to atmospheric conditions.

- If working at vacuum pressures, open the bleed valve first and then then switch off the vacuum pump. This prevents any sort of mechanical shock that the setup may have by bringing the system back to atmospheric pressure before switching the pump off.
- Click on the “Power” button on the touch screen interface and reduce the power to a zero value.
- Click on the “Jacket” button on the touch screen interface and reduce the temperature to a zero value or room temperature value.
- Leave the water pump and stirrer on for at least ten minutes before switching them off as well. This allows the still to cool down gradually.

Once the heating chamber and the still have cooled down, the power switch on the left hand side panel and the man power switches on the wall can all be switched off. The still is now ready for draining and washing.

E-6: Emergency shut down

The emergency shut down procedure is as follows:

- Briskly open the bleed valve so as to open the system to atmosphere
- Switch off the main power switch at the wall socket
- Immediately close the nitrogen cylinder if operating at overpressure OR
- Switch off the vacuum pump at the wall socket if operating at vacuum conditions

E-7: Draining and washing

Once the still is cooled down and the system switch off, the feed can be drained at the bottom of the heating chamber and stored for either disposal or recycling. The feed should be completely drained, this will take about 5 minutes. The cartridge heater should also be removed as some feed collects between it and the drain valve. The cartridge heater can be removed by gently unscrewing it from the still and carefully sliding it out.

Compressed air can also be used to dry or direct any collection of liquid in a difficult-to-drain area such as in the pressure connection tube or the Cottrell tube overflow drain. The compressed air line should not be connected by disconnecting the vacuum and overpressure lines and directing the flow of air through the proportional valve as this will cause the pipes to come off their connections.

Once drained, the drain stop valve should be closed and the still should be loaded with acetone in such a way as if it is a feed material. The operation procedure can then be followed to boil the acetone through the still. This cleans the still as it operates and does not need to be operated at either vacuum or overpressure conditions. During operation, the still should be opened to atmosphere and the fume hood for the still should be closed and switched on. The still should run with acetone being boiled for at least one hour to ensure that the still is clean.

The operation can then be stopped using the shut down procedure and consequently drained using the procedure explained above. Thereafter, the still can be dried using compressed air. One should make sure that the pressure does not exceed 110 kPa while suing compressed air. To be safe, one should use 106 kPa as a maximum air pressure within the still while drying.

Every nuke and corner in the still should be dried by adjusting the stop valves and manipulating air flow through different parts of the still, drying each part as it passes through. The stop valves can be removed from the still by unscrewing them and hence taken apart and dried separately as well.

The total time for drying the entire still could take anything between 30 minutes to 1 hour, however, this will depend on how effectively each part is dried as well.

Appendix F: Hazard and operability study (HAZOP)

A basic HAZOP was performed on the constructed still in terms of the process and operational procedure [98]. It applies to all operational modes including commissioning, start up, shut down and normal operation.

Figure 8.9 shows the new equilibrium still together with the specific nodes (areas) analysed in this HAZOP [98]. Node 1 refers to the cartridge heater that is used to heat up the feed to the system. Node 2 refers to the vacuum pump used to achieve the sub-atmospheric conditions in the system. Node 3 refers to the thermal insulation jacket which has the added ability to heat up, itself and in turn the Gillespie chamber. Node 4 refers to the hot sections in this equilibrium still setup. Finally, node 5 refers to the entire still. Tables 8.9 and 8.10 present the HAZOP for the process and operational procedure respectively.

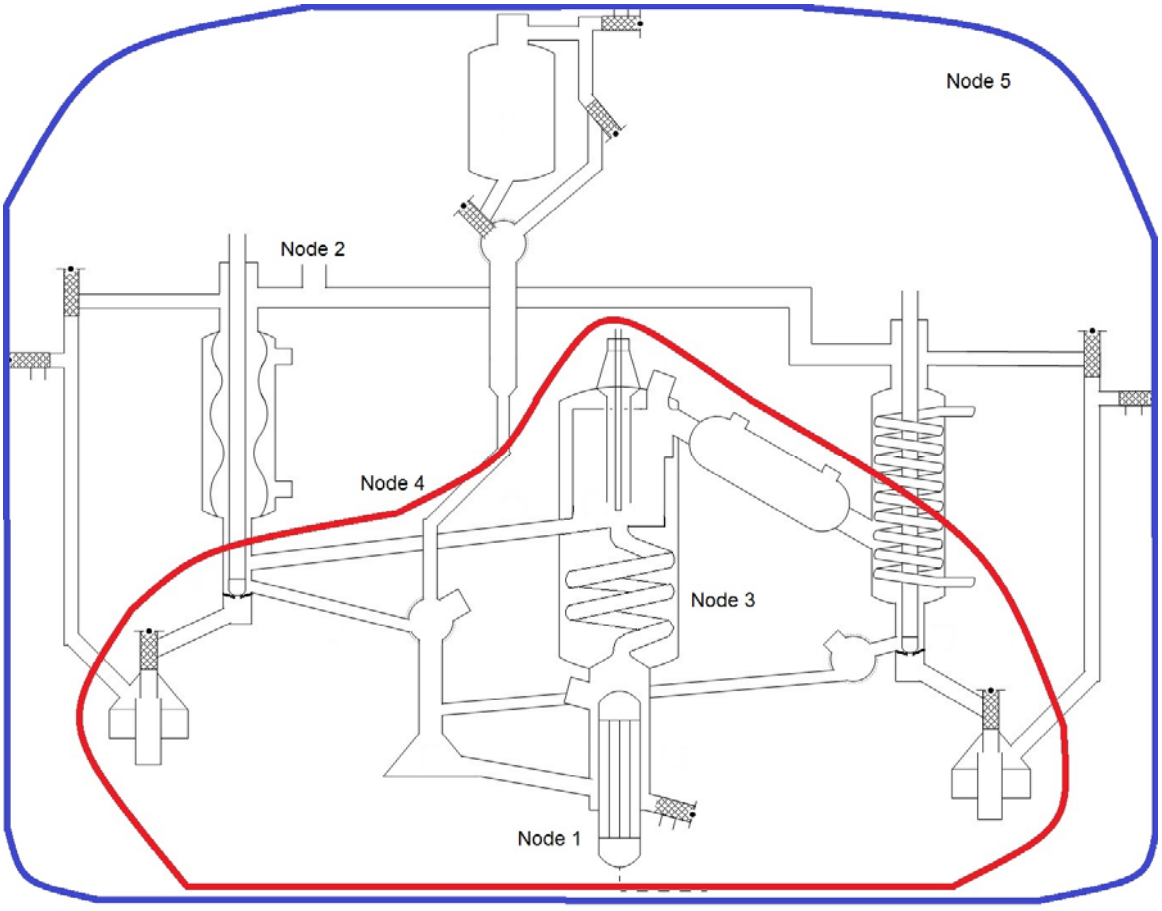

Figure 8.9: Nodes of equilibrium still on which HAZOP study was done

Table 8.9: Process HAZOP

Node	Parameter	Guide-word	Intent	Causes	Consequences	Safeguards
1	Heat	Too much	Specific amount	Heater continuously on	Excessive boiling – too much vapour	Solid state relay – PID.
	Heat	None / Too little	Specific amount	Heater not working	Equilibrium will not be reached	Ensure wattage.
2	Suction	Too little	~ 40 kPa Abs	Leaks Vacuum pump not powerful	Desired pressure unattainable	Close all valves; check for leaks; ensure pump capacity.
	Suction	Too much	~ 40 kPa Abs	Excessive vacuum	Desired pressure unattainable	Proportional valve.
3	Heat	Too much	Specific temperature	Heater continuously on	Excessive boiling – too much vapour	Solid state relay – PID.

Table 8.10: Operational procedure HAZOP

Node	Parameter	Guide-word	Intent	Causes	Consequences	Safeguards
4	Glass	Break	Able to withstand high temperatures	Glass cracks due to excessive heat	Leakages; equilibrium cannot be reached; system crash	Ensure strength and durability of glass during manufacture.
5	Glass	Break	Glass strength / Careful handling	Mishandling of equipment / Horseplay	System crash	Double check each decision during operation;

	Handle with care.

Appendix G: Vapour Pressure Data

Figures 8.10 to 8.12 display the vapour pressure data collected for limonene, *p*-cymene and butylbenzene in this study. The figures also plot reference data as indicated on the graphs. Table 8.11 shows the regression results together with the AAD and AARD values for pressure and Table 8.12 presents the experimental vapour pressure data obtained for limonene, *p*-cymene and butylbenzene. Visually as well as through the AAD and AARD values, the vapour pressure data collected matches that of literature, confirming the temperature and pressure measurement capability of the newly built still.

Table 8.11: Vapour pressure regression results using Antoine equation in Aspen Plus® DRS

	A	B	C	Lower limit	Upper limit	*AAD* (*P*)	*AARD* (*P*)
	Pa	Pa.K	K	K	K	kPa	%
Limonene	74.803	-7269.2	-27.043	199	653	0.3	0.4
p-Cymene	114.01	-18044.2	167.28	206	652	0.3	0.5
Butylbenzene	98.944	-7368.9	-46.959	186	660	0.6	1.0

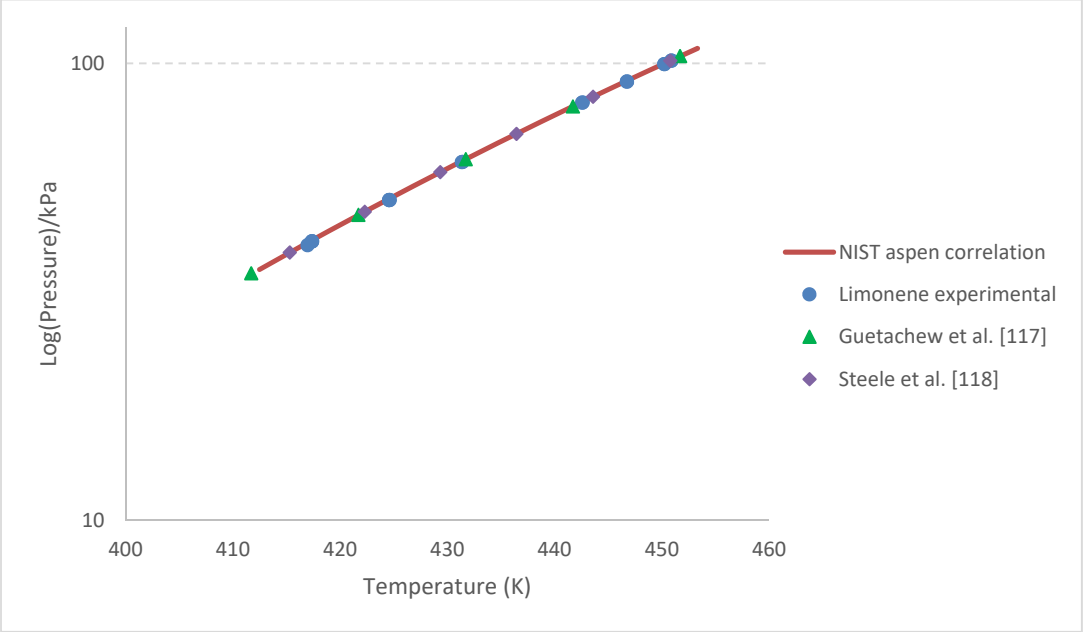

Figure 8.10: Experimental vapour pressure data for limonene compared to literature data [117, 118]

Table 8.12: Vapour pressure data for limonene, *p*-cymene and butylbenzene

Limonene		*p*-Cymene		Butylbenzene	
P (kPa)	*T* (K)	*P* (kPa)	*T* (K)	*P* (kPa)	*T* (K)
40.0	417.0	29.9	406.2	30.5	413.0
40.8	417.4	39.6	416.2	30.9	413.5
40.8	417.4	39.6	416.3	40.0	421.9
40.8	417.4	40.0	416.4	42.7	424.3
50.2	424.6	40.0	416.4	50.0	429.7
50.2	424.6	49.7	423.8	50.4	430.0
50.2	424.6	49.9	423.9	59.7	433.9
60.8	431.4	59.3	430.4	59.9	434.1
60.8	431.4	60.0	430.5	68.9	441.4
82.1	442.6	69.7	436.1	69.0	441.4
82.0	442.6	69.9	436.0	69.0	441.4
91.3	446.8	70.1	436.2	80.0	447.0
91.2	446.8	79.7	441.1	80.1	447.0
99.6	450.2	80.5	441.3	89.9	451.1
99.6	450.3	89.5	445.6	100.8	456.1
101.4	450.9	90.1	445.7	101.4	456.3
101.3	450.9				

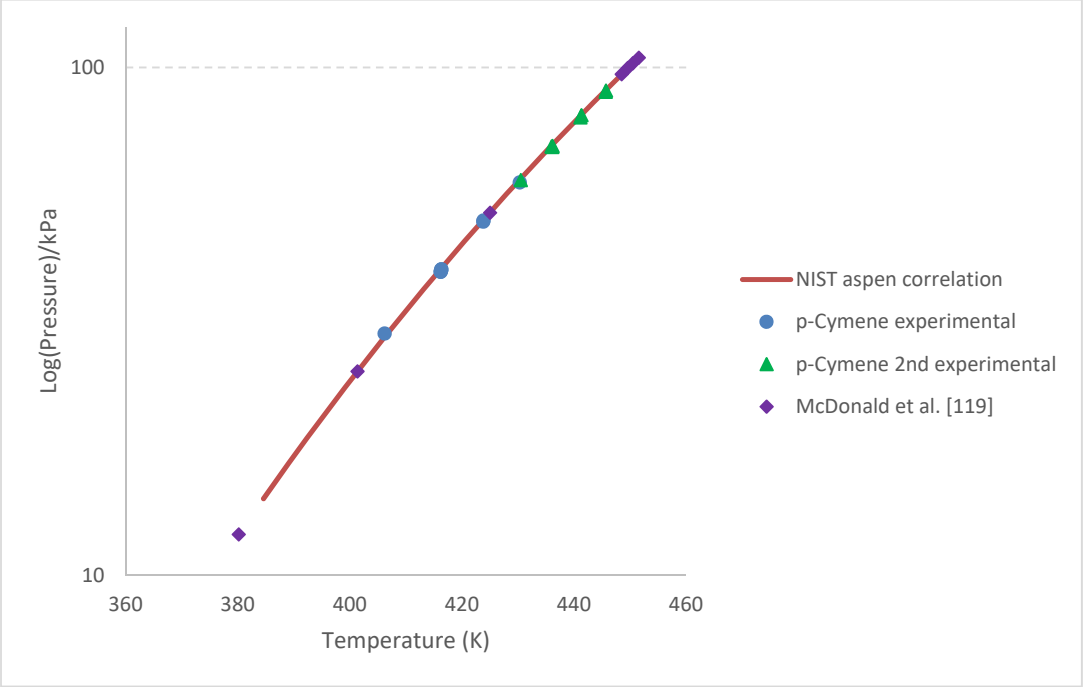

Figure 8.11: Experimental vapour pressure data for *p*-cymene compared to literature data [119]

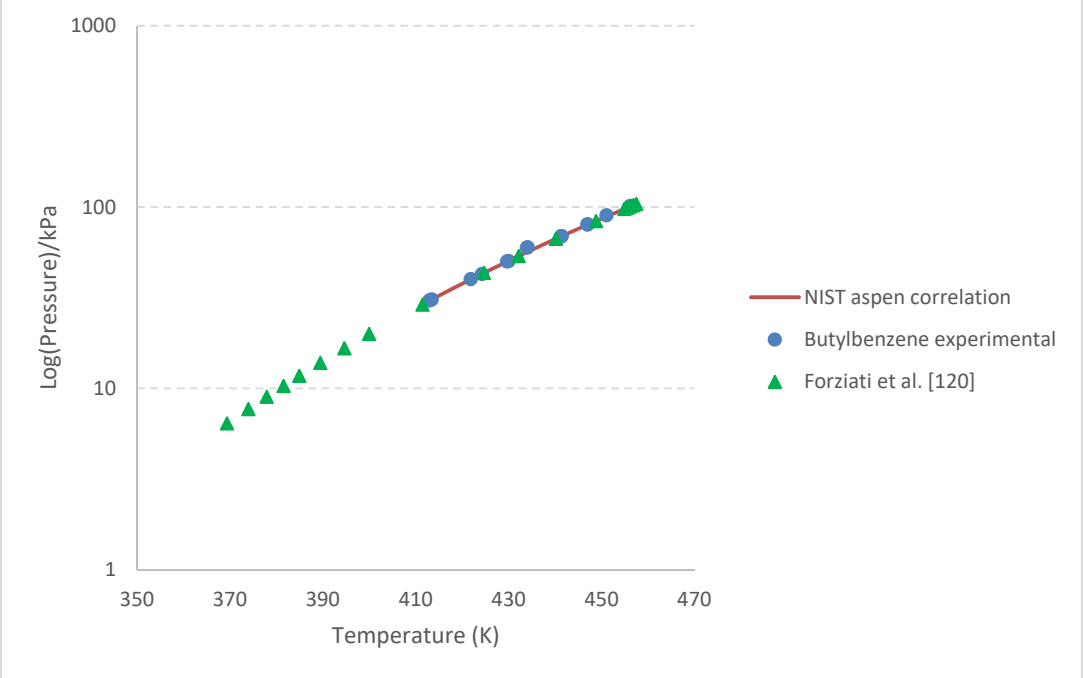

Figure 8.12: Experimental vapour pressure data for butylbenzene compared to literature data [120]

Appendix H: Degradation results

In order to quantify the degradation taking place in a single binary system, experiments were run at 40 kPa under an Argon environment using a single mixtures of fixed feed concentrations. A 100 mL feed mixture was used to start up the still. Once equilibrium was reached in each experiment, samples were taken regularly and the times recorded.

The figures in each sub-appendix depict temperature degradation profiles, concentration degradation profiles, temperature-composition diagrams and the percentage change of limonene fractions compared to the feed respectively, for the respective systems.

The graphs obtained ultimately illustrate general fluctuations for the systems and indicate that 4 hours of operation should be safe enough to obtain reliable data.

H-1: Limonene/*α*-pinene at 40 kPa

A 0.30 mole fraction limonene mixture was used for this test.

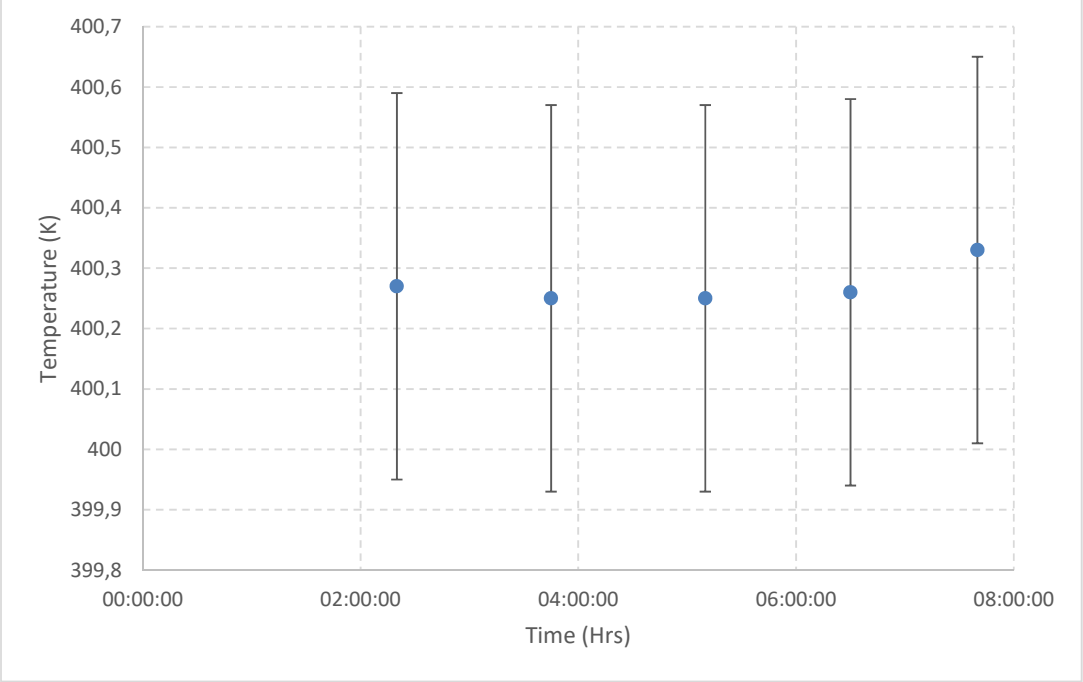

Figure 8.13: Temperature degradation profile for limonene/*α*-pinene system at 40 kPa with +/- 0.32 K error bars illustrating negligible drift within 6 hours of operation

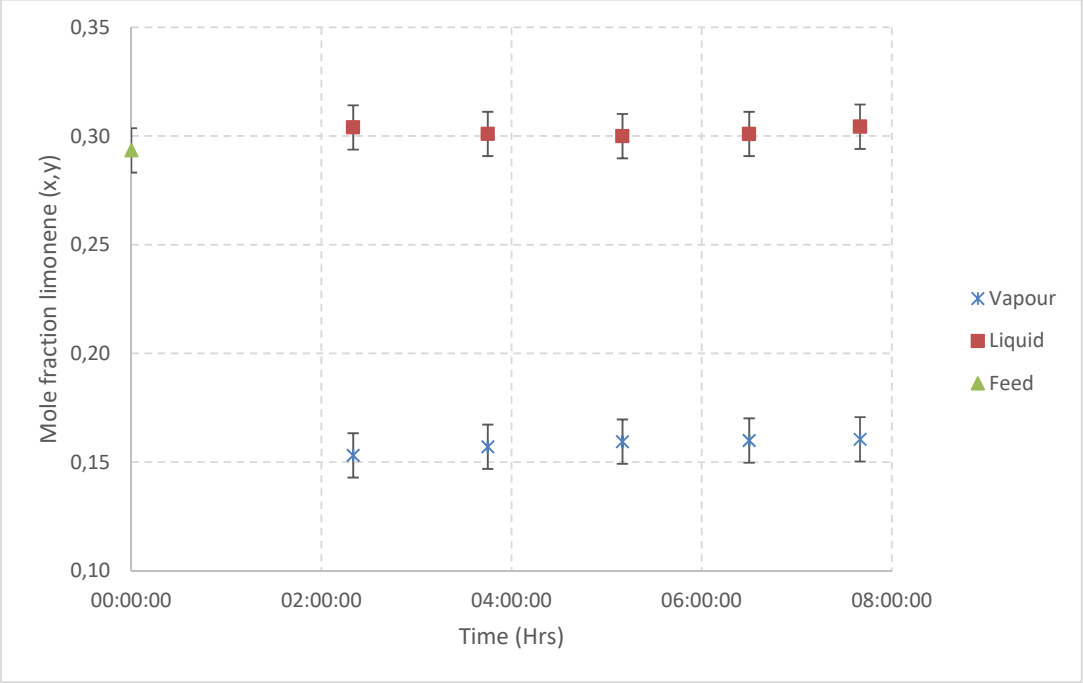

Figure 8.14: Concentration degradation profile for limonene/*α*-pinene system at 40 kPa with +/- 0.0102 mole fraction error bars illustrating negligible drift within 4 hours of operation

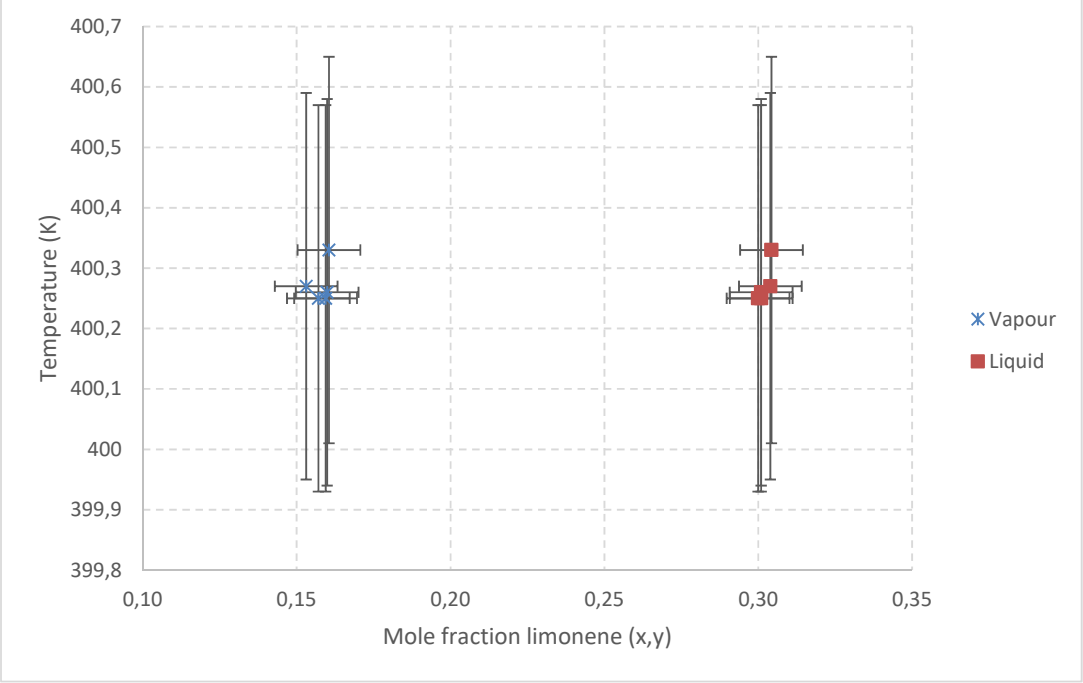

Figure 8.15: Temperature-composition diagram for limonene/*α*-pinene system at 40 kPa illustrating general concentration fluctuation

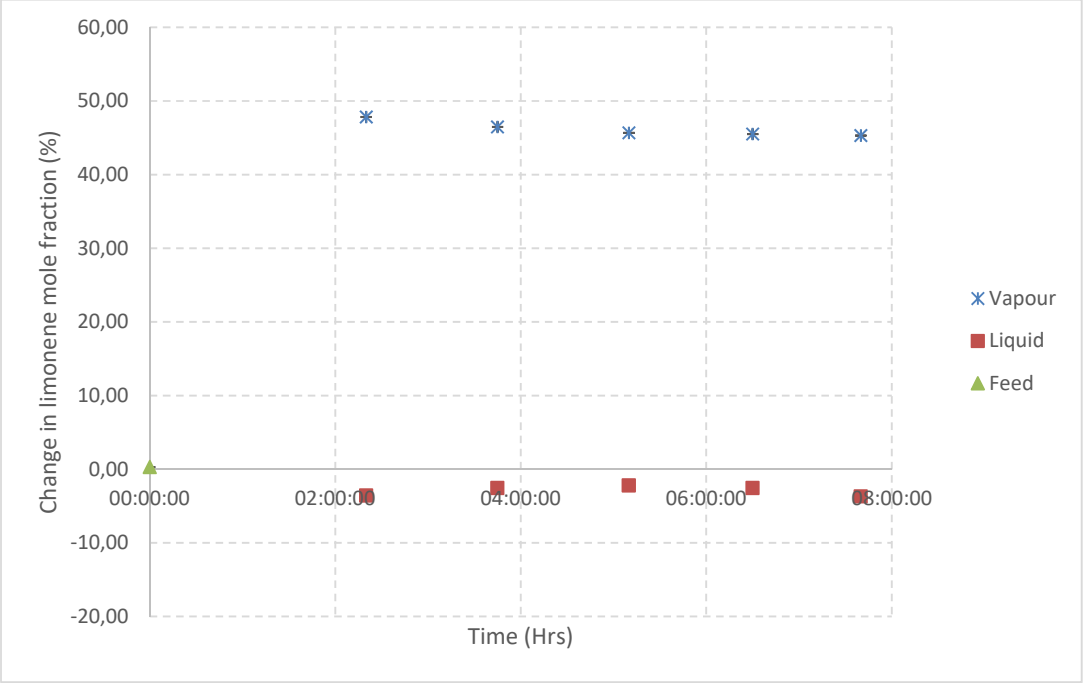

Figure 8.16: Percentage change in limonene fraction compared to feed in limonene/*α*-pinene system at 40 kPa

H-2: Limonene/*p*-cymene

A 0.38 mole fraction limonene mixture was used for this test.

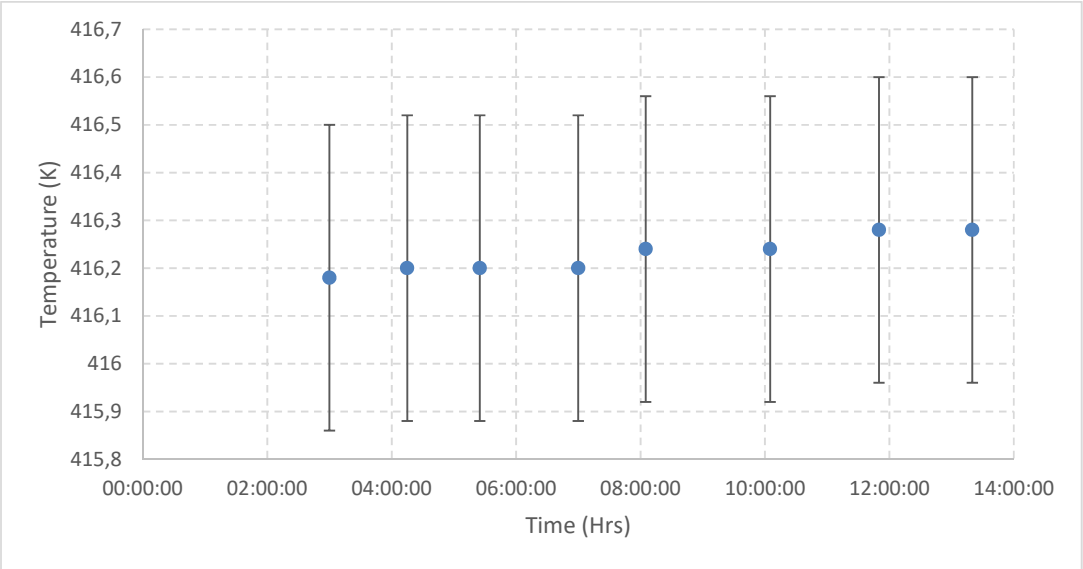

Figure 8.17: Temperature degradation profile for limonene/*p*-cymene system at 40 kPa with +/- 0.32 K error bars illustrating negligible drift within 6 hours of operation

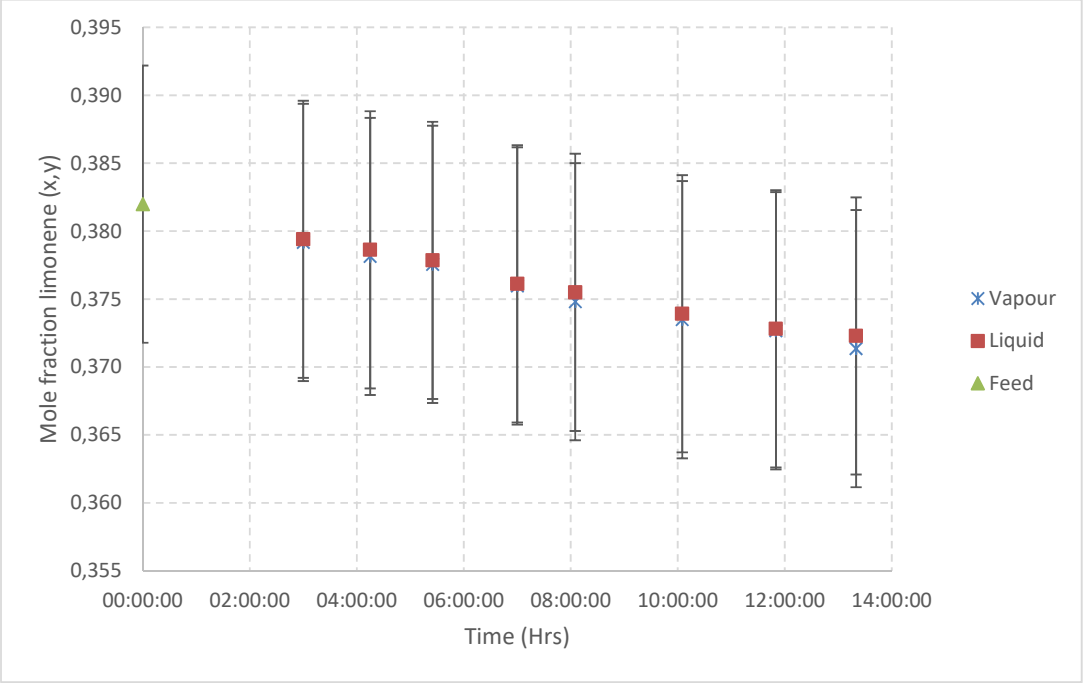

Figure 8.18: Concentration degradation profile for limonene/*p*-cymene system at 40 kPa with +/- 0.0102 mole fraction error bars illustrating reasonable drift within 4 hours of operation

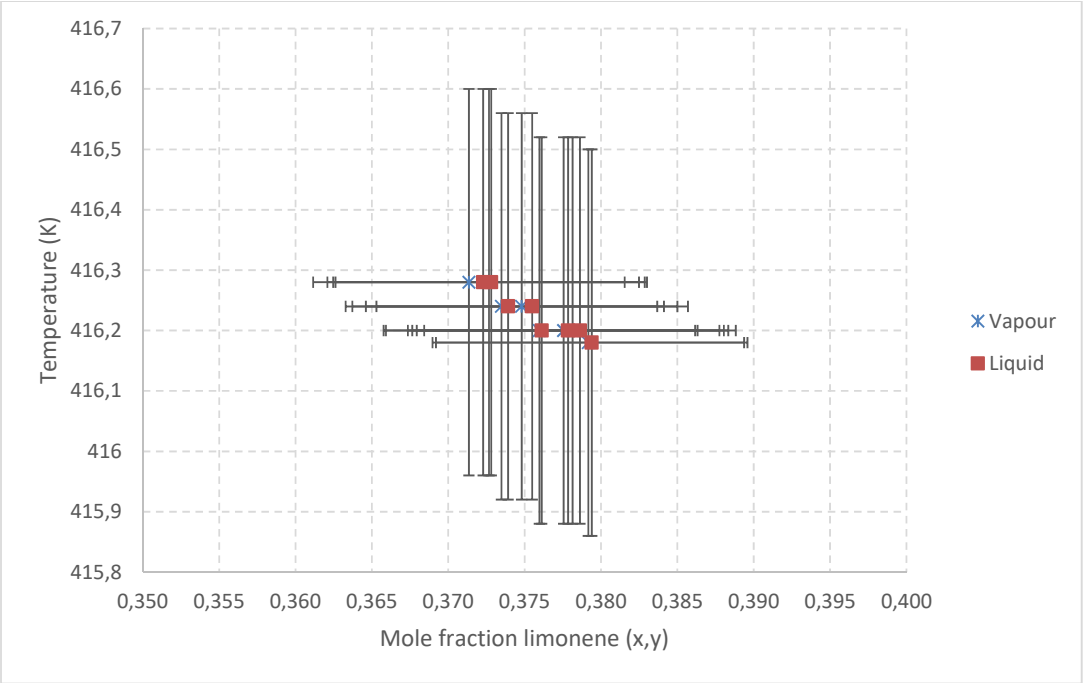

Figure 8.19: Temperature-composition diagram for limonene/*p*-cymene system at 40 kPa illustrating general concentration fluctuation

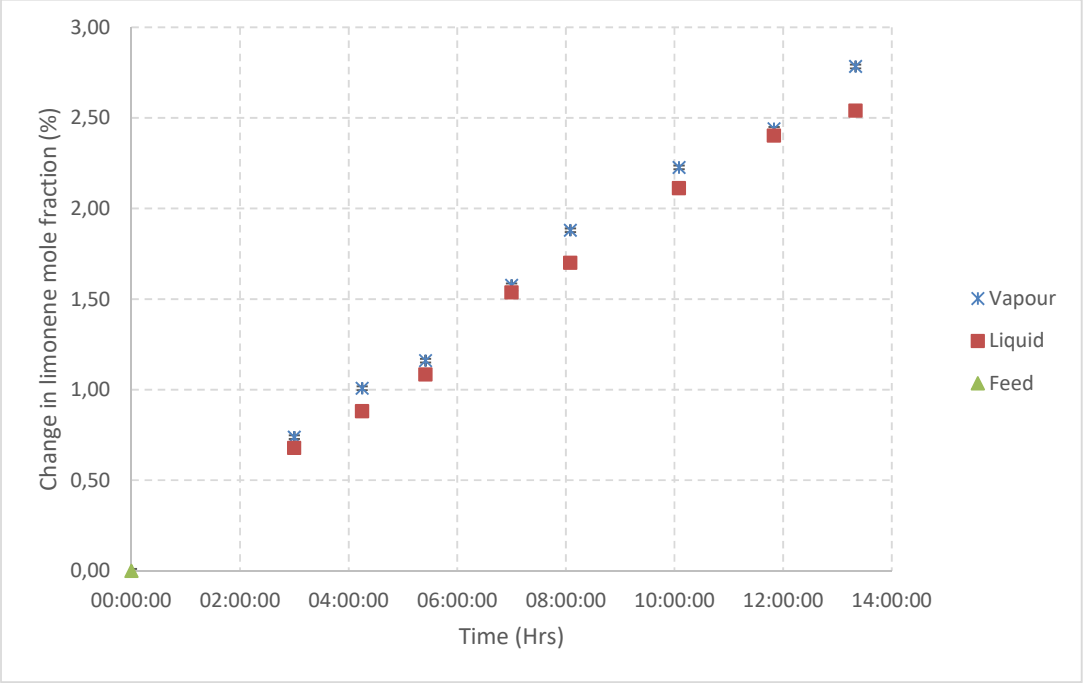

Figure 8.20: Percentage change in limonene fraction compared to feed in limonene/*p*-cymene system at 40 kPa

H-3: Limonene/butylbenzene

A 0.16 mole fraction limonene mixture was used for this test.

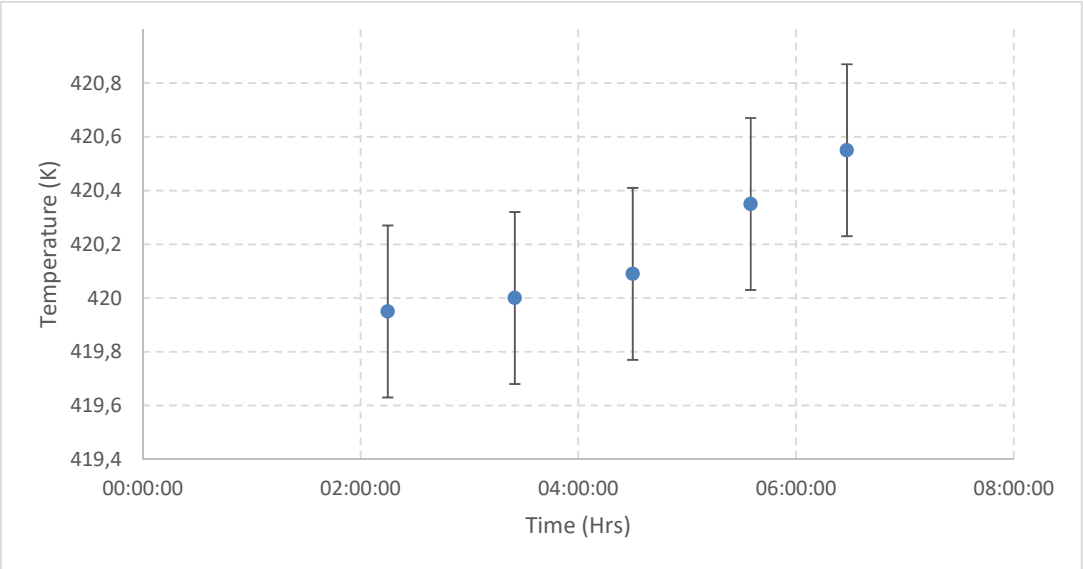

Figure 8.21: Temperature degradation profile for limonene/butylbenzene system at 40 kPa with +/- 0.32 K error bars illustrating reasonable drift within 4 hours of operation

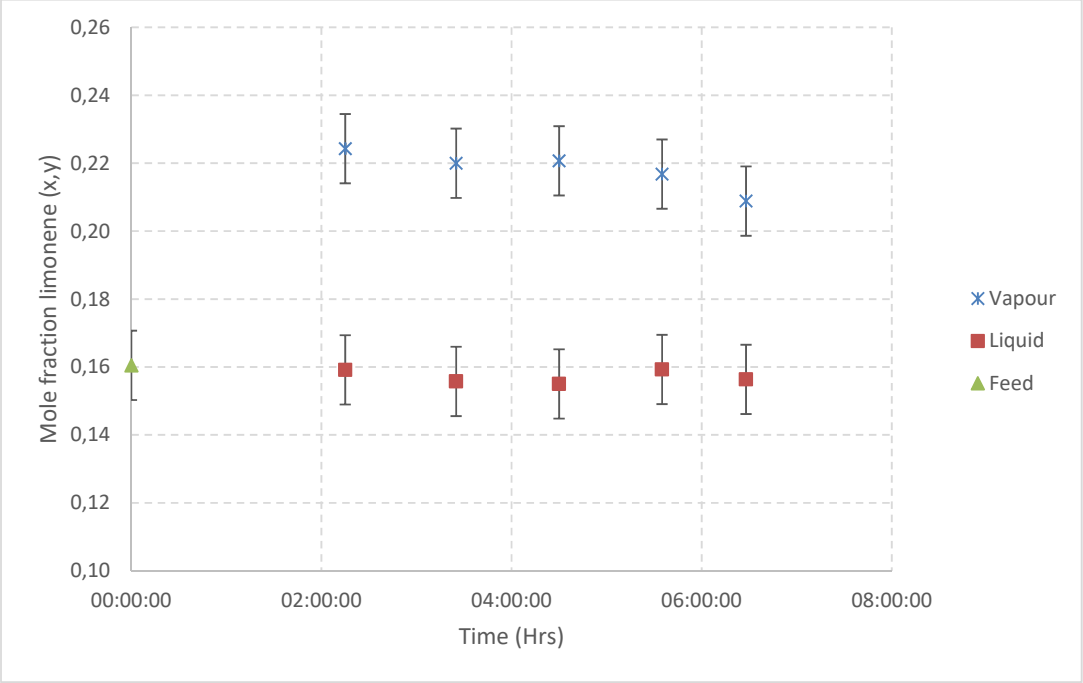

Figure 8.22: Concentration degradation profile for limonene/butylbenzene system at 40 kPa with +/-0.0102 mole fraction error bars illustrating negligible drift within 4 hours of operation

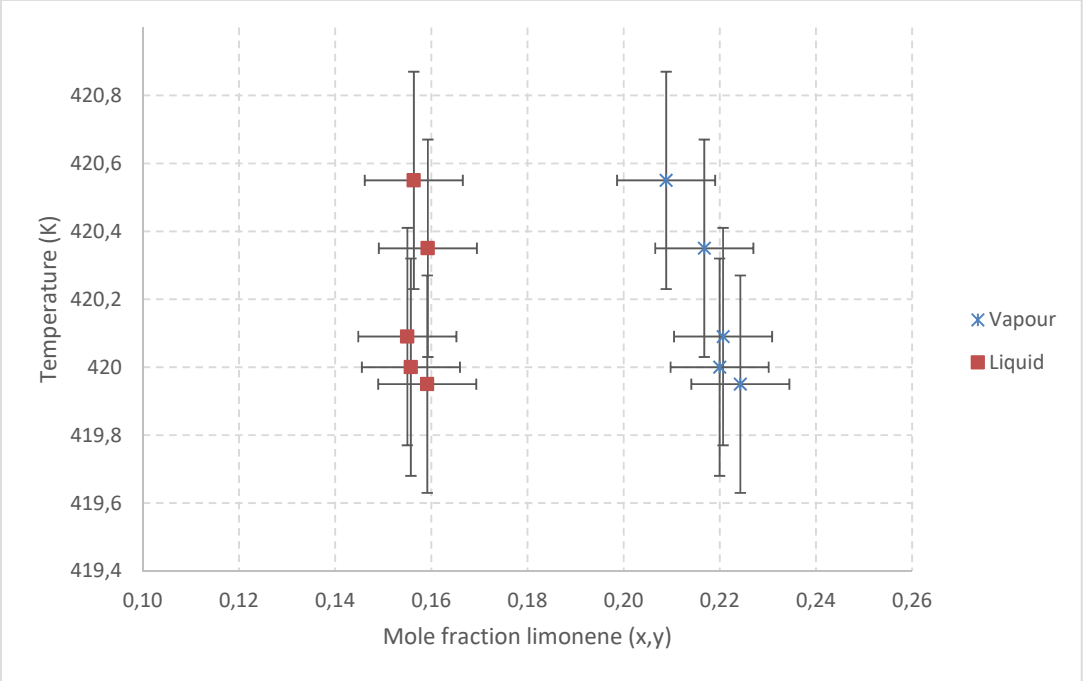

Figure 8.23: Temperature-composition diagram for limonene/butylbenzene system at 40 kPa illustrating general concentration fluctuation

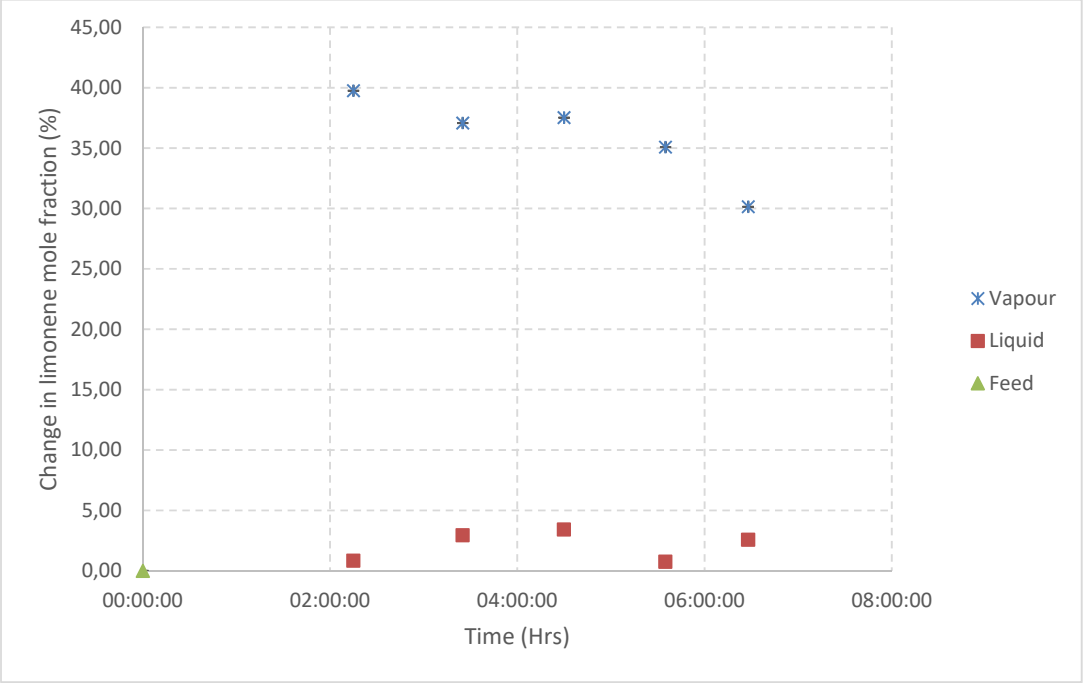

Figure 8.24: Percentage change in limonene fraction compared to feed in limonene/butylbenzene system at 40 kPa

H-4: *p*-Cymene/butylbenzene

A 0.70 mole fraction *p*-cymene mixture was used for this test.

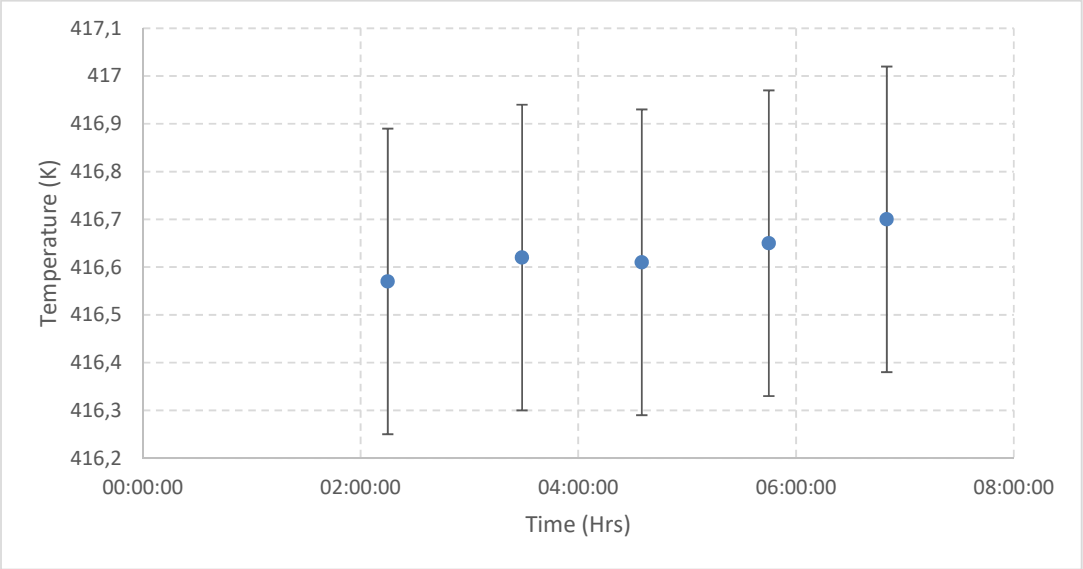

Figure 8.25: Temperature degradation profile for *p*-cymene/butylbenzene system at 40 kPa with +/- 0.32 K error bars illustrating negligible drift within 6 hours of operation

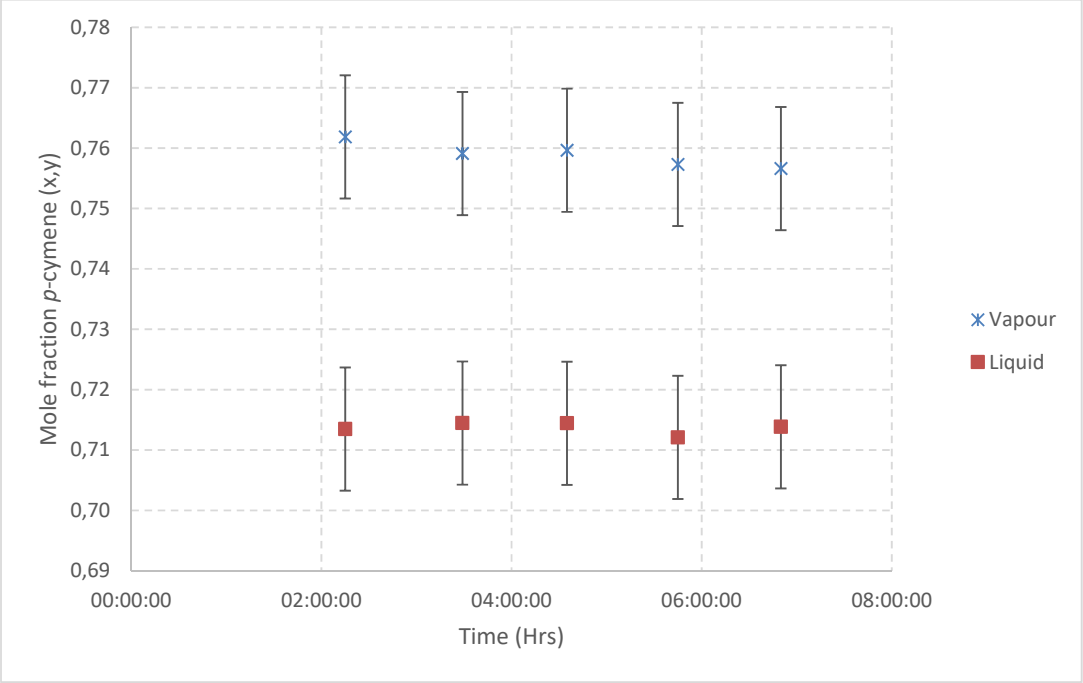

Figure 8.26: Concentration degradation profile for *p*-cymene/butylbenzene system at 40 kPa with +/- 0.0102 mole fraction error bars illustrating negligible drift within 4 hours of operation

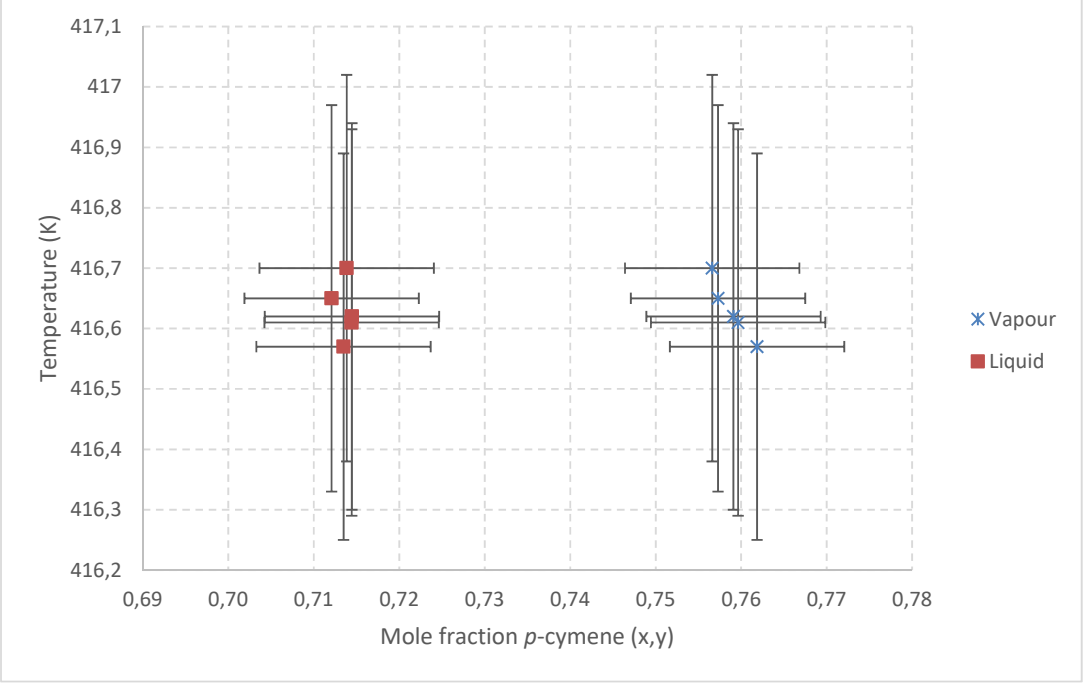

Figure 8.27: Temperature-composition diagram for *p*-cymene/butylbenzene system at 40 kPa illustrating general concentration fluctuation

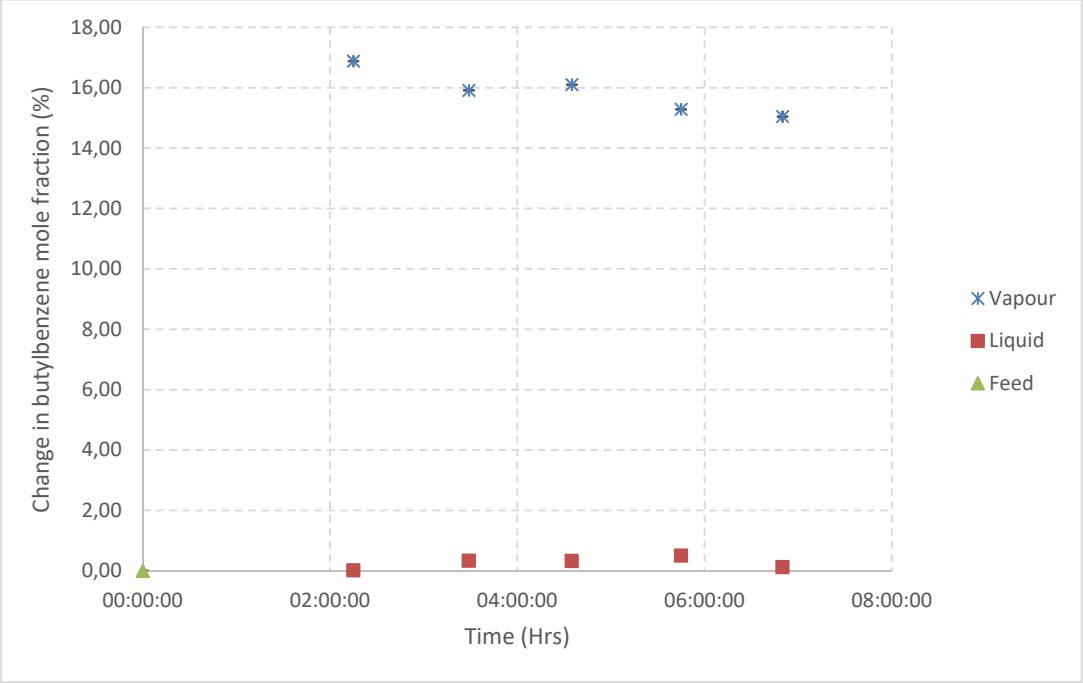

Figure 8.28: Percentage change in butylbenzene fraction compared to feed in *p*-cymene/butylbenzene system at 40 kPa

H-5: Limonene/indane

A 0.73 mole fraction limonene mixture was used for this test.

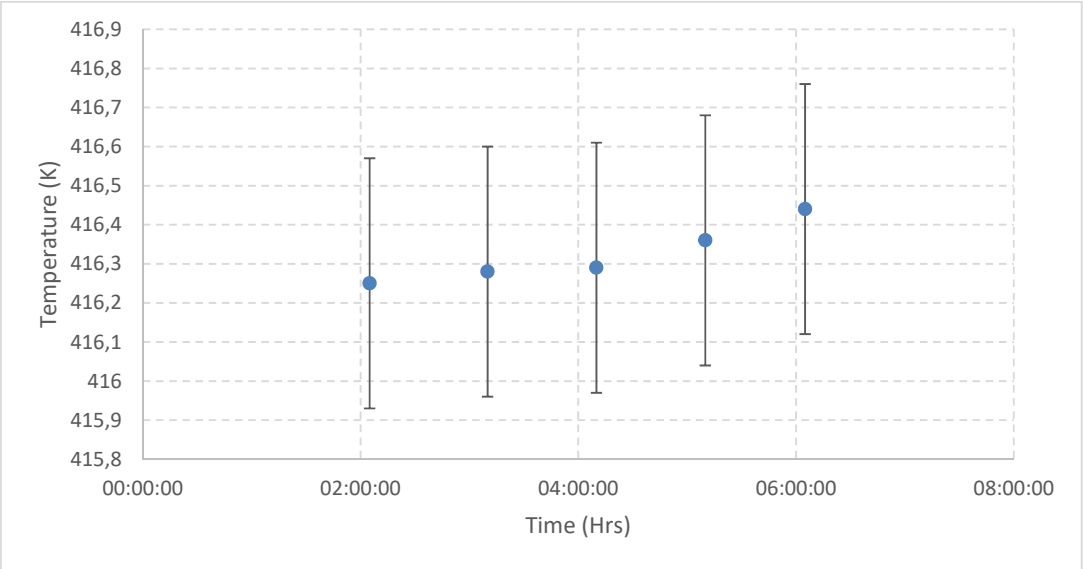

Figure 8.29: Temperature degradation profile for limonene/indane system at 40 kPa with +/- 0.32 K error bars illustrating negligible drift within 4 hours of operation

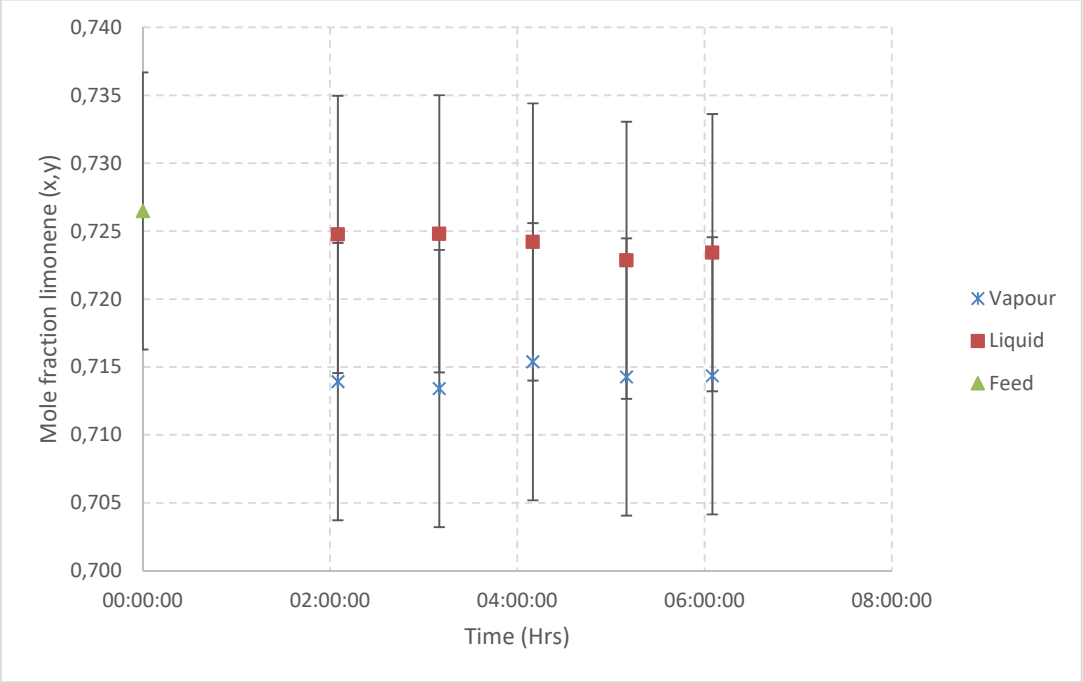

Figure 8.30: Concentration degradation profile for limonene/indane system at 40 kPa with +/- 0.0102 mole fraction error bars illustrating negligible drift within 4 hours of operation

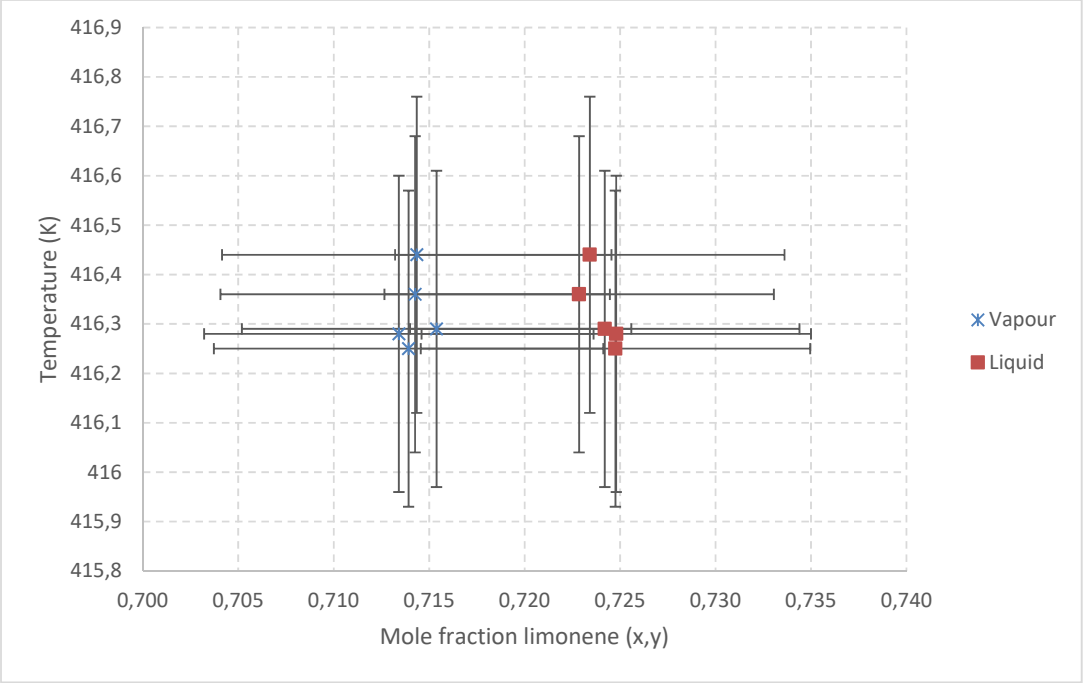

Figure 8.31: Temperature-composition diagram for limonene/indane system at 40 kPa illustrating general concentration fluctuation

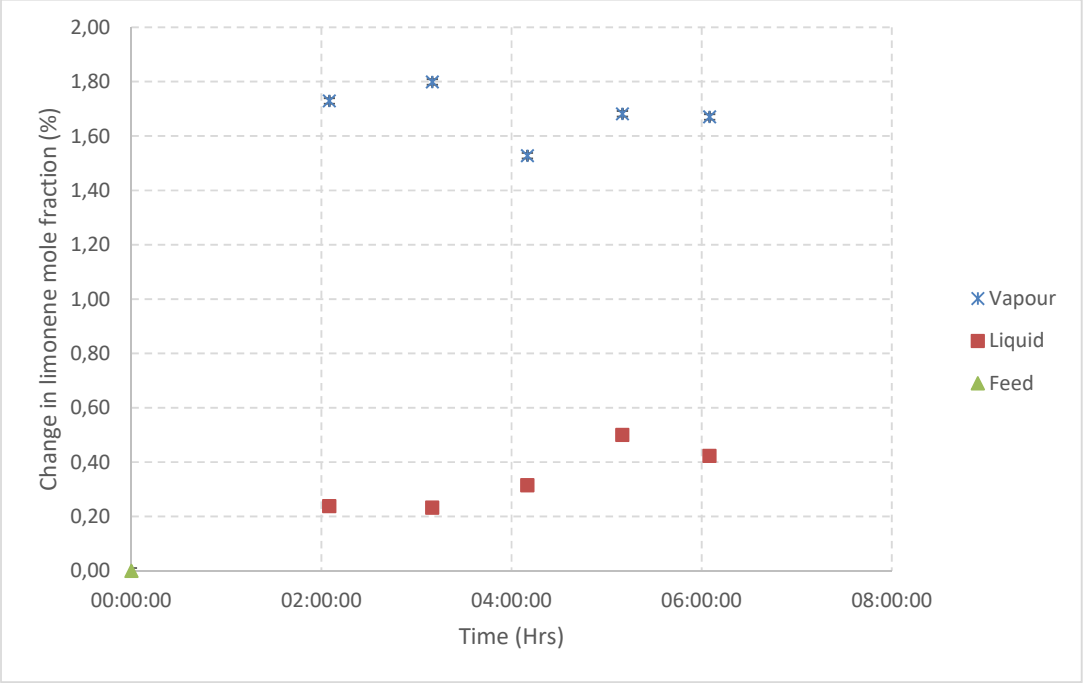

Figure 8.32: Percentage change in limonene fraction compared to feed in limonene/indane system at 40 kPa

H-6: Limonene/1,2,3-trimethylbenzene/*p*-cymene/indane

A 0.87 mole fraction limonene mixture was used for this test.

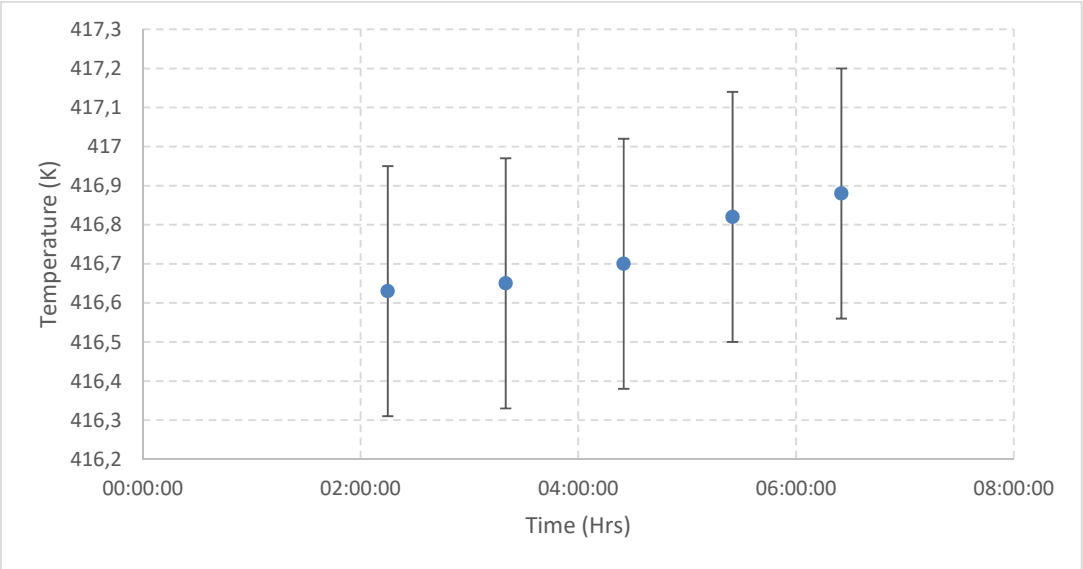

Figure 8.33: Temperature degradation profile for limonene/1,2,3-trimethylbenzene/*p*-cymene/indane system at 40 kPa with +/- 0.32 K error bars

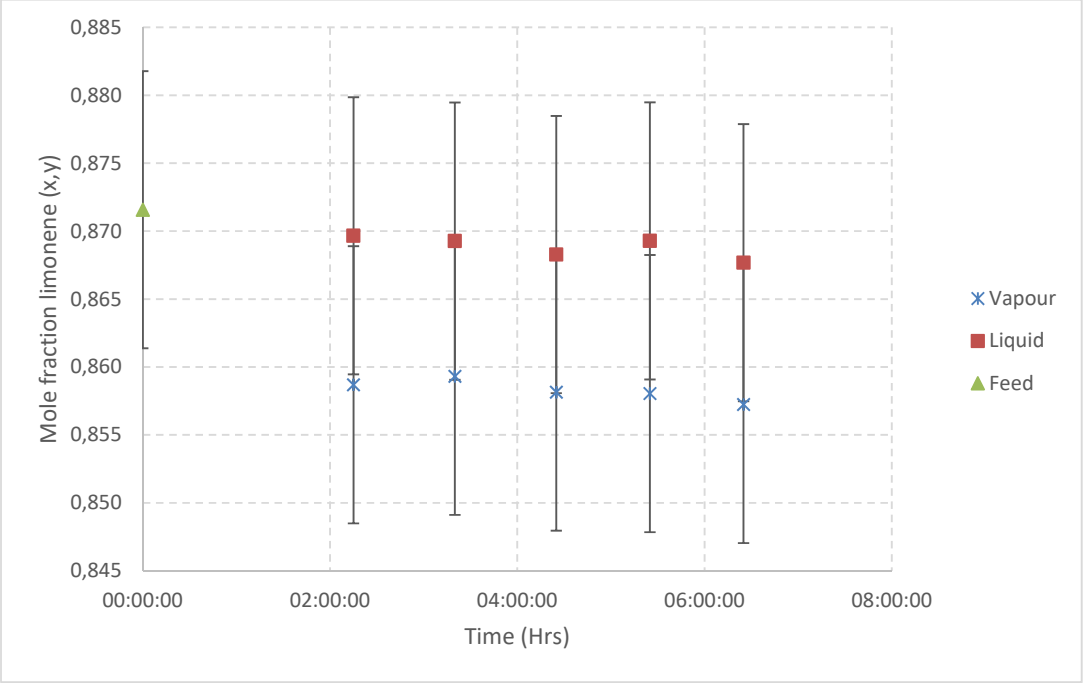

Figure 8.34: Concentration degradation profile for limonene/1,2,3-trimethylbenzene/*p*-cymene/indane system at 40 kPa with +/- 0.0102 mole fraction error bars

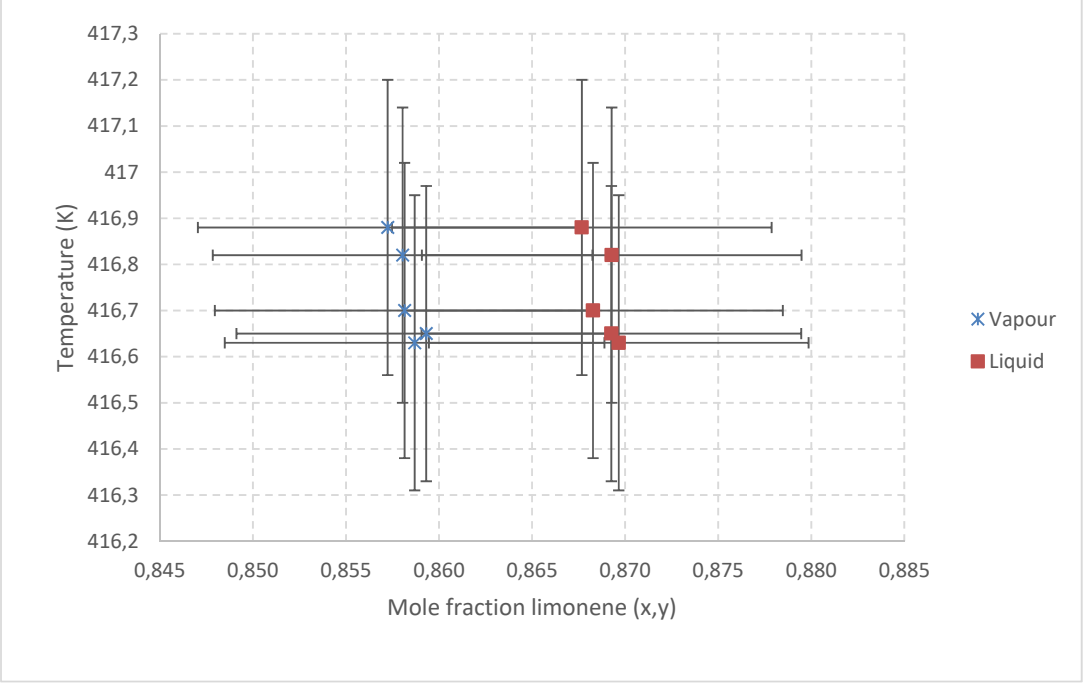

Figure 8.35: Temperature-composition diagram for limonene/1,2,3-trimethylbenzene/*p*-cymene/indane system at 40 kPa illustrating general concentration fluctuation

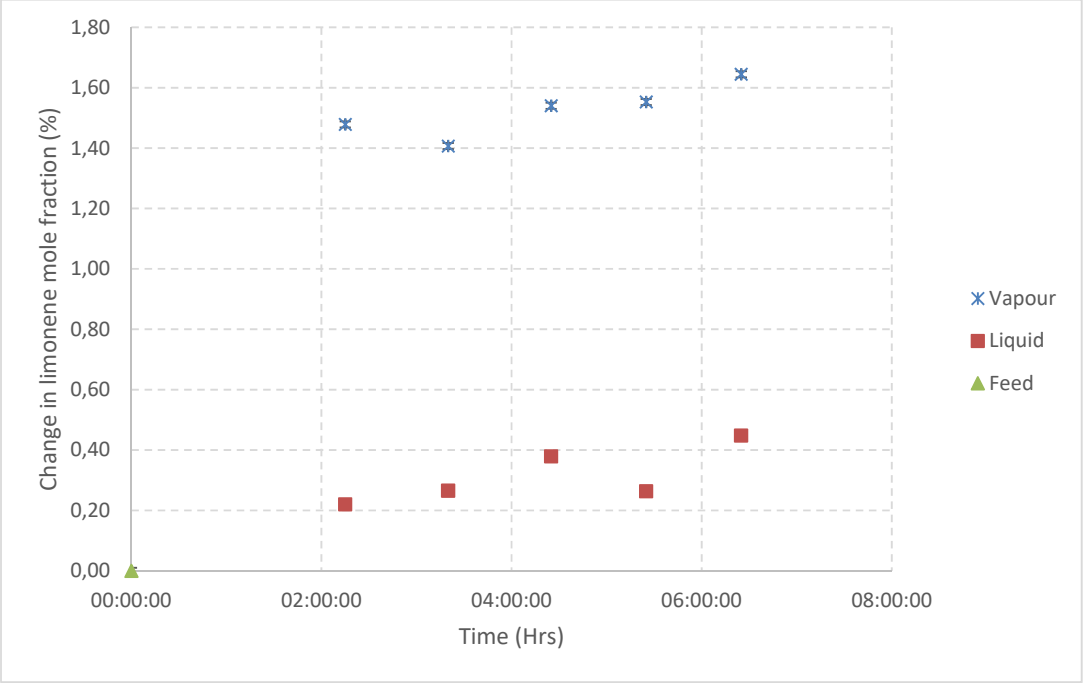

Figure 8.36: Percentage change in limonene fraction compared to feed in limonene/1,2,3-trimethylbenzene/*p*-cymene/indane system at 40 kPa

Appendix I: GC-Calibration curves

The calibration curves for each system were generated by preparing four samples with fixed masses of the internal standard and varying masses of the mixture compounds. Each sample had different ratios between the standard and compounds and were run through the GC with the areas of peaks recorded, producing four points, which was enough for a straight line calibration curve.

Table 8.13 contains the typical compound volumes used for preparing the samples that were used in generating the calibration curves. In addition to the volumes, the masses and peak areas were also recorded. With the area and the mass of the standard known, the following equation can be used to determine the mass of a component in a sample [61]:

$$m_{comp} = n\left(\frac{m_{std} * Area_{comp}}{Area_{std}}\right) \tag{8.1}$$

Where m_{comp} is the mass of the component being analysed, m_{std} and $Area_{std}$ are the mass and area of internal standard respectively and are known, $Area_{comp}$ is the area of the component returned by the GC analyser and n is the gradient of the calibration curve generated [61].

Table 8.13: Typical volumes used in preparation of samples for generation of calibration curves

Sample vial	1	2	3	4
IS: Toluene (µL)	250	250	250	250
Compound i (µL)	10	125	250	375
Compound j (µL)	10	125	250	375

Table 8.14 contains the calibration curve gradients and R^2 values used in the determination of each compounds mass and mole fractions, for each system analysed. In order to minimise the effect of retention time drift, new calibration curves were generated for each system being analysed.

Table 8.14: Calibration curve gradients and R^2 values for each system analysed

Compound	*n*	R^2
ethanol/1-butanol		
Ethanol	1.4646	0.9996
1-Butanol	1.0307	0.9998
n-decane/2-heptanone		
n-decane	1.0919	1
2-heptanone	1.5337	0.9987
n-decane/3-heptanone		
n-decane	1.1304	1
3-heptanone	1.4271	1
n-nonane/1-pentanol		
n-nonane	0.8053	1
1-pentanol	1.0942	1
limonene/*α*-pinene		
limonene	1.1752	0.9992
α-pinene	1.0465	0.9995
limonene/*p*-cymene		
limonene	1.0448	1
p-cymene	1.0200	1
limonene/butylbenzene		
limonene	1.1491	0.9998
butylbenzene	1.0235	0.9997
p-cymene/butylbenzene		
p-cymene	1.0004	0.9997
butylbenzene	0.9949	0.9997
limonene/indane		
limonene	1.0371	0.9991
indane	1.0269	0.9994
limonene/1,2,3-trimethylbenzene/*p*-cymene/indane		
limonene	1.0932	1
1,2,3-trimethylbenzene	0.9679	1
p-cymene	1.2081	0.9986
indane	1.1301	1

Appendix J: Experimental data

This appendix contains the experimental data obtained for the systems limonene/butylbenzene, *p*-cymene/butylbenzene, limonene/indane, limonene/*p*-cymene, and limonene/1,2,3-trimethylbenzene/*p*-cymene/indane at 40 kPa. Consistency test results for the McDermott-Ellis and L/W consistency tests are also shown for each binary system. The L/W consistency test however was not performed on the quarternary system results.

Table 8.15: Limonene(1)/butylbenzene(2) at 40 kPa with consistency test results

T (K)	x_1	x_2	y_1	y_2	γ_1	γ_2	L/W	D	D_{max}
421.82	0.000	1.000	0.000	1.000					
421.40	0.082	0.918	0.099	0.901	0.998	1.003	0.95		
420.80	0.195	0.805	0.236	0.764	1.009	0.988	-0.46	-0.0229	0.2051
420.77	0.207	0.793	0.239	0.761	0.963	1.000	-0.01	0.0006	0.1909
420.23	0.302	0.698	0.353	0.647	0.989	0.981	0.14	-0.0150	0.1951
420.00	0.360	0.640	0.412	0.588	0.975	0.979	0.31	-0.0122	0.1930
419.74	0.416	0.584	0.465	0.535	0.957	0.984	0.36	-0.0082	0.1941
419.43	0.484	0.516	0.535	0.465	0.956	0.976	0.40	-0.0099	0.1951
419.35	0.504	0.496	0.547	0.453	0.941	0.991	0.41	-0.0002	0.1955
419.00	0.563	0.437	0.611	0.389	0.949	0.977	0.39	-0.0043	0.1966
418.67	0.630	0.370	0.671	0.329	0.941	0.983	0.40	-0.0051	0.1976
418.40	0.688	0.312	0.727	0.273	0.939	0.979	0.42	-0.0056	0.1984
418.15	0.742	0.258	0.776	0.224	0.936	0.976	0.43	-0.0063	0.1994
417.95	0.784	0.216	0.815	0.185	0.935	0.972	0.43	-0.0036	0.2001
417.20	0.941	0.059	0.950	0.050	0.927	0.984	0.44	-0.0114	0.2472
416.95	1.000	0.000	1.000	0.000					

Table 8.16: *p*-Cymene(1)/butylbenzene(2) at 40 kPa with consistency test results

T (K)	x_1	x_2	y_1	y_2	γ_1	γ_2	L/W	D	D_{max}
416.35	1.000	0.000	1.000	0.000					
416.50	0.966	0.034	0.970	0.030	0.996	1.017	6.36		
417.01	0.879	0.121	0.895	0.105	0.995	1.004	7.01	-0.0039	0.2445
417.39	0.791	0.209	0.825	0.175	1.007	0.965	-6.25	0.0069	0.2091
417.59	0.769	0.231	0.799	0.201	0.998	0.995	202.18	-0.0005	0.2013
418.10	0.659	0.341	0.703	0.297	1.010	0.980	-1.80	0.0084	0.2034
418.63	0.553	0.447	0.598	0.402	1.008	0.997	-0.45	0.0112	0.1999
419.04	0.483	0.517	0.526	0.474	1.005	1.003	-0.29	0.0027	0.1964
419.60	0.363	0.637	0.411	0.589	1.028	0.996	0.31	0.0110	0.1970
419.85	0.322	0.678	0.360	0.640	1.006	1.010	0.35	0.0035	0.1937
420.45	0.227	0.773	0.268	0.732	1.042	0.997	0.40	0.0005	0.1950
420.78	0.161	0.839	0.185	0.815	1.007	1.012	0.55	0.0108	0.1937
421.57	0.038	0.962	0.047	0.953	1.073	1.008	0.63	0.0055	0.2386
421.88	0.000	1.000	0.000	1.000					

Table 8.17: Limonene(1)/indane(2) at 40 kPa with consistency test results

T (K)	x_1	x_2	y_1	y_2	γ_1	γ_2	L/W	D	D_{max}
416.15	0.220	0.780	0.239	0.761	1.025	0.998	1.00		
416.08	0.262	0.738	0.279	0.721	1.007	1.001	1.68	-0.0040	0.1934
415.99	0.373	0.627	0.388	0.612	0.987	1.003	-2.18	-0.0100	0.1967
415.95	0.404	0.596	0.420	0.580	0.988	1.001	-1.60	-0.0017	0.1939
415.92	0.440	0.560	0.449	0.551	0.972	1.012	-1.07	-0.0011	0.1946
415.88	0.479	0.521	0.486	0.514	0.967	1.016	-0.85	-0.0005	0.1945
415.87	0.499	0.501	0.504	0.496	0.963	1.019	-0.71	-0.0010	0.1943
415.94	0.561	0.439	0.559	0.441	0.948	1.033	-0.19	-0.0038	0.1954
416.00	0.587	0.413	0.584	0.416	0.945	1.033	-0.04	-0.0036	0.1942
416.17	0.691	0.309	0.683	0.317	0.935	1.046	0.20	-0.0046	0.1966
416.25	0.725	0.275	0.714	0.286	0.929	1.059	0.26	-0.0019	0.1940
416.48	0.811	0.189	0.800	0.200	0.924	1.075	0.36	-0.0013	0.1963
416.50	0.819	0.181	0.810	0.190	0.926	1.061	0.36	-0.0013	0.1926
416.57	0.841	0.159	0.833	0.167	0.926	1.061	0.38	0.0000	0.1927
416.88	0.944	0.056	0.941	0.059	0.923	1.063	0.45	-0.0054	0.2179

417.04	1.000	0.000	1.000	0.000

Table 8.18: Limonene(1)/*p*-cymene(2) at 40 kPa with consistency test results

T (K)	x_1	x_2	y_1	y_2	γ_1	γ_2	L/W	D	D_{max}
416.35	0.000	1.000	0.000	1.000					
416.30	0.008	0.992	0.010	0.990	1.065	0.996	5.27		
416.30	0.017	0.983	0.019	0.981	1.051	0.995	4.68	-0.0023	0.1995
416.25	0.074	0.926	0.078	0.922	0.994	0.994	2.99	-0.0070	0.2471
416.22	0.098	0.902	0.101	0.899	0.972	0.996	2.61	-0.0002	0.1949
416.24	0.118	0.882	0.120	0.880	0.963	0.996	2.13	-0.0020	0.1943
416.22	0.152	0.848	0.152	0.848	0.944	0.999	1.76	-0.0002	0.1957
416.22	0.158	0.842	0.158	0.842	0.943	0.999	1.70	-0.0003	0.1943
416.17	0.191	0.809	0.194	0.806	0.957	0.998	1.47	0.0035	0.1952
416.17	0.203	0.797	0.206	0.794	0.957	0.997	1.38	-0.0016	0.1939
416.21	0.228	0.772	0.228	0.772	0.946	0.999	1.20	-0.0018	0.1946
416.17	0.248	0.752	0.250	0.750	0.951	0.999	1.11	0.0025	0.1944
416.24	0.275	0.725	0.276	0.724	0.950	0.996	1.00	-0.0050	0.1944
416.23	0.324	0.676	0.323	0.677	0.941	1.000	0.85	-0.0001	0.1951
416.23	0.353	0.647	0.352	0.648	0.940	1.001	0.78	0.0006	0.1945
416.27	0.448	0.552	0.447	0.553	0.939	1.000	0.63	-0.0021	0.1960
416.33	0.530	0.470	0.527	0.473	0.936	1.002	0.56	-0.0011	0.1954
416.33	0.532	0.468	0.528	0.472	0.934	1.005	0.56	0.0005	0.1942
416.40	0.591	0.409	0.578	0.422	0.918	1.027	0.53	-0.0004	0.1953
416.39	0.591	0.409	0.582	0.418	0.925	1.016	0.52	0.0002	0.1941
416.47	0.656	0.344	0.647	0.353	0.925	1.017	0.50	0.0007	0.1945
416.53	0.711	0.289	0.703	0.297	0.925	1.017	0.49	0.0000	0.1942
416.55	0.731	0.269	0.715	0.285	0.914	1.050	0.48	0.0006	0.1940
416.67	0.797	0.203	0.793	0.207	0.927	1.006	0.48	0.0014	0.1962
416.79	0.900	0.100	0.896	0.104	0.926	1.015	0.46	0.0009	0.2046
416.97	1.000	0.000	1.000	0.000					

Table 8.19: Limonene(1)/1,2,3-trimethylbenzene(2)/*p*-cymene(3)/indane(4) at 40 kPa with consistency test results

T (K)	x_1	x_2	x_3	x_4	y_1	y_2	y_3	y_4	γ_1	γ_2	γ_3	γ_4	D	D_{max}
415.40	0.251	0.618	0.013	0.118	0.250	0.620	0.013	0.117	1.005	1.006	1.007	1.024		
415.47	0.294	0.583	0.012	0.111	0.291	0.587	0.012	0.110	0.996	1.007	1.005	1.021	-0.0034	0.3729
415.56	0.351	0.536	0.011	0.102	0.347	0.540	0.011	0.102	0.992	1.005	1.002	1.028	-0.0035	0.3730
415.67	0.400	0.490	0.016	0.095	0.395	0.500	0.010	0.095	0.988	1.015	0.624	1.035	-0.0048	0.3952
415.72	0.432	0.464	0.014	0.090	0.423	0.470	0.016	0.091	0.978	1.006	1.140	1.034	0.0012	0.3931
415.90	0.503	0.402	0.016	0.079	0.493	0.412	0.015	0.080	0.974	1.012	0.930	1.030	-0.0053	0.3737
416.05	0.585	0.335	0.014	0.065	0.573	0.345	0.015	0.067	0.969	1.012	1.058	1.028	-0.0016	0.3737
416.19	0.656	0.275	0.014	0.055	0.645	0.286	0.013	0.056	0.969	1.018	0.913	1.027	-0.0011	0.3744
416.20	0.673	0.262	0.013	0.052	0.658	0.274	0.014	0.054	0.963	1.023	1.059	1.047	0.0009	0.3715
416.40	0.757	0.190	0.013	0.041	0.747	0.202	0.011	0.040	0.967	1.034	0.827	1.002	-0.0007	0.3802
416.63	0.870	0.110	0.000	0.021	0.859	0.119	0.000	0.022	0.961	1.045	1.000	1.095	-0.0014	0.3008
416.77	0.945	0.045	0.000	0.010	0.936	0.053	0.000	0.011	0.960	1.133	1.000	1.091	0.0108	0.3037
416.89	1.000	0.000	0.000	0.000	1.000	0.000	0.000	0.000	0.966					

Appendix K: Verification data

This appendix presents the experimentally obtained data during the verification tests of the constructed setup. Each data set obtained is presented together with results of the L/W and McDermott-Ellis consistency tests. Furthermore, this Appendix contains the vapour pressure data collected for ethanol and 1-butanol during the verification process.

Table 8.20: VLE data obtained for ethanol(1)/1-butanol(2) system at 101.3 kPa

T (K)	x_1	x_2	y_1	y_2	γ_1	γ_2	L/W	D	D_{max}
390.54	0	1	0	1					
386.68	0.044	0.956	0.171	0.829	0.836	0.998	1.22		
385.11	0.063	0.937	0.237	0.763	0.848	0.990	1.24	0.0058	0.2856
383.65	0.085	0.915	0.312	0.688	0.863	0.963	1.28	-0.0111	0.2929
381.18	0.123	0.877	0.394	0.606	0.807	0.967	1.33	-0.0602	0.3052
378.47	0.179	0.821	0.496	0.504	0.760	0.947	1.48	-0.0787	0.3212
376.68	0.206	0.794	0.556	0.444	0.778	0.923	1.49	-0.0036	0.3334
375.88	0.223	0.777	0.572	0.428	0.758	0.936	1.54	-0.0114	0.3414
372.52	0.292	0.708	0.668	0.332	0.753	0.904	1.7	-0.0433	0.3607
371.92	0.324	0.676	0.684	0.316	0.707	0.923	2.04	-0.0395	0.3755
369.42	0.360	0.640	0.740	0.260	0.745	0.886	1.93	0.0080	0.3911
369.21	0.368	0.632	0.743	0.257	0.738	0.893	1.99	-0.0014	0.4024
364.2	0.506	0.494	0.823	0.177	0.700	0.963	3.92	0.0404	0.4316
356.69	0.749	0.251	0.946	0.054	0.702	0.804	-1.53	-0.1033	0.5858
355.7	0.793	0.207	0.957	0.043	0.696	0.804	-0.92	-0.0082	0.6122
355.15	0.827	0.173	0.967	0.033	0.687	0.765	-0.57	-0.0640	0.6389
354.17	0.850	0.150	0.976	0.024	0.699	0.659	-0.57	-0.1356	0.7019
353.38	0.873	0.127	0.979	0.021	0.703	0.701	-0.51	0.0688	0.7366
353.09	0.905	0.095	0.984	0.016	0.688	0.739	-0.28	0.0336	0.7299
352.56	0.929	0.071	0.988	0.012	0.686	0.761	-0.21	0.0272	0.7201
351.76	0.950	0.050	0.991	0.009	0.693	0.819	-0.2	0.0850	0.7178
351.78	0.989	0.011	1.000	0.000					

Table 8.21: VLE data obtained for limonene(1)/*α*-pinene(2) system at 40 kPa

T (K)	x_1	x_2	y_1	y_2	γ_1	γ_2	L/W	D	D_{max}
396.14	0.0092	0.9908	0.0000	1.0000					
396.63	0.0351	0.9649	0.0167	0.9833	0.939	0.795	0.14		
396.65	0.0423	0.9577	0.0187	0.9813	0.944	0.738	0.08	-0.0685	0.2481
396.85	0.0734	0.9266	0.0369	0.9631	0.952	0.834	-0.18	0.1272	0.2579
397.3	0.0993	0.9007	0.0500	0.9500	0.954	0.824	-0.23	-0.0096	0.2392
397.67	0.1006	0.8994	0.0548	0.9452	0.941	0.881	0.01	0.0531	0.2341
397.58	0.1088	0.8912	0.0459	0.9541	0.961	0.685	-0.16	-0.2284	0.2461
399.02	0.1951	0.8049	0.1097	0.8903	0.954	0.873	-0.45	0.2137	0.2595
399.33	0.2424	0.7576	0.1294	0.8706	0.983	0.821	-2.39	-0.0271	0.2290
401.06	0.3412	0.6588	0.1917	0.8083	1.001	0.82	-7.71	0.0188	0.2284
404.57	0.5170	0.4830	0.3495	0.6505	0.999	0.889	-15.09	0.0642	0.2220
404.2	0.5193	0.4807	0.3444	0.6556	1.022	0.882	5.84	0.0149	0.2049
405.27	0.5547	0.4453	0.3680	0.6320	1.033	0.855	-51.53	-0.0189	0.2051
409.34	0.7298	0.2702	0.5575	0.4425	1.072	0.875	-1.62	0.0626	0.2048
412.38	0.8534	0.1466	0.7376	0.2624	1.083	0.908	-0.31	0.0439	0.1939
414.18	0.9179	0.0821	0.8343	0.1657	1.167	0.908	0.09	0.0795	0.1857
414.67	0.9392	0.0608	0.8783	0.1217	1.143	0.921	0.12	-0.0073	0.1775
415.89	0.9712	0.0288	0.9351	0.0649	1.248	0.917	0.34	0.0865	0.1837
416.61	0.9977	0.0023	0.9834	0.0166	3.928	0.92	0.39	1.1802	0.3187
416.91	1.0000	0.0000	1.0000	0.0000					

Table 8.22: VLE data obtained for *n*-decane(1)/2-heptanone(2) system at 40 kPa

T (K)	x_1	x_2	y_1	y_2	γ_1	γ_2	L/W	D	D_{max}
413.35	1.000	0.000	0.964	0.036					
405.71	0.867	0.133	0.667	0.333	0.991	1.687	1.06		
404.11	0.827	0.173	0.602	0.398	0.985	1.629	1.05	-0.0210	0.1799
399.91	0.668	0.332	0.447	0.553	1.035	1.336	1.03	-0.0262	0.1997
397.56	0.564	0.436	0.365	0.635	1.079	1.256	1.03	0.0039	0.2003
397.15	0.516	0.484	0.341	0.659	1.118	1.187	1.02	-0.0136	0.2018
396.29	0.451	0.549	0.298	0.702	1.153	1.144	1.02	-0.0084	0.2029
396.79	0.504	0.496	0.325	0.675	1.106	1.199	1.02	0.0094	0.2039
396.95	0.526	0.474	0.344	0.656	1.115	1.215	1.02	0.0212	0.2012

Table 8.23: VLE data obtained for *n*-decane(1)/3-heptanone(2) system at 40 kPa

T (K)	x_1	x_2	y_1	y_2	γ_1	γ_2	L/W	D	D_{max}
413.53	1.000	0.000	0.971	0.029					
408.97	0.936	0.064	0.798	0.202	0.994	1.764	0.99		
408.02	0.910	0.090	0.732	0.268	0.966	1.702	0.98	-0.0583	0.1710
404.29	0.830	0.170	0.624	0.376	1.015	1.409	0.98	0.0370	0.1854
401.02	0.744	0.256	0.484	0.516	0.976	1.412	0.98	-0.0608	0.1885
400.10	0.714	0.286	0.448	0.552	0.971	1.387	0.97	-0.0172	0.1925
397.92	0.620	0.380	0.389	0.611	1.044	1.235	0.97	0.0193	0.2015

Table 8.24: VLE data obtained for *n*-nonane(1)/1-pentanol(2) system at 40 kPa

T (K)	x_1	x_2	y_1	y_2	γ_1	γ_2	L/W	D	D_{max}
384.49	1.000	0.000	1.000	0.000					
383.94	0.981	0.019	0.937	0.063	1.232	3.398	1.02		
382.47	0.943	0.057	0.842	0.158	1.208	3.023	1.02	-0.0468	0.1847
380.12	0.855	0.145	0.709	0.291	1.213	2.395	1.02	-0.0397	0.1896
379.42	0.795	0.205	0.651	0.349	1.225	2.095	1.02	-0.0306	0.1831
378.84	0.746	0.254	0.619	0.381	1.266	1.886	1.02	0.0025	0.1856
389.75	0.031	0.969	0.090	0.910	3.141	0.780	0.92	-0.3751	0.5680
390.10	0.013	0.987	0.078	0.922	6.556	0.766	0.93	-0.0036	0.1849
381.25	0.151	0.849	0.382	0.618	3.571	0.833	1.13	0.0548	0.3084

Table 8.25: Vapour pressure data obtained for 1-butanol and ethanol

1-Butanol		Ethanol	
P (kPa)	T (K)	P (kPa)	T (K)
101.35	390.70	101.33	351.51
100.75	390.47	101.28	351.49
90.75	387.58	100.00	351.18
90.75	387.57	90.96	348.81
90.84	387.62	81.00	346.00
83.09	385.15	69.99	342.42
83.04	385.13	59.95	338.81
82.96	385.12	49.65	334.45
69.68	380.41	39.95	329.66
69.71	380.43	29.88	323.48
59.82	376.52	20.08	315.48
59.77	376.47	16.34	311.54
50.06	372.08		
40.03	366.65		
30.22	360.10		
20.05	351.05		
14.61	344.63		
14.60	344.60		